AD-A038 491 JOHNS HOPKINS UNIV LAUREL MD APPLIED PHYSICS LAB F/G 17/7
SYSTEM DEFINITION AND INVESTIGATION OF THE ON-SITE PROCESSING O--ETC(U)
SEP 76 J W THOMAS, E C WETZLAR, L H ZITZMAN DOT-FA75WA-3553

UNCLASSIFIED APL/JHU-FP8-E-024-1 FAA-RD-77-12-1 NL

1 OF 3
AD
AD38491

Report No. FAA-RD-77-12, I

SYSTEM DEFINITION AND INVESTIGATION OF THE ON SITE PROCESSING OF EN ROUTE SENSOR SIGNALS

VOLUME 1
- SUMMARY OF RESULTS
- SYSTEM DEFINITION
- RADAR PROCESSING

J. W. THOMAS
E. C. WETZLAR
L. H. ZITZMAN

FLEET SYSTEMS DEPARTMENT
THE JOHNS HOPKINS UNIVERSITY • APPLIED PHYSICS LABORATORY
JOHNS HOPKINS ROAD • LAUREL, MARYLAND • 20810

SEPTEMBER 1976

FINAL REPORT

Prepared for

U.S. DEPARTMENT OF TRANSPORTATION
FEDERAL AVIATION ADMINISTRATION
Systems Research & Development Service
Washington, D.C. 20590

NOTICE

This document is disseminated under the sponsorship of the Department of Transportation in the interest of information exchange. The United States Government assumes no liability for its contents or use thereof.

Technical Report Documentation Page

1. Report No.	2. Government Accession No.	3. Recipient's Catalog No.
FAA-RD-77-12-I		

4. Title and Subtitle
System Definition and Investigation of the On-Site Processing of Sensor Signals. Volume I, Summary of Results, System Definition, Radar Processing.

5. Report Date
September 1976

6. Performing Organization Code

7. Author(s)
J.W. Thomas, E.C. Wetzlar and L.H. Zitsman

8. Performing Organization Report No.
APL/JHU-FP8-E-024-1

9. Performing Organization Name and Address
Fleet Systems Department, Johns Hopkins University,
Johns Hopkins Road
Laurel, Maryland 20810

10. Work Unit No. (TRAIS)

11. Contract or Grant No.
DOT-FA75WA-3553

12. Sponsoring Agency Name and Address
Department of Transportation
Federal Aviation Administration, SRDS
2100 2nd Street, SW
Washington, DC 20591

13. Type of Report and Period Covered
Final rept.
September 1974 - September 1976

14. Sponsoring Agency Code
ARD-111

15. Supplementary Notes
An Addendum to this work, concerned with beacon ringaround problems, is scheduled for publication in August 1977.

16. Abstract

The objective of this program was twofold: (1) to define requirements from the primary radar system and from the Air Traffic Control Radar Beacon System (ATCRBS) for the en route automation portion of the National Airspace System and (2) to unload the data line from the on-site surveillance system. The primary thrust of this investigation was directed towards the Common Digitizer (CD); the requirements placed on the CD by the Air Route Traffic Control Center's Central Computer Complex, the processing capabilities and limitations of the CD and the requirements the CD places on the surveillance sensors. This report documents the analytical and empirical investigations that were conducted in these areas in support of the stated objectives.

Due to the magnitude of the results of this program, this report has been prepared in three volumes. This Volume I consists of (1) a summmary of major results, conclusions, and recommendations for the entire program, (2) a description of the work accomplished and results obtained in the area of primary radar processing, and (3) a discussion of the ATCRBS jitter problem from the overall surveillance system standpoint. Volume II discusses processing of the ATCRBS (secondary radar) information within the Common Digitizer. Volumes I and II are essentially independent so that the reader concerned with ATCRBS processing can concentrate on Volume II and vice versa. Volume III contains the appendices which present backup information in support of the Volume I and II discussions.

17. Key Words	18. Distribution Statement
Air Traffic Control Radar Beacon	Document is available to the public through the National Technical Information Service, Springfield, Virginia 22151.

19. Security Classif. (of this report)	20. Security Classif. (of this page)	21. No. of Pages	22. Price
Unclassified	Unclassified	291	

Form DOT F 1700.7 (8-72) Reproduction of completed page authorized

031650

METRIC CONVERSION FACTORS

Approximate Conversions to Metric Measures

Symbol	When You Know	Multiply by	To Find	Symbol
	LENGTH			
in	inches	*2.5	centimeters	cm
ft	feet	30	centimeters	cm
yd	yards	0.9	meters	m
mi	miles	1.6	kilometers	km
	AREA			
in^2	square inches	6.5	square centimeters	cm^2
ft^2	square feet	0.09	square meters	m^2
yd^2	square yards	0.8	square meters	m^2
mi^2	square miles	2.6	square kilometers	km^2
	acres	0.4	hectares	ha
	MASS (weight)			
oz	ounces	28	grams	g
lb	pounds	0.45	*kilograms*	kg
	short tons (2000 lb)	0.9	tonnes	t
	VOLUME			
tsp	teaspoons	5	milliliters	ml
Tbsp	tablespoons	15	milliliters	ml
fl oz	fluid ounces	30	milliliters	ml
c	cups	0.24	liters	l
pt	pints	0.47	liters	l
qt	quarts	0.95	*liters*	l
gal	gallons	3.8	liters	l
ft^3	cubic feet	0.03	cubic meters	m^3
yd^3	cubic yards	0.76	cubic meters	m^3
	TEMPERATURE (exact)			
°F	Fahrenheit temperature	5/9 (after subtracting 32)	Celsius temperature	°C

*1 in = 2.54 (exactly). For other exact conversions and more detailed tables, see NBS Misc. Publ. 286, Units of Weights and Measures, Price $2.25, SD Catalog No. C13.10:286.

Approximate Conversions from Metric Measures

Symbol	When You Know	Multiply by	To Find	Symbol
	LENGTH			
mm	millimeters	0.04	inches	in
cm	centimeters	0.4	inches	in
m	meters	3.3	feet	ft
m	*meters*	1.1	yards	yd
km	kilometers	0.6	miles	mi
	AREA			
cm^2	square centimeters	0.16	square inches	in^2
m^2	square meters	1.2	square yards	yd^2
km^2	square kilometers	0.4	square miles	mi^2
ha	hectares (10,000 m^2)	2.5	acres	
	MASS (weight)			
g	grams	0.035	ounces	oz
kg	kilograms	2.2	pounds	lb
t	tonnes (1000 kg)	1.1	*short tons*	
	VOLUME			
ml	*milliliters*	0.03	*fluid ounces*	fl oz
l	liters	2.1	pints	pt
l	liters	1.06	quarts	qt
l	liters	0.26	gallons	gal
m^3	cubic meters	35	cubic feet	ft^3
m^3	cubic meters	1.3	cubic yards	yd^3
	TEMPERATURE (exact)			
°C	Celsius temperature	9/5 (then add 32)	Fahrenheit temperature	°F

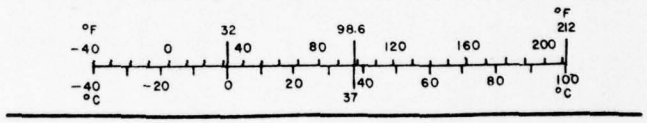

THE JOHNS HOPKINS UNIVERSITY
APPLIED PHYSICS LABORATORY
LAUREL MARYLAND

PREFACE

This report describes the work performed by The Johns Hopkins University Applied Physics Laboratory (APL) for the Federal Aviation Administration under contract DOT-FA75WA-3553. The Technical Representative for this effort is Dr. James A. Shannon of Air Traffic Control System Division (ARD-111) of the Systems Research and Development Service (SRDS).

Grateful acknowledgement is made to NAFEC personnel; Messrs. W. Swanseen, E. Mancus, R. Gilmartin, M. Hulse, M. Holtz, M. Schoenthal and others for their cooperation and technical assistance in testing the CD enhancements and providing data for the beacon and en route system analysis.

Acknowledgement is made to the following APL/JHU personnel for their contributions to this task:

E. L. Brickner - Investigation of the Radar Data Requirements and Processing Capability of the Air Route Traffic Control Center (ARTCC), Section 3.0.

M. I. Marks - Performance Capability of the Air Route Surveillance Radars (ARSR-1, 2), Section 4.1.

R. J. Prengaman - Automatic ACE Curve Selection, Section 5.3.1.

W. G. Bath - Scan Correlated Feedback Control of the Rank Quantizer, Section 5.3.2.

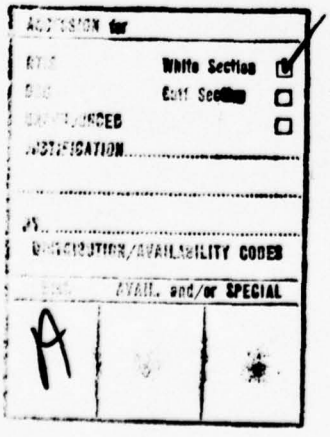

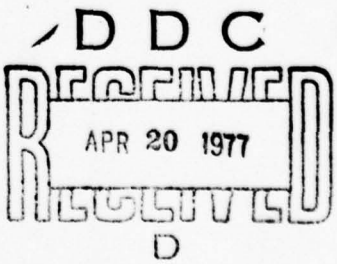

GLOSSARY

ACE	Automatic Clutter Eliminator
ACP	Azimuth Change Pulse
AI	Auxiliary Interpreter (same as the D-machine)
APL	The Johns Hopkins University Applied Physics Laboratory
ARP	Azimuth Reference Pulse
ARSR	Air Route Surveillance Radar
ARTCC	Air Route Traffic Control Center
ARTG	Azimuth Range Timing Group
ARTS	Automated Radar Terminal System
ASR	Airport Surveillance Radar
ATCBI	Air Traffic Control Beacon Interrogator
ATCRBS	Air Traffic Control Radar Beacon System
AVP	Adaptive Video Processor
BRG	Beacon Reply Group
CCC	IBM 9020 Computer Complex
CD	Common Digitizer
CE	Compute Element
CFAR	Constant False Alarm Rate
CPV	Correlation Preference Value
CRT	Cathode Ray Tube
DDI	Delayed Decision Integration
D-Machine	A minicomputer manufactured by Burroughs Corp. which has been interfaced to the Common Digitizer at Elwood, N.J. (Also called the Auxiliary Interpreter (AI))
FLAT	Flight Plan Aided Track
FR-1800	Intermediate band analog recorder used to record output of modem receiver at the ARTCC
FR-950	Wide band analog recorder made by Ampex
FREE	A track in the ARTCC system not aided by a flight plan
FTC	Fast Time Constant

GLOSSARY (cont'd)

HPF	High Pass Filter
HWD	Hit Width Discrimination
IFT	Intermediate Format Tape
IOCE	Input/Output Control Element
LSA	Large Search Area
LSB	Least Significant Bit
MCG	Memory Control Group
MDS	Minimum Detectable Signal
MISAL	Radar-Beacon Misalignment Detection Program
M/N	Number of hits (M) in a sliding window of N opportunities
MTI	Moving Target Indicator
MTU	Magnetic Tape Unit
NAFEC	National Aviation Facilities Experimental Center
NAS	National Airspace System
PCD	Production Common Digitizer. Also CD
PDF	Probability Density Function
P_{fa}	Probability of false alarm reports exiting the Common Digitizer
PPI- RAPPI	Plan Position Indicator - Random Access PPI (manufactured by Ampex). Console unit that permits display of raw in-process and completed target report message data. It is part of the PCD.
P_n	Probability of false alarms exiting the radar quantizers
PRF	Pulse Repetition Frequency
PSA	Primary Search Area
RSB	Radar Search Box
SCF	Scan Correlated Feedback
S/N	Signal/Noise Ratio
SPI	Special Position Identification Pulse
Spiky	Occasional large excursions in the signal amplitude of short duration
SSA	Small Search Area
SST	Standard Sweep Tape

GLOSSARY (cont'd)

TDG	Target Detection Group
T_L	Target lead edge threshold for the azimuth sliding window
TOT	Target Ordered Tape
TPG	Target Processing Group
TRAAP	Target Report Ambiguity Analysis Package
TRQA	Target Report Quality Analysis program
TSB	Track Search Box
T_T	Trailing edge threshold in the sliding window
T_V	Validation threshold in the sliding window
UC	Unselected Centroid
VCA	Voltage Controlled Amplifier
VQR	Video Quantizer Recorder

TABLE OF CONTENTS

TABLE OF CONTENTS (cont'd)

TABLE OF CONTENTS (cont'd)

TABLE OF CONTENTS (cont'd)

TABLE OF CONTENTS (cont'd)

TABLE OF CONTENTS (cont'd)

TABLE OF CONTENTS (cont'd)

TABLE OF CONTENTS (cont'd)

TABLE OF CONTENTS (cont'd)

LIST OF FIGURES

LIST OF FIGURES (cont'd)

LIST OF FIGURES (cont'd)

LIST OF FIGURES (cont'd)

LIST OF FIGURES (cont'd)

LIST OF FIGURES (cont'd)

LIST OF FIGURES (cont'd)

LIST OF FIGURES (cont'd)

LIST OF TABLES

LIST OF TABLES (cont'd)

LIST OF TABLES (cont'd)

1.0 INTRODUCTION

The broad objective of this program is to assist the FAA in enhancing the performance of the National Airspace System (NAS) in the areas of acquisition, transfer, and processing primary radar and Air Traffic Control Radar Beacon System (ATCRBS) data. The statement of work further specifies this objective by giving the following two objectives for the contract:

> "(1) to define requirements from the primary radar system and from the ATCRBS for the en route automation part of NAS; and
>
> (2) to unload the data line from the on-site surveillance system."

Although the major thrust of this contract was directed toward the Common Digitizer (CD), it must be remembered that the CD is only one part in the entire en route automation system. Therefore in order to achieve the above-mentioned objectives, a certain amount of systems analysis has been performed on the en route automation system as a whole. Figure 1.1 shows a simplified block diagram of this system. Radar and beacon video from the Air Route Surveillance Radar (ARSR) and ATCRBS along with certain control signals, are transferred to the CD which forms target reports that are in turn transmitted over modem lines to an Air Route Traffic Control Center (ARTCC). This center houses an IBM 9020 computer complex (CCC) which correlates the reports from scan to scan (tracks the reports), merges them with flight scheduling information, and finally generates various displays.

This report is divided into three separate volumes. Volume I consists of a summary of major results, conclusions, and recommendations from the entire report. In addition Volume I also describes work completed in the area of primary radar processing (one exception to this is Section 4.2 which discusses jitter in the beacon system). Volume II discusses processing of the secondary radar (beacon) information within the CD. Volumes I and II are essentially independent so that the reader mainly concerned with beacon processing can concentrate on Volume II and vice versa. Volume III contains the appendices for this report.

A summary of the major results, conclusions, and recommendations are presented in Section 2. Appropriate references to the detailed discussions contained in the body of this report are also cited.

As mentioned before the primary thrust of this investigation was directed toward the Common Digitizer. However, because the CD is only one link in the entire chain of en route automation and system optimization of the functions performed by the Common Digitizer must take into consideration the capabilities and requirements of other system components, a portion of the program was directed towards investigating the other system components.

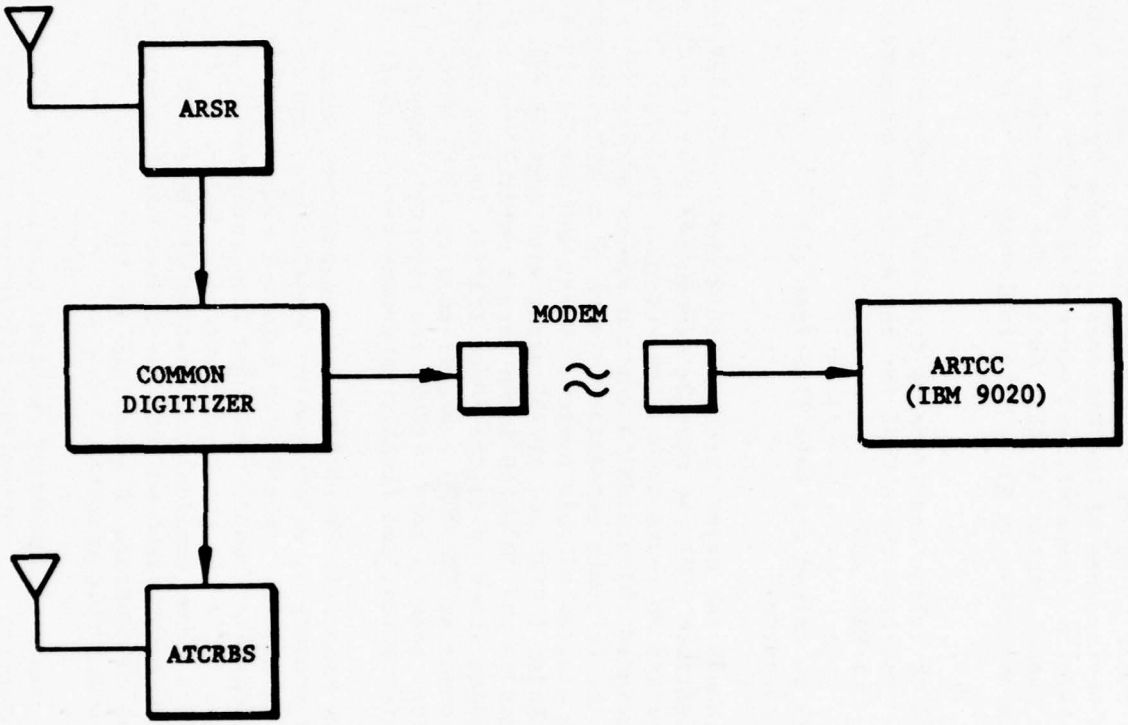

FIGURE 1.1

BLOCK DIAGRAM OF THE EN ROUTE SYSTEM

This consisted of a combination literature search and theoretical investigation of the ARSR and the ARTCC with the two-fold purpose of (1) providing background material and familiarization in those areas and (2) identifying any special requirements placed upon the CD by either the ARSR or the ARTCC. A similar study was not directly performed for the ATCRBS. Instead, it was recognized that a significant problem in the area of beacon processing is that of range splits; therefore, a theoretical investigation was undertaken into the various sources of jitter from sweep to sweep in the ATCRBS including the CD. Section 3 contains material on the ARTCC and Section 4 discusses the ARSR and ATCRBS jitter problem.

The primary radar processing within the Common Digitizer itself is discussed in Section 5. This section begins with a theoretical investigation of some aspects of a group of experimental modifications to the Common Digitizer purchased under contract DOT-FA74WA-3426. In addition to theoretical studies, Section 5 also includes a description of evaluation tests which were performed on the new modifications.

In contrast to Sections 3 and 4 which involved theoretical investigations of the ARSR and ARTCC, Sections 6 and 7 discuss experimental measurements and analyses made of actual field data of the video leaving the ARSR and the target reports entering the ARTCC. Therefore these two sections consist of an experimental evaluation of the information entering and exiting the Common Digitizer as it presently exists in the field. Section 6 addresses the statistical characteristics of the video of ARSR returns from various types of clear and clutter environments, and Section 7 addresses the quality of the target reports (radar and beacon) exiting the Common Digitizer.

Section 8 is concerned with beacon (secondary radar) processing within the CD. Evaluations are performed on the video entering the CD, the target reports exiting it, as well as the replies which are formed from the video and in turn combined to form the reports.

All of the originally planned investigations as outlined above were not completed due primarily to problems in obtaining the necessary CD test information (see Sections 5 and 8). In view of fiscal limitations, the FAA and the Laboratory (APL) agreed to suspend this program and recommence in the future should such a course of action prove to be advisable. Sections 5, 6, 7, and 8 are directly affected by this action and, of course, Section 2 indirectly.

SECTION 2.0

SUMMARY OF RESULTS,
CONCLUSIONS AND RECOMMENDATIONS

2.0 SUMMARY OF RESULTS, CONCLUSIONS AND RECOMMENDATIONS

2.1 INTRODUCTION

This program has the overall objective of assisting the FAA in enhancing the performance of the en route portion of the National Airspace System (NAS). The following two specified subobjectives have been addressed:

- The definition of requirements from the primary radar system and from the Air Traffic Control Radar Beacon System (ATCRBS) for the en route automation portion of NAS; and
- The unloading of the data line from the on-site surveillance system.

Many significant results were obtained toward satisfying the overall objective and the two subobjectives. These results are summarized on both an overall basis and with regard to specifics in the subsections to follow. In pursuit of subobjective one, various key aspects of the radar and ATCRBS data processing requirements and capabilities for both the Common Digitizer (CD) and the Air Route Traffic Control Center (ARTCC) have been investigated in depth. The empirical investigation into the potential performance capability of the Common Digitizer Enhancements as implemented at the Elwood, New Jersey site has not been fully completed at this time; however, due primarily to the unavailability of certain system data taken under operationally representative conditions. Pursuit of the second subobjective revealed that the data line is not a problem; the compute capability of the ARTCC computer complex will be exceeded before the data line reaches full capacity. Therefore, the direction of the investigation supporting this subobjective was changed to place emphasis on reducing the number of false target reports which must be processed by the ARTCC rather than just reducing the number of digitized returns which are transported over the data line.

Lastly, it is appropriate to note that an extensive and powerful capability has been developed for the FAA to investigate certain aspects of the Common Digitizer video and information processing for both radar and/or ATCRBS inputs. This capability has been used as appropriate to extract the results which were used as the basis for the conclusions and recommendations to follow. This capability can be used by the FAA in the future to investigate other problem areas on a cost benefit basis since the development of these basic tools has been, for the most part, completed.

2.2 GENERAL CONCLUSIONS AND RECOMMENDATIONS

One of the most important long range problems facing the en route automation system is the heavy utilization of the IBM 9020 computer systems (in both compute power and memory). This problem is not only related to anticipated increased data rates resulting from increases in air traffic but can place severe restrictions on the number and quality of additional automated functions performed by the CCC such as collision and terrain avoidance. Approaches used in the past to solve this problem include enhancing the IBM 9020 computer system with increases in both memory and computer power, restriction on additional function allowed to be placed in the computer, and optimization of the existing code. These methods all have their merit; however, an additional approach is recommended here which has enough promise to warrant further investigation. The saturation of the IBM 9020 computer complex is an en route automation systems problem and as such should be attacked from a systems point of view. (The previous approaches have concentrated on the 9020 itself.) Much of this report is directed toward a beginning of a systems approach to this problem. An investigation is made into ways of reducing the number of false radar (primary) target reports exiting the Common Digitizer. Of the proposed enhancements which were investigated those which showed the most promise are the rank order quantizer and the scan correlated feedback to the quantizers. Much work remains before these enhancements are perfected and continued investigation in this area is recommended.

In comparison with radar reports, beacon processing in the Common Digitizer does not produce large quantities of false reports; therefore, rather than the reduction of large volumes of false reports the beacon work performed had as its objective the investigation of specifically troublesome false target reports such as splits, missing reports, reflections, etc. The beacon report analysis appropriately characterizes and quantifies these problem reports. The portion of the reply analysis which has been completed raised many interesting questions which should be investigated further. Primary among them being the fact that replies which produced range splits in the Common Digitizer were measured by the Auxiliary Interpreter (AI), an Elwood, New Jersey CD Enhancement feature, to all be in the same range cell. It is recommended that the next step in this area be the construction of a computer simulation which takes replies from the AI and centroids them into target reports utilizing the algorithm in the Common Digitizer. This will help to clarify the ranging differences between the AI and the CD. It will also provide a means to test proposed improvements to beacon processing. No extensive work was performed on beacon video; nevertheless, the analysis techniques developed were successfully demonstrated and proved to be very powerful. To our knowledge this is the first time beacon replies and video have been investigated in this manner and to this detail. Both techniques show a potential for discovering in more detail than before the internal operations of the Common Digitizer with regard to beacon processing and the development of effective solutions to the problems which exist. Their continued development and use are recommended.

Another systems approach to the saturation problem which merits investigation is the continued transformation from one central, large computer performing all functions to a distributed network of computers operating in a pipeline fashion where some of the functions (such as initial or site tracking) presently being implemented in the 9020 would be placed in smaller satellite computers which could be located either at the ARTCC or radar site. In this way the system computer resources (compute power and memory) could be enhanced. This trend was initiated with the establishment of the Input/Output Compute Element (IOCE), but could be expanded greatly. In these days of drastic reductions in computer hardware costs distributed computer system architectures are becoming increasingly attractive from an overall cost effective point of view and it is recommended that this approach be seriously investigated and initial engineering and development projects started.

A large portion of the problems and delays associated with this work can be directly attributed to the inability of the Elwood New Jersey AI enhancement feature to support the required test operations. In spite of this, it is recommended that if the AI is used only to support the present enhancements and data collection modes, then the present difficulties should be rectified. The data collection capability provided by the AI makes it a valuable tool in investigating the performance capability of the Common Digitizer and should be maintained. On the other hand, if it is anticipated that the capabilities performed by the AI will be enhanced and such enhancements will require large amounts of software development, it is recommended that serious consideration be given to replacement of the AI with a computer system which is more widely supported and maintained in the commercial sector.

2.3 SPECIFIC SUMMARY

2.3.1 Investigation of the Radar Data Requirements and Processing Capability of the Air Route Traffic Control Center (Section 3)

The ARTCC 9020 system was analyzed to determine the quantity and quality of Common Digitizer data it can satisfactorily handle. The analyses indicate that the output data rate of the CD is more than adequate to meet the future capacity data requirements of the en route system (Section 3.2.2). The limiting factor in the ARTCC system is 9020A compute capacity. The 9020D configuration can satisfactorily handle the projected 1985 track loads while the 9020A cannot. The 9020A limitation can be reduced by implementing one or all of the following (Section 3.3):

- Expand the 9020A compute capacity
- Reconfigure the hardware and software for more efficient operation
- Preprocess the centroid data at the Common Digitizer or the ARTCC site.

Four specific findings of this investigation are as follows.

Radar and discrete beacon centroids should have a positions measurement accuracy (standard deviation) of 0.22 nmi in range and 0.14 degrees (1.6 ACP's) in azimuth in order to be tracked properly in the ARTCC (Section 3.2.3).

Measured positions are used for display to the air traffic controller. Since the variance in the filtered track position is nearly one-fourth that of the measured data, filtered positions should be displayed (Section 3.2.4).

The size of the small (SSA) and large (LSA) search area windows is not varied as a function of target range. A fixed sized window has the disadvantage of being too small at long ranges and too large at short ranges. Tracking window sizes should be varied according to the range of the centroid from the radar (Section 3.2.4).

Investigations into the requirement for unloading the data lines from the surveillance systems site to the ARTCC have indicated the data line capabilities are not the system problem area. The compute capabilities of the ARTCC computer complex will be exceeded before the data lines reach full capacity. On the other hand, much of the work accomplished was directed towards reducing the number of false target reports, thereby indirectly aimed at satisfying the system problem underlying the subobjective of unloading the data lines.

2.3.2 Performance Capability of Long Range Search Radar (Section 4.1)

Signal to clutter ratios were plotted for both land clutter and rain clutter. Utilizing the advertised subclutter visibility of the ARSR-1, 2 radars which is 27 dB, Figure 4.10 shows that rain clutter for the assumed worst case of 16 mm/hr rain rate and one square meter target, does not prevent target detection (i.e., all the curves are well above -27 dB).

Figure 4.9 shows that in most normal cases land clutter is not a limiting factor. However, when the terrain backscatter coefficient is -20 dB and a 1 square meter target is considered, detection is limited between about seven nautical miles and twenty-four nautical miles.

2.3.3 Results of the Analysis of ATCRBS Range Jitter (Section 4.2)

The primary thrust of the investigation of the beacon processing performance of the CD described in Section 8 was directed toward the CD. However, it was recognized that a significant problem in the area of beacon processing is that of range splits. Therefore, a theoretical investigation of the various sources of range jitter in ATCRBS, including the CD, was undertaken. This theoretical investigation emphasizes the contributions of the Air Traffic Control Beacon Interrogator (ATCBI) and the transponder to the range jitter problem. Consequently the discussion of the investigation is included in Section 4 entitled Analysis of Sensors.

The variation in the range of successive replies from a target during a single scan past the target as determined by the CD was theoretically considered by this analysis. The maximum variation in range possible for successive replies received from a fixed target was analyzed. There are several significant sources of range jitter in ATCRBS. These are listed below.

- o The CD range clock synchronization with the ARSR pretrigger.
- o Synchronization of the Beacon Interrogator timing with the radar pretrigger.
- o Jitter between the beacon interrogator trigger and the RF transmission.
- o Transponder timing.
- o Beacon Reply Group Time Quantization.

The jitter values were obtained from appropriate reference specifications and not verified experimentally.

The individual range jitters from the above jitter sources were statistically combined to obtain a measure of the relative contribution of each source to the total effective system jitter. The results were used to show that modifying the CD processing alone to reduce its contribution to overall system jitter will probably not achieve range accuracy sufficient to significantly reduce the split problem.

It is recommended that the range jitter introduced by each component be physically measured in a real system, so that more representative values can be used. Such measurements could, for example, reveal that the jitter values used for the theoretical analysis (which are presumed to be maximum allowable) are significantly higher than those of a typical system. If this were the case, CD modification might be more effective.

2.3.4 Automatic ACE Curve Selection (Section 5.3.1)

The analysis of the Automatic ACE Curve Selection enhancement indicates that the technique will be only modestly successful. When correlated clutter occurs the number of false targets can increase significantly, e.g. from 80 to 1000 false targets. The correlation estimator is particularly weak if clutter is correlated in azimuth but not in range (Section 5.3.1.6). At best a 2 to 1 reduction in false target reports could be expected. Better results can be obtained if the clutter is correlated in both azimuth and range. For strong correlation a 10 to 1 false target report reduction might be achieved, while a 5 to 1 reduction is possible in moderately correlated clutter (Section 5.3.1.4). A 10 to 1 and 5 to 1 reduction is necessary in order to keep the number of false targets close to the number occurring under uncorrelated conditions. A 2 to 1 reduction (1000 to 500) in false targets would still overload the system.

The above expected results assumed ideal conditions of clutter correlation thresholds chosen to match a well regulated hit probability (P_n). Changes in the hit probability will modify the automatic selection operation considerably. In addition, if target reports extend over more than one range cell they may trigger the auto select thresholds. If this occurs, suboptimal thresholds must be chosen. This would further reduce the performance of the technique.

There are other methods available that will adjust the target detection threshold (second threshold) to maintain a constant false target detection probability based upon the correlation of the input video. In particular, the FAA has been testing a method proposed by MITRE. Because the subject enhancement is projected to be only modestly successful, the MITRE method and others should be investigated and the relative capabilities determined prior to pursuing further testing.

2.3.5 Rank Quantizer (Sections 5.3.2 and 5.4.2)

A rank quantizer, configured to obtain independent range samples of video that has the same probability distribution for all samples, produces a first threshold false hit rate (P_n) that is independent of the video probability distribution. This distribution-free characteristic makes the rank quantizer a desirable first threshold device to enhance target detection by controlling the false hit rate under varied video conditions.

A 24 tap, 1 μsec tap spaced delay line rank quantizer prototype was added to the Common Digitizer. The CD/quantizer interface incorporated the capability of operating the quantizer both nonparametrically and parametrically with scan correlated feedback. Analysis results from previous FAA contracts were reviewed and new analyses performed to define a test program to assess the performance of the quantizer. References 1 and 2 provided significant information applicable to first threshold quantizers and Scan Correlated Feedback (SCF). Significant findings applicable to the rank quantizer based upon previous analysis are as follows:

1. The sample tap spacing (1 μsec) does not match the ARSR-2 pulse width (2 μsec). Therefore, the video samples along the delay line are not independent and the performance of the rank quantizer should be affected by the statistical characteristics of the input video.

2. Parametric operation with SCF should be implemented with additive gain control when using log video not with the multiplictive gain control as is now being used.

3. The use of a quantizer thermal loop for non clutter situations is not a cost effective means of P_{fa} regulation.

The parametric operating capability provides a means of controlling P_n should the nonparametric operation not prove to be successful. Three analyses were made to determine the effectiveness of the SCF loop in maintaining a well regulated false alarm rate. The analyses performed were:

- o Appraisal of SCF Technique
- o Estimate of SCF Detection Loss
- o Performance of SCF in non Rayleigh Clutter with the use of Guard Bands.

Conclusions and recommendations concerning parametric operation with SCF are as follows:

- Scan correlated feedback can provide a hit probability easily regulated to within 20-30% in noise or lightly correlated clutter. This implies a system false alarm probability well regulated to within an order of magnitude (Section 5.3.2.1.3).

- Scan correlated feedback is limited by the zone density sample size to hit probability (P_n) greater than 10^{-3} (Section 5.3.2.1.4). Thus in heavily correlated clutter where the system false alarm and hit probability are nearly equal, system false alarm probabilities (P_{fa}) less than 10^{-5} could not be maintained (Section 5.3.2.1.4).

- The rank quantizer with SCF operates with a detection loss when compared to an ideal thresholding system because the presence of a target will trigger the SCF loop to bias the first detection threshold upward (Section 5.3.2.2). The magnitude of this loss was computed and found to be less than 0.6 dB over a typical range of operating values (P_n = 0.05 to 0.1). If operation at lower P_n values is desired, the detection loss can be minimized by adjusting the SCF gains to limit the downward range of P_n.

- SCF control of the rank quantizer center tap bias maintains the desired probability of false alarm when the clutter power changes as well as when the clutter distribution changes (Section 5.3.2.3.2).

- The center tap bias range required to maintain P_n control in "spiky" clutter is larger than when controlling for thermal noise or Rayleigh clutter (Section 5.3.2.3.2).

- The use of a SCF guard band in the control of the center tap bias improves the steady state characteristic of the control loop by damping out oscillations. A guard band of ±10 hits in a zone with 1000 hit opportunities is recommended (Section 5.3.2.3.3).

Satisfactory nonparametric performance of the rank quantizer was obtained for log and MTI receiver noise after a correct calibration procedure was determined (Section 5.4.2.1). Performance characteristics (receiver noise) for the 24 tap configuration are as follows:

- The quantizer shows little sensivitity to the rank selected, input voltage level and type of input video.

- An increase in the video correlation results in a reduction in the value of P_n. The video correlation effect was simulated by reducing the video bandwidth with receiver noise input to the CD.

Hardware failures, digital recording problems, and a lack of documentation to calibrate, operate and maintain the CD enhancements, all combined to have a severe impact on the successful completion of the test program (Section 5.4.2). Due to the limited testing that was accomplished it is difficult to assess how the proposed quantizer will perform in clutter conditions. It is recommended that dynamic tests be performed to measure the effects on P_n control and target detection of the absence of a target buffer zone and operation with non independent samples. Since the quantizer is calibrated in receiver noise under correlated conditions (0.5 MHz delay line bandwidth), dynamic video correlation may not be a problem. For comparison purposes, all dynamic tests should also be performed on a quantizer with a target buffer zone and independent tap spacing. Several quantizer configurations were tested in receiver noise. The 10 tap, 2 μsec tap spaced, 3 μsec target buffer zone configuration showed the static performance required to obtained proper dynamic operation (Section 5.4.2.2).

2.3.6 Hit Width Discriminator (Sensitivity of Signal Conditioning, Section 5.4.2.3)

The results of test 2.3 (Section 5.4.2.3) show that changes in hit width discrimination (HWD) influence the P_n characteristics of the rank quantizer. The combined operation of the HWD and 1/4 nmi peak detector approximately doubles P_n. Since the nonparametric P_n is changed the rank quantizer will have to be operated parametrically to obtain the desired P_n. It is recommended that further analysis and testing be performed to determine the best method of P_n control that includes the HWD and detector effects. The minimum hit width target discrimination (1/32 nmi) presently used by the CD is the preferred value. Values greater than 1/32 nmi drastically reduce noise hits out of the discriminator.

2.3.7 MTI Video (Section 5.4)

During rank quantizer testing it was observed that significant limiting of the MTI signal occurs in rain clutter (Section 5.4; 24, 25, 26 September Test Interval). Signal limiting results in a loss of target information. It is recommended that MTI video not be used during rain clutter conditions unless a method is available to adjust the receiver so that limiting will not occur.

2.3.8 Zone Control of the Lead Edge Threshold (Section 5.4.3)

Zone control of the second threshold lead edge (T_L) is accomplished by counting the targets declared in a zone. If the count exceeds an expected count plus a delta value (Δ), a T_L modifier is incremented and added to the sensitive lead edge switches. The two parameters, expected count and Δ, are single values to be used for the entire coverage area.

It is recommended that the zone control of T_L be palced low on the priority scale for test and development because it is highly speculative. The distribution of aircraft within the radar coverage area will not be uniform. Air traffic density varies significantly over the radar coverage area due to traffic patterns, the time of day, and because the area covered by a zone (4 nmi x 5.6 degrees) increases with range. It is questionable whether it will be possible to select a value for the expected number of targets in a zone that will be constant with respect to time and be applicable for all zones in the radar coverage area. The beacon analysis presented in Sectio 8.4.2 supports these statements.

2.3.9 Input Signal Characteristics (Section 6)

A literature search of several texts and papers on statistical modeling of the radar environment shows that it has been determined that radar clutter returns are very complex. Ground clutter returns are affected by the terrain and season. Contour variations of the terrain cause significant spatial variations. Seasonal variations result from the amount of foliage on trees and the moisture content of the soil. Weather clutter is even more complex because it is affected by turbulence and wind shear and whether the rainfall fills the radar beam.

The objective of this task was to measure the various statistical characteristics of the ARSR-2 video. A library of models would then be available that could be used to predict how the CD modifications would perform when tested. Some preliminary statistics on ground clutter were measured prior to suspension of the task. These measurements verify that different statistics are obtained from area to area. Due to the requirements of the unanticipated problems encountered during the Common Digitizer Enhancement test program, which was considered to be of higher priority, only ten percent of this task as originally conceived was completed.

The analysis of radar signals is enhanced by the availability of digitized radar signal recordings. Future work should include a method to calibrate the recorded amplitude to the input signal amplitude (Appendix A Reference 40). This would enhance the statistical modeling effort by providing a scaled amplitude for power spectrum analysis and the comparison of amplitude data between different recordings made at the same site or at different sites.

2.3.10 Output Signal Characteristics (Section 7.3)

The investigation of Output Signal Characteristics involved the measurement of the quantity and quality of target reports (radar and beacon) produced by the Common Digitizer. Only a limited amount of data was processed; however, the following conclusions and recommendations can be made. The vast majority of radar reports exiting the CD are false (approximately 90%, Section 7.3). In view of this large false radar report rate the potential for major improvements exists and it is recommended that efforts be made to reduce the rate and thereby take some of the work load off of the IBM 9020 Central Computing Complex (Section 7.3).

Primary radar information processed in the CD is of value both in increasing blip-scan ratios and track continuity during beacon fades and in increasing confidence in the validity of a beacon report through radar reinforcement (Section 7.3).

Run length and radar reinforcement are two measured parameters which may be useful in determining the validity of a target report (radar and beacon). These parameters have been used in the past to discriminate against false radar reports; however, careful examination of their characteristics may uncover more effective uses (see Section 7.3).

2.3.11 Beacon Processing Investigation (Section 8)

The first step in the analysis of beacon processing was to single out specific problem areas for detailed investigation. The important results obtained from the study of each problem are presented followed by remaining important findings and significant data collection problems encountered during the study.

2.3.11.1 Problems Identified to be Investigated (Section 8.1.3.2)

There were five problems identified for further study:

- o Beacon Target Report Ambiguities
- o Radar-Beacon Misalignment
- o Missing Beacon Reports
- o Jagged Tracks
- o Incorrectly Reported Beacon Codes.

2.3.11.2 Beacon Target Report Ambiguities (Section 8.1.3.2.1)

Target report ambiguities occur when the CD produces two or more beacon reports corresponding to a single target in the same scan. Five types of ambiguities were identified. They are categorized according to the separations between the reports that comprise the ambiguity. Although the separation characteristics were used to type the ambiguities, the names of the categories relate directly to the suspected causes for each ambiguity type. The five categories are:

- o Range Splits
- o Azimuth Splits
- o Sidelobe Ambiguities
- o Reflections
- o Mainbeam Reflections

2.3.11.2.1 Range Splits (Sections 8.4 and 8.5)

Range splits occur in adjacent range cells and have a small azimuth separation. They were the most frequent type of ambiguity observed, occurring for about one to three percent of the beacon reports and occasionally as high as four percent (see Section 8.4.3.2 and Tables 8.15 and 8.17). Most range splits occur in pairs (Section 8.4.3.2). Normally, at least ninety-five percent of the reports in a range split are separated by less than 3° in azimuth and are exactly 1/8 nmi apart in range (Section 8.4.3.7).

The suspected cause of range splits is the jittering of successive replies received from a single target back and forth between adjacent range cells in sufficient quantity to declare a beacon target report in both cells. It was expected that an analysis of Auxiliary Interpreter Mode 2 reply data would allow direct verification of the range jitter theory via observing the ranges of successive replies that resulted in a range split. Unfortunately, the range jitter could not be observed in the reply data (see Section 8.5.4). The fact that the jitter cannot be observed is attributed to the difference between the way that the Auxiliary Interpreter extracts the range of the beacon replies and the way that the CD assigns the replies to range cells. It is recommended that the differences be resolved. Other evidence supporting the range jitter theory was present. In Section 4.2, a theoretical analysis of range jitter is discussed. The analysis shows that not only does the CD introduce range jitter into the system, but other components (interrogator, transponder) contribute significantly to range jitter as well.

Several characteristics of range splits that were observed experimentally can also be explained by, and therefore support, the range jitter theory. As was stated, the suspected cause of range splits is the jittering of replies back and forth between adjacent range cells. Of course, only Mode 3/A replies are used for detection, but the Mode C replies, which will also jitter in range, are associated with a particular range cell for altitude determination. A minimum number of Mode 3/A replies are required for detection of a target, and a minimum number of Mode C replies are required to validate the altitude. In most cases, the mode interlace pattern was 3/A, 3/A, C. It was observed that the majority of range splits consisted of pairs with the same beacon code, but one target with Mode C validated and one without Mode C validated (Section 8.4.3.2). As the interlace was providing more Mode 3/A interrogation than Mode C interrogations, there would be enough Mode 3/A replies going into two adjacent range cells (assuming the range jitter theory) to declare a target present in both. On the other hand, since fewer Mode C replies are received, there may be an insufficient quantity to validate Mode C data in two adjacent cells. In one case, the interlace pattern was 3/A,C so that an equal number of Mode 3/A and Mode C replies were received. This was the only case for which the majority of range splits with Mode C data consisted of pairs with both reports having validated Mode C altitude. Thus the range jitter theory is consistent with this observation.

Next, it was noted that the range split rate was a function of the rate of Mode 3/A interrogation (Section 8.4.3.4). The greater the 3/A interrogation rate, the higher the range split rate. This too is consistent with the range jitter theory. Since the Mode 3/A replies are jittering back and forth between adjacent range cells, there may be an unequal amount of Mode 3/A replies in each cell. In fact, one of the two target reports comprising a range split may be generated with the minimum required Mode 3/A replies in the range cell. If this were the case, a lower 3/A interrogation rate would cause the report generated with the minimum number of replies to not be generated at all. Thus this observation is consistent with the range jitter theory.

Finally, the azimuth separation characteristics presented in Section 8.4.3.7 support the range jitter theory. The characteristics show that both reports forming a range split are generated simultaneously. This eliminates the possibility that most range splits are caused by a target with a radial velocity to the sensor merely flying across a range cell boundary, in which case the pair would be generated successively rather than simultaneously, and strengthens the range jitter hypothesis.

Section 4.2 presents a theoretical analysis of the range jitter in the system and shows that significant contributions to the range jitter are coming from non-CD sources. This range jitter was observed in the VQR analysis of Section 8.5.9. This observation lends credence to the analysis of Section 4.2, which says that such jitter exists.

Two recommendations concerning range splits are made. First, it is recommended that the CD detection and centroiding for beacon replies be simulated in software using the Auxiliary Interpreter reply data as an input. This effort may uncover specific CD processing problems. In addition, it is probably the most effective way to evaluate the AI Mode 2 reply data for a variety of other problems.

Second, the jitter sources listed in Section 4.2 should be measured to determine their actual characteristic, since the analysis was based solely on design specifications. The measurements would provide a more accurate, empirical assessment of the range jitter problem. A conclusion of Section 4.2, restated here, is that CD modifications to improve the range accuracy will not significantly reduce the range split rate because of significant contributions to range jitter from non-CD sources. (See conclusion of Section 2.3.3).

2.3.11.2.2 Azimuth Splits (Sections 8.4.3 and 8.5.8)

Azimuth splits occur in the same range cell, are always pairs, and are usually separated by less than 3° (see Sections 8.4.3 and 8.5.8). They are caused when an intermittent beacon fade causes a trailing edge followed by a leading edge to be declared for a target during a single scan of the antenna mainbeam past the target. Azimuth splits were quite rare - on the order of less than 0.1 percent and therefore not regarded as a significant problem.

2.3.11.2.3 Sidelobes (Section 8.4.3)

The reports in sidelobe ambiguities have narrow range separations but may be widely separated in azimuth. Sidelobe ambiguities occur when a target is interrogated and replies received in sufficient quantity to declare a report while the mainbeam of the antenna is not pointed at the target (i.e., through a sidelobe of the antenna). Sidelobe ambiguities occurred between 0.5 and 1.0 percent of the time (see Section 8.4.3).

Normally, sidelobe ambiguities occur in pairs, so that the 0.5 to 1 percent rate does not appear to be significant. However, on some occasions, sidelobe ambiguities can create far more than one extra target report per ambiguity (i.e., a single target may result in many reports. Such an event is called a single ambiguity using the definition of Section 8). An extreme case is called ring around, where one target causes reports to be generated for 360° of antenna scan.

Cases where a single target was producing several reports per scan (more than two or three) were observed (see Section 8.4.3.8). These were observed for targets that were within a few miles of the sensor. It was noticed that this type of sidelobe ambiguity, which in the observed cases was either ring around or nearly ring around, was related to the installation of the NADIF antenna modification at Elwood. While it can be stated with reasonable confidence that the NADIF modification was responsible for the problem at NAFEC, it can not be inferred that all NADIF installations will result in ring around problems of similar magnitude. It is, however, recommended that care be taken whenever the NADIF modification is employed to insure that ring arounds are kept to a minimum. In fact, it may be judicious only to employ this modification at sites where local conditions warrant its use.

2.3.11.2.4 Reflections (Section 8.4.3)

Reflections (Section 8.4.3) occur when a target is either interrogated or replies via a reflected path. Generally, reflections will have different ranges and azimuths than the true target report. The separation characteristics used were a range separation larger than 1/4 nmi and an azimuth separation larger than five degrees. With these criteria, many of the reports flagged as reflection ambiguities were actually two aircraft using the same code. Real reflections were observed to occur at insignificant levels at NAFEC. This may, however, be an important problem at other sites. Reflections are, of course, a highly site-dependent problem.

Some algorithms for eliminating reflections via software processing have been prepared but none are within the scope of reasonable changes to the CD. These algorithms process report data and require a knowledge of known reflecting surfaces. Such processing is best done by a minicomputer receiving CD output. Further study at the various levels (reply and video) of processing may reveal that some useful discriminants exist which could be used to reduce reflection. These discriminants may be of such a nature that they could be implemented in CD processing.

2.3.11.2.5 Mainbeam Reflections (Section 8.4.3)

Mainbeam reflections (Section 8.4.3) occur within the mainbeam but are not in adjacent range cells. Hence they are less than five degrees apart and have a greater separation than .250 nmi in range. They are called mainbeam reflections because when first observed, they appeared to be the result of reflected paths occurring within the mainbeam. However, the data collected tends to show that they are a result of range jitter of replies between range cells that are not adjacent. Theoretically, this is possible, though it should be rare. Mainbeam reflections were indeed rare, occurring at less than 0.3 percent of the time in all cases.

2.3.11.3 Radar-Beacon Misalignments (Section 8.4.4)

Radar-beacon misalignment (Section 8.4.4) refers to the failure of the CD to properly correlate radar returns with the corresponding beacon returns to produce a single beacon report which is radar reinforced. When this failure occurs, both a radar and a beacon report are outputted by the CD.

The effectiveness of the correlation is measured as radar reinforcement rate which is the percentage of beacon reports that are radar reinforced. Radar reinforcement was measured for the Los Angeles ARSR, which is a commissioned site, to be only about 42 percent for beacon reports which were part of beacon tracks.

There are several reasons why radar reinforcement is not 100%. First, the radar simply does not see all the beacon targets. As a result, some beacon targets have no corresponding radar report. Even for those beacon targets which have corresponding radar returns, radar reinforcement is prevented from occurring in some cases for two reasons. First, a non zero average offset usually exists between the radar and beacon range processing. This average offset, however small, will always cause some radar returns to fail to correlate with beacon returns in the CD. Second, there is a time varying offset between the radar and beacon processing in the CD which causes correlation failure for some targets even if the average offset is zero.

2.3.11.4 Missing Reports (Section 8.4.5)

For the Los Angeles ARSR data examined, approximately 13% of the beacon reports on established beacon tracks were missing. Additional data from NAFEC was visually studied to locate missing reports. The corresponding replies were examined and it was determined that insufficient number of replies caused the missing reports. This deficiency might be solved by lower T_L or adjusting the video quantizers, but a tradeoff will result in adverse effects on the false target rate and possibly increases in ambiguity rates. The effects should be investigated to see if an optimal setting for T_L exists.

2.3.11.5 Jagged Tracks (Section 8.4.5)

Jagged tracks are a result of individual beacon reports deviating from a smoothed predicted position based on prior and subsequent reports. Since en route aircraft normally fly a smooth flight path it is assumed that when individual reports deviate from a smoothed track position, they are being positioned incorrectly.

Collected data shows that the jagged tracks are caused by azimuthal deviation from predicted position. Range variations are minimal. Examination of replies from jagged tracks confirmed this. Typically, the transponder was replying inconsistently, which affected the centroiding of the report in the CD. There are other centroiding algorithms besides the one used by the CD. The possibility of using one of these should be investigated if track jaggedness is to be reduced.

2.3.11.6 Code Changes (Section 8.4.5)

About 4.7 percent of the beacon reports on beacon tracks in data collected at the Los Angeles ARSR was found to have incorrectly reported codes. Half were code 0000, which indicates that the CD recognized the corresponding replies as severely garbled and assigned a code of 0000 to the report. The remainder (2.3%) were non zero codes. Of these, the majority incorrectly interpreted the pulse train between the framing pulses by one pulse. Most of the remaining codes had between two and seven pulses in error. Investigation of beacon video may help to determine the exact causes for this and uncover ways to more efficiently degarble what are now considered garbled replies.

2.3.11.7 Target Report Characteristics (Section 8.4.2)

In addition to identifying anomalies, the nature of target report data was studied. The main conclusion of this investigation concerns the spatial distributions of the target reports (Section 8.4.2.1). The distributions of reports with respect to range, azimuth, and altitude were all considered. No single distribution was characteristic in all cases, but the shape of the distribution differed for each data collection.

2.3.11.8 VQR Analysis (Section 8.6)

Though there were no major conclusions extracted from the Video Quantizer Recorder data, the power of the analysis technique was demonstrated. Beacon replies were examined at the video level. Code, altitude, and garbling conditions were studied. In addition, the actual pulse shapes can be carefully studied. It is strongly recommended that this technique, which displays quantized beacon video as a function of range and azimuth, be utilized in the future to study beacon video characteristics. Jitter in the range of beacon replies was observed (Section 8.6.2.1).

2.3.11.9 Data Problems (Sections as noted)

Three data problems were discovered during this analysis. First, Auxiliary Interpreter beacon reply data cannot be recorded whenever the beacon interrogator is turned on. Consequently real time data cannot be collected. This situation severely restricts any analysis of beacon replies and should be rectified (Section 8.2.4.7).

Second, beacon video is studied via use of VQR tapes containing quantized beacon video. The video to be quantized is selected by specifying a small window (typically 8 nmi by 147 ACP's). The windows are specified so that they contain the region of video of interest. A proper procedure has yet to be established whereby a specified range-azimuth window can be obtained. An offset problem of some type exists in the procedure, which should be corrected (Section 8.6.2.6).

Finally, it was found that results of CD processing when FR-950 analog recordings of beacon video were used often differed significantly from results obtained when the corresponding video direct from the beacon receiver was used. Since FR-950 recordings play an important roll in many engineering and development projects within the FAA, the exact cause for these differences should be determined (Sections 8.4.2 and 8.4.3).

3.0 INVESTIGATION OF THE RADAR DATA REQUIREMENTS AND PROCESSING CAPABILITY OF THE AIR ROUTE TRAFFIC CONTROL CENTER (ARTCC)

3.1 INTRODUCTION

The Common Digitizer (CD) processes sensor data (primary radar and beacon) and transmits target, weather, and status data to the Air Route Traffic Control Center (ARTCC). The data processing system at ARTCC was investigated to determine the quantity and quality of data it requires for satisfactory performance. The results of this study set the output requirements of the CD.

Emphasis has been placed on the processing of target report data. Weather, sensor status, and airborne hazard messages have not been considered in detail.

Data used in this investigation was obtained via discussion with ARTCC system designers at NAFEC and via existing published information (see References 3 to 9). Additional supporting analyses were performed as required.

3.2 SENSOR DATA PROCESSING

3.2.1 Background

Sensor data is transmitted to the ARTCC via (up to) three 2400 bit/second modem lines. Data consist of beacon and primary centroid data, test, strobe, status, and map messages. Map messages may be fixed, normal, sensitive, low intensity weather, and high intensity weather. The fixed, normal, and sensitive map messages indicate the performance of the CD, but are not used by ARTCC. Received data may be rejected if parity errors are detected in particular portions of the message.

Received centroids are adjusted for sensor registration and collimation errors and then subjected to range, bearing filtering. The coverage regions of a sensor is divided into sectors indicating that centroids in a sector are either preferred, supplementary, or not desired. Thus the ARTCC control region is divided into sectors in which there is one or more preferred data source and one or more supplementary data source. Range, bearing filtering is the first attempt to exclude undesired data.

The output from range, bearing filtering may then be slant range corrected. If Mode C altitude is available, exact slant range correction is performed. Non-Mode C centroids within 16 nmi of the sensor are approximate slant range corrected according to a table of values based on target range. This approximate correction is intended to minimize the maximum height-induced error for aircraft below positive controlled airspace.

The data are transformed into X-Y coordinates and placed into radar search boxes (RSB) that are 16 nmi square. The X-Y coordinate system is established so that every RSB of the ARTCC has a positive X and positive Y coordinate (see Figure 3.1). Each RSB contains a list of preferred data sites, and a flag indicating if supplementary data is desired. Data falling in the area of an RSB which is not from a preferred or supplementary site, or is supplementary but the "supplementary flag" is not set, is discarded.

Data in the RSB are used to update tracks each tracking subcycle (every 6 seconds). A track update cycle consists of two subcycles. As can be seen in Figure 3.2, each RSB covers a quarter of the area of four track search boxes (TSB). The TSBs have the same dimensions as the RSBs and comprise a grid superimposed on the RSB coordinates with an offset of 8 nmi in both the X and Y directions. A primary search area (PSA) 10 nmi square and aligned with the X-Y axis, is centered on a centroid in an RSB and tracks in the four adjacent TSBs are searched to determine if the track is within the PSA box. When tracks are found within the PSA box, their position is time corrected to correspond with the time of the centroid.

The coordinates of the centroid are then compared with the coordinates of each track within the PSA. If the centroid has not been exact slant-range corrected (i.e., it is not a beacon centroid with validated Mode C altitude), the centroid will be exact slant-range corrected if the track with which the coordinate comparison is being made had a valid Mode C altitude reported on previous scans or has a pilot-reported altitude on file or has an assigned altitude on file.

The differences in coordinates between track and centroid are compared with the small search area (SSA) and then the large search area (LSA). The SSA is a circle one nmi in radius around the track position. The LSA is a six nmi radius circle for beacon centroids and an area shown in Figure 3.3 for radar centroids. If a centroid falls within the SSA or LSA a correlation preference value (CPV) is assigned to the match as shown in Table 3.1.

If the centroid correlates with several tracks, the match with the lowest CPV is retained. If the CPVs are equal, the match closest in distance to the centroid is saved. A match in the SSA has priority over an LSA match. No correlation is attempted between beacon centroids and radar tracks.

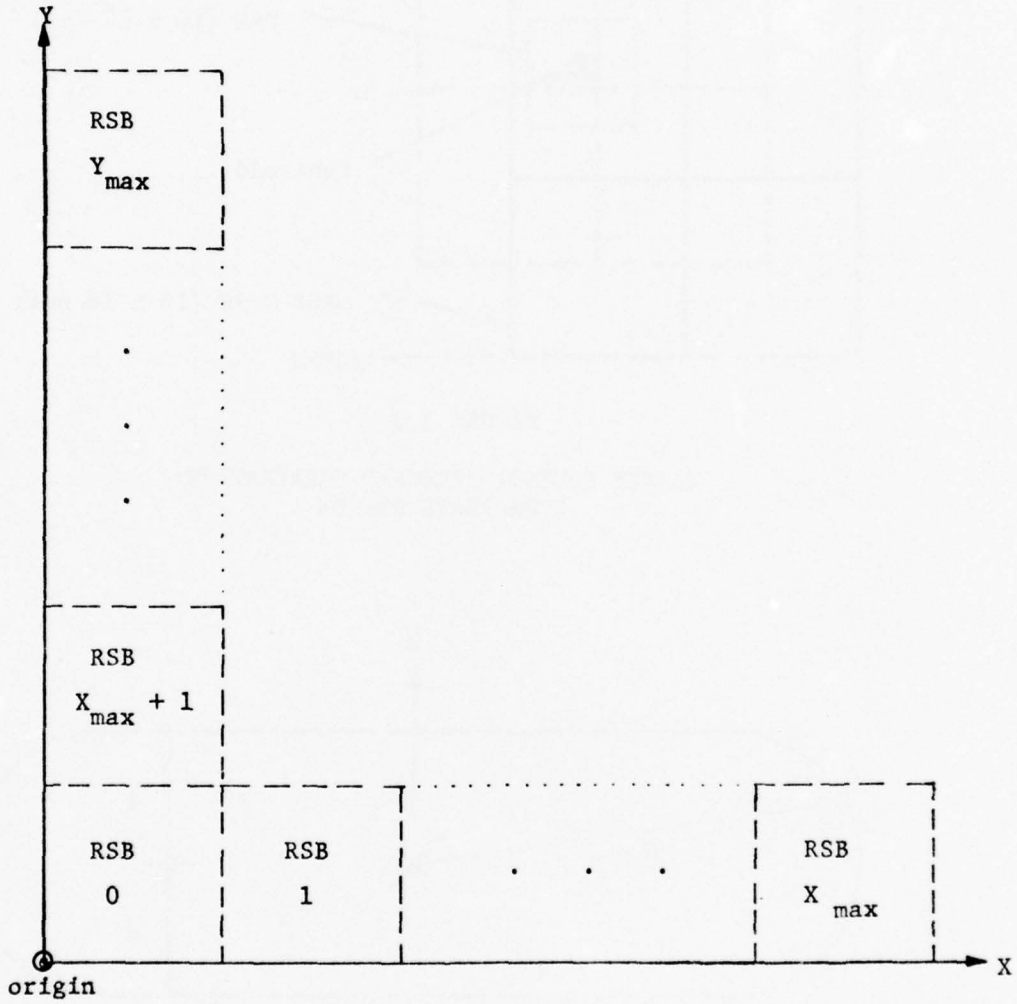

FIGURE 3.1

Radar Sort Boxes in X, Y Coordinate System. Y-Axis is aligned with true north. The System is a plane with point of tangency at the origin.

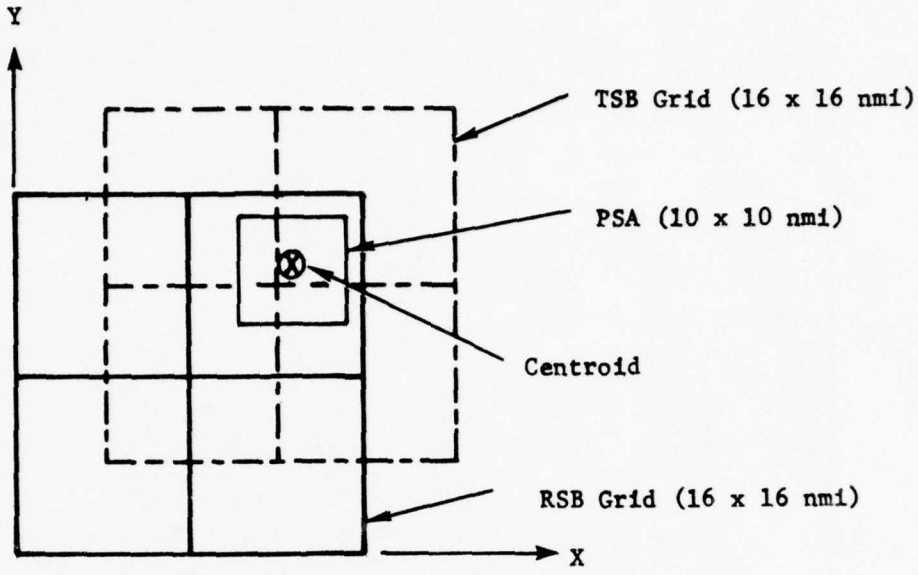

FIGURE 3.2

TARGET CENTROID/TRACKER CORRELATION
COORDINATE SYSTEM

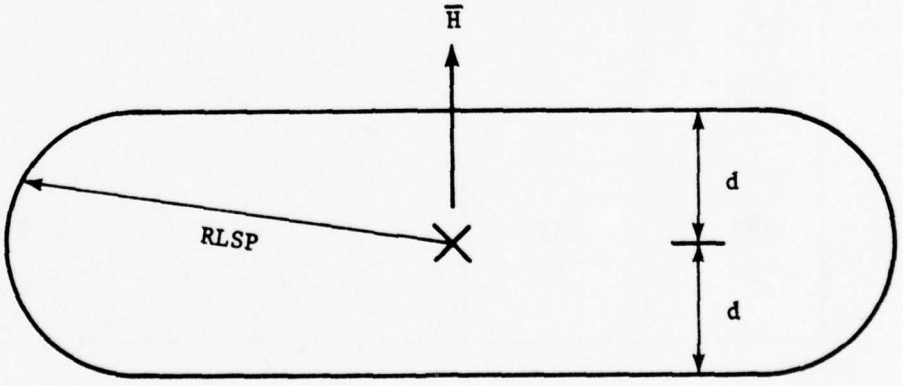

FIGURE 3.3

Large search area for radar data. $\bar{H}$ = track heading, X = time corrected track position, RLSP = 4 nmi, d = 2.5 nmi.

TABLE 3.1 CORRELATION PREFERENCE VALUES

Radar Datum Class	Track Class	Condition	Correlation Preference Value
Mode 3/A Beacon Datum Preferred	Beacon	Received Code = Assigned Code	1
Mode 3/A Beacon Datum Supplementary	Beacon	Received Code = Assigned Code	2
Mode 3/A Beacon Datum Preferred	Beacon	Received Code = Established Code	3
Mode 3/A Beacon Datum Supplementary	Beacon	Received Code = Established Code	4
Mode 3/A Beacon Datum Preferred	Beacon	Received Code ≠ Assigned or Established Code or is unvalidated	5
Mode 3/A Beacon Datum Supplementary	Beacon	Received Code ≠ Assigned or Established Code or is unvalidated	6
Primary Datum Preferred	Beacon or Primary	Long Run Length	7
Primary Datum Supplementary	Beacon or Primary	Long Run Length	8
Primary Datum Preferred	Beacon or Primary	Short Run Length	9
Primary Datum Supplementary	Beacon or Primary	Short Run Length	10

Assigned Code = Code assigned to the aircraft by the air traffic controller

Established Code = Code the aircraft has responded during recent history

When radar centroids are being correlated with a track, four counts are maintained of radar centroids falling within the LSA of the track during the last two tracking subcycles (12 seconds). The counts are:

a. Preferred radar centroid - long run length
b. Preferred radar centroid - short run length
c. Supplementary radar centroid - long run length
d. Supplementary radar centroid - short run length.

The track is considered in a clutter situation if any count > 2. No correlation will be attempted for this track with the offending data during the current tracking subcycle. If long run length data is offending the corresponding short run length data will also be disallowed.

Discrete beacon centroids (centroids whose last two numbers in their beacon code ≠ 00) are processed differently. The RSB table is bypassed by comparing the beacon code with codes of aircraft in track. If a code match is found, the SSA and LSA tests are employed. If the track is not within the LSA and the track has not received a correlation in the three preceeding tracking cycles the LSA is expanded to a square 32 nmi on a side centered on the track position.

When a code match is not found or the centroid is not within the search areas, a discrete beacon centroid is the only report type that can automatically initiate a track. Automatic initiation will occur if the beacon code matches that of a filed flight plan and the return is within a 50 nmi square centered around the expected entry point of the flight. Discrete centroids which do not correlate with a discrete track or flight plan are reprocessed by the standard correlation technique mentioned previously.

Let us now investigate the types of tracks in the ARTCC tracking system. A track is either FLAT (flight plan aided track) or FREE (no use of flight plans). The FLAT tracking mode uses flight plan speed, heading, and planned maneuvers to aid tracking. The FLAT tracking mode matches track position and heading with a segment of its filed flight plan. All tracks, except FLAT tracks with discrete beacon code, must be manually initiated.

At the end of the subcycle, track prediction is performed for the next subcycle. Prediction of track position is made for the mid-time of the next subcycle (see Figure 3.4). Small window data is used each subcycle to update the track. Large window data is used each cycle (see Figure 3.4). All preferred data and correlated supplementary data is sent to the air traffic controller displays.

The smoothing and prediction algorithms require the following information concerning the track-centroid correlation: ΔX, ΔY between track and centroid positions, LSA or SSA correlation, CPV, and subcycle of correlation. If the track is FREE, FLAT in a turn (as indicated by the flight plan), or FLAT and correlated with a discrete centroid with CPV ≤ 2, FLAT and flight plan calculated ground speed ≤ 0, then smoothed velocity is determined after a SSA correlation by using the centroid data. Otherwise, FLAT tracks use flight plan velocity as the smoothed velocity. The small search area (SSA) smoothing equations are:

$$X_s = X_p + a\ \Delta X$$

$$\dot{X}_s = \dot{X}_p + \frac{\alpha\ \Delta X}{T}$$

where X_s = track smoothed X position, X_p = track predicted X position as calculated on the previous update subcycle, $\dot{X}_s$ = track smoothed X velocity, $\dot{X}_p$ = track predicted X velocity calculated on the previous update subcycle, T = time since last correlation, a and α are tracking parameters shown in Table 3.2.

As was mentioned previously, large search area (LSA) data is used to update a track only in the second subcycle. If a SSA correlation was received during the previous cycle and the LSA correlation was not a discrete beacon centroid with CPV = 1 through 4, the smoothing equations are:

$$X_s = X_p + c\ \Delta \dot{X}$$

$$\dot{X}_s = \dot{X}_p + \frac{\gamma\ \Delta X}{T}$$

Note that the equations are the same form as the SSA equations. Checking the tracking parameter values c and γ in Table 3.2, it is seen that the equations are identical.

For LSA correlations not covered by the above conditions, the smoothing equations are:

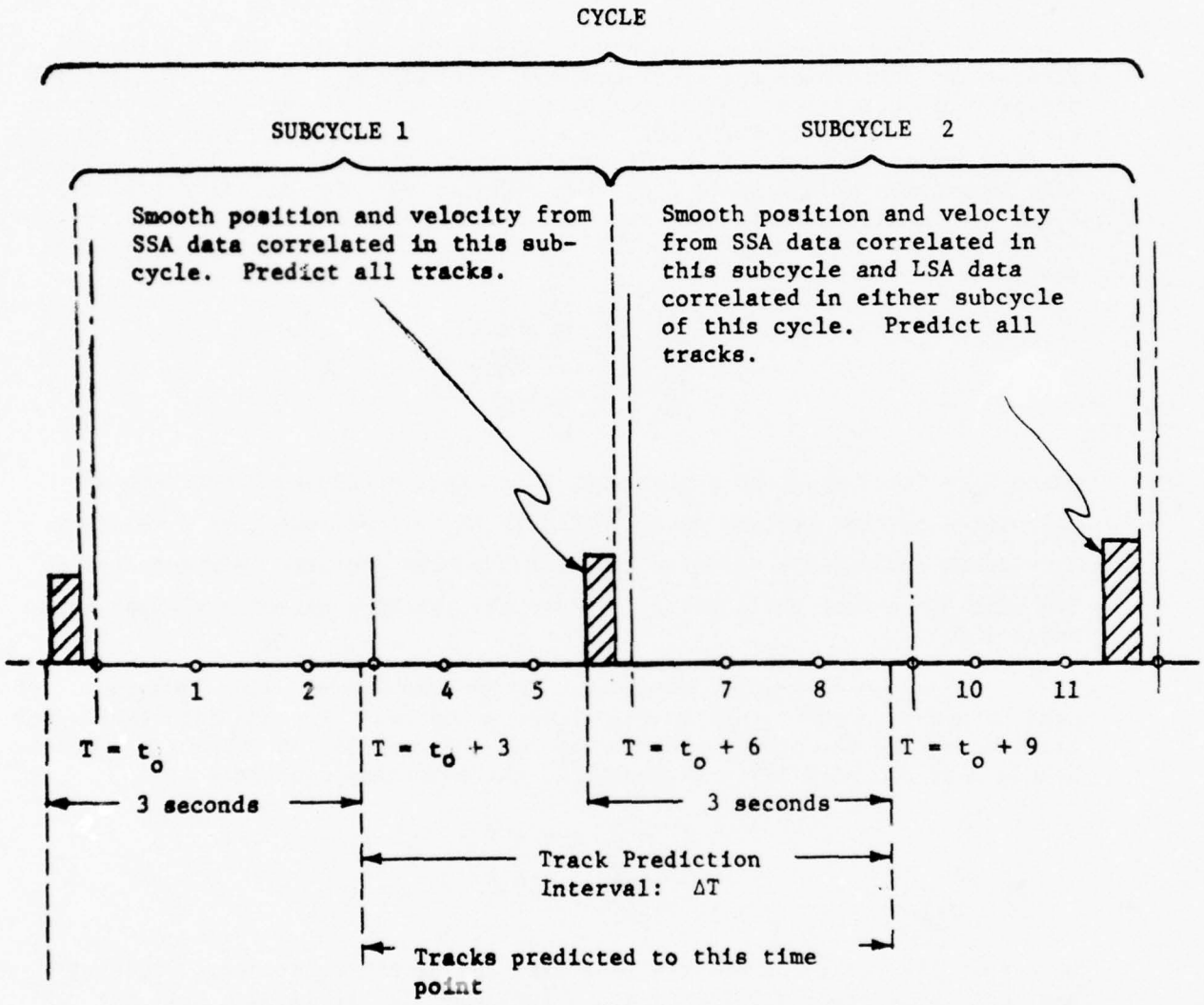

FIGURE 3.4

TRACK POSITION AND VELOCITY SMOOTHING AND POSITION PREDICTION

Centroid Type	CPV	a	α	b_1	b_2	β_1	β_2	c	γ
Discrete Beacon	1-2	.313	.047	1.0	1.0	.156	.156	NA	NA
Non-Discrete Beacon	1-2	.203	.047	.406	.406	.109	.109	.203	.047
Beacon	3-4	.203	.047	.406	.406	.109	.109	.203*	.047*
Beacon	5-6	.313	.016	.203	.25	.016	.031	.313	.016
Radar	7-10	.313	.047	.50	.50	.156	.156	.313	.047

TABLE 3.2

Tracking Parameters as a Function of Correlated Centroid Type and Correlation Preference Value (CPV).

*Not applicable to discrete beacon

$$X_s = X_p + \frac{b_1 \dot{X}_p}{V^2} \left(\Delta X \dot{X}_p + \Delta Y \dot{Y}_p \right) + \frac{b_2 \dot{Y}_p}{V^2} \left(\Delta X \dot{Y}_p - \Delta Y \dot{X}_p \right)$$

$$\dot{X}_s = \dot{X}_p + \frac{\beta_1 \dot{X}_p}{TV^2} \left(\Delta X \dot{X}_p + \Delta Y \dot{Y}_p \right) + \frac{\beta_2 \dot{Y}_p}{TV^2} \left(\Delta X \dot{Y}_p - \Delta Y \dot{X}_p \right)$$

where $V^2 = \dot{X}_p^2 + \dot{Y}_p^2$. This form of smoothing is usually referred to as "track-oriented smoothing". For example, if $b_1 > b_2$ then the tracking system will be more responsive to variation in data along the heading of the track. If $b_1 < b_2$ then the system is more responsive to variation in data orthogonal to the heading of the track. Note that if $b_1 = b_2$ and $\beta_1 = \beta_2$ then the equations reduce to:

$$X_s = X_p + b_1 \Delta X$$

$$\dot{X}_s = X_p + \frac{\beta_1 \Delta X}{T}$$

Because LSA smoothing is only performed after the second subcycle, track position and velocity is appropriately adjusted if LSA data from the first subcycle is used.

After smoothing, all tracks are predicted for the following subcycle using the equations:

$$\dot{X}_p = \dot{X}_s$$

$$X_p = X_s + \dot{X}_p t$$

where t = subcycle period (6 seconds) except for LSA smoothing adjusted for the first subcycle (12 seconds).

Please remember that this description of the tracking system is intended to give the reader a broad overview of the design concept. Many fine details have been omitted for brevity. For further detail, please see the references used for this report.

3.2.2 Capacity and Requirements

ARTCC sensor data processing capacity was determined from information contained in Reference 3.

The ARTCC computer system can be either a 9020A or a 9020D. The normal on-line components of the 9020A system include two input/output control elements (IOCE and three 9020A computing elements (CE). The 9020D has two IOCE's and two 9020D CE's. The 9020D system has 1.9 times the compute capability of the 9020A system because the 9020D C# is faster than the 9020A CE.

Data from the common digitizer is input to an IOCE. Each IOCE can handle eight common digitizers. The ARTCC system can handle a maximum of fifteen digitizer inputs. However, the Salt Lake ARTCC is expected to have the largest number of inputs - eleven. The worst-case situation would be eight common digitizers feeding one IOCE. If each digitizer were reporting at its maximum rate of 7200 bits/second, only 1.1% of the compute capacity of the IOCE would be used in maintaining this input load.

Each common digitizer sends 42 map messages, a status message and a test message per scan. Strobe and error messages may also be transmitted. All messages sent to the ARTCC are 52 bits in length except for beacon centroids which are 91 bits. Assuming an average of 5 messages/second for maps, etc., there are 6940 bits/second of centroid data available for transmission. This corresponds to 133 radar centroids/second, 76 beacon centroids/second, or a mixture of both.

In addition to input of digitizer data, the IOCE also performs the initial processing of that data. This includes parity checks, registration and collimation correction, range-bearing filtering, slant range correction, coordinate conversion, and filtering the appropriate data into the radar sort boxes. The amount of IOCE compute capability required for this task depends on the type of data received. For example, if each aircraft were seen by three radars but the ARTCC required only one preferred site and one supplementary site, then 33% of the data would be eliminated after range-bearing filtering. The projected maximum number of returns per second in 1985 is expected at the Atlanta ARTCC 9020D system. With an average of 3.8 returns per track, initial processing of the projected 858 centroids per second would require 68% of the compute capability of one IOCE. Since there are two IOCEs, this averages to 34% each. The maximum for a 9020A site will be at Jacksonville with 702 peak centroids per second, 3.7 returns per track, requiring 57% of the compute capability of one IOCE.

Processed centroids from the IOCE are placed in a report table for track correlation. The size of this table depends on the data load of each ARTCC.

The data load used for performance testing, assuming an ARTCC with inputs from 12 Radar/Beacon sites, is defined by the following data:

	9020D	9020A
ARTCC controlled tracks (average)	444	222
Noise centroids from each radar site		
Maximum per second	18	9
Average per second	8	4
Minimum per second	5	2
ARTCC aircraft centroids		
Average beacon per second	250	123
Average radar per second	214	112
ARTCC centroids after range-bearing filtering		
Average beacon per second	197	100
Average radar per second	176	85
ARTCC uncontrolled tracks (VFR)	812	406
Map messages per radar per scan	42	42

The RSB selective rejection passes 47.5% of the centroids which pass the range-bearing filter.

Using this data mix, it is estimated that the 9020A system could handle approximately up to 295 controlled tracks. The 9020D has been tested to handle 676 controlled FLAT tracks. The projected peak number of controlled tracks at a 9020D site in 1985 is 551 at Chicago. The projected peak at a 9020A site is 413 at Jacksonville.

By investigating each component in the ARTCC data handling system it can be seen that the only component which limits capacity is the CE compute capability of the 9020A system. The capacity of the three modem line data link (3 x 2400 = 7200 bits/second) between the CD and the ARTCC is adequate to handle the maximum expected CD data rate (6940 bits/second). If projections are correct, the Jacksonville, Memphis, Boston, Houston, and Denver ARTCCs will be CE compute limited by 1985 if the current software-hardware configuration is retained. Each of these centers will have in excess of 320 peak-minute controlled tracks.

The common digitizer can send ARTCC at least 76 centroids per second. This corresponds to 760 centroids per scan for usual FAA radar scan period of ten seconds. This data rate should be well in excess of 1985 requirements. Each IOCE at ARTCC can receive data from up to eight common digitizers. IOCE centroid processing capacity is nearly double that of the worst case 1985 requirements. Processed centroids from the IOCE are entered in a report table in the CEs. The size of the table is fitted to the requirements of each ARTCC. Data in this table is used to update controlled tracks. The controlled track capacity of the 9020D ARTCCs exceed their expected peak-minute 1985 requirements. Meanwhile, some 9020A ARTCCs will have stripped the capacity of the present system.

3.2.3 Common Digitizer - Required Accuracy and False Alarm Rate

By investigating parameters of the ARTCC tracking algorithms the constraints on accuracy and false alarm rates (P_{FA}) can be calculated. Centroid accuracy can be determined from the size of the small search area (SSA) and the gains used in SSA filtering (a, α). Centroids are slant-range corrected before correlation in order to reduce the height-induced range error to less than .125 nmi. In addition to the height-induced error, a radar centroid has an associated error ellipse (Figure 3.5). The size of the ellipse reflects the uncertainty in measurement accuracy. For instance, a one standard deviation (1σ) ellipse has one axis $2\ \sigma_B$ in length and one $2\ \sigma_R$ in length where σ_B = standard deviation of bearing measurement error and σ_R = standard deviation of range measurement error. There is then a 63% chance that the target is within the $1\ \sigma$ error ellipse.

Measurement error is reflected through the filtering and prediction equations and thus determines the size of the correlation window. The ratio of the variance in filtered track position to the variance in measurement error is given by:

$$FPR = \frac{2a^2 + \alpha(2-3a)}{a(4-\alpha-2a)}$$

where a and α are the filtering gains shown in Table 3.2. The ratio of the variance in predicted position to the variance in measurement error is given by:

$$PPR = \frac{2a^2 + a\alpha + 2\alpha}{a(4-\alpha-2a)}$$

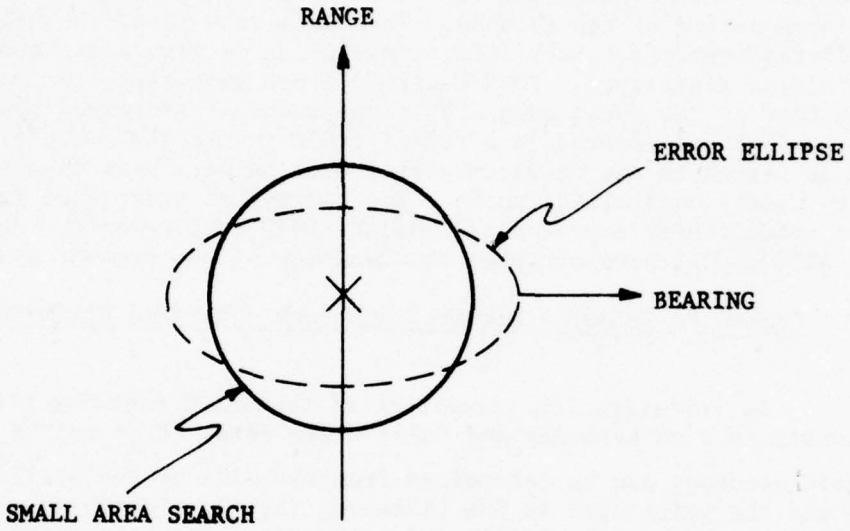

FIGURE 3.5

Error ellipse associated with a centroid reported at coordinates R_X, Θ_X.

These are steady-state ratios valid after start-up or maneuver transients have dissipated. Inserting a = .313 and α = .047 we obtain FPR = .257 and PPR = .871. This indicates that the standard deviation of filtered position accuracy = $\sigma_F = \sqrt{FPR}\ \sigma_m$ where σ_m is the measurement error. Hence $\sigma_F = .506\ \sigma_m$.

The standard deviation of predicted position accuracy = $\sigma_p = \sqrt{PPR}\ \sigma_m = .871\ \sigma_m$. The size of the correlation window depends on the prediction accuracy and the measurement accuracy. A one standard deviation window would have the dimension $\sigma_w = \pm \sqrt{\sigma_p^2+\sigma_m^2} = \pm\ \sigma_m \sqrt{1.871} = \pm\ 1.37$ The size of the small search area is selected to have a high probability of correlation success. A circle with a radius of 3 σ_w will have correlation success ≥ 95%.

The small search area is a circle of one nmi radius. To determine the required range measurement error (σ_R), subtract the maximum height-induced error (.125 nmi). Thus

$$3\sigma_w = 3 \times 1.37\sigma_R = \pm\ (1-.125)\ \text{nmi}$$

$$\sigma_R = \frac{\pm\ .875}{3 \times 1.37}$$

$$\sigma_R = \pm\ .222\ \text{nmi}$$

A complication arises when determining the bearing measurement error (σ_B) since the size of the error when measured in nautical miles is dependent on the target range. A .1° error subtends twice the arc at 150 nmi range as it does at 75 nmi. The tracking design philosophy for ARTCC was to "optimize" the window at 100 nmi. Thus

$$3\sigma_w = 3 \times 1.37\sigma_B = \pm\ 1\ \text{nmi}$$

$$\sigma_B = \pm\ .244\ \text{nmi @ 100 nmi range}$$

$$\sigma_B = \tan^{-1} \frac{.244\ \text{nmi}}{100\ \text{nmi}} = .14°$$

$$= 1.59\ \text{ACPs}$$

The allowable Probability of a False Alarm (P_{fa}) can be determined from system logic and search window sizes. Assuming a radar pulse every 0.1° and a possible false alarm every .25 nmi, the SSA has approximately 1420 sample areas at 5 nmi while the radar LSA has from 15400 to 17000 (depending on track heading) at 5 nmi. The number of samples decreases with increasing range due to the 0.1° pulse of the radar. Figure 3.6 depicts the P_{fa} which will guarantee the occurrence of a false centroid within the SSA or LSA regions on each scan. At 5 nmi, a $P_{fa} = 6 \times 10^{-5}$ will guarantee a centroid in the LSA and a $P_{fa} = 7 \times 10^{-4}$ will guarantee a centroid in the SSA. For comparison, the data load described in Section 3.2.2 for performance testing uses a $P_{fa} \simeq 3 \times 10^{-5}$.

For proper track/centroid association, a $P_{fa} \leq 6 \times 10^{-6}$ will reduce the probability of false correlation of short range tracks. For example, at 5 nmi a $P_{fa} = 6 \times 10^{-6}$ gives the probability of a false alarm within the LSA = .10. If the track blip/scan is .8, then the probability of false correlation on noise for one radar is

$$.1 \times (1-.8) = .02; \text{ e.g.,}$$

a false correlation every 50 scans. The effects of a second, supplemental radar can be neglected because of the large distance between radar sites. Thus if a track is close to one en route radar, it will usually be at long range to a second, supplemental radar. False alarm rates double those in the LSA curve of Figure 3.6 must be avoided because of the clutter detection logic of the correlation routine. For example, a $P_{fa} = 1.2 \times 10^{-4}$ at 5 nmi will allow two noise false alarms. These, when added to the target return, will exceed the clutter centroid count limit. This will cause all radar data of that type to be discarded during that tracking subcycle.

3.2.4 Radar Tracking Software Problems

As a result of the analysis of the ARTCC to determine the radar requirements and processing capability, the existence of several tracking software problems became evident. The primary problem areas are associated with the criteria to select track correlation windows and gains, track correlation window size, and track gain magnitudes. These problems and several others are discussed in the following paragraphs.

The small search area (SSA) window size (a circle of one nmi radius) used for target centroid/tracker correlation was chosen to be optimum at a range of 100 nmi. A fixed size window (SSA and LSA) has the disadvantage of being too small at long ranges and too large at short ranges. For instance, a 3σ window at 100 nmi becomes a 12σ window at 25 nmi. The probability of a non-maneuvering target being within a 5σ window exceeds 0.99. Thus the use of a 12σ window dramatically increases the chances of incorrect centroid correlation on a noise false alarm or a nearby track. Track quality is compromised and computer time wasted. Tracking window sizes must be varied according to the range of the centroid from the radar.

Properly sized SSAs will give a high degree of correlation confidence. The probability of correlation success should be near 0.95 in the en route environment if a 3σ window is used. Then if a SSA correlation is not made, a correlation in the large search area (LSA) would be a strong indicator of target maneuver. Tracking systems usually use an LSA = 1.5 x SSA. The en route LSA is much larger than this norm and will also increase the chances of false correlation.

Problems with the search area sizes have apparently been seen in system operations. This is evidenced by the choice of tracking gains for LSA correlations. Normally, tracking gains are increased for LSA correlations because a maneuver is assumed to be in progress. The en route tracker makes no change in its gains for the first LSA correlation but waits until the second consecutive LSA correlation to make a change. This reflects a lack of confidence in the first LSA correlation.

Track-oriented smoothing is used on the second and subsequent consecutive LSA correlation. However, because of the choice of gains, the equations revert to the original non-oriented algorithm in most instances.

Supplemental data are not used for track update until primary data are missed for an entire tracking cycle. Thus supplemental data may be available during the first scan of the primary data fade but is not used. Since fades are often associated with aircraft maneuvers, the maneuver-following capability of the en route system is hampered.

Measured positions are used for display to the air traffic controller. Since the variance in the filtered track position is nearly one-fourth that of the measured data, filtered positions should be displayed.

3.3 CONCLUSIONS AND RECOMMENDATIONS

The output data rate of the common digitizer (7200 bits/sec) is more than adequate for providing ARTCC with centroid data. If proper P_{fa} is maintained, most radars could operate at a lower rate without sacrificing performance. The only apparent limiting factor in the ARTCC data processing system is 9020A compute capacity. The capacity of the three modem line data link between the CD and the ARTCC is not a limiting factor. Projected 1985 controlled track loads exceed the 9020A capacity in the current hardware/software architecture. The 1985 track loads can be handled satisfactorily by the 9020D. The solution to the problem is to expand the 9020A compute capacity or else reconfigure the hardware and software for more efficient operation. On-site data processing in the common digitizer should be investigated as a possible answer.

The size of the large search area (LSA) used for radar tracking dictates that the P_{fa} should be maintained at an order of magnitude less than the LSA curve of Figure 3.6. P_{fa} should reach a peak of about 3×10^{-5} at 25 nmi and remain near that value for longer ranges. This implies that the strictest P_{fa} control must be maintained in the short range region of the radar search area. This is a difficult task since clutter and their resultant false alarms are dominant in the short range region.

The size of the small search area (SSA) used for tracking, combined with the gains used in the filtering equations dictate that common digitizer reports have measurement standard deviation in range of less than .22 nmi. In bearing, the standard deviation should be below 0.14° (1.6 ACPs). These measurement accuracy results also apply to discrete beacon centroids.

The size of the small (SSA) and large (LSA) search area windows is not varied as a function of target range. A fixed sized window has the disadvantage of being too small at long ranges and too large at short ranges. Tracking window sizes should be varied according to the range of the centroid from the radar.

Measured positions are used for display to the air traffic controller. Since the variance in the filtered track position is nearly one-fourth that of the measured data, filtered positions should be displayed.

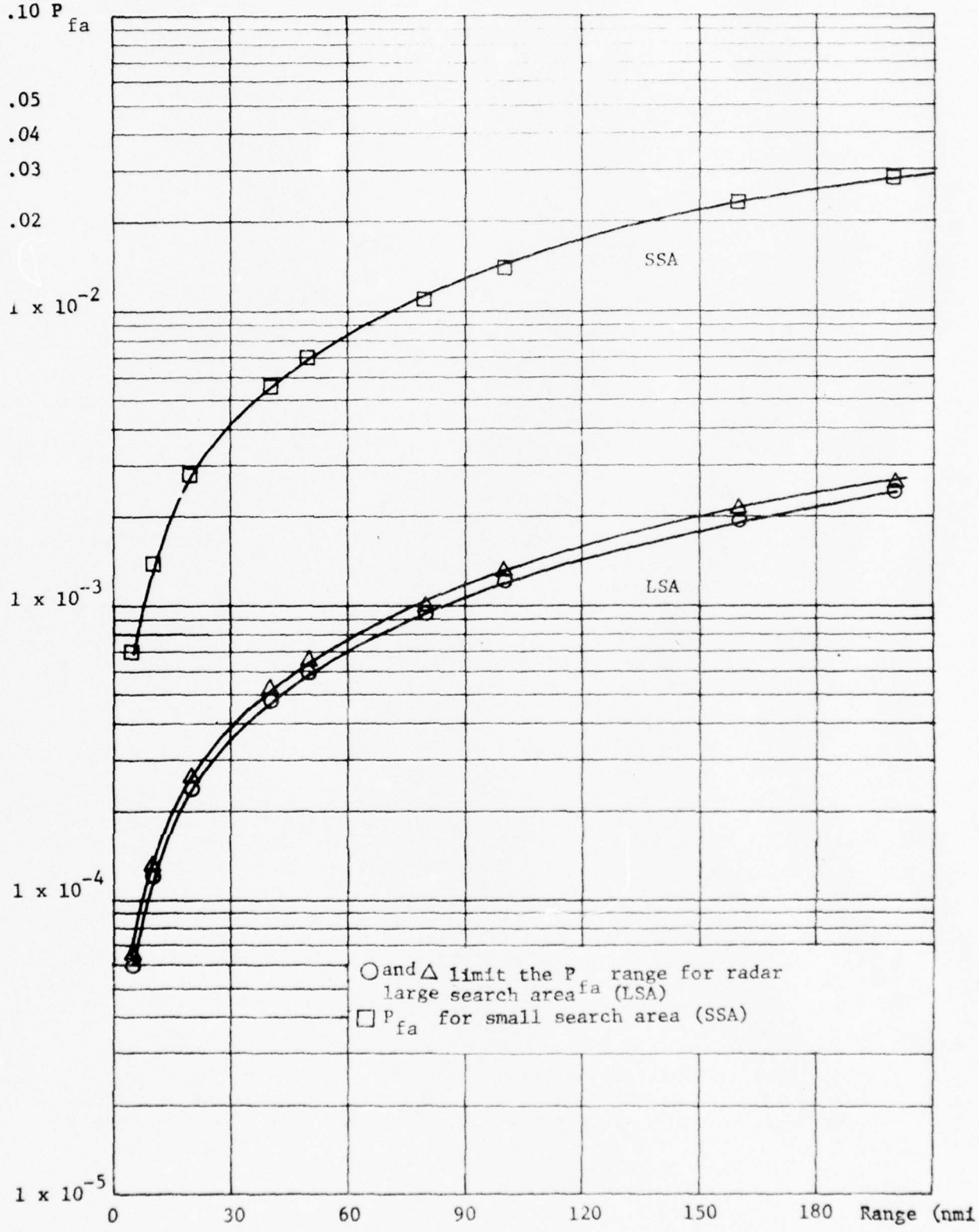

RADAR P_{fa} TO OBTAIN
ONE SSA OR LSA FALSE CENTROID PER SCAN
FIGURE 3.6

4.0 ANALYSIS OF THE SENSORS

4.1 PERFORMANCE CAPABILITY OF THE AIR ROUTE SURVEILLANCE RADARS (ARSR-1, 2)

4.1.1 Introduction

The purpose of this investigation is to determine analytically the basic performance capability of the ARSR-2 radar. In particular, the quality of the data, in terms of signal-to-noise ratio, is of great import to the performance of the Common Digitizer (CD) which is fed by the radar. Signal-to-noise ratios, as a function of range, have been computed for various clutter models, and from these target detection statistics can be generated. A few examples of these latter computations are also included.

4.1.2 Background

There are approximately 80 ARSR radars installed in the United States. These radars have been procured over the last 25 years and have been continually upgraded over that period of time. Currently they are represented typically by the ARSR-2 and the FPS-66 (USAF). The ARSR-3 is currently being procured. Major characteristics of these radars are shown in Table 4.1. Note that only the ARSR-3 has solid-state circuitry and employs digital signal processing.

Although the use of digital techniques does not inherently increase the radar capability, the analog systems drift out of adjustment over a period of time. Thus, digital techniques result in improvement in the average performance obtained in the field.

4.1.3 Receiver Details

Table 4.2 lists the significant characteristics of the ARSR-2 receiving system. This material was obtained from the ARSR-2 Manual, Revised May 1973.

4.1.3.1 MTI Processing

The effect of MTI processing is to provide visibility for moving targets in clutter, even when the signal is well below that of the clutter. The effectiveness of the MTI processing is measured as the ratio of the received clutter power to the minimum target signal that can be seen in the clutter and is called subclutter visibility. The advertised subclutter visibility for the ARSR-1, 2 MTI processors is 27 dB. Thus, for a signal to clutter ratio above -27 dB, a moving target is visible on the PPI display.

TABLE 4.1

ATC LONG RANGE SEARCH RADAR CHARACTERISTICS

Characteristic	Units	ARSR-1, 2	FPS-66	ARSR-3
Antenna Scan Rate	rpm	6	5	6
Instrumented Range	nmi	200	200	200
Pulse Width	μs	2	6	2
Azimuth Beamwidth	deg	1.2	1.3	1.2
Elevation Coverage	deg	0.2-45	0.2-45	0.2-46
Polarization (selectable)		hor/circ	hor/vert/circ	hor/vert/circ
Prf Average	Hz	360	360	360
Frequency	GHz	1.28-1.35	1.25-1.35	1.25-1.35
Diplex Operation		no	yes	yes
Subclutter Visibility	dB	27	25	30
MTI Improvement Factor	dB	33	30	39
Blind Speed (first)	knots	1150	80	1200
Antenna Gain	dB	34	35	34.5
Peak Power	kW	4000	2000	5000
Average Power	W	2900	2000	3500
Receiver Sensitivity	dBm	-116	-114	-114
Noise Figure	dB	4	8	4
Circuitry		tubes	tubes	solid state
Signal Processing		analog	analog	digital

TABLE 4.2

ATC LONG RANGE SEARCH RADAR RECEIVER CHARACTERISTICS

Frequency range	1280 to 1350 MHz
Type	Superheterodyne
RF parametric preamplifier	15 to 18 dB across band
RF preselector	10 MHz bandwidth, tunable with 60 dB image rejection
Mixer	Broad band crystal matched to waveguide
Normal detector	Crystal diode, nonlimiting AM detector
MTI detector	Dual crystal diode, limiting phase detector
Intermediate frequency	30 MHz $\pm$ .5 MHz
MTI bandwidth	3 MHz $\pm$ .5 MHz (3 dB)
Normal bandwidth	1 MHz $\pm$ .122 MHz
MTI feature	3-pulse canceller with 3-period staggered repetition rate and feedback for velocity response shaping. Blind speeds at 0 and 1150 knots.
Anti-clutter circuits	STC, CFAR
Overall system noise figure	4 dB maximum
Local oscillator	2C40 lighthouse triode with AFC, tuned above magnetron frequency, manually controllable
Subclutter visibility	27 dB
Cancellation ratio	33 to 36 dB
Minimum discernible signal	-109 dBm (normal) -112 dBm (integrated) -107 dBm (MTI)

4.1.4 Antenna Pattern

The early ASR and ARSR radars of the 1950's had antenna patterns with "cosecant squared" coverage. This means that the elevation pattern was a function of the cosecant squared of the elevation angle. This results in constant received power from a target flying at a constant altitude. This pattern proved to be inadequate because of the increase in clutter as the aircraft approaches the radar. The ARSR-2 antenna (first delivered in 1961) greatly increases the energy radiated at high elevation angles to increase the signal-to-clutter ratio. See Figure 4.1. This antenna resulted in some improvements in detecting close-in targets but still was not totally adequate.

In more recent years, another modification was made involving a two-beam approach. The two beams are generated by adding a second receive-only feedhorn beneath the high-power, normal transmit-and-receive feedhorn on the reflector antenna. The resulting coverage patterns are shown in Figure 4.2. The near-in, high-angle coverage is obtained by transmitting on the lower beam but receiving on the upper beam. At some preselected range, the receiver is switched from the upper beam to the lower beam, and normal coverage results beyond that range. The shaded area in Figure 4.2 shows where coverage is not obtained when using the high beam. The choice of range where the switching takes place is a compromise.

Raytheon undertook an R&D program from the FAA to study the feasibility of obtaining intermediate beam positions by combining the energy from the two beams using appropriate phase shifts. This work largely proved to be successful; however, the scheme will not be implemented on the ARSR-3, because the feasibility of appropriate phase control between the two waveguide runs at the time of the ARSR-3 procurement had not been established.

The ARSR antenna has a very large vertical aperture (23 feet). This permits careful control of the elevation pattern. It makes possible a sharp cutoff on the lower edge of the beam. This results in very little energy radiated below the horizon, which greatly enhances the ability to provide accurate azimuth estimation on targets near the horizon.

4.1.5 Target and Clutter Models

Prediction of radar performance must be done on a statistical basis because the radar energy returned from a target depends upon a large number of variables which can be specified only on a statistical basis. Legitimate signals from targets compete with unwanted signals returned from the ground and other non-aircraft targets. The ability to detect a target in the presence of these spurious or clutter signals is the major performance parameter of a radar in coping with low altitude targets.

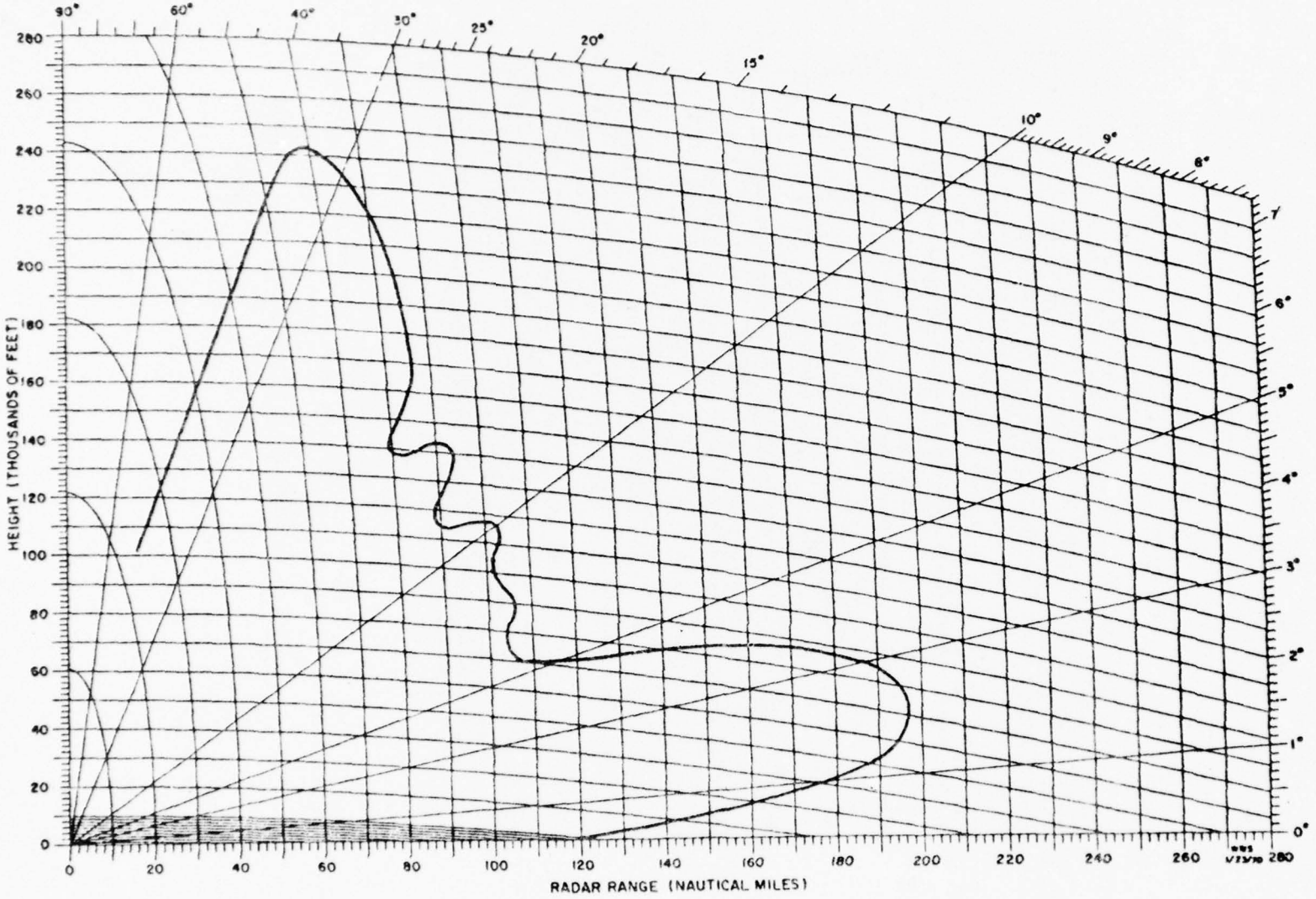

FIGURE 4.1

ARSR-2 RADAR SYSTEM COVERAGE

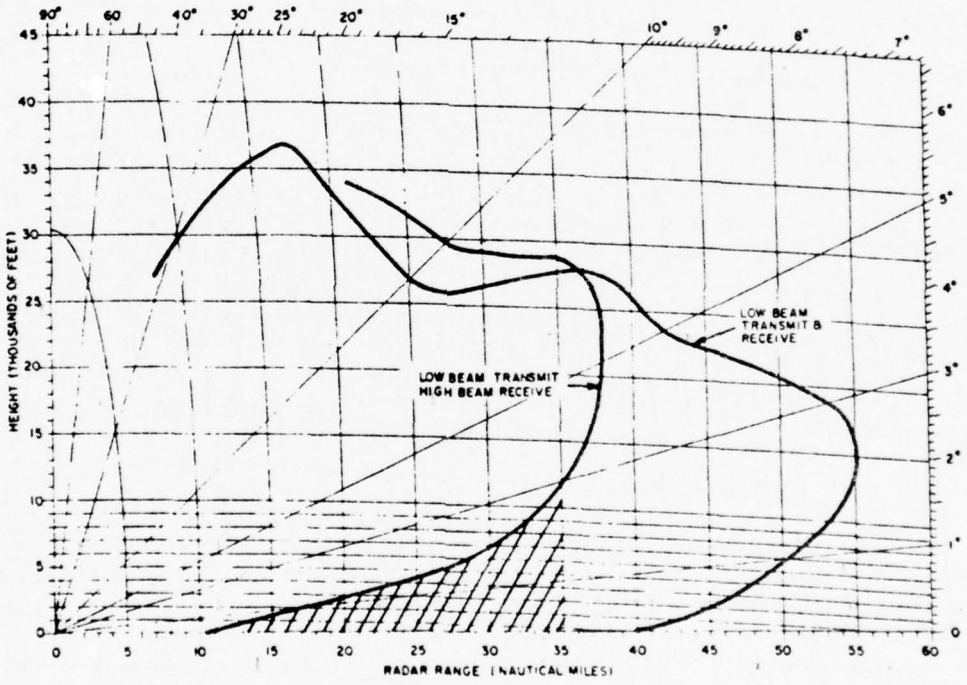

FIGURE 4.2

EXAMPLE OF COVERAGE OBTAINED WITH TWO-BEAM ANTENNA

To predict radar performance in a meaningful way, one must construct realistic models of both targets and clutter. The problem is further complicated by the fact that the ARSR radars are situated in widely dispersed geographical areas in which land clutter characteristics vary over a wide range. Thus the performance of a radar predicted in this study will be based on a model assuming certain "typical" parameters. The performance of a specific ARSR radar may be better or worse than that predicted for the model assumed here. If data on clutter surrounding a particular site is available, then performance predictions can be made more exact.

4.1.5.1 Target Model

The FAA radars must reliably handle the smallest en route aircraft. A median radar cross section of one square meter is representative of the smallest target for vertical or horizontal polarization (see Reference 10). If circular polarization is used, a 2 dB loss (to 0.63 square meter) in median radar cross section is conservative for the nose-on ±50° case.

The Rayleigh fluctuation distribution is appropriate for translating median cross section into the statistical description needed for radar performance prediction. Detection probabilities can be calculated for this case using the Swerling Case 1 (Reference 18) model for fixed frequency radar operation.

4.1.5.2 Environmental Model

Land clutter, weather clutter, undesired targets, anomalous propagation, and radio frequency interference are environmental conditions which are responsible for radar performance degradation. The environmental characteristics for which the ARSR-1, 2 must maintain its required coverage on a one square meter target are summarized below along with the rationale for selecting the levels of environmental conditions.

4.1.5.2.1 Land Clutter

Land clutter is radar return from terrain features and fixed man-made objects in the field of view of the radar. Radar return from land clutter is expressed as effective radar cross section per unit area illuminated by the radar, σ_o, commonly referred to as terrain backscatter coefficient. The units of σ_o are m^2/m^2 (square meters of radar cross section per square meter illuminated by the radar) so σ_o is effectively unitless. Land clutter is proportional to the area of the ground illuminated and the backscatter coefficient of the terrain.

A terrain backscatter coefficient of -20 dB (0.01 square meter cross section per square meter illuminated by the radar) was chosen to define the average land clutter with which the ARSR-1, 2 must cope. In data published by Nathanson (Reference 11), this value was exceeded only 5 percent of the time for measurements made in the Rocky Mountains and only 16 percent of the time for cities. These very large returns are usually due to isolated man-made features such as radio towers and large buildings which can mask small aircraft which are in the same resolution cell. The effect of losing position reports on small aircraft over strong clutter reflectors can be minimized by proper scan-to-scan processing of the radar track data.

In general, clutter signals decrease with decreasing grazing angle. Figure 4.3 illustrates a typical situation at a radar site. Up to the optimal horizon (for a smooth spherical earth), the backscattered signals from the ground will be more intense because the grazing angle is relatively large. As the horizon is approached, and grazing angles approach zero, the clutter signals begin to fall off more rapidly. Beyond the horizon (in the diffraction region), the clutter signals drop off even more rapidly. However, terrain features such as mountains which are in the radar beam beyond the smooth earth horizon will of course produce large clutter signals. Thus, land clutter signals for a particular site will be relative to the height of the radar antenna above the surface (which determines the horizon distance) and the terrain features. Attempts to reduce land clutter signals (other than through signal processing) involve reducing the antenna gain at low angles by biasing the center of the beam upward.

4.1.5.2.2 Rain Clutter

Radar return for rain is expressed as the effective radar backscattering cross section per unit volume illuminated by the radar and is denoted as ρ. This may be referred to as the rain backscatter coefficient and has the units m^2/m^3 (square meters of radar cross section per cubic meter of volume illuminated by the radar). Rain clutter is proportional to the volume of rain illuminated by the radar and the effective radar backscattering cross section per unit volume for rain.

The probability of occurrence of the rain must also be taken into account. For the continental United States, rainfall in excess of light drizzle (0.25 millimeters of accumulation per hour) occurs about 6 percent of the time at any given location. Since violent storms must be avoided by small aircraft, there is a practical upper limit on the rainfall rates in which the radar must be required to detect small aircraft. The value chosen for the ARSR-1, 2 is 16 millimeters per hour. In New Orleans, which is a high rainfall area, rainfall is below 16 mm/hour 99.5 percent of the time. This corresponds to about 44 hours per year for rains heavier than 16 mm/hr. The mean diameter of such a storm is about 8 nmi. The effects of rain attenuation at the frequency of operation of the ARSR-1, 2 is negligible. Table 4.3 summarizes the rain clutter model. The information was obtained from Reference 11.

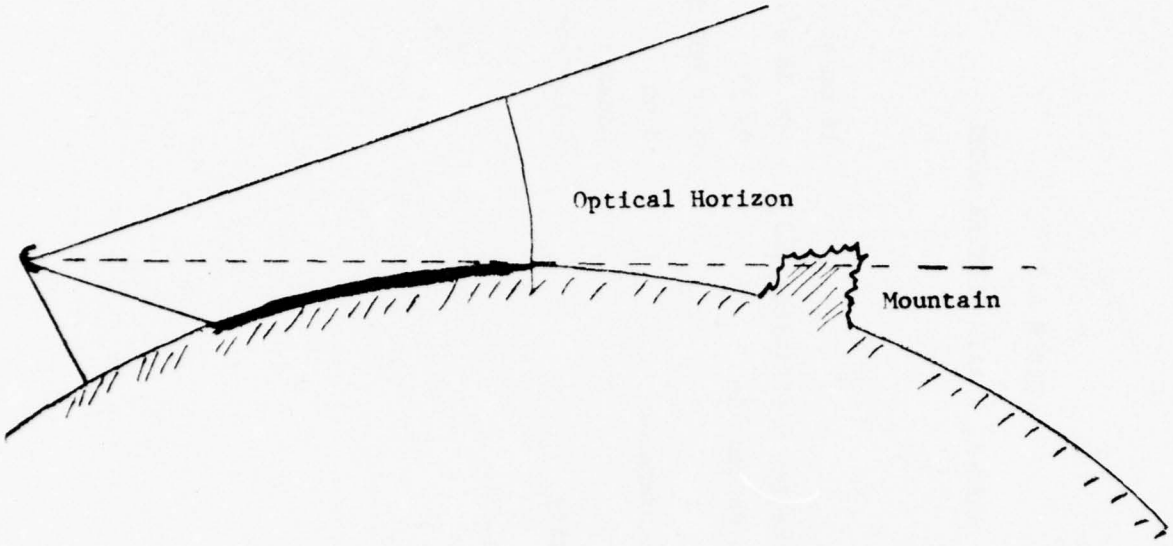

FIGURE 4.3

LAND CLUTTER GEOMETRY

TABLE 4.3

ARSR-1, 2 RAIN CLUTTER MODEL

Intensity	16 mm/hr
Rain Backscatter Coefficient (ρ)	-86 dB m^2/m^3
Occurrence Percentile	99.5%
Altitude	0-10,000 ft.
Mean Storm Diameter	8 nm
Spectrum	Gaussian
Mean Velocity	0-16m/sec

4.1.5.2.3 Anomalous Propagation and Undesired Moving Targets

Anomalous propagation is the term often applied to propagation which does not follow the "free-space" $1/R^4$ model. Variations in the refractive index of the atmosphere (usually due to an inversion layer) can produce ducting which can lead to "second-time'around" land clutter appearing at much shorter ranges on the displays. Multipath propagation involving reflection of signals from the ground or large objects such as mountains can change signal levels above or below what is predicted by the $1/R^4$ model. Not enough detailed data are available to work these effects into a model to produce useful results. However, it is important to be aware of them.

Undesired moving targets are produced by a number of sources. These include ground vehicular traffic and "angels". The latter term is used to describe returns from birds, insects, and atmospheric irregularities. A number of recent studies have detailed the effects of angel clutter (see References 15 and 16). It is most likely that this type of interference can best be handled at the digital processor level.

4.1.6 Results

4.1.6.1 Signal-to-Noise Ratio Versus Range

Figure 4.4 shows the signal-to-noise ratio as a function of range for two-target cross-section values and two-radar loss figures. Radar losses may vary from 6 to 12 dB depending upon many unpredictable variables for each radar. Such factors as component age, degree of maintenance, calibration and alignment will all influence the actual loss number. Therefore, it is more prudent to show a range for the loss factors. Cross section (nose-on) for a small private aircraft is on the order of one square meter, and for a commercial aircraft 10 square meters.

The curves are based on the equation

$$\frac{S}{N} = \frac{P_t G^2 \lambda^2 \sigma_{TARGET}}{(4\pi)^3 R^4 KTB \overline{NF} L} \qquad (4\text{-}1)$$

where

P_t is the transmitted pulse power

G is the antenna gain

λ is the wavelength of the rf energy

σ_{TARGET} is target cross section

R is the range

KTB is the receiver thermal noise with which the signal must compete

$\overline{NF}$ is the receiver noise figure

L are the radar losses (6-12 dB)

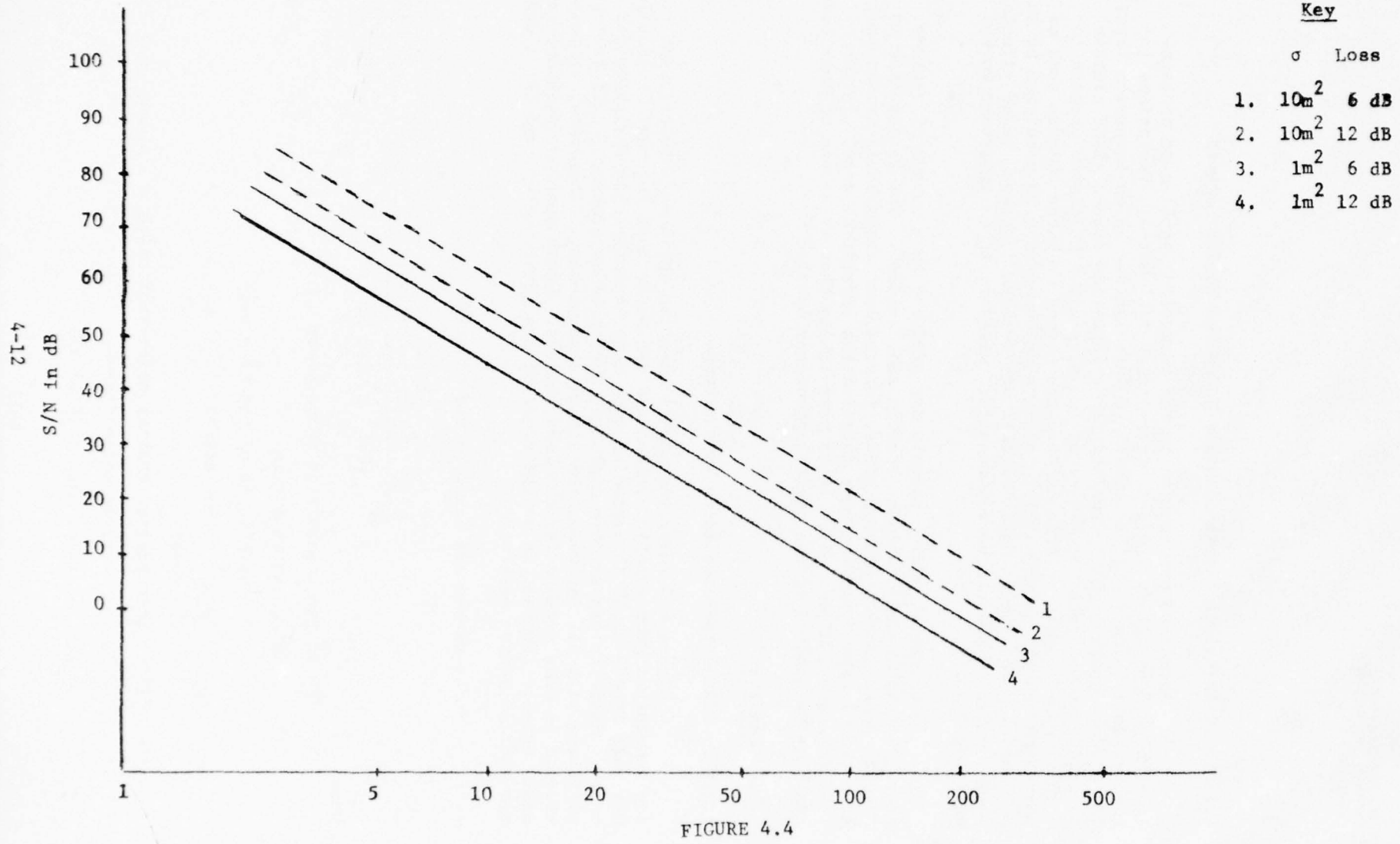

FIGURE 4.4

S/N VS RANGE FOR ARSR-1, 2 RADAR (FREE SPACE)

The S/N required for a given probability of detection and false alarm rate is given in Table 4.4.

TABLE 4.4

REQUIRED SIGNAL-TO-NOISE RATIO FOR DETECTION

Req'd S/N (dB)	No. of Pulses Integrated	Prob. of Detection	Prob. of False Alarm
15.8	1	.5	10^{-12}
12.8	1	.5	10^{-6}
24.0	1	.9	10^{-12}
21.0	1	.9	10^{-6}

The table shows the S/N for single pulse for various conditions when square law detection is used. Results for a linear law detector are about the same. A fixed threshold detector is assumed. By using Table 4.4 in conjunction with Figure 4.4 it is a very simple matter to estimate the free-space detection range under various conditions (excluding clutter).

4.1.6.2 Clutter-to-Noise Ratios for Land and Rain

4.1.6.2.1 Land Clutter

The clutter-to-noise ratio is computed from an equation identical to 4.1 except that the clutter cross section is substituted for the target cross section. The land clutter cross section is a function of the area illuminated by the antenna beam within the range resolution dictated by the pulsewidth and the terrain radar backscatter coefficient of the area. This is expressed in equation (4-2).

$$\sigma_{land} = \sigma_o \, R \, \theta_{az} \, \frac{c\tau}{2} \qquad (4\text{-}2)$$

where

σ_{land} = effective radar cross section of the land clutter (m^2)

σ_o = terrain radar backscatter coefficient (m^2/m^2)

θ_{az} = beamwidth in azimuth (radians)

c = velocity of light (m/second)

τ = pulse width (seconds)

R = range (m)

When (4-2) is substituted into (4-1), the dependence on range becomes $\frac{1}{R^3}$ as shown in (4-3).

$$\frac{C}{N} = \frac{P_t G^2 \lambda^2}{(4\pi)^3 R^3 L} \quad \frac{\sigma_o \theta_{az} c\tau}{2KTB\ NF} \tag{4-3}$$

Figure 4.5 shows the resulting plot of equation (4-3) for two values of σ_o and two values of radar losses as described in Section 4.1.5. A σ_o of -20 dB is a median number and -40 dB would represent smoother terrain such as in the Central Plains or desert regions.

The curves follow equation (4-3) up to the optical horizon and then drop off at a rate of approximately -15 dB per octave (see Barton, Reference 17). The optical horizon shown (18 nmi) corresponds to a high sited radar (200 ft). For radars whose horizon is different from that shown, simply determine the optical horizon and draw the slope at -15 dB per octave. If the clutter comes from high terrain which is above the smooth earth horizon, then the C/N for that case would be determined from the line falling off at 9 dB per octave (equation 4-3), shown dotted beyond the horizon line. For different σ_o, the curves may be translated up or down by the corresponding difference from that shown.

4.1.6.2.2 Rain Clutter

Clutter-to-noise for rain clutter is computed similarly to the land clutter C/N. In this case, the rain clutter cross section is a function of the volume that is bounded by the antenna beam cross section and a linear distance equal to the range resolution (dictated by the pulsewidth) of the radar. Cross section for rain is expressed by:

$$\sigma_{rain} = \rho R^2 \theta_{az} \phi_{el} \frac{c\tau}{2} \tag{4-4}$$

where

σ_{rain} = effective radar backscattering cross section for rain (m^2)

ρ = the effective radar cross section per unit volume for rain and is dependent on the severity of the rain storm (m^2/m^3)

ϕ_{el} = the elevation beamwidth (radians)

θ_{az} = beamwidth in azimuth (radians)

c = velocity of light (m/sec)

τ = pulse width (seconds)

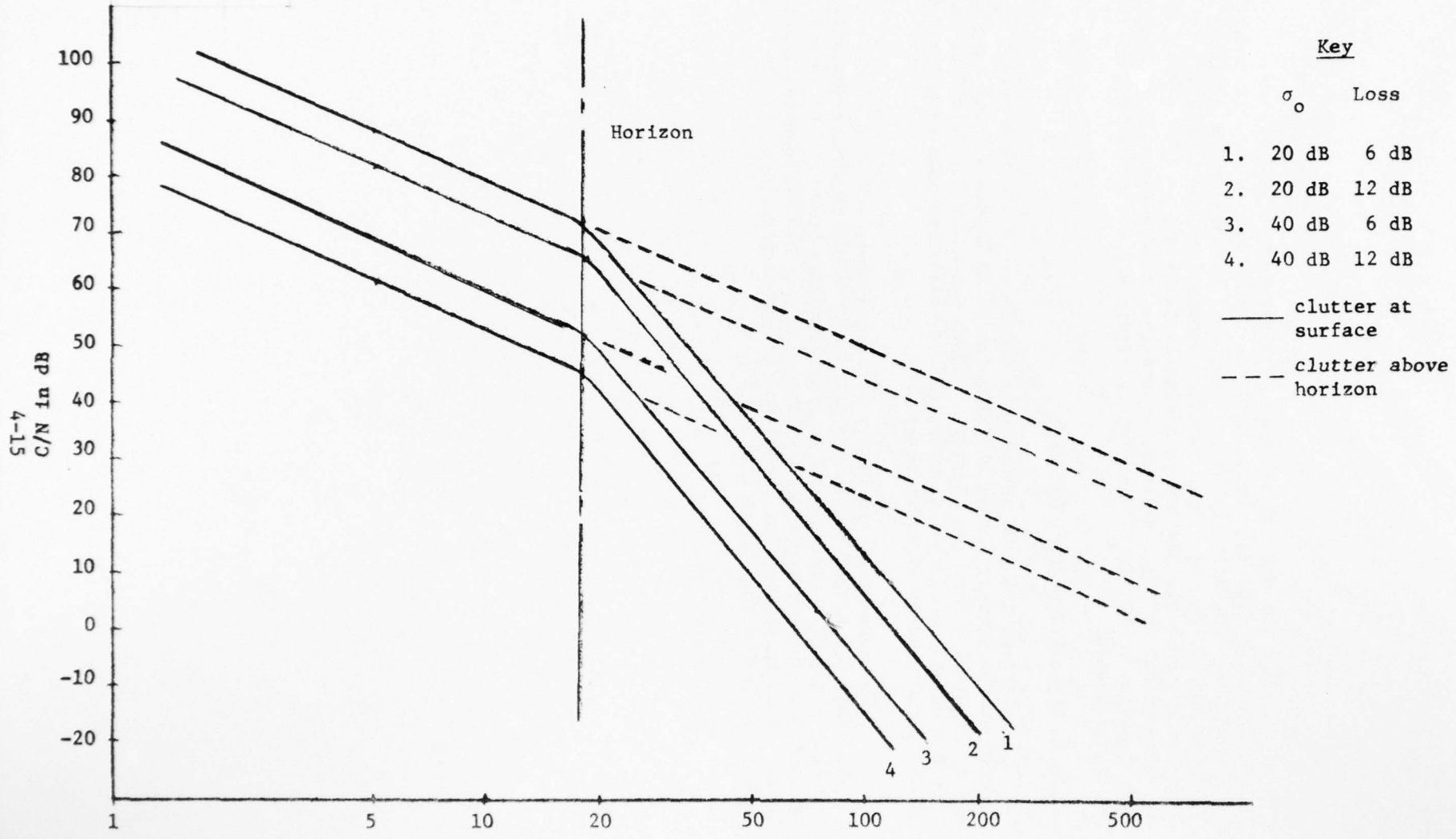

FIGURE 4.5

C/N VS RANGE FOR ARSR-1, 2 IN LAND CLUTTER

Since the maximum altitude of a rain storm seldom exceeds 10K ft, the rain will not always fill the beam. Such a case is shown in Figure 4.6. The storm is beyond the radar horizon at the surface, the only portion of the radar beam receiver energy from the rain particles. Thus, up to the radar horizon rain clutter falls off as $1/R^2$ (cross section is proportional to R^2). However, beyond the horizon the clutter falls off more rapidly. This is illustrated in Figure 4.7 for two values of rain rate and radar losses.

4.1.6.3 Signal-to-Clutter Ratios

Perhaps the most interesting curves are those that relate the clutter to the signal. These are illustrated in Figure 4.8 for land clutter and in Figure 4.9 for rain clutter. Since the radar losses affect both target signals and clutter signals equally, they disappear from the S/C which is independent of radar losses.

The subclutter visibility for the ARSR-1, 2 MTI is advertised as 27 dB. Thus for signal to clutter ratios above -27 dB the target will be visible on the PPI. For signal to clutter ratios below -27 dB it will not be visible. The heavy horizontal line on Figure 4.8 represents this cutoff level. This indicates that signal-to-clutter ratios above the line will result in visible targets on the PPI.

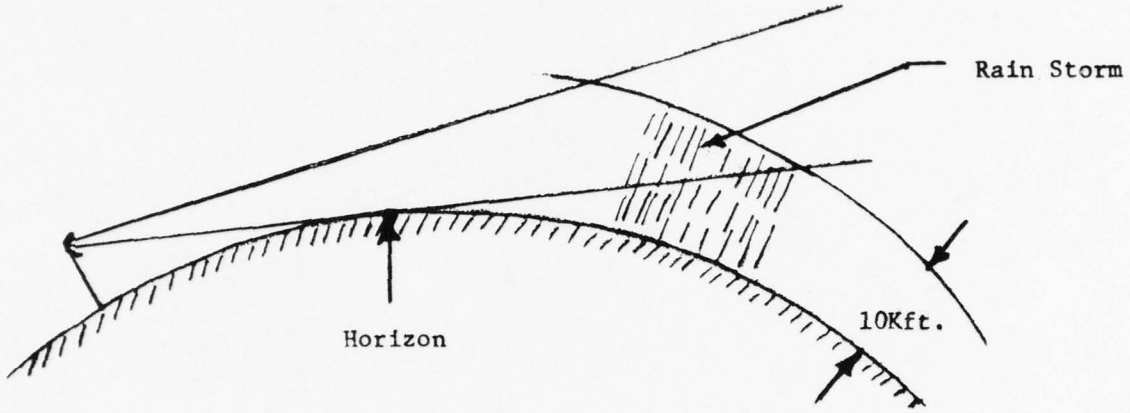

FIGURE 4.6

RAIN BEYOND RADAR HORIZON

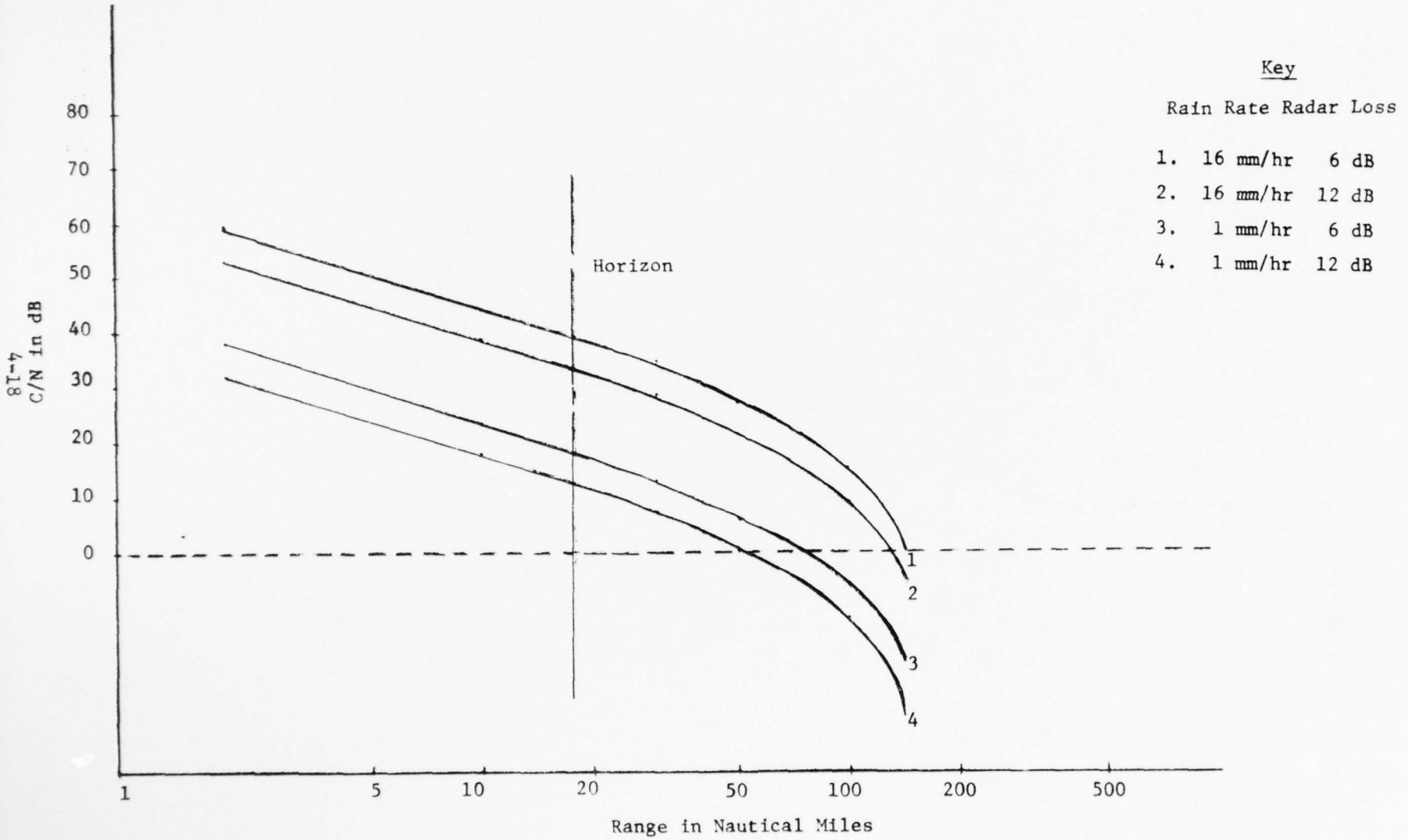

FIGURE 4.7 C/N VS RANGE FOR ARSR-1, 2 RADAR IN RAIN CLUTTER

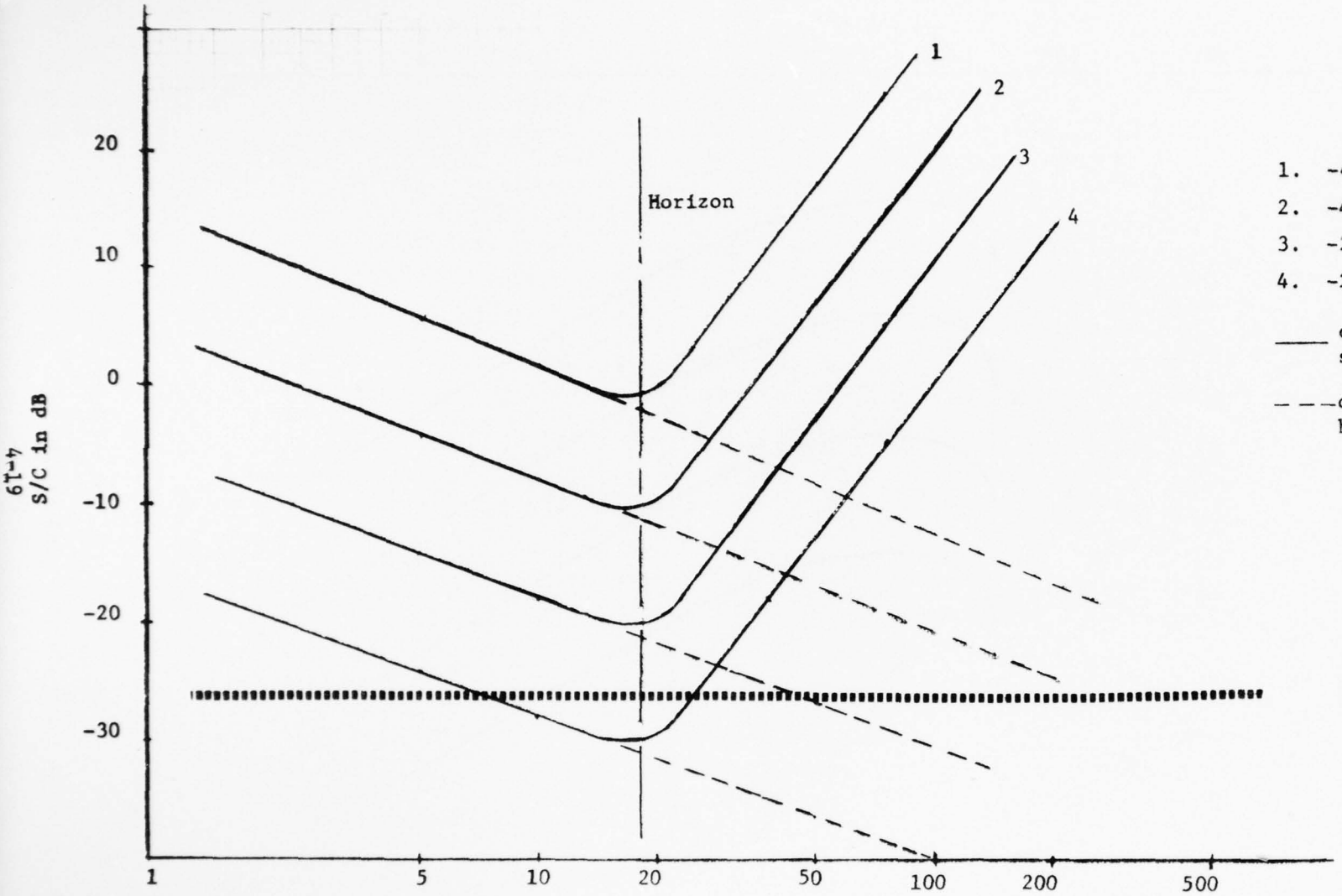

FIGURE 4.8

S/C VS RANGE FOR ARSR-1, 2 IN LAND CLUTTER

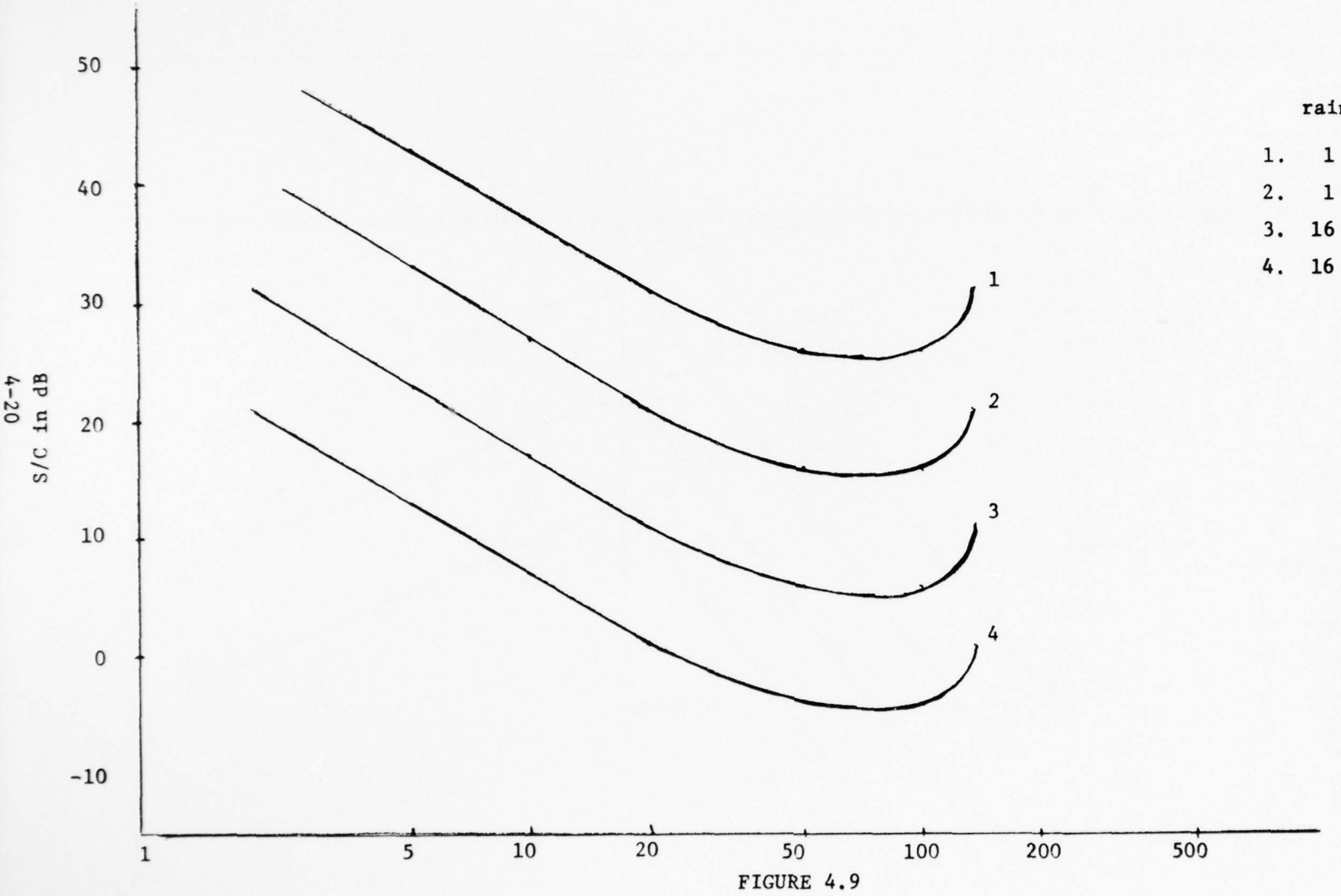

FIGURE 4.9

SIGNAL-TO-CLUTTER RATIO FOR ARSR-1, 2 IN RAIN

4.2 ANALYSIS OF BEACON SYSTEM RANGE JITTER IN ATCRBS

The primary thrust of the investigation of the beacon processing performance of the CD described in Section 8 was directed toward the CD. However, it was recognized that a significant problem in the area of beacon processing is that of range splits. Therefore, a theoretical investigation of the various sources of range jitter in ATCRBS, including the CD, was undertaken. This theoretical investigation emphasizes contributions of the Air Traffic Control Beacon Interrogator (ATCBI) and the transponder to the range jitter problem. Consequently the discussion of the investigation is included in Section 4 entitled Analysis of Sensors.

4.2.1 Introduction

This analysis was initiated in response to a proposed modification to the Common Digitizer (CD) being considered by the FAA which would disable the 18.112 MHz clock (55.2 nsec) in the Azimuth Range Timing Group (ARTG) and the 9.655 MHz clock (103.6 nsec) in the Beacon Reply Group (BRG) and replace them with a single clock operating at either 38.621 MHz (25.9 nsec) or 77.241 MHz (12.9 nsec) and appropriate down counters to provide the required CD timing. The proposed modification was evaluated by the Laboratory with respect to the improvement in range jitter and beacon target split rate that would theoretically be realized.

In this analysis, it is shown that there are significant jitters in the ATCRBS that are external to the CD. For this reason, it makes little sense to make expensive modifications to the CD in an attempt to detect the beacon hits to within a few nanoseconds because the received replies already have jitters much larger than this. This analysis was based mostly on the jitter values listed in design specifications for the involved equipment. It is suggested that it be verified by taking actual measurements.

Section 4.2.2 addresses the present system configuration and shows how the CD range system is synchronized for proper range determination. This configuration was extracted from the appropriate references. Important points were verified with NAFEC personnel. Section 4.2.3 presents the analysis approach used, including a comparison of results obtained when the choice of the arbitrarily chosen reference pulse is changed from the radar pretrigger to the beacon interrogation P_3 pulse. Section 4.2.4 applies the results of Section 4.2.3 to form a comparison of total system jitter for the present system configuration, the synchronized clock modification and the single clock modification for both of the proposed single clock rates. Section 4.2.5 is the conclusion section.

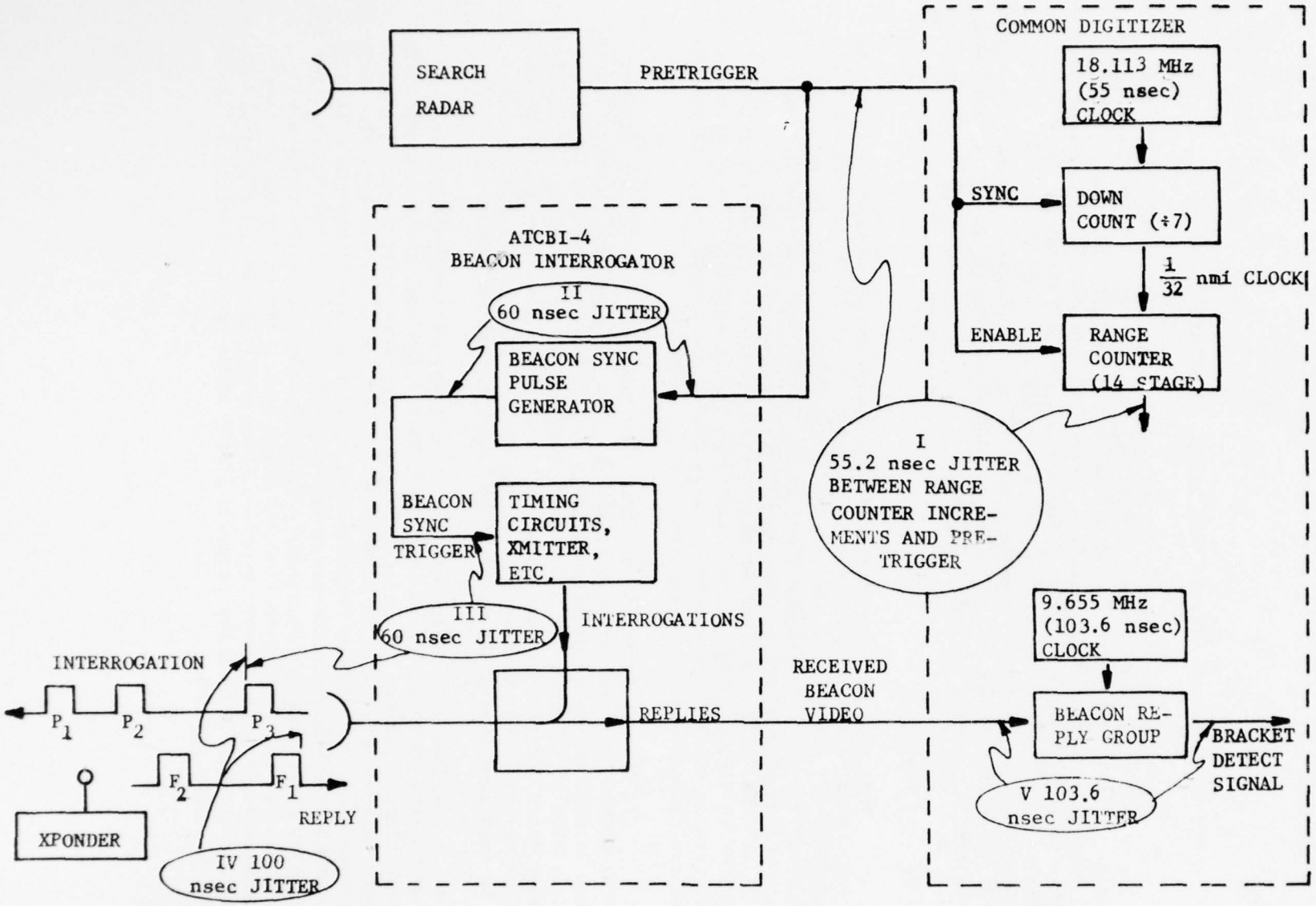

FIGURE 4.10

PRESENT SYSTEM CONFIGURATION

4.2.2 Description of the System

Figure 4.10 is a block diagram of the system under discussion showing the relevant components of the Search Radar, the Beacon Interrogator, and the Common Digitizer. This diagram was developed from information in References 19 and 20 and verified via discussions with NAFEC personnel. The system shown is for the Air Traffic Control Beacon Interrogator-4 (ATCBI-4) in associated operation which means that the timing of the Beacon Interrogator is established by a pretrigger from the associated search radar (information being presented here also applies to the ATCBI-3). Nearly all sites, including NAFEC, are operated this way. The alternative is to have the Beacon Interrogator in self-triggered operation, which is used only at a few military sites.

The range clock in the CD is synchronized to the search radar pretrigger (Reference 20, pages 4-6, paragraphs 4-12). The 18.113 MHz (55.2 nsec) clock is a free running stable oscillator. The divide by 7 circuit produces the 1/32 nmi clock used by the range counter. The radar pretrigger is received by the ARTG, shifted through a five stage shift register at the 18.113 MHz rate and leading edge detected at the first stage flip flop to produce a signal used to synchronize the divide by 7 counter.

The pretrigger signal is again leading edge detected at the end of the five stages and used to set a flip flop which enables the 14 bit range counter to begin counting. This means that the pretrigger from the search radar first synchronizes the divide by 7 counter then enables the range counter to begin counting. Figure 4.11, which was taken from Reference 20 presents this information in detail. In Figure 4.11, note that a divide by two counter is included for providing the wire strap selectable alternative to the 1/32 nmi range clock which is the 1/16 nmi clock. Figure 4.11 presents only the 1/32 nmi system which is the system normally used in the field and the one being considered by this discussion.

The pretrigger input to the ATCBI-4 from the search radar is fed through pulse shaping circuits and used to produce a signal called the beacon sync trigger. This trigger is the master timing pulse in the ATCBI-4, and is used to trigger interrogation at the proper time. The interrogation, consisting of a P_1, P_2, P_3 pulse triplet, is received by a transponder which, after a delay of 3 μsec from receipt of the P_3 leading edge (Reference 21), transmits a reply consisting of two framing pulses F_1 - F_2 spaced 20.3 μsec apart (Reference 21), and code data between the framing pulses. The reply is received by the BRG in the CD, which is driven by a free running stable oscillator that has a period of 103.6 nsec and samples the video to detect an F_1 - F_2 bracket pair. When an F_1 - F_2

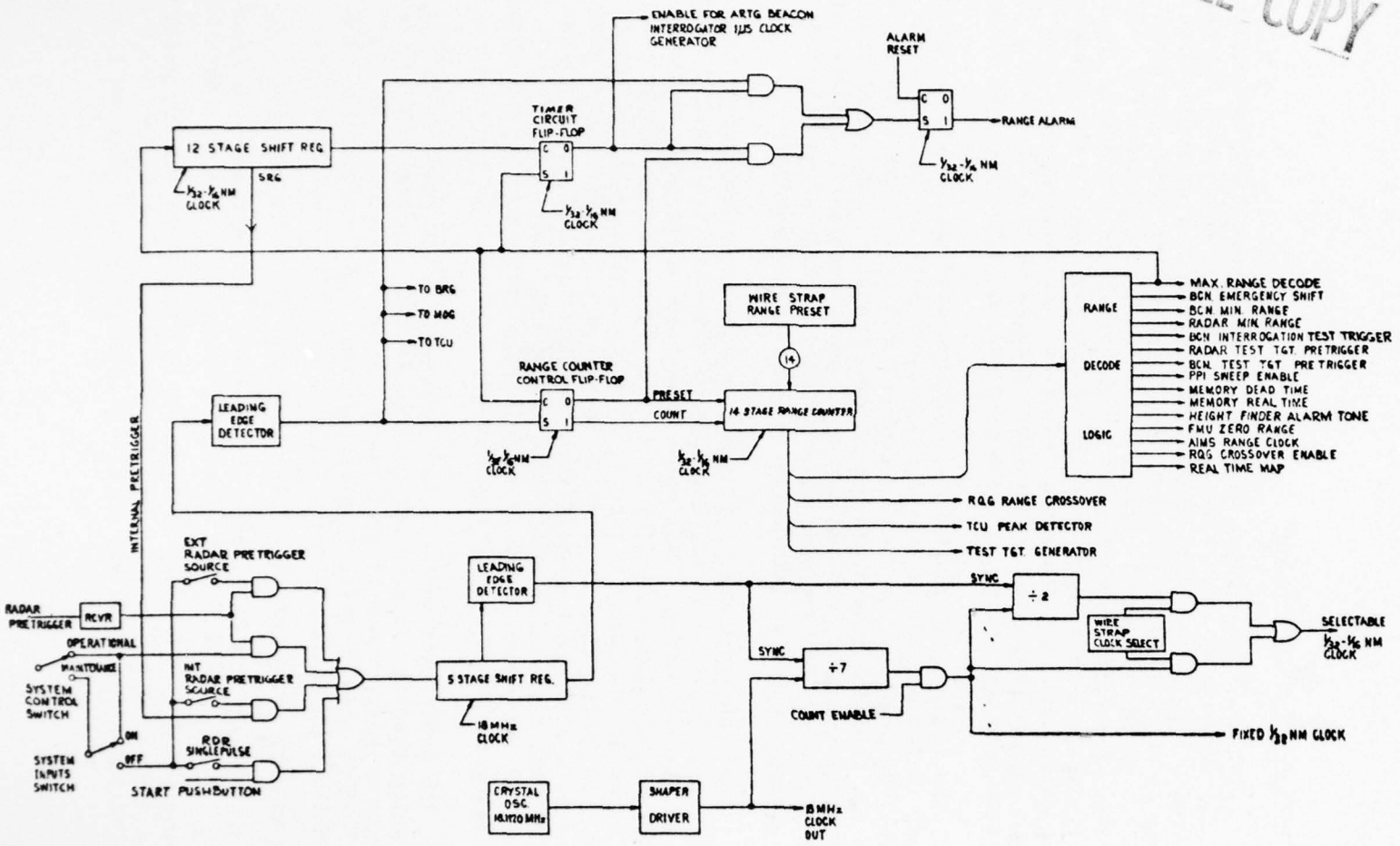

FIGURE 4.11

ARTG RANGE UNIT BLOCK DIAGRAM

coincidence is detected a bracket detect signal is outputted by the BRG. This signal essentially tells the CD to read the range on the counter, so that the bracket pair will have the correct range assigned to it. Of course, to obtain the proper range, it is desired to compute the time elapsed between the leading edge of the P_3 pulse at the interrogator antenna and the occurrence of the leading edge of the F_1 pulse at the same place. Target range is (speaking in terms of classical physics, not hardware implementation) the product of this elapsed time, less the 3 μsec transponder delay, and one half the rate of propogation of electromagnetic waves in free space. In order that the range counter in the CD be equal to what this calculation would yield when the bracket detect signal occurs, various presets and delays are incorporated into the system. For example, the range counter is normally set to a negative range and starts counting from this point upon receipt of the pretrigger. (This by the way, is one reason why the counter is incremented in 1/32 nmi counts, even though the range cells are 1/4 nmi; i.e., to obtain necessary resolution in the preset.) In addition there are pre-adjustable shift register delays in the ATCBI-4 and the BRG of the CD, which are used to adjust the equipment for the proper range determination and for radar-beacon range correlation.

4.2.3 Development of Analysis Methods

Known jitters are indicated on Figure 4.10 and identified in Table 4.5. For purposes of analysis, the elements between each pair of associated points where a jitter is indicated in Figure 4.10 shall be represented as a single network N_i, as shown in Figure 4.12. For an input to N_i of $S_{IN}(t)$, the output is $S_i(t + C_i + \Delta t_i)$ where C_i is a constant delay introduced to preserve the causal nature of the system, and Δt_i is a random variable with probability density function (PDF) of $p_i(\alpha)$. The Δt_i are assumed to be statistically independent. The PDF of the Δt_i associated with each of the jitters indicated in Figure 4.10 is assumed to be uniformly distributed over $\pm J_i/2$ as shown in Figure 4.13, where the J_i's are the values of jitter indicated in Figure 4.10.

TABLE 4.5

REFERENCES USED FOR DETERMINATION OF JITTERS - PRESENT SYSTEM (See Figure 4.10)

I. Jitter between the range counts and the pretrigger will be 55.2 nsec. This is obtained from Reference 20 . The fact that the 55.2 nsec clock is not synchronized to the pretrigger, but rather the divide by 7 counter is synchronized, means that there will always be a 55.2 nsec ambiguity here.

II. The jitter between the radar pretrigger and the beacon sync pulse is 60 nsec, obtained from page xix of Reference 19.

III. The jitter between the beacon sync trigger and any r.f. interrogation pulse (which would include the pulse of interest P_3) is 60 nsec, from page xvii of Reference 19 .

IV. The jitter between the leading edge of the P_3 pulse received by the transponder and transmission of the reply is required to be less than 100 nsec by Reference 21 . One AT-50 was tested at APL and found to have between 80-100 nsec of jitter. It is not known if this is typical.

V. The jitter between the receipt of a reply and the bracket detect signal is 103.6 nsec, obtained from Reference 20 and is a result of the ARTG being driven by a free running (rather than synchronized) stable oscillator.

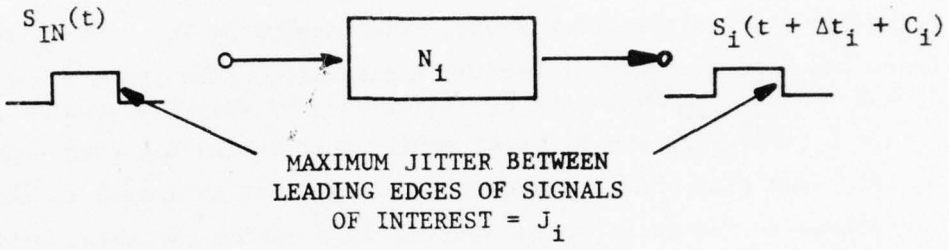

FIGURE 4.12

NETWORK N_i

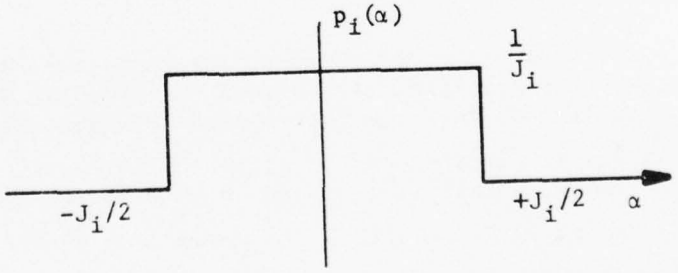

FIGURE 4.13

UNIFORM PROBABILITY DENSITY FUNCTION

Some examples will clarify the discussion. Jitter IV in Figure 4.10 is the jitter between the P_3 pulse of the interrogation pulse set and the F_1 pulse of the transponder reply. The network of interest N_4 is the free space transmission channel and the transponder. The input signal of interest to the channel $S_{IN}(t)$ is the P_3 pulse, and the output signal of interest $S_4(t + C_4 + \Delta t_4)$ is the F_1 pulse received at the ATCBI. The constant delay C_4 is 3 μsec plus whatever time the signal takes to travel to the transponder and return to the interrogator and Δt_4 is a random variable, uniformly distributed over ± 100 nsec/2.

Jitter I is indicated as the jitter between the radar pretrigger and the time at which the range counter increments. Thus, since the range counter increments on each 1/32 nmi clock pulse, this jitter is between the radar pretrigger and an arbitrarily chosen pulse from the 1/32 nmi clock. The network N_1 consists of the 55.2 nsec clock and divide by 7 counter. The input signal to this network $S_{IN}(t)$ is the radar pretrigger, and the output $S_1(t + C_1 + \Delta t_1)$ is a 1/32 nmi clock pulse. The constant delay C_1 determines which clock pulse is chosen while Δt_1 is uniformly distributed over ± 55 nsec/2.

The total jitter of interest occurs between the range counter increments and the bracket detect signal, as shown in Figure 4.10. Figure 4.14 is a block diagram of the same system with the elements reduced to the N_i networks, and also illustrates the jitter of interest, between signals S_1 and S_5. The time delay introduced by this jitter shall be designated by Δt_{TOTAL}, a random variable with a PDF determined by the constraints of the system model set forth. It is this value of Δt_{TOTAL} that we wish to investigate. The signals being discussed, S_o through S_5 are shown in Figure 4.14 and elements lumped into each network are indicated. An arrow going into a network is an input to that network, an arrow coming out is an output of that network.

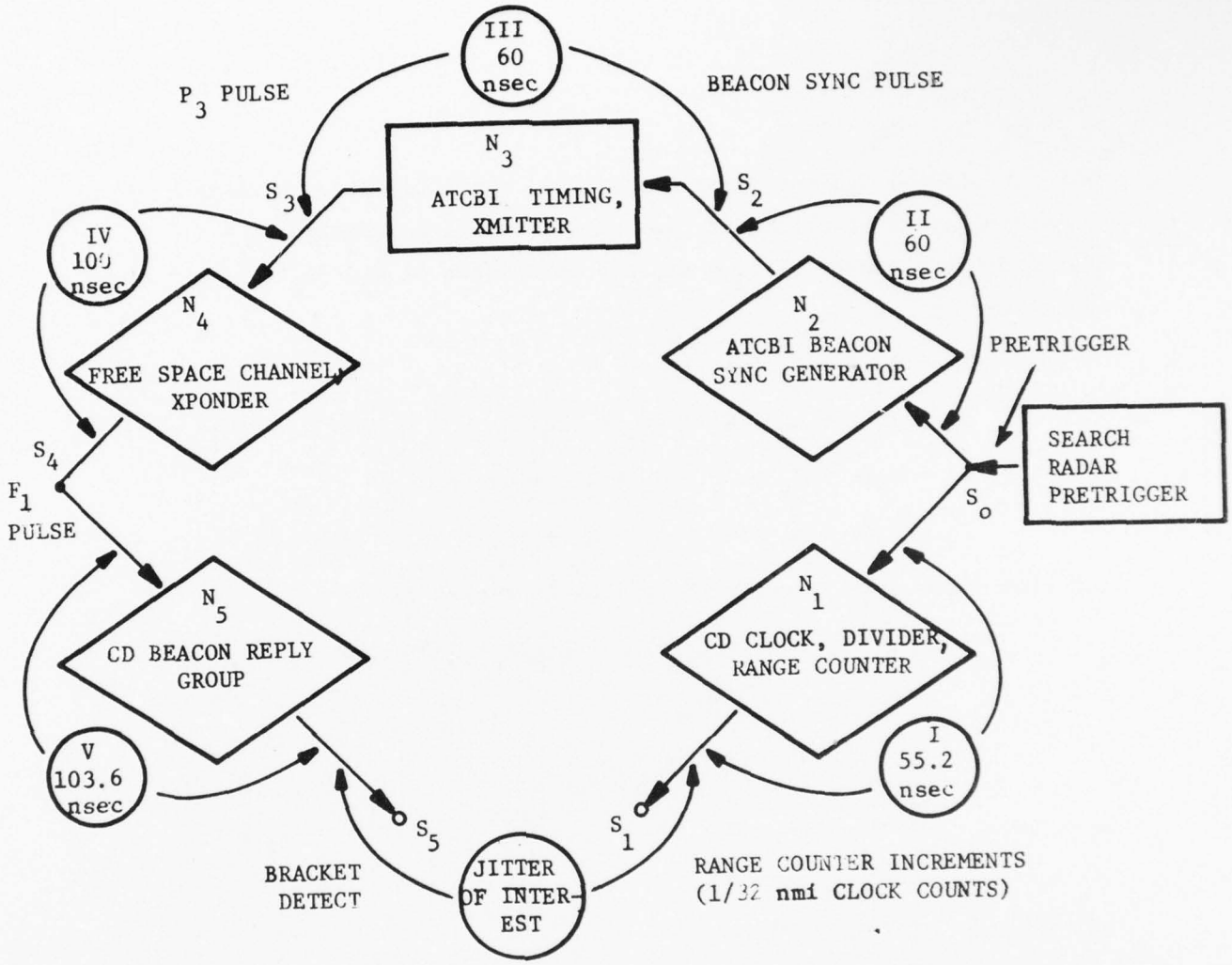

FIGURE 4.14

SIMPLIFIED BLOCK DIAGRAM

AD-A038 491 JOHNS HOPKINS UNIV LAUREL MD APPLIED PHYSICS LAB F/G 17/7
SYSTEM DEFINITION AND INVESTIGATION OF THE ON-SITE PROCESSING O--ETC(U)
SEP 76 J W THOMAS, E C WETZLAR, L H ZITZMAN DOT-FA75WA-3553
UNCLASSIFIED APL/JHU-FP8-E-024-1 FAA-RD-77-12-1 NL

2 OF 3
AD A038491

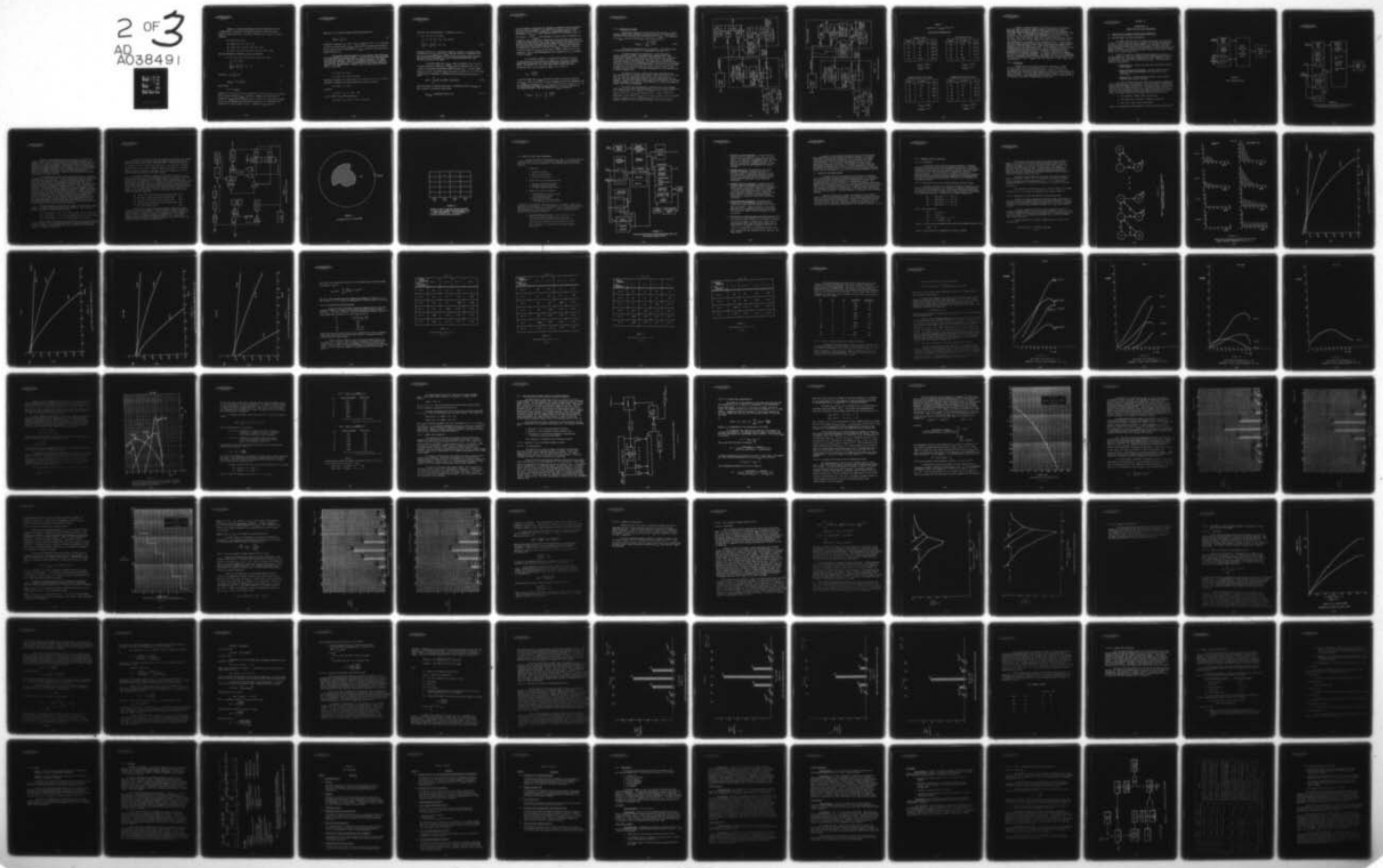

Signal S_o, the radar pretrigger, shall be chosen with no loss of generality as occurring at time zero and will be written as $S_o(t)$. Signal S_1 then occurs at $C_1 + \Delta t_1$ and is written as $S_1 = S_1(t + C_1 + \Delta t_1)$. Similarly

$$S_2 = S_2(t + C_2 + \Delta t_2)$$

$$S_3 = S_3(t + C_2 + C_3 + \Delta t_2 + \Delta t_3)$$

$$S_4 = S_4(t + C_2 + C_3 + C_4 + \Delta t_2 + \Delta t_3 + \Delta t_4)$$

$$S_5 = S_5(t + C_2 + C_3 + C_4 + C_5 + \Delta t_2 + \Delta t_3 + \Delta t_4 + \Delta t_5)$$

The time difference T between S_1 and S_5 is therefore

$$T = [t + C_2 + C_3 + C_4 + C_5 + \Delta t_2 + \Delta t_3 + \Delta t_4 + \Delta t_5] -$$

$$[t + C_1 + \Delta t_1] =$$

$$\left\{ \sum_{i=2}^{5} C_i + \sum_{i=2}^{5} \Delta t_i \right\} - C_1 - \Delta t_1 \qquad 4\text{-}5$$

Letting $K = -C_1 + \sum_{i=2}^{5} C_i$ and

$$\Delta t_{TOTAL} = -\Delta t_1 + \sum_{i=2}^{5} \Delta t_i \qquad 4\text{-}6$$

this becomes

$$T = K + \Delta t_{TOTAL} \qquad 4\text{-}7$$

Equation (4-7) says that the time difference T between S_1 and S_5 is a constant plus a random variable Δt_{TOTAL}. We wish to examine the statistical properties of Δt_{TOTAL} given by Equation (4-6). Because the uniform PDF's assumed for the Δt_i are symmetrically distributed about zero, the statistical properties of Δt_i are the same as $(-\Delta t_i)$. Similarly, Δt_{TOTAL} given by

Equation 4-6 will have the same statistical properties as

$$\Delta t'_{TOTAL} = \sum_{i=1}^{5} \Delta t_i \qquad 4\text{-}8$$

obtained by replacing $-\Delta t_1$, with $-(-\Delta t_1)$ in Equation (4-6). It is important to note the random variable $\Delta t'_{TOTAL}$, which shall be investigated because it has the same statistical properties as Δt_{TOTAL}, is given by the same sum of random variables Δt_i.

The concept being discussed here is the relative time differences that exist between the various signals. The choice of the radar pretrigger as the ultimate reference (hence the pulse with no jitter) in the above discussion was arbitrary. This fact is sometimes confusing. To clarify the situation, the analysis will be repeated with the P_3 pulse (signal S_3) chosen as the reference pulse. Assume S_3 (the P_3 pulse) occurs at time 0, and $S_3 = S_3(t)$ then

$$S_4 = S_4(t + C_4 + \Delta t_4)$$

$$S_5 = S_5(t + C_4 + C_5 + \Delta t_4 + \Delta t_5)$$

Referring to Figure 4.15, recall that S_2 is an input to N_3, S_3 is an output. Therefore, consistent with the definition set forth for the N_i,

$$S_2 = S_2(t - C_3 - \Delta t_3)$$

Similarly

$$S_o = S_o(t - C_3 - C_2 - \Delta t_3 - \Delta t_2)$$

S_o is an input to N_1 which produces S_1,

$$S_1 = S_1(t - C_3 - C_2 + C_1 - \Delta t_3 - \Delta t_2 + \Delta t_1).$$

Thus the total time difference T' between S_1 and S_5 is

$$T' = (t + C_4 + C_5 + \Delta t_5 + \Delta t_5) -$$

$$(t - C_3 - C_2 + C_1 - \Delta t_3 - \Delta t_2 + \Delta t_1) =$$

$$\left\{ \sum_{i=2}^{5} C_i + \sum_{i=2}^{5} \Delta t_i \right\} - C_1 - \Delta t_1 \qquad (4\text{-}9)$$

Equation (4-9) for T' is the same as Equation (4-5) for T, and will result in equations for Δt_{TOTAL} and $\Delta t'_{TOTAL}$ that are identical to Equations (4-6) and (4-8) respectively showing that the choice of reference does not affect the results of the analysis; i.e., one is discussing differences, thus absolute references do not apply.

It has been shown that Δt_{TOTAL}, given by Equation (4-6) will have the same statistical properties as $\Delta t'_{TOTAL}$ given by Equation (4-8), which is a sum of the uniformly distributed random variables (Δt_i). For two random variables, X and Y, with PDF's $p_X(x)$ and $p_Y(y)$, the PDF of Z = X + Y for X and Y statistically independent is obtained by convolving $p_X(x)$ with $p_Y(y)$ as shown:

$$p_Z(z) = \int_{-\infty}^{\infty} p_X(x)\ p_Y(z-x)dx = p_X(x) * p_Y(y) \qquad (4\text{-}10)$$

where the symbol (*) denotes convolution. Obtaining the PDF of Δt_{TOTAL} is then a matter of successive convolutions:

$$p_{\Delta t_{TOTAL}} = \left([(p_1 * p_2) * p_3] * p_4 \right) * p_5 \qquad (4\text{-}11)$$

As the successive convolutions are completed, a piecewise function develops, such that when the argument of the function lies within a given interval, the value of the function is defined by a corresponding equation. The development of $P_{\Delta t_{TOTAL}}$ is quite tedious because of the piecewise nature of the function. If $P_{\Delta t_{TOTAL}}$ were obtained, it could be used to determine the probability that a reply from a target with a given position with respect to a range cell boundary will occur in the adjacent range cell because of jitter, where the own cell contains the nominal target position and adjacent cells are those which fall on either side of own cell. Because of the difficulty in obtaining the closed form of the PDF for Δt_{TOTAL}, a program to generate successive values for Δt_{TOTAL} and use them to predict range split rate was considered. The en route investigations were suspended prior to development of such a program.

It is possible, however, to evaluate the variance of Δt_{TOTAL}, or some function of the variance, and compare the result with values obtained when various source of jitter are reduced or eliminated from the system. The variance σ^2_i for a zero mean random variable uniformly distributed over $\pm J_i/2$ as shown in Figure 4.13 is given by

$$\sigma^2_i = \frac{(J_i/2)^2}{3} \tag{4-12}$$

It has been shown that Δt_{TOTAL} will have the same statistical properties as $\Delta t'_{TOTAL}$, which is given by the sum of assumed statistically independent random variables in Equation (4-8). It is well known that the variance of the sum of statistically independent random variables is the sum of variances of the random variables. Thus the variance of Δt_{TOTAL} is given by

$$\sigma^2_{TOTAL} = \sum_{i=1}^{5} \sigma^2_i = \sum_{i=1}^{5} \frac{(J_i/2)^2}{3} \tag{4-13}$$

4.2.4 Evaluation of Jitter

This section compares the system jitter that results for various system configurations (including the proposed single clock modification, Reference 22) by comparing the resulting values of $2\sigma_{TOTAL}$. The expression for $2\sigma_{TOTAL}$ is derived from Equation (4-13) and is given by

$$2\sigma_{TOTAL} = 2\sqrt{\sum_{i=1}^{5} \frac{(J_i/2)^2}{3}} \qquad (4\text{-}14)$$

Three system configurations are considered. The present system configuration shown in Figure 4.10 is described in Section 4.2.2.

The synchronized clock modification is being designed by Airways Facilities at NAFEC. The modification replaces the 9.7 MHz (103.6 nsec) oscillator in the BRG with a 38.6 MHz (25.9 nsec) oscillator. A divide by 4 counter is used to down count the clock to the required 103.6 nsec period for BRG functions. The signal used to synchronize the divide by 7 counter for the ARTG range clock will also be used to synchronize the divide by 4 counter in the BRG every sweep. The effect is that N_5 shown in Figure 4.14 will introduce only 25.9 nsec of jitter, instead of the previous 103.6 nsec jitter. The system configuration for this modification is shown in Figure 4.15.

The single clock mod, a modification being considered by the FAA (see Reference 22), disables both the 55.2 nsec clock and the 103.6 nsec clock in the CD and replaces both with either a 25.9 nsec clock or a 12.9 nsec clock and appropriate dividers to operate existing BRG and ARTG elements. The BRG shift register shift times are fixed relative to the range counter increments, so no jitter is introduced by N_5. Figure 4.16 shows the single clock system configuration.

For each of the configurations, including both of the proposed clock rates for the single clock modification, the N_i are listed in Table 4.6 with corresponding J_i, σ^2_i obtained from Equation (4-12) σ^2_{TOTAL} from Equation (4-13) and $2\sigma_{TOTAL}$ from Equation (4-14). Table 4.6 shows an improvement in the value of $2\sigma_{TOTAL}$ of 18.1 nsec in going to the synchronized clocks. In going to the 25.9 nsec single clock a gain of 24.4 nsec is realized, while 25.5 nsec is realized in going to the 12.9 nsec clock.

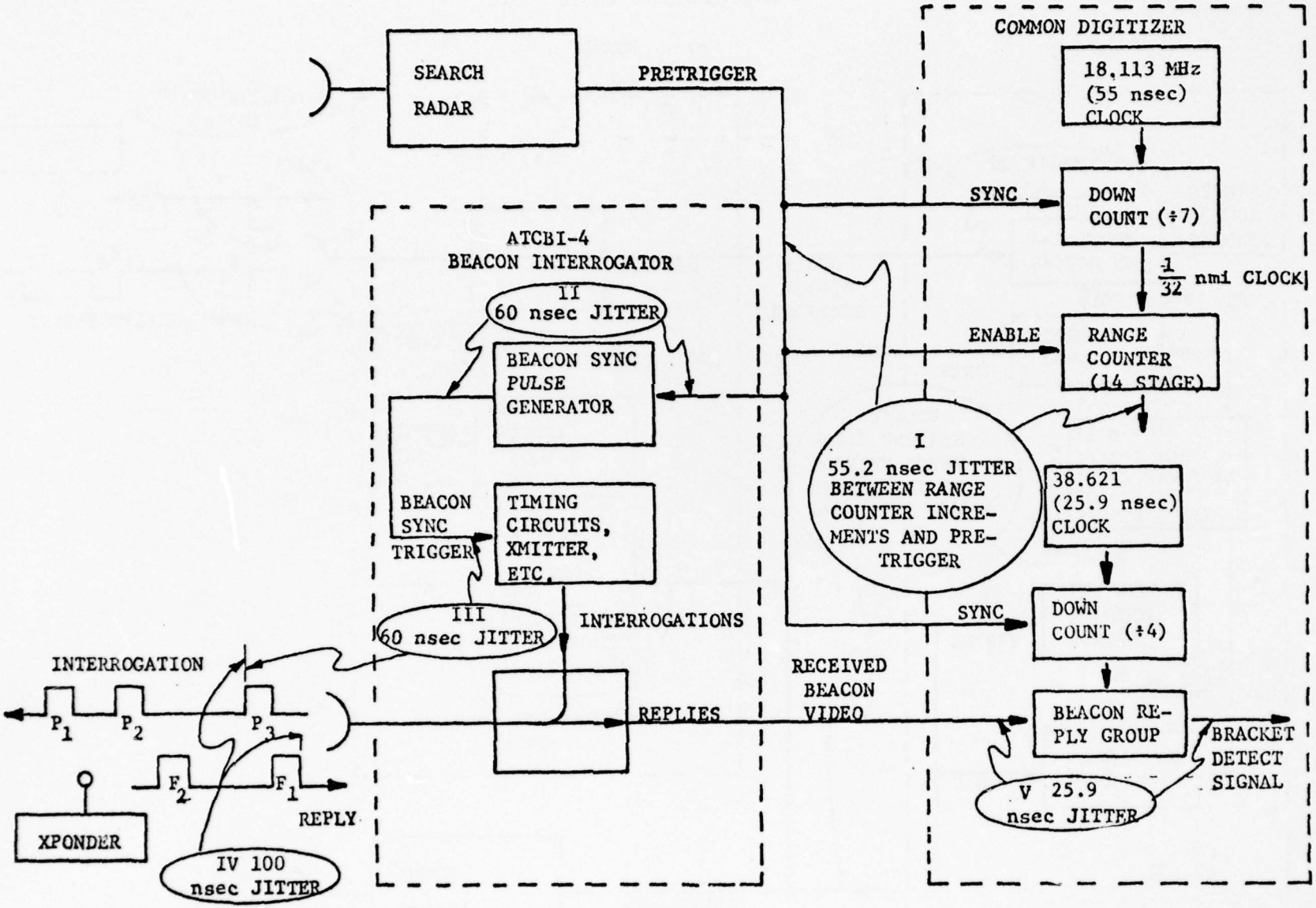

FIGURE 4.15

SYNCHRONIZED CLOCKS CONFIGURATION

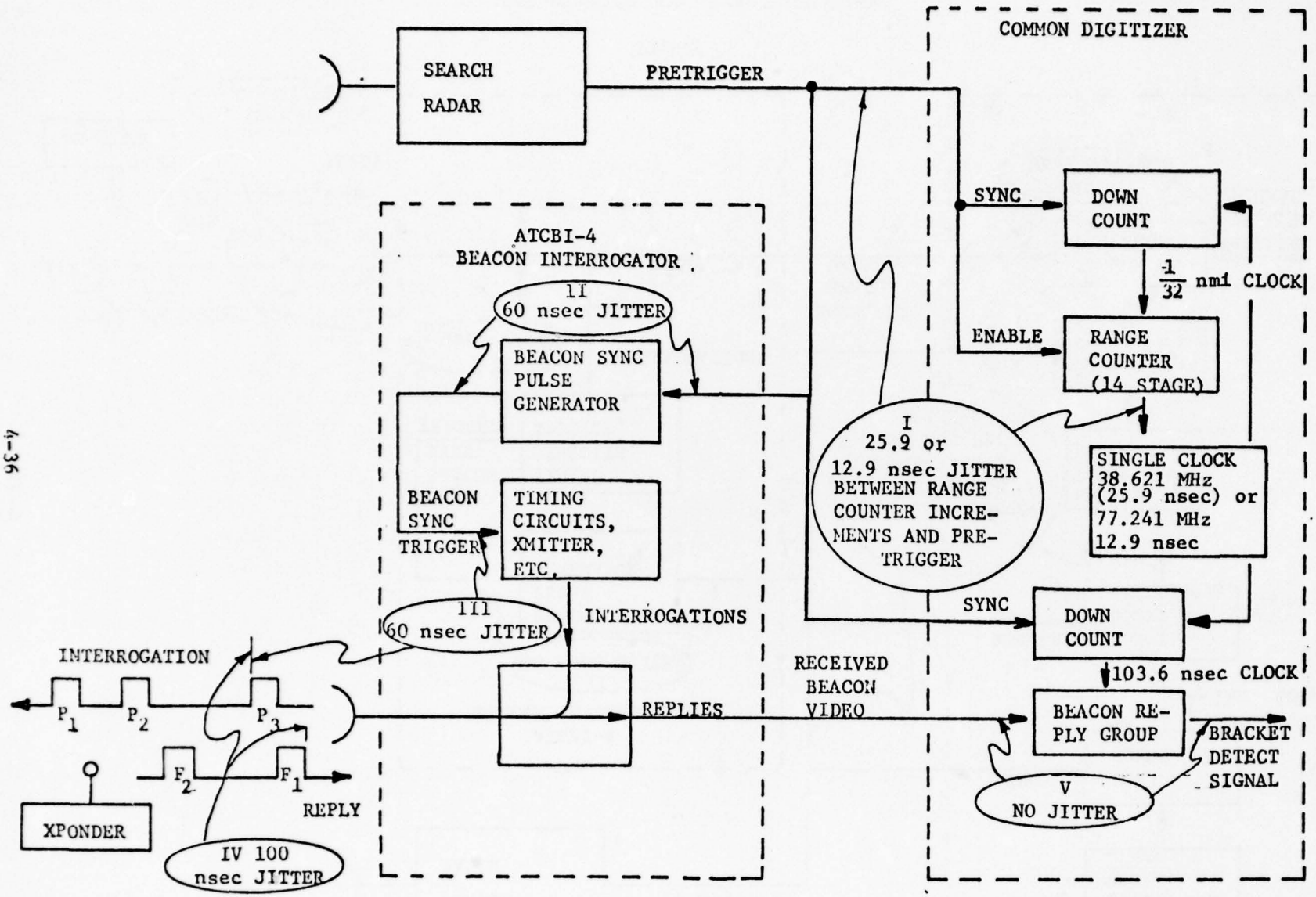

FIGURE 4.16

SINGLE CLOCK CONFIGURATION

TABLE 4.6

Comparison of $2\sigma_{TOTAL}$ Values for

Four System Configurations

Present System

Source	J_i (nsec)	σ^2_i
N_1	55.2	253.9
N_2	60	300.0
N_3	60	300.0
N_4	100	833.3
N_5	103.6	894.4

$\sigma^2_{TOTAL} = 2581.7$

$2\sigma_{TOTAL} = 101.6$

Synchronized Clock

Source	J_i (nsec)	σ^2_i
N_1	55.2	253.9
N_2	60	300.0
N_3	60	300.0
N_4	100	833.3
N_5	25.9	55.9

$\sigma^2_{TOTAL} = 1743.2$

$2\sigma_{TOTAL} = 83.5$

Single Clock Mod (25.9 nsec)

Source	J_i (nsec)	σ^2_i
N_1	25.9	55.9
N_2	60	300.0
N_3	60	300.0
N_4	100	833.3
N_5	0	0

$\sigma^2_{TOTAL} = 1489.2$

$2\sigma_{TOTAL} = 77.2$

Single Clock Mod (12.9 nsec)

Source	J_i (nsec)	σ^2_i
N_1	12.9	13.9
N_2	60	300.0
N_3	60	300.0
N_4	100	833.3
N_5	0	0

$\sigma^2_{TOTAL} = 1447.2$

$2\sigma_{TOTAL} = 76.1$

Further, as shown by Table 4.6, the major portion of the improvement (18.1 nsec) is obtained simply by going to synchronized clocks, providing this modification results in the assumed 25.9 nsec introduced by the BRG (which is determined by how stable the 55 nsec clock and 103.5 nsec clock are). Only 7.4 nsec additional improvement in the value of $2\sigma_{TOTAL}$ is gained over the synchronized clock configuration by going to a 12.9 nsec single clock system. Note that, as shown by the difference between the $2\sigma_{TOTAL}$ value for 25.9 nsec single clock and the 12.9 nsec clock, very little is gained by increasing the clock frequency further. This is because the jitter being introduced by the clock is becoming an increasingly smaller fraction of the total system jitter, which may be observed in Table 4.6 by comparing the σ^2_1 for each jitter source. It was indicated on January 16, 1976 by FAA personnel that much of the work to effect the synchronized clock configuration has already been done. According to NAFEC personnel this modification is relatively inexpensive. It should, therefore, be completed if it has not already been completed. The single clock mod is not recommended, because it represents little potential improvement over the synchronized clocks (7.4 nsec in the value of $2\sigma_{TOTAL}$) and is not expected to reduce range split significantly.

4.2.5 Conclusions

Because the analysis shows that several components of ATCRBS contribute range jitter at significant levels, it is recommended that an investigation of the system be undertaken to measure the range jitter introduced by the individual ATCRBS components so that proper corrective action can be initiated. It does not make sense to modify the CD to detect beacon replies to within a few nanoseconds when successive replies received by the CD are jittering by an order of magnitude more than this.

SECTION 5.0

INVESTIGATION OF

COMMON DIGITIZER RADAR ENHANCEMENTS

5.0 INVESTIGATION OF COMMON DIGITIZER RADAR ENHANCEMENTS

5.1 BASELINE COMMON DIGITIZER CONFIGURATION

The Common Digitizer (CD) is a single channel logic processor which is used to convert radar and beacon information into digital data messages for use by a central computer complex (ARTCC). The raw radar video input is first quantized in binary form and then processed to determine range and azimuth information. A statistical detection scheme is utilized to distinguish genuine (aircraft) target returns from thermal noise and other random interference, e.g., weather clutter, etc.

Figure 5.1 presents a simplified block diagram of the basic CD. In this diagram the search radar target detection and transmission operations are simplified into 3 operations performed by the Radar Quantizer, Target Detection and Processing, and the Output Buffer Groups. The functions performed by each group are:

- o Radar Quantizer - Accepts raw radar video and produces digital output pulses.
- o Target Detection and Processing - Performs target detection, range and azimuth determination, and radar/beacon target correlation.
- o Output Buffer - Performs message buffering, output message selection, and message formatting.

In order to improve the search radar target detection capabilities of the Common Digitizer, particularly in clutter environments, experimental modifications were made to the Quantizer and Target Detection and Processing Groups of the CD at NAFEC (Elwood, N.J.). The modifications, installed in 1971, include the addition of a new radar quantizer, designated the Improved Quantizer, and three modifications to the Target Detection and Processing Group. The Target Detection and Processing Group modifications were:

1. Hit Placement - Reduce range cell splitting
2. ACE remove cell of interest - Eliminate target bias
3. ACE clutter jump - Faster ACE response

Figure 5.2 illustrates the configuration of the CD with these modifications.

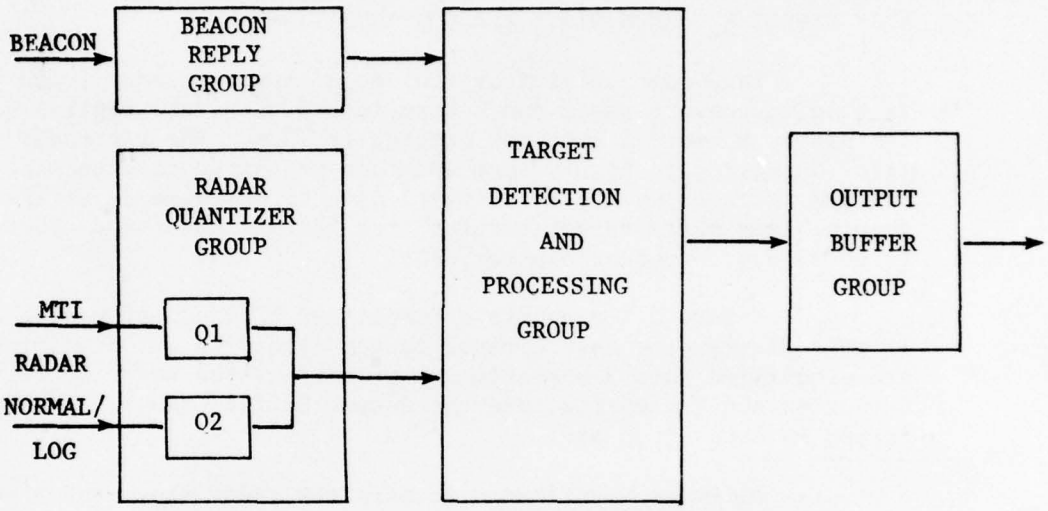

FIGURE 5.1

BASIC COMMON DIGITIZER

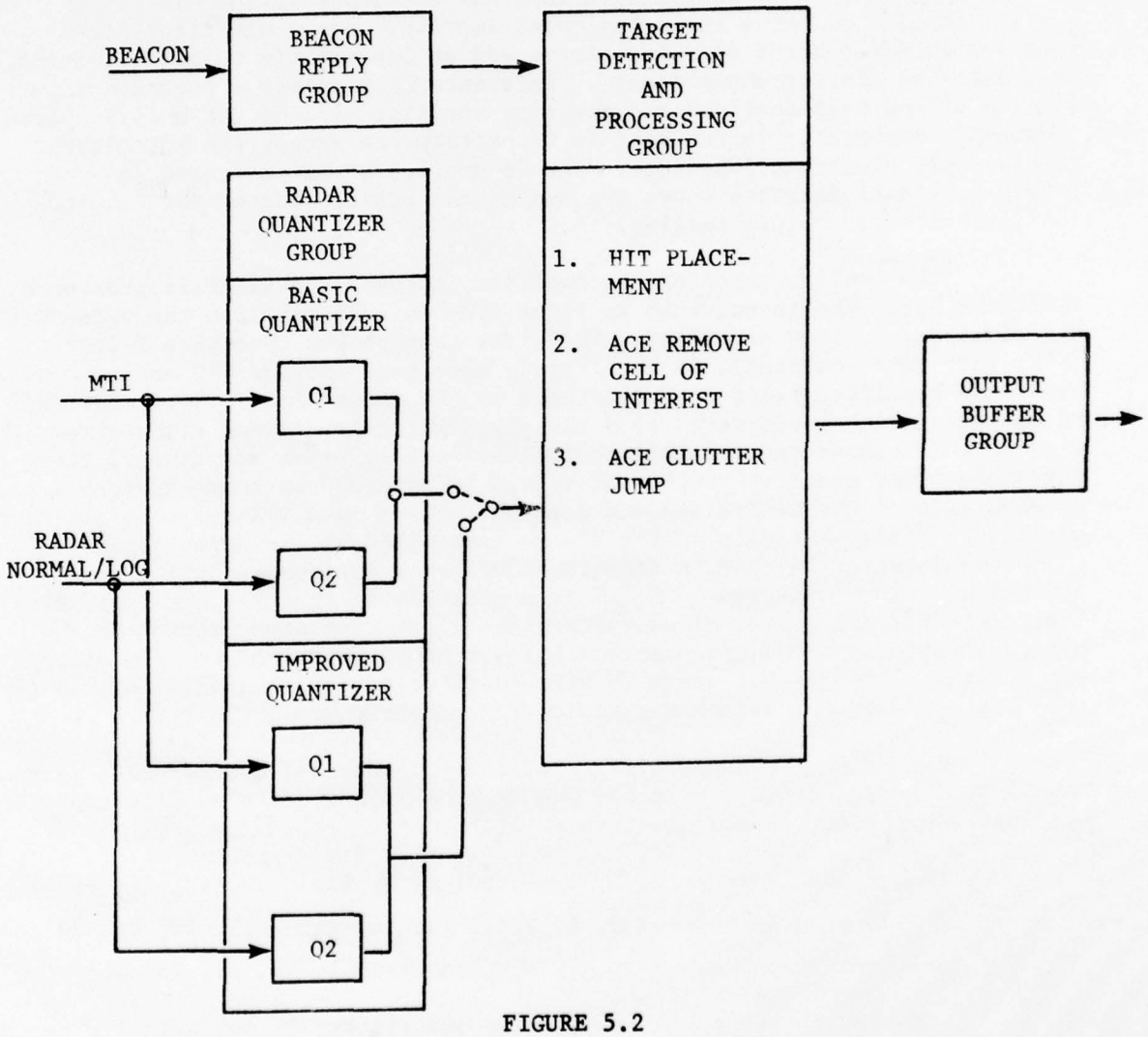

FIGURE 5.2

COMMON DIGITIZER WITH IMPROVED QUANTIZER AND ACE MODIFICATIONS (NAFEC, ELWOOD, N.J.)

Testing of these modifications was completed in late 1972. The overall results of these tests indicated improved Common Digitizer performance in the control of false alarms and an increase in target detection capability in clutter environments. Reference 23 presents a detailed discussion of the modifications and the test results. All of the modifications produced a measurable improvement in CD performance except the ACE clutter jump and hit placement functions. The CD configuration presented in Figure 5.2, excluding the above two functions, was considered the Baseline configuration for future testing.

The configuration of the baseline improved quantizer is presented in Figure 5.3. The input video is first time delayed to align the video with the clutter detection circuitry. The video then passes through a filter (FTC; fast time constant), is antilogged, undergoes another FTC and is precision rectified prior to being input to the delay line. The center tap of the delay line is compared to a threshold which is derived either from a slow-loop (2 second integration) thermal noise loop or an adaptive clutter threshold. The adaptive clutter threshold is obtained by summing video taps on each side of the center tap and feeding the sum to a voltage controlled amplifier (VCA). The gain of the VCA is controlled by a clutter noise meter (2 second integration). Hits from the comparator must pass minimum and maximum hit width criteria. The minimum criteria is that the hit last at least two 1/32 nmi clock pulses. Since the clock runs asynchronous to the hit declaration process, the minimum hit may be between 1/32 to 1/16 nmi. The maximum allowable hit width is site selectable. Width qualified hits are then processed by the second threshold M/N integrator.

The break-frequency of the FTC's are 35 KHz for quarter-mile systems (ARSR) or 3.5 KHz for half-mile systems (e.g. AN/FPS-7). Delay line tap spacing is dependent on the radar pulse width:

(a) 2 μsec pulse: 0, 2, 4, 6, 8 (center tap), 10, 12, 14, 16 μsec

(b) 3 μsec pulse: 0, 3, 6, 9, 12 (center tap), 15, 18, 21, 24 μsec

(c) 6 μsec pulse: 0, 3, 6, 12 (center tap), 18, 21, 24 μsec

The baseline CD operates with two quantizers; Q1 for normal video and Q2 for MTI video. Q2 is used from zero range to a preselected range where Q1 commences operation. The crossover range can be varied over three bearing segments as exampled in Figure 5.4.

The clutter loop in the improved quantizer is enabled by the clutter detection circuit. This circuit sets a reference voltage obtained from a 70% P_n noise meter whose input is dead-time video. A fraction of this 70% P_n voltage is used to threshold the input video. This fraction is usually set for 25% P_n. If the output from the comparator is high for $\geq$ 2.5 pulse widths, a clutter situation is declared. The clutter signal will reset if the comparator goes low for $\geq$ 1.25 pulse widths.

The clutter signal is sliced each range cell and fed to a 3 x 5 matrix (five range cell by three radar dwell matrix) for automatic switching to improved Q1 (MTI video) when Q2 (normal video) is in operation. See Figure 5.5 for an example of a 3 x 5 matrix clutter detection situation. Q1 is used whenever the matrix count $\geq$ 4. However, the operator can wire-strap the CD to inhibit switching to Q1 beyond a designated range. Furthermore, the operator can wire-strap the CD to disable the noise meters within a specified range. That is, a noise meter will not be effected by hits declared at a range less than that specified. Thus the operator must set five CD parameters for quantizer operation:

(a) normal video thermal noise meter minimum range (Q2)

(b) MTI video thermal noise meter minimum range (Q1)

(c) MTI video clutter noise meter minimum range (Q1)

(d) normal video clutter noise meter minimum range (Q2)

(e) MTI video maximum range (Q1)

Declaration of clutter also enables dynamic minimum run length criteria for the second threshold. Second threshold targets declared in a clutter region are counted and if the count exceeds 64 clutter targets per scan, the dynamic minimum run length is incremented by 2. The largest possible value of the dynamic minimum run length is 28. If the second threshold targets declared in a clutter region per scan falls below 32, the dynamic minimum run length is decremented by 2.

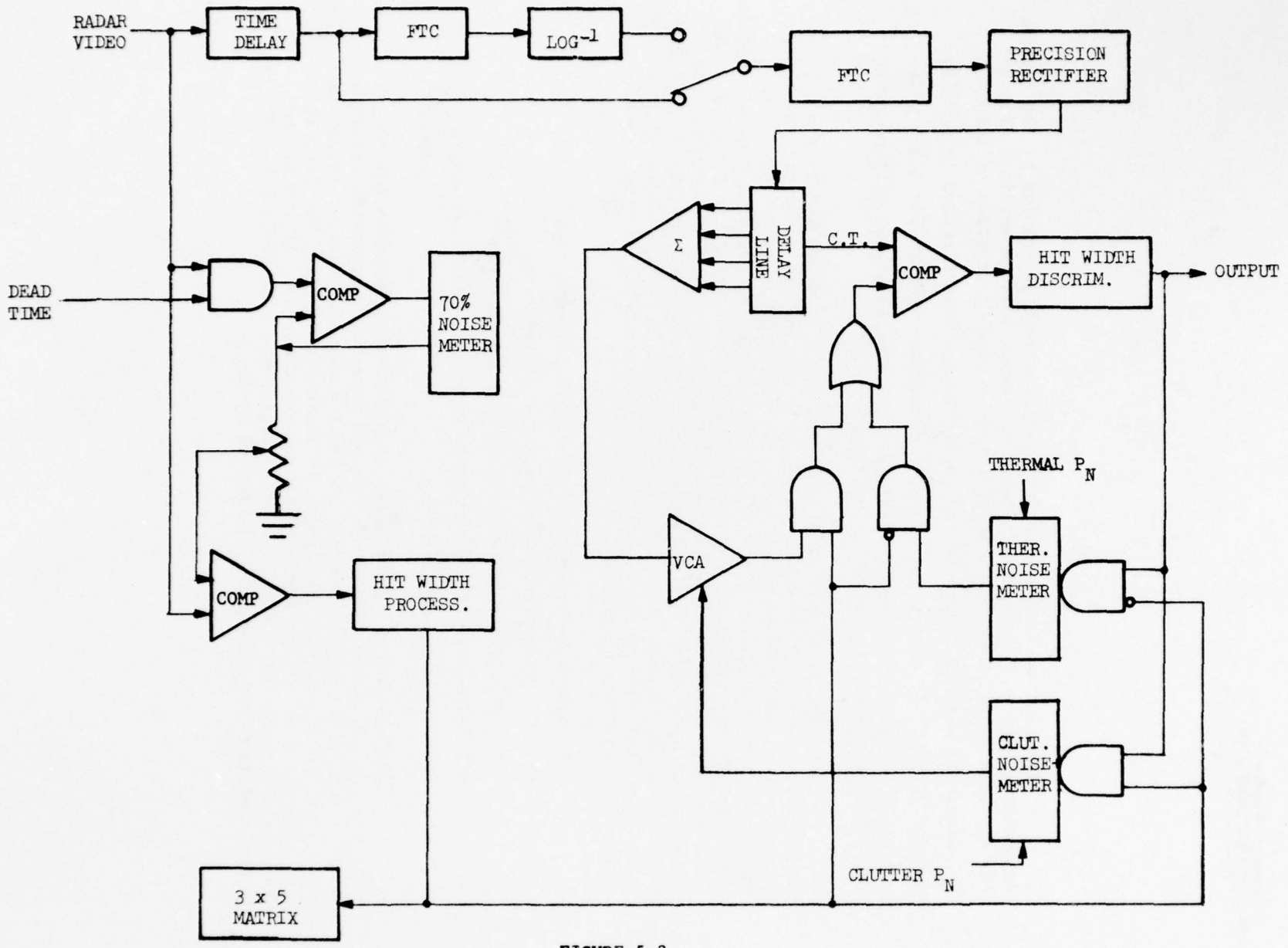

FIGURE 5.3

IMPROVED QUANTIZER (BASELINE)

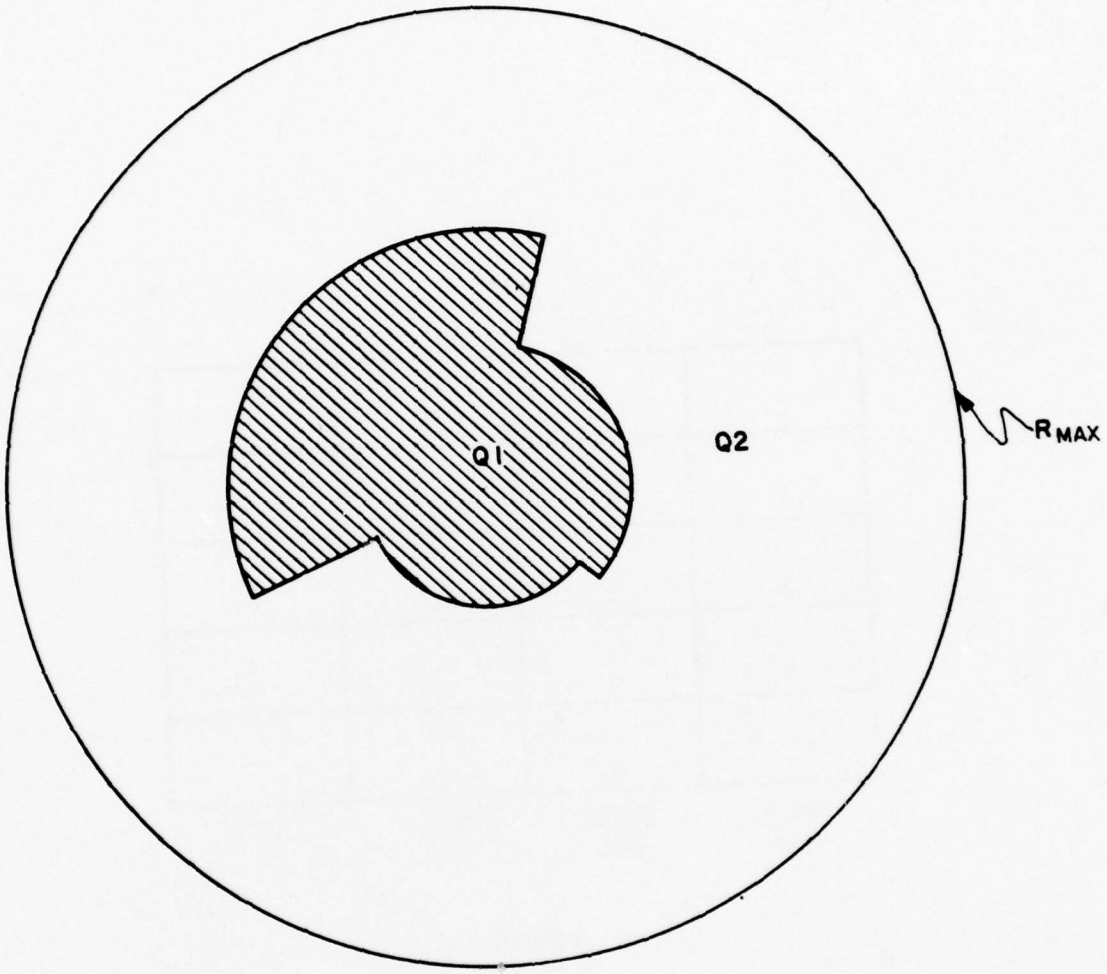

FIGURE 5.4

AN EXAMPLE OF Q1, Q2 CROSSOVER

0	0	0	
1	1	1	
0	1	0	X
1	0	0	
0	0	1	
DWELL N-3	DWELL N-2	DWELL N-1	DWELL N

FIGURE 5.5

EXAMPLE OF MATRIX USED FOR CLUTTER DETECTION.
X = RANGE CELL CURRENTLY BEING PROCESSED BY Q2.
1 = FIRST THRESHOLD HIT. IN THIS EXAMPLE, A CLUTTER SITUATION WOULD BE DECLARED.

5.2 COMMON DIGITIZER RADAR ENHANCEMENTS

Several experimental modifications were made to the Common Digitizer at NAFEC (Elwood, N. J.) for the purpose of upgrading the primary search radar video hit processing capability. The following areas of the CD were modified:

1. Quantizers
   - o Improved Q_1 and Q_2
   - o Added Q_3 rank quantizer
   - o Quantizer Select Logic
2. Target Detection and Processing Group
   - o Automatic ACE Curve Selection
   - o Delayed Decision Integration
   - o Lead Edge Threshold (T_L) Control
3. Added Scan Correlation Hardware
   - o Video Monitoring - Clutter, Limit, Hit Density, ACE Blank
   - o Processing Algorithms
   - o Video Control - Quantizer select, Threshold gain, T_L zone control

In addition, a digital data recording capability was added to enhance the analysis of CD performance. The configuration of the CD with these modifications installed is illustrated in Figure 5.6. Refer to Reference 24 for a detailed discussion of each modification. A brief description of each modification is presented as follows:

1. Improved Quantizers Q_1 and Q_2 - The video input to Q_1 was disconnected and replaced with a wire strap selection so that the video can be input to Q_1 or Q_3. Improved Q_2 was modified with the addition of a five bit D/A converter to provide scan correlated automatic gain control.

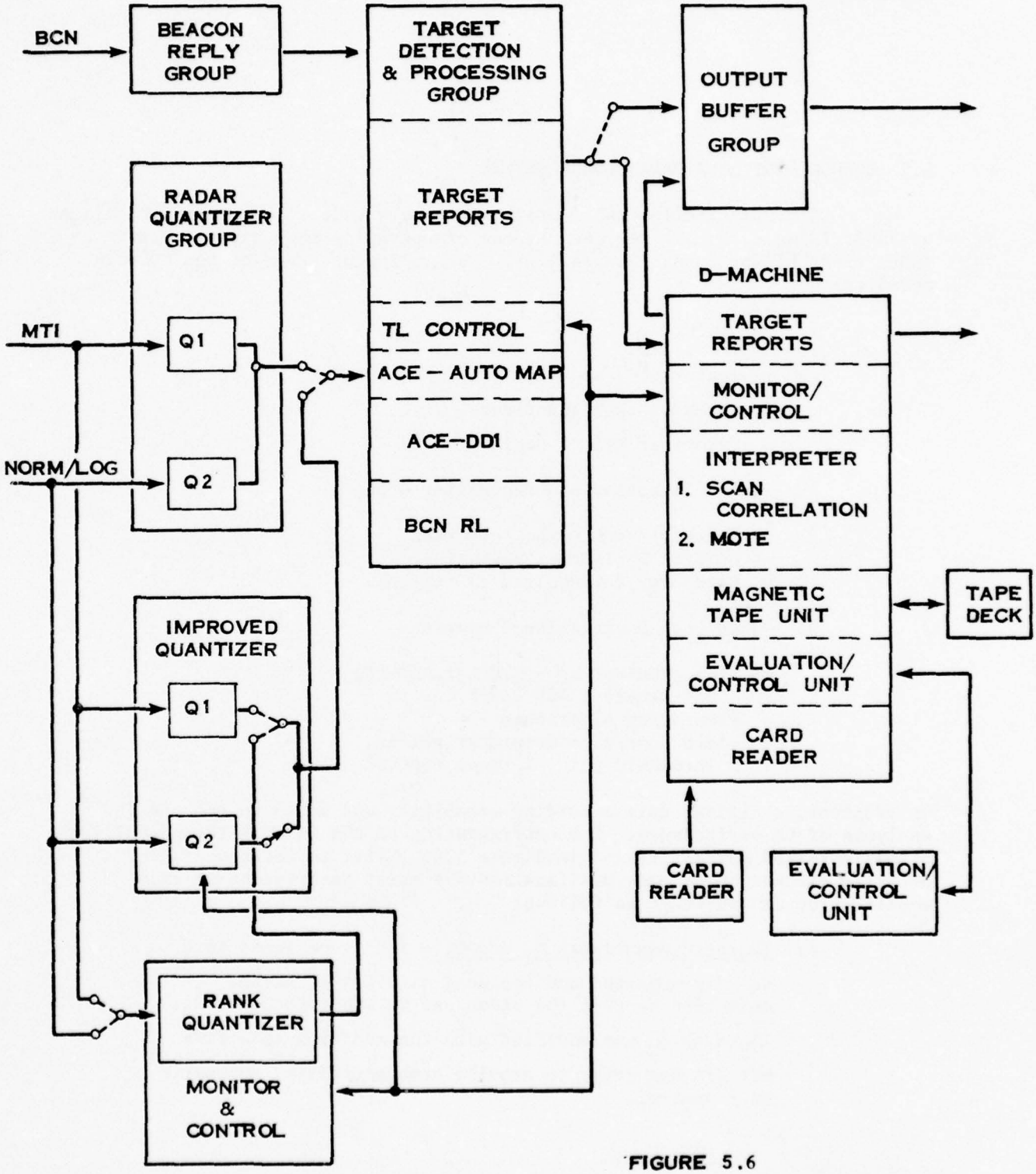

FIGURE 5.6

COMMON DIGITIZER WITH RANK QUANTIZER, SCF, ACE, AND OTHER MODIFICATIONS

2. Quantizer Q_3 (rank quantizer) - A single rank order quantizer has been added as a wire strap selectable option. The quantizer is configured so that its input video can be either MTI or Normal/Log video. The quantizer incorporates a thermal quantizer for clear operation and uses the rank quantizer for clutter operation.

3. Quantizer Selection - New quantizer select logic provides for quantizer selection with the CD operational panel or with scan correlation control. Scan correlation of appropriate statistics is used to select the quantizer that will provide the best target detection capability for the operating environment.

4. Automatic ACE Curve Selection - Automatic ACE Curve Selection selects the appropriate Target Detection threshold false alarm curve, based on the correlation of the clutter encountered, to attempt to maintain a constant target false alarm rate. Three false alarm curves are available. They are adjustable and may be modified to reflect the desired detector threshold for a percent hit count with a particular correlation.

5. Delayed Decision Integration - Delayed Decision Integration provides smoothing of the ACE derived leading edge target detection threshold (T_L) in both range and azimuth. Targets detected on a lowerlead edge will not be completed and reinitiated by raising and lowering the leading (T_L) and trailing (T_T) edge erratically.

6. Zone Control of Target Detection Lead Edge Threshold (T_L) - The Target Detection Threshold (T_L) Lead Edge is adjusted to control the number of targets over a small area of radar coverage (zone 4 nmi by 64 ACPs), based upon scan correlation of the number of targets in the zone. T_L control is accomplished by increasing/decreasing the T_L value selected with the operational panel sensitive lead edge switches.

A portion of the Quantizer and Target Detection and Processing Group enhancements are made possible through the addition of a computer (D machine) to perform scan correlation. The correlation of pertinent video information from scan to scan significantly enhances the target detection process. Scan correlation is implemented in three steps: monitoring, processing, and control. The monitor and control parameters are recorded on magnetic tape in order to provide information on system performance and the operation of the scan correlation processing algorithms. Target centroid information is also recorded for system performance analysis.

5.3 ANALYSIS OF THE MODIFICATIONS

An analysis of the various modifications was made to determine the technical basis (no written information was available) of each modification and to determine whether improved CD performance will result through the implementation of the modifications or combinations thereof. The modifications were analyzed in detail or in general depending upon importance, whether initial operating parameter values were required to perform operational tests and the availability of analysis time. Computer analysis programs were also developed to facilitate the evaluation of the impact that each modification had on CD performance. Pertinent analyses are presented in the following sections.

Appendix A presents the program specifications for the Common Digitizer Data List and Analysis Program. The program is designed to provide data lists and statistical information of selected "D" machine recorded scan correlated feedback data and target data. Statistical information includes calculations of the data mean, standard deviation, and autocorrelation function as well as graphical presentations of the probability density function.

5.3.1 Automatic ACE Curve Selection

5.3.1.1 Introduction

The Automatic Curve Selection technique attempts to recognize correlated clutter by counting and thresholding azimuth hits, and further counting and thresholding the first threshold crossings over a range window. If appropriate first and second threshold crossings are obtained, an ACE curve is selected to increase M/N and thus reduce false reports in correlated clutter. Since no analysis or parameter selection was supplied with the information available with this modification, considerable effort was devoted to determine optimum parameter selection and to evaluate the resulting performance.

5.3.1.2 Distribution of the Sum of Binary Quantized Correlated Video

In order to evaluate the correlation recognition capability of the ACE Auto Select mechanization, it is necessary to compute the distribution of the sum of binary quantized video under various correlation assumptions. The development follows the assumption that quantized clutter can be modeled as a binary Markov process. In particular, we define probabilities:

$$P1 = \text{Prob}\,(X_i+1 = 1 \mid X_i = 1)$$
$$P0 = \text{Prob}\,(X_i+1 = 1 \mid X_i = 0)$$
$$Q1 = \text{Prob}\,(X_i+1 = 0 \mid X_i = 1)$$
$$Q0 = \text{Prob}\,(X_i+1 = 0 \mid X_i = 0).$$

Now it can be shown that

$$P1 = (1-\rho)\,P_n + \rho$$
$$P0 = (1-\rho)\,P_n$$
$$Q1 = (1-\rho)\,(1-P_n) = 1 - P1$$
$$Q0 = 1 - (1-\rho)P_n = 1-P0$$

where ρ is the one-step correlation coefficient for the Markov process so that

$$\rho(k) = \rho^k$$

and P_n is the quantizer hit probability in noise or clutter.

Now with this model we can construct a Markov chain as shown in Figure 5.7 to represent the azimuth binary integration process with an azimuth window size of 12. Each of the Markov states shown in Figure 5.7 represent an azimuth hit count (i.e. M hits in the 12 cell window). The chain can then be iterated 12 times to provide density and distribution functions. This was performed in a computer program which modeled the chain, provided the 12 iterations and printed out density and distribution functions for various values of P_n and ρ.

An example of the density and distribution functions is shown in Figure 5.8 with P_n = .2 and ρ = 0, .5, .9 and .99. Note that the density function changes from the standard Binomial at ρ = 0 to a density with two discrete values (i.e. fm = P_n at m = 12 and fm = 1-P_n at m = 0) at high correlation.

This same data is plotted as P_{fd} (i.e. 1-Fm) in Figures 5.9 through 5.12 for P_n = .2, .1, .05 and .01 respectively and several values of ρ.

5.3.1.3 Probability of False ACE Selection in Uncorrelated Noise

The ACE auto select implementation provides double thresholding to initiate selection of alternate curves in correlated environments. The first threshold is the azimuth M/N threshold described above. The second threshold is based on a count of first threshold crossings in a range window spanning 8 cells.

In order to examine the ACE auto select capability we need to establish acceptable values of first and second thresholds. That is, we wish to select thresholds which provide low probabilities of triggering falsely the auto select logic in an uncorrelated environment since this will adversely affect target detection.

The net probability of falsely triggering the auto select can be obtained from:

$$P_{fd}\ (T_1=M,\ T_2=J) = \sum_{i=J}^{8} \binom{8}{i} (1-F_M)^i\ F_M^{8-i}$$

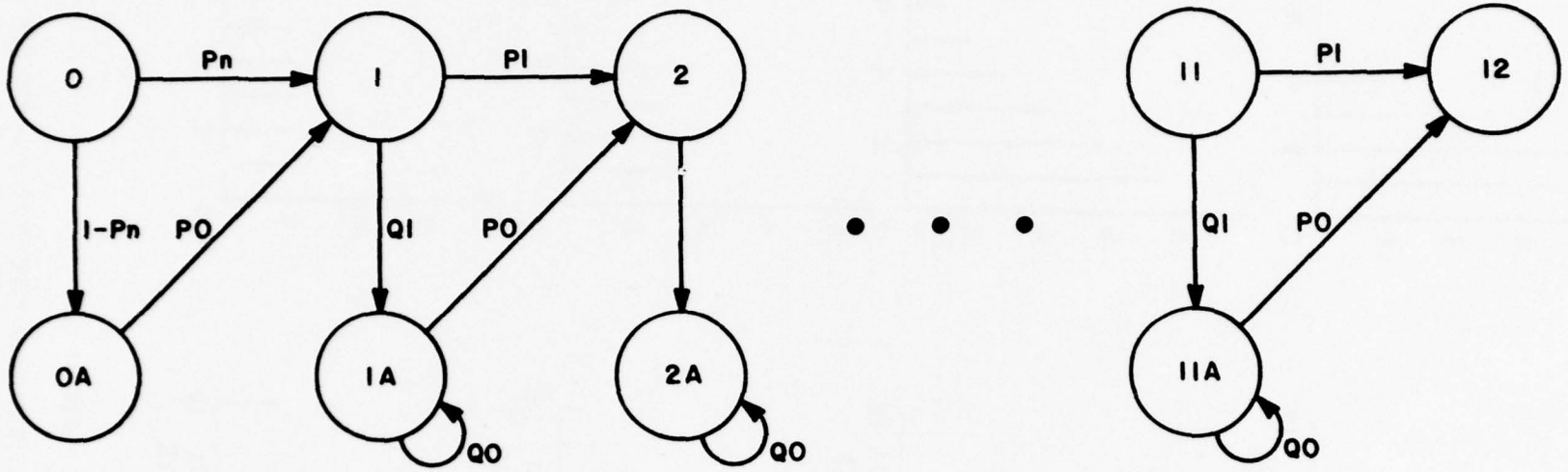

FIGURE 5.7

MARKOV CHAIN REPRESENTATION OF BINARY INTEGRATION PROCESS FOR A WINDOW SIZE OF 12

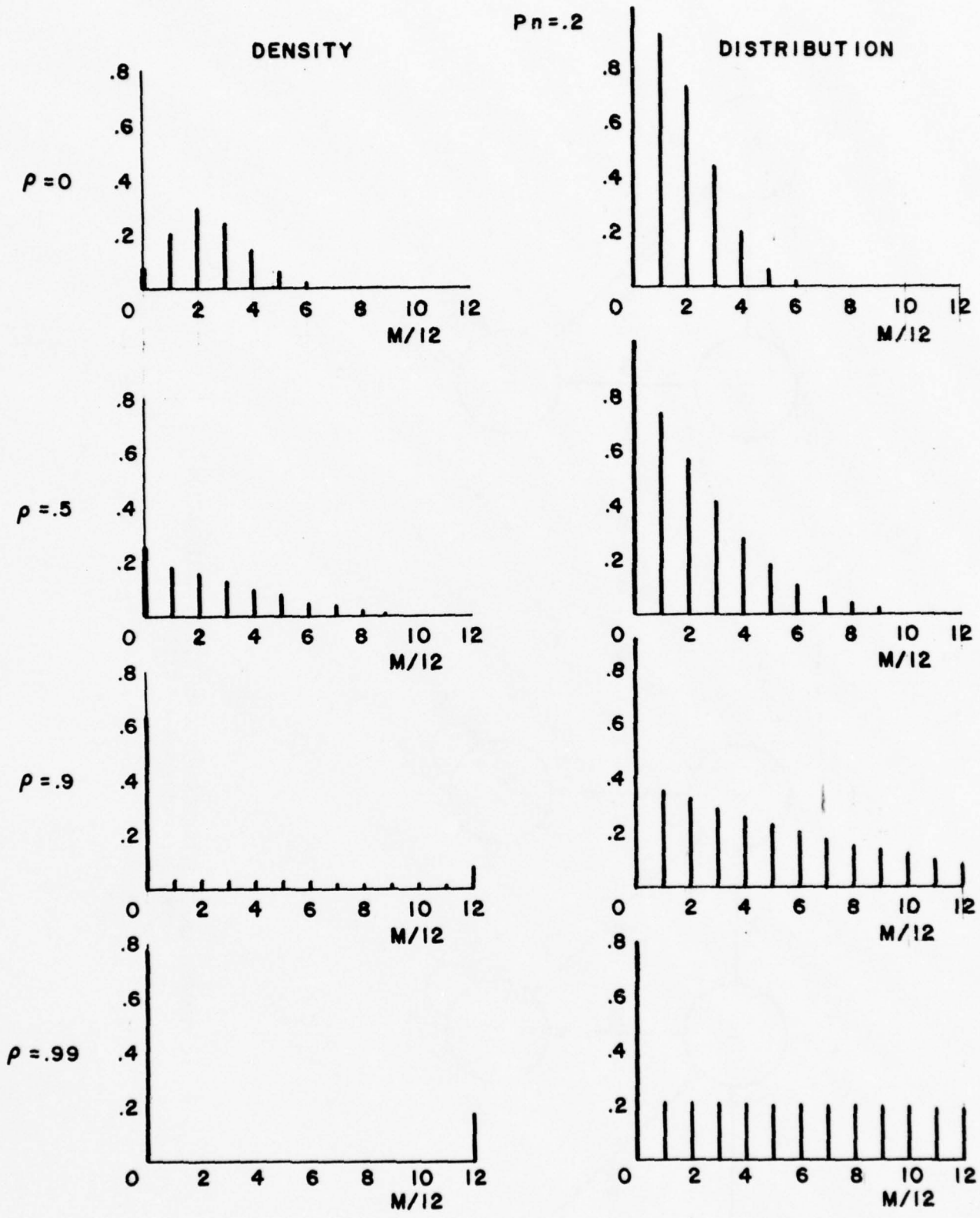

FIGURE 5.8

DENSITY AND DISTRIBUTION FUNCTIONS FOR THE SUM OF BINARY QUANTIZED CORRELATED VIDEO AT $P_n = .2$

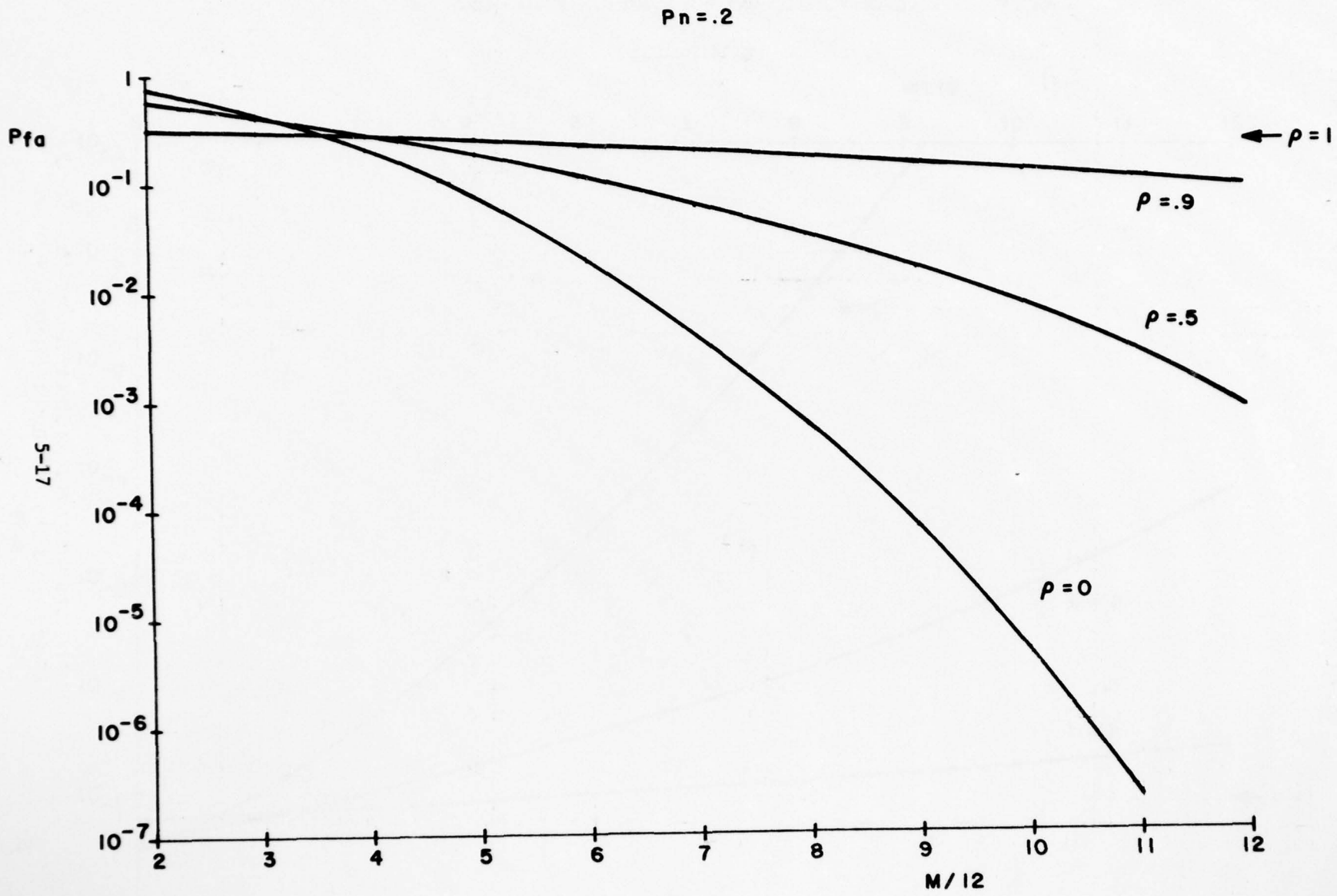

FIGURE 5.9

P_{fa} VS M FOR A M/N DETECTOR AND CORRELATED DATA (P_n = .2)

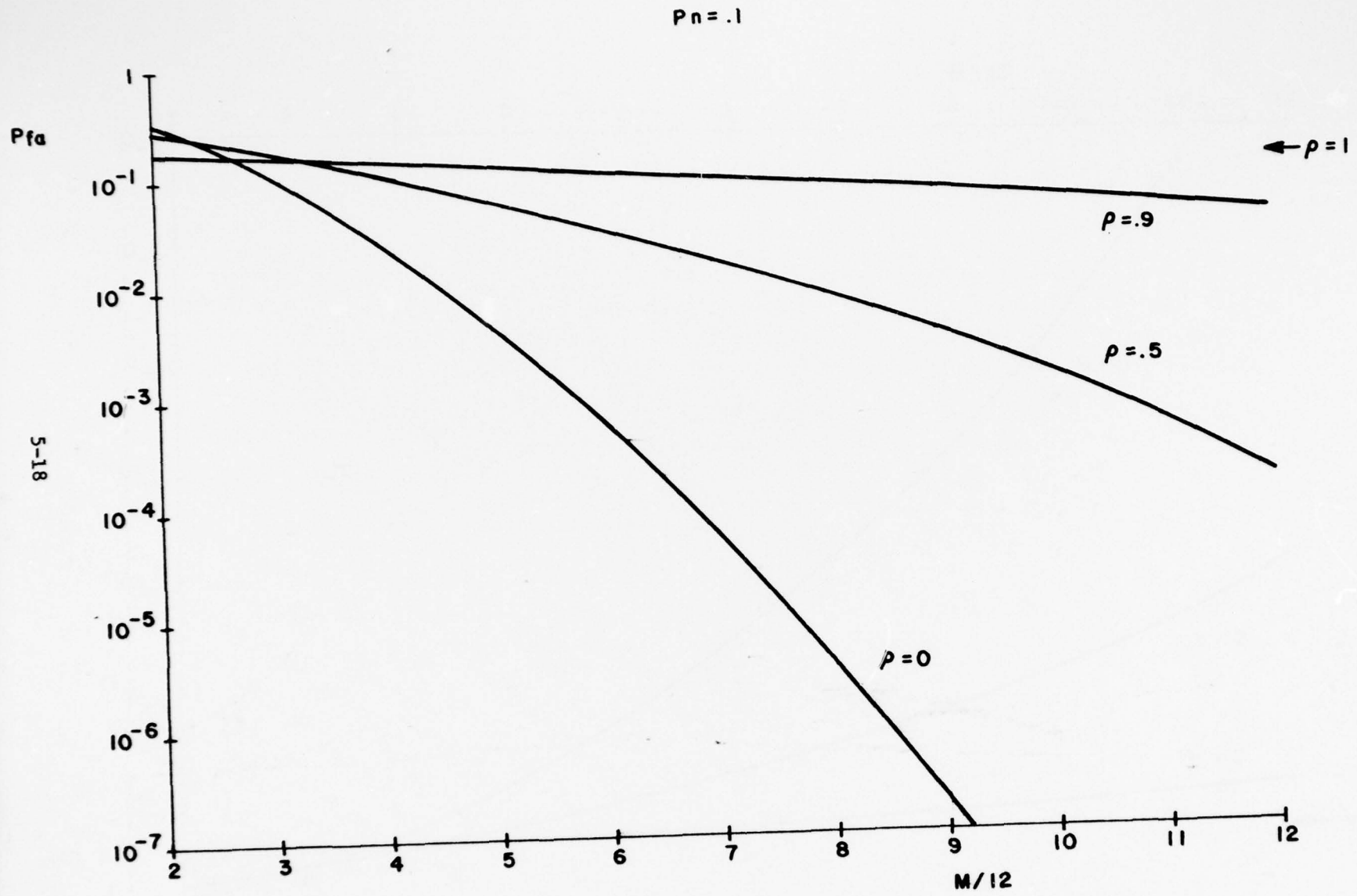

FIGURE 5.10

P_{fa} VS M FOR A M/N DETECTOR AND CORRELATED DATA (P_n = .1)

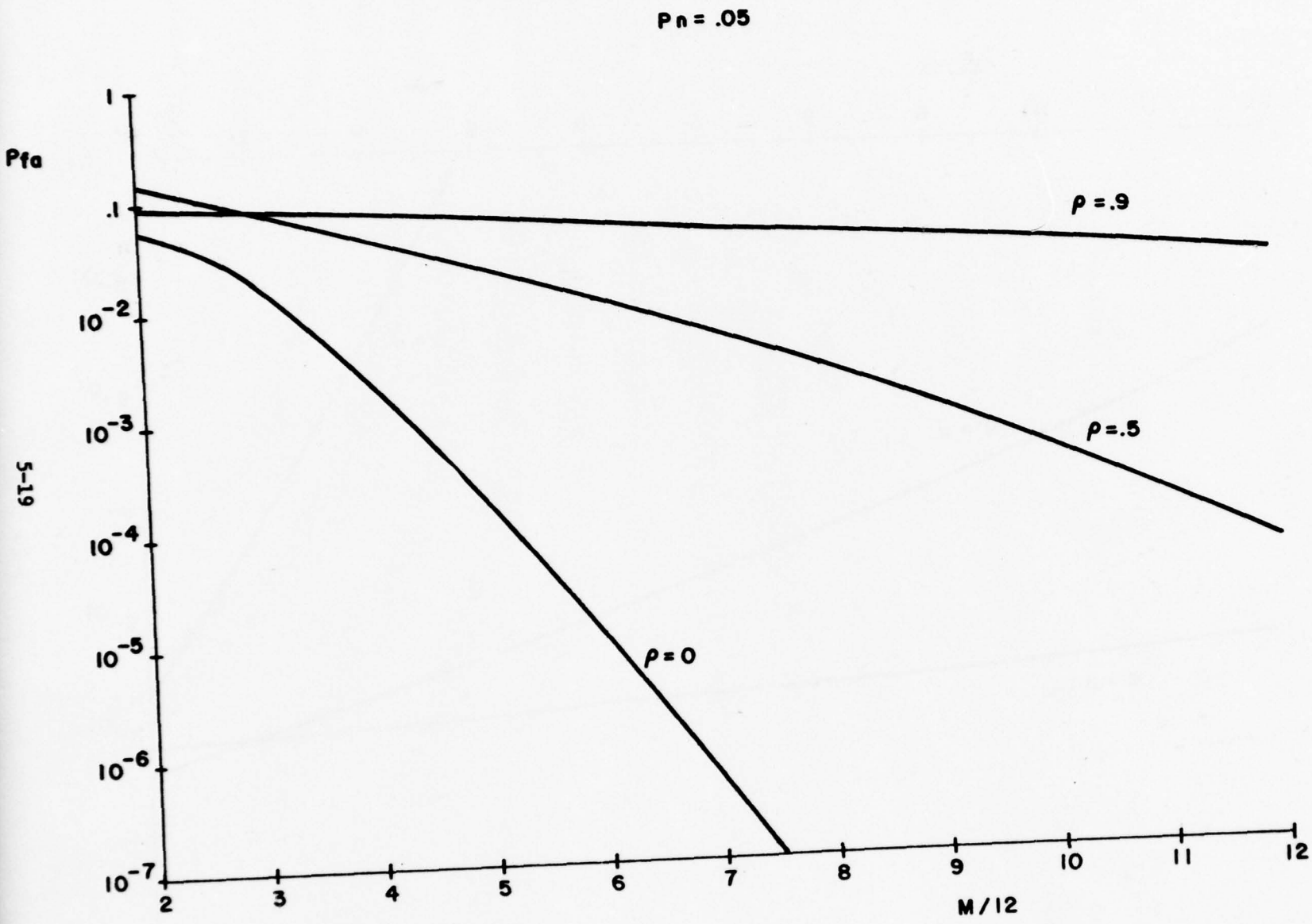

FIGURE 5.11

P_{fa} VS M FOR AN M/N DETECTOR AND CORRELATED DATA (P_n = .05)

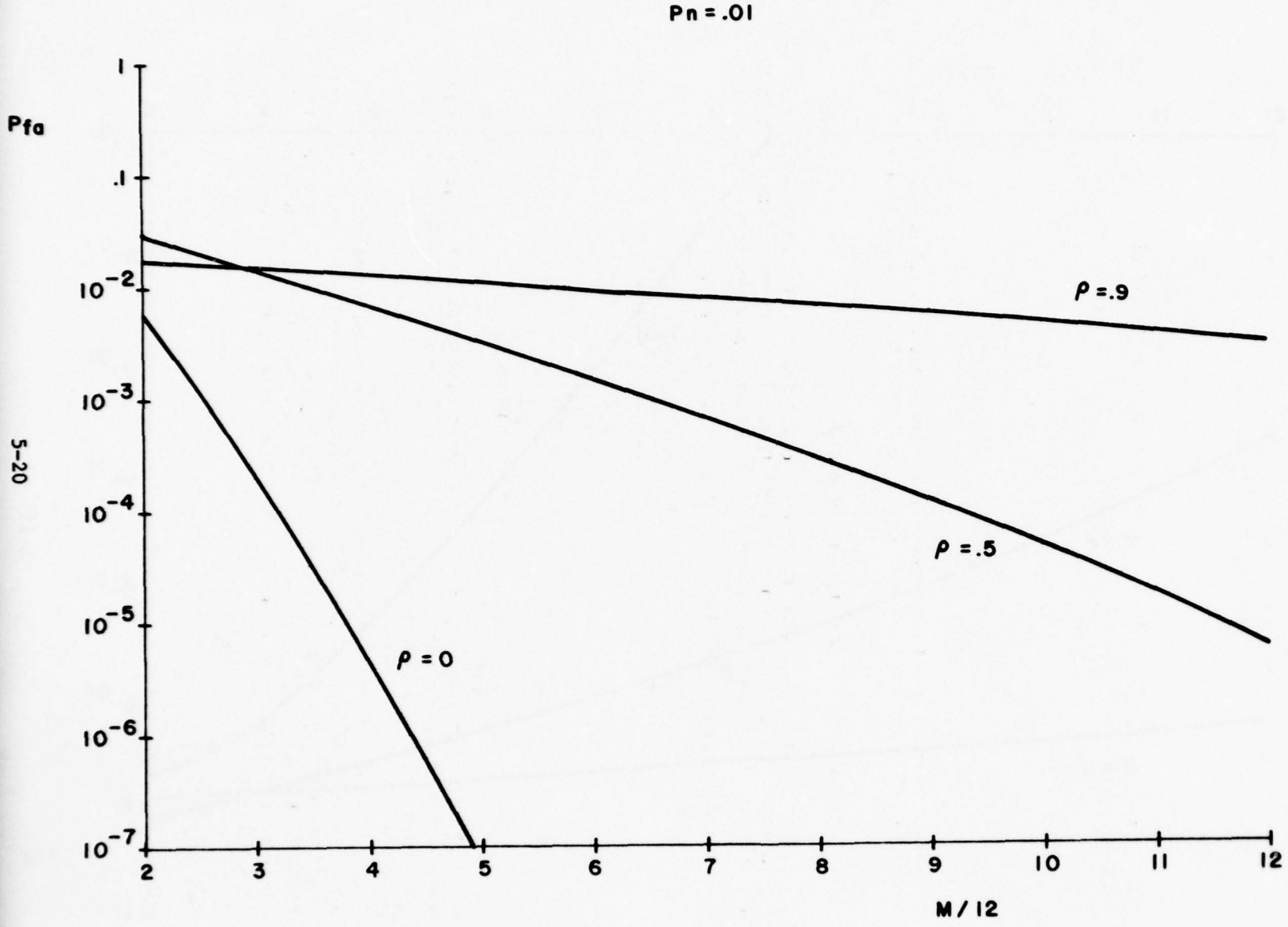

FIGURE 5.12

P_{fa} VS M FOR AN M/N DETECTOR AND CORRELATED DATA (P_n = .01)

where F_M is the distribution function (at $\rho=0$) computed above the M/12 azimuth thresholding. That is:

$$F_M(\rho=0) = \sum_{i=M}^{12} \binom{12}{i} P_n^i (1-P_n)^{12-i} .$$

The false alarm probabilities were computed and tabulated in Tables 5.1, 2, 3 and 4 for P_n = .2, .1, .05 and .01 respectively for various values of T_1 and T_2.

5.3.1.4 Acceptable Operating Thresholds

We can not select acceptable operating thresholds based on the data compiled in Tables 5.1 through 5.4 and typical operating points for target detection. If we wish to maintain a detection threshold providing a P_{fa} of 10^{-4} then leading edge thresholds (i.e. M/12) would be set at:

P_n	M/12 for $P_{fa} \simeq 10^{-4}$
.2	M=9
.1	M=7
.05	M=5 or 6
.01	M=3 or 4.

These would provide an upper limit of first threshold choice since a threshold higher than these values could allow false reports to be generated without activating the auto select logic.

Another obvious criteria is that the second threshold must be set at a value of 2 or greater. This criteria is necessary to avoid target self-suppression since target returns are included in the ACE auto select range window. It may, in fact, be necessary to increase the minimum second threshold criteria if it is found that targets of interest span more than one range cell.

$P_n = .2$

SECOND THRESHOLD / FIRST THRESHOLD	$T_2 = 1$	$T_2 = 2$	$T_2 = 3$	$T_2 = 4$
M = 4	.84	.51	.215	.1
M = 5	.45	.11	.016	.008
M = 6	.145	.01	.0004	.0003
M = 7	.03	.0004	$< 10^{-4}$	$< 10^{-4}$
M = 8	.0046	$< 10^{-4}$	$< 10^{-4}$	$< 10^{-4}$
M = 9	.0005	$< 10^{-4}$	$< 10^{-4}$	$< 10^{-4}$

TABLE 5.1

Auto Select P_{fa} for $P_n = .2$
($\rho = 0$)

$P_n = .1$

SECOND THRESHOLD / FIRST THRESHOLD	T = 1	T = 2	T = 3	T = 4
M = 2	.96	.82	.55	.27
M = 3	.61	.22	.05	.007
M = 4	.19	.017	.0009	$< 10^{-4}$
M = 5	.034	.0005	$< 10^{-4}$	$< 10^{-4}$
M = 6	.004	$< 10^{-4}$	$< 10^{-4}$	$< 10^{-4}$
M = 7	.0004	$< 10^{-4}$	$< 10^{-4}$	$< 10^{-4}$
M = 8	$< 10^{-4}$	$< 10^{-4}$	$< 10^{-4}$	$< 10^{-4}$

TABLE 5.2

Auto Select P_{fa} for $P_n = 0.1$.

($o = 0$)

$P_n = .05$

SECOND THRESHOLD / FIRST THRESHOLD	T = 1	T = 2	T = 3	T = 4
M = 1	.99	.94	.80	.55
M = 2	.64	.24	.06	.009
M = 3	.15	.01	.0004	$< 10^{-4}$
M = 4	.018	.0001	$< 10^{-4}$	$< 10^{-4}$
M = 5	.0015	$< 10^{-4}$	$< 10^{-4}$	$< 10^{-4}$
M = 6	.0001	$< 10^{-4}$	$< 10^{-4}$	$< 10^{-4}$

TABLE 5.3

Auto Select P_{fa} for $P_n = .05$

($\rho = 0$)

$P_n = .01$

SECOND THRESHOLD / FIRST THRESHOLD	T = 1	T = 2	T = 3	T = 4
M = 1	.62	.23	.05	.008
M = 2	.05	.001	$< 10^{-4}$	$< 10^{-4}$
M = 3	.0016	$< 10^{-4}$	$< 10^{-4}$	$< 10^{-4}$
M = 4	$< 10^{-4}$	$< 10^{-4}$	$< 10^{-4}$	$< 10^{-4}$

TABLE 5.4

Auto Select P_{fa} for $P_n = .01$

($\rho = 0$)

With these criteria we can then select lowest first and second threshold values which provide best auto select sensitivity with low probability of suppressing targets. The latter criteria to be used will be that probability of triggering the auto select with a single range cell target will be kept at .05 or less. The minimum values of these thresholds with all criteria applied are listed below. The P_{fa} values shown use the probability of false auto select triggering in noise and in the presence of a single range cell target.

P_n	T_1	T_2	P_{fa}(Noise)	P_{fa}(Target)
.2	7	2	.0004	.03
.2	6	3	.0004	.01
.2	5	4	.008	.016
.1	5	2	.0005	.034
.1	4	3	.0009	.017
.1	3	4	.007	.05
.05	4	2	.0001	.018
.05	3	3	.0004	.01
.05	2	5	$< 10^{-4}$	.009
.01	2	2	.001	.05
.01	1	5	$< 10^{-4}$	.008

5.3.1.5 Power of the Auto Select Test - Range Independence

To determine the effectiveness of the auto select correlation test, we compute the power of the test, defined as the probability that the test will indicate correlation (i.e. T_1 and T_2 crossed) given a value of ρ. The initial assumption is that the data in range is independent which is the usual case for most radar environments. Furthermore, we assume that the quantizer false alarm rate (P_n) is held constant.

The power of the test can then be found from

$$P\ (T_1 = M,\ T_2 = J \mid \rho) = \sum_{i=J}^{8} \binom{8}{i} (1-F_m(\rho))^i\ F_m\ (\rho)^{8-i}$$

where $F_m\ (\rho)$ is the value of the distribution function at m computed earlier for correlation coefficients ρ.

Of particular interest is the power of the test given that a first threshold crossing has occurred on one range sample. This is really the only measure of importance since if no first threshold crossing of the auto select occurs, then no target report could be generated because the auto select thresholds are always less than or equal to the leading edge thresholds. This conditional probability is found from

$$P\ (T_1 = M,\ T_2 = J-1 \mid \rho)$$

where the seocnd threshold is reduced by one to account for the first threshold crossing precondition.

Curves of the conditioned power of the auto select test or a function of correlation coefficient are shown in Figures 5.13 through 5.16 for P_n = .2, .1, .05 and .01 respectively. Notice that best performance of the auto select tests occurs for high values of P_n (i.e. P_n = .2) and low values of second threshold (i.e. T_1, T_2 = 1). Notice, also, that the test is remarkably weak overall. For example, for P_n = 0.5, the best power produced is a probability of .425. This means that even if auto select totally eliminates false alarms when correlation is recognized, the net reduction of 40% is negligible when one considers the magnitude of increase in false report rate due to correlation. Thus one might conclude that the auto select estimators will be ineffective in range independent, azimuth correlated clutter.

5.3.1.6 Auto Select Performance in Azimuth and Range Correlated Video

The full evaluation of the auto select test in environments where data is correlated in both azimuth and range is considerably more difficult than the azimuth-only case considered above. However, if we limit, the cases considered, a reasonable estimate of performance can be obtained. Therefore we limit our consideration to a typical operating point of P_n = .05. This is good choice becuase the false alarm rate is low enough that correction for moderate correlation is possible by raising the M/12 criteria.

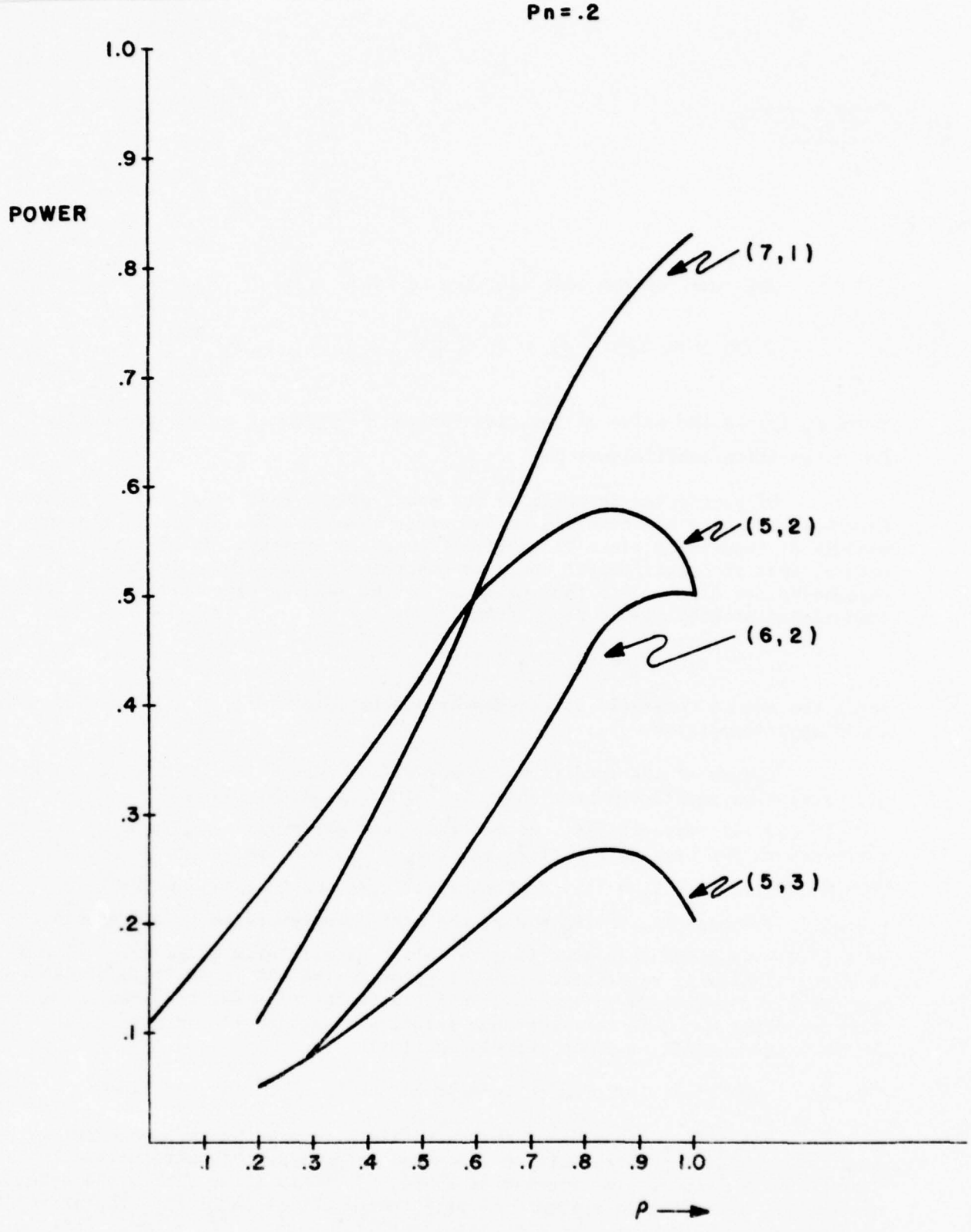

FIGURE 5.13

AUTO SELECT TEST POWER FOR P_n = .2

PARAMETER IS FIRST, SECOND THRESHOLDS (T1, T2-1)

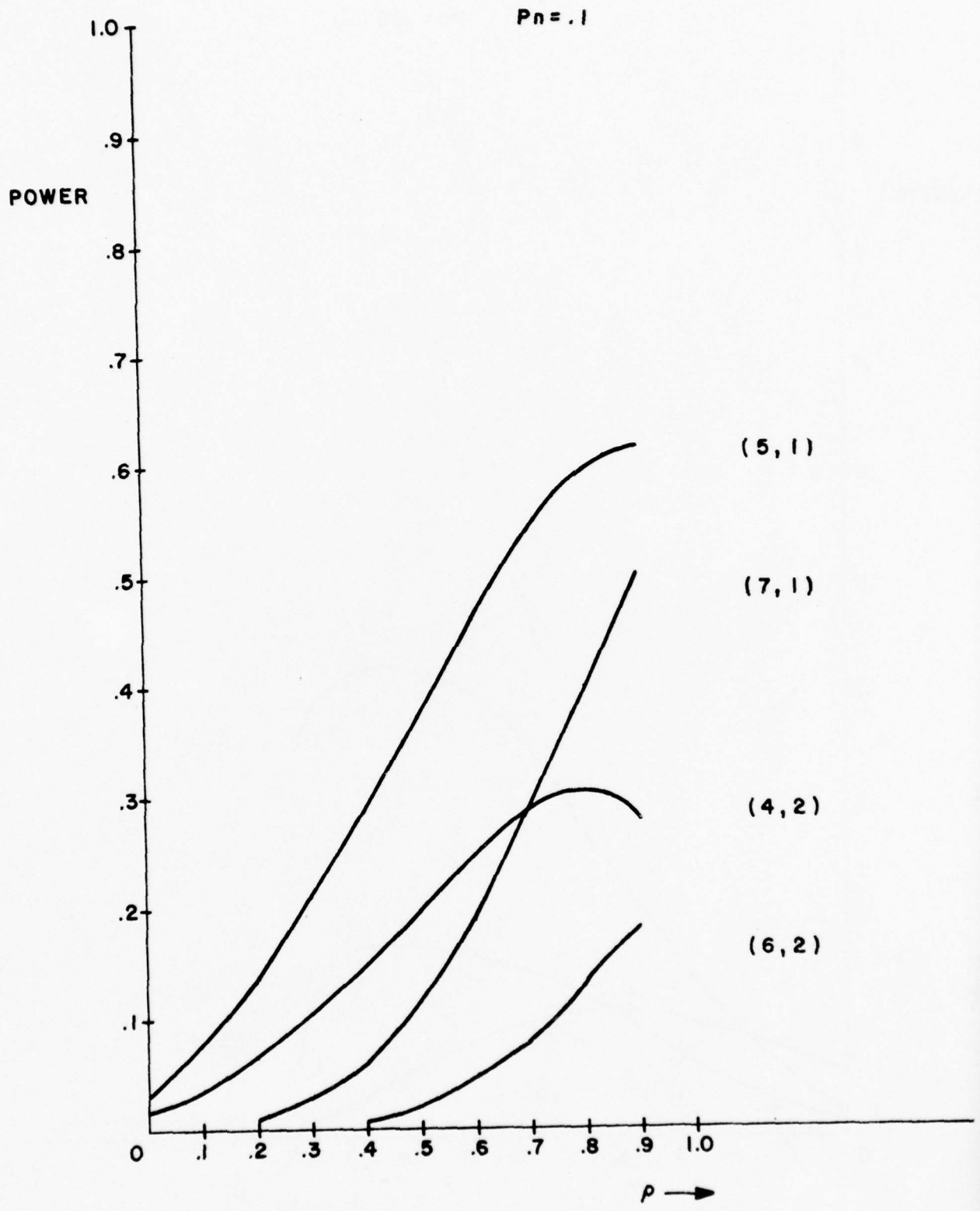

FIGURE 5.14

AUTO SELECT TEST POWER FOR P_n = .1
PARAMETER IS FIRST, SECOND THRESHOLD (T1, T2-1)

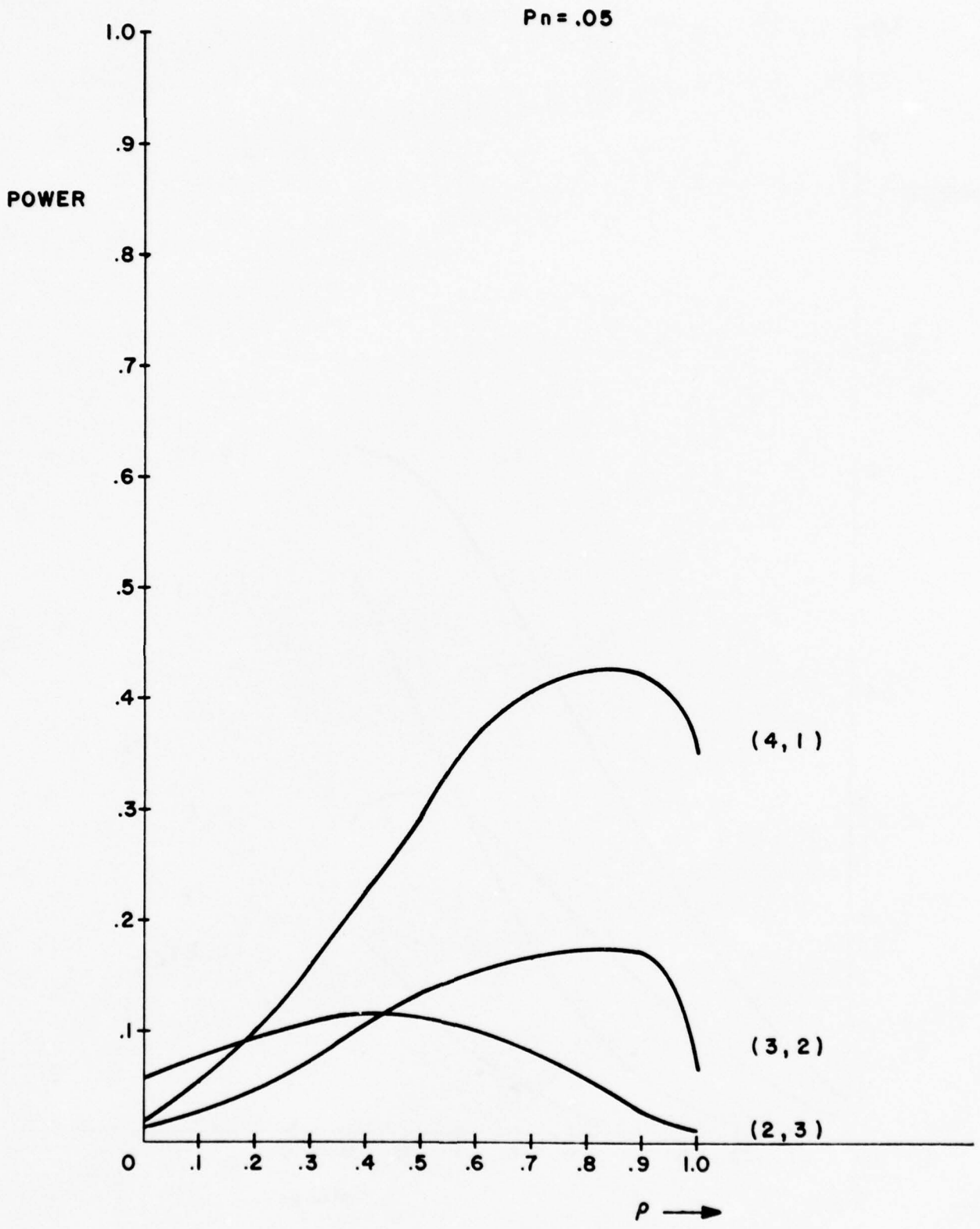

FIGURE 5.15

AUTO SELECT TEST POWER FOR P_n = .05
PARAMETER IS FIRST, SECOND THRESHOLDS (T1, T2-1)

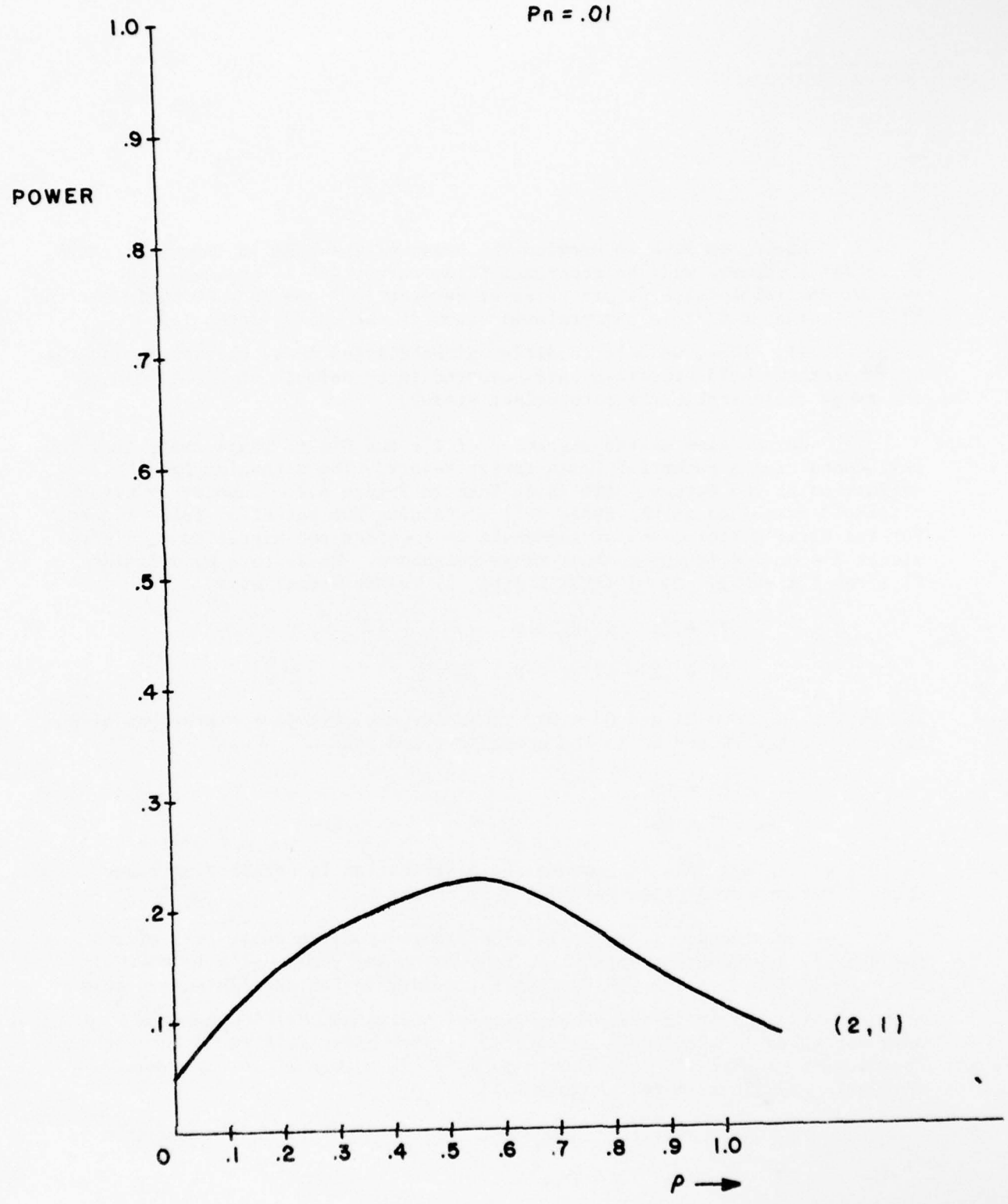

FIGURE 5.16

AUTO SELECT TEST POWER FOR P_n = .01

PARAMETER IS FIRST, SECOND THRESHOLD (T1, T2-1)

Again, we wish to examine the power of the test in important cases where false reports will be generated if no correction is applied. For typical desirable false report rates of between 10^{-4} and 10^{-5} we would set the M/12 criteria at 6/12 in uncorrelated video at the .05 P_n level (see Figure 5.11). Thus, we will condition probabilities under the assumption that 6 or more threshold crossings have occurred in an azimuth window in one of the range cells within the auto select window.

We now examine the migration of 1's and 0's to range cells near the cell containing a potential false target report. The mechanism for the evaluation is the Markov chain as defined in Figure 5.7. Suppose we have k threshold crossings in the range cell containing the potential false report. For the first k iterations of the chain we consider the migration of 1's to either 1's or 0's in the nearest range neighbors. We do this by defining P1 (Prob 1 given 1) and Q1 (Prob 0 given 1) in the normal way:

$$P1 = (1 - \rho)\, P_n + \rho$$

$$Q1 = (1 - \rho)\, (1 - P_n)$$

and by setting P0 = P1 and Q0 = Q1. Then for the next 12-k iterations of the chain we define P0 and Q0 in the normal way and let

$$P1 = P0$$

$$\text{and} \quad Q1 = Q0.$$

In this way we are able to compute the distribution in neighboring range cells under a Markov correlation assumption in range.

For example, if we begin with 7 detections in range cell of interest, the density function for detections in neighboring range cells is shown in Figure 5.17 for P_n = .05 and various range correlation coefficients. This shows clearly the increased probability of additional M/12 detections in neighboring cells with range correlations. For example if range correlation coefficient reached .99 then there would be 93% chance of seeing exactly 7 threshold crossings in neighboring cells.

Now the acceptable thresholds for P_n = .05 previously computed as

$$T1 = 4 \quad T2 = 2$$

$$\text{and } T1 = 3 \quad T2 = 3.$$

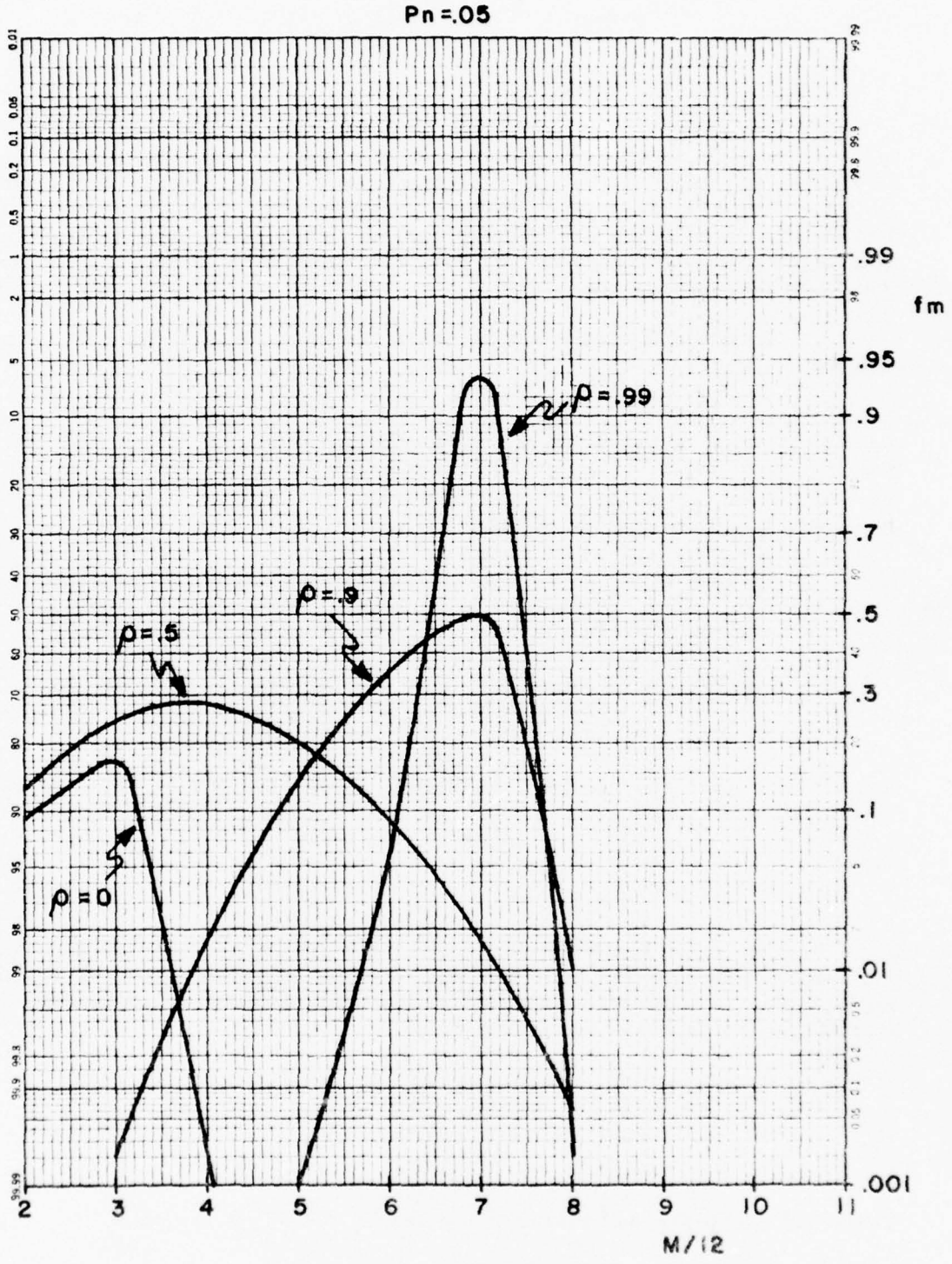

FIGURE 5.17

DENSITY FUNCTION P (EXACTLY M OF 12) FOR RANGE CORRELATED DATA WITH 7 DETECTIONS IN NEAREST RANGE CELL. (PARAMETER IS RANGE CORRELATION COEFFICIENT)

For the first case, we see that to pass the test we need one azimuth count of 4 or more in either of the nearest neighbors to the range cell which produced at least 6 detections. In the second case (T1 = 3, T2 = 3) we need at least 3 crossings in both the neighboring cells. Other cases such as less than 3 in a neighboring cell followed by more than 3 in another cell are so unlikely that they need not be considered.

To compute test power in the first case (T1 = 4, T2 = 2) we need to compute

$$\text{Power} = \sum_{k=6}^{12} P_n\,(4 \mid k)\; P\,(k \mid \geq 6)$$

where the probabilities in the sum are

$P_n\,(4 \mid k)$ = probability of obtaining at least 4 threshold crossings in a neighbor cell given k crossings in the cell producing 6 or more crossings.

$P\,(k \mid \geq 6)$ = probability of obtaining exactly k crossings in the cell producing 6 or more given that at least 6 were produced in that cell.

We recognize that the second conditional probability can be obtained from results already computed. That is

$$P\,(k \mid \geq 6) = \frac{P(k)}{1-F(6)}$$

where P(k) is the probability of obtaining k crossings under azimuth correlation and 1-F(6) is the probability of obtaining 6 or more crossings with azimuth correlation. The first conditional probability is that which we can obtain with the modified chain described above.

Because of the many steps involved we limit consideration to two cases:

(1) ρ azimuth = .5, ρ range = .5

(2) ρ azimuth = .9, ρ range = .5

Table 5.5 shows the computations for the $T_1 = 4$ $T_2 = 2$ case.

Case 1 $\rho_{az} = .5$, $\rho_{range} = .5$

k	P (k | 6 or more)	P (≥ 4 | k)
6	.5317	.4373
7	.2579	.586
8	.1204	.709
9	.0539	.803
10	.0228	.870
11	.010	.93
12	.0033	.98

$$\Sigma\ P\ (k \mid \geq 6)\ P\ (\geq 4 \mid k) = .545$$

Case 2 $\rho_{az} = .9$, $\rho_{range} = .5$

k	P (k | 6 or more)	P (≥ 4 | k)
6	.5317	.148
7	.2579	.130
8	.1204	.114
9	.0537	.099
10	.0228	.086
11	.010	.075
12	.0033	.347

$$\Sigma\ P\ (k \mid \geq 6)\ P\ (\geq 4 \mid k) = .716$$

TABLE 5.5

Calculations for Range and Azimuth Correlations with $T_1 = 4$, $T_2 = 2$ or the probability in either cell. Thus

Power ($\rho_{az} = .5$, $\rho_{range} = .5$) = .792

Power ($\rho_{az} = .9$ $\rho_{range} = .5$) = .92

The probabilities shown in the table are for nearest neighbor cells. Since either nearest neighbor is acceptable we compute the net power as:

$$\text{Power} = \geq 2P - p^2.$$

for $T_1 = 4$, $T_2 = 2$. Thus we can reject up to 79% and 92% of false reports for the respective correlations with this test.

The same calculations were done for the other acceptable thresholds $T_1 = 3$, $T_2 = 3$ but the calculations are not shown in detail. The results are

$$\text{Power } (\rho_{az} = .5, \rho_{range} = .5) = .63$$

$$\text{Power } (\rho_{az} = .9, \rho_{range} = .9) = .83$$

Thus, with correlation assumption the first thresholds ($T_1 = 4$, $T_2 = 2$) would be preferred. If we used these thresholds up to 10 to 1 and 5 to 1 reduction in false reports could be achieved in highly and moderately correlated clutter respectively. However, if target spreading in range is a problem, the second, less efficient threshold net would be preferred.

5.3.1.7 Summary and Conclusions

The analysis of the Automatic ACE Curve Selection modification indicates that the technique will be only modestly successful. Correlation effects can cause the P_{fa} to increase from 10^{-5} to 10^{-2}. This results in a large increase in the number of false targets per scan; e.g. from 80 to 1000. If clutter is correlated in azimuth but not in range, the estimator is particularly weak. At best a 2 to 1 reduction in false reports could be expected. This is relatively insignificant compared to the very large increases in false reports due to correlation, i.e. the system overloads with 500 or 1000 false targets.

If clutter is correlated in both azimuth and range, somewhat better results will be obtained. For strong correlation a 10 to 1 false report reduction might be achieved while a 5 to 1 reduction is possible in moderately correlated clutter. A 10 to 1 and 5 to 1 reduction keeps the number of false targets close to the number obtained under non-correlated conditions.

It should be noted that these results assume ideal conditions of thresholds chosen to match a well regulated hit probability. Changes in the hit probability modify the auto select operation considerably. In addition if target reports spread in range they may trigger auto select thresholds. If this occurs,suboptimal thresholds must be chosen - this would further reduce the performance of the technique.

5.3.2 Scan Correlated Feedback Control of the Rank Quantizer

One modification to the Common Digitizer at Elwood, New Jersey is the addition of a rank quantizer with a bias controlled by scan correlated feedback (SCF). The rank quantizer will accept as input either linear or log video. The video is fed into an analog delay line with 24 taps. The center tap is adjusted by a variable bias and then compared to the other taps to determine its rank. If this rank exceeds the preset reference rank, then a hit has occurred. This hit is, then, input to a M/N binary azimuth integrator which outputs target reports. For analysis purposes a radar having a range coverage of 200 nmi and 4096 sweeps (pulses) per antenna scan was assumed. It was also assumed that the combined effect of the video synchronizer, hit width discriminator and timing circuits produces a false hit rate into the M/N azimuth integrator roughly equal to the quantized false hit rate P_n.

Three analyses were made to determine the effectiveness of the SCF loop in maintaining a well-regulated false alarm rate. The analyses performed were:

- Appraisal of Scan Correlated Feedback Technique
- Estimate of Scan Correlated Feedback Detection Loss
- Performance of Scan Correlated Feedback in Non-Rayleigh Clutter with the use of Guard Bands.

These analyses are discussed in the following sections.

5.3.2.1 Appraisal of Scan Correlated Feedback Technique

5.3.2.1.1 SCF Mechanization

The ARSR-2 en route radar coverage is divided into 4096 zones. Each zone extends 4 nmi in range and 64 ACP's in azimuth. With .25 nmi range cells, there will be 1024 hit opportunities per zone. The video quantizer monitor collects, for each zone, a hit density count. This count is simply the number of hits occurring in the given zone.

Figure 5.18 illustrates the rank quantizer with the SCF bias control. Closed loop control of P_n, the probability of a hit occurring in a given range cell, is accomplished by feeding back the zone hit density count. The feedback path is implemented in "D" machine software. For each zone, the "D" machine accepts the hit density count as input and generates as output a 5 bit control word. This control word is used to provide the variable bias for the center tap video. The quantizer can process either linear or log video by switching the bias function from an additive bias (log video) to a multiplicative bias (linear video). Biasing the center tap downward by either manner will decrease the hit probability P_n. The closed loop system is referred to as scan correlated feedback (SCF).

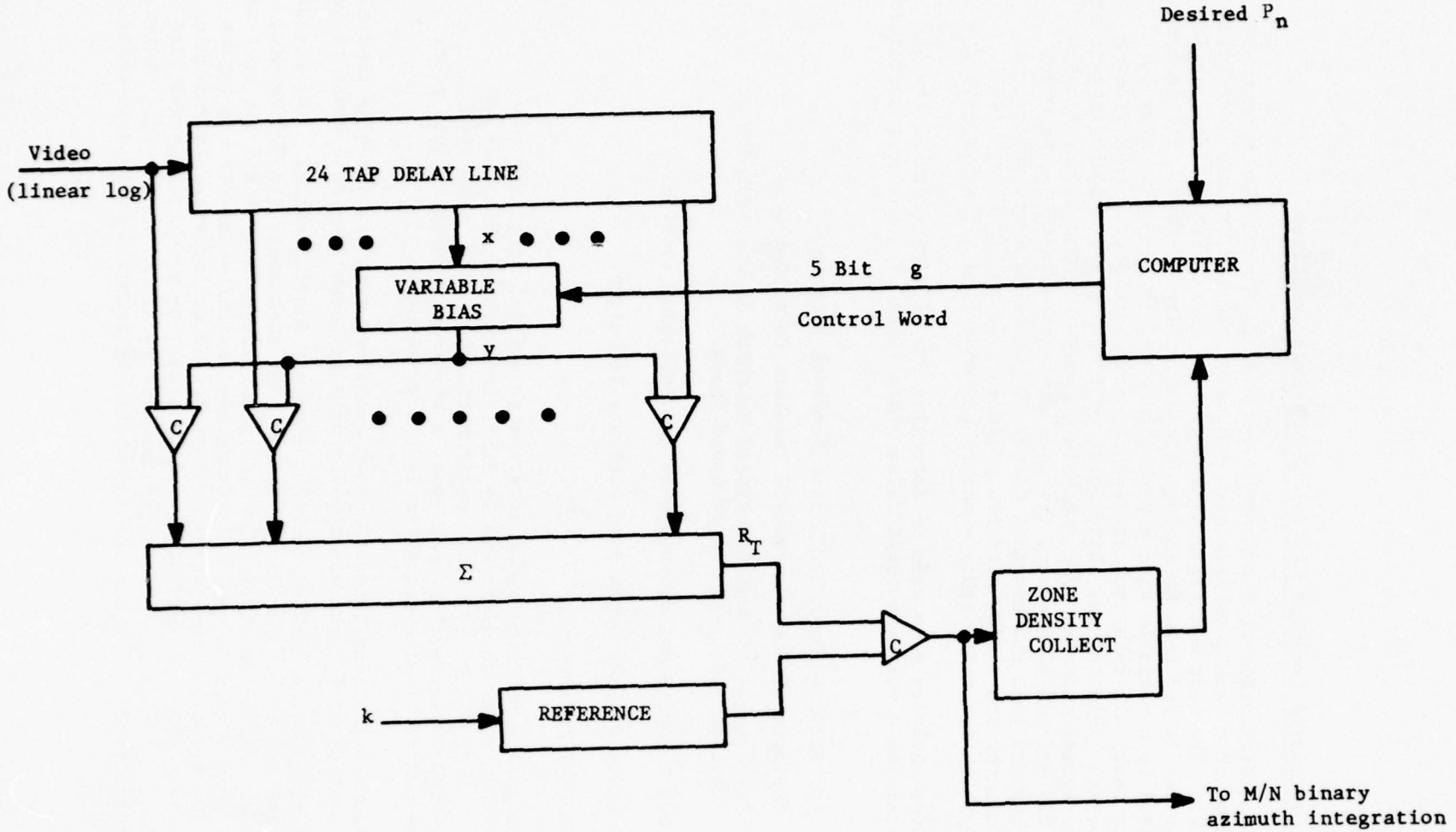

RANK QUANTIZER WITH SCAN CORRELATED FEEDBACK

FIGURE 5.18

5.3.2.1.2 Variable Bias Implementation

The quantizer is non-parametric in the sense that with zero bias the probability, P_n, of a false hit is independent of the distribution of the radar video. In the case of zero bias, the summer pictured in Figure 5.18 computes the rank, R_T, of the center tap among N + 1 = 25 video samples. Assuming the video is stationary for the 24 μsec duration, it is no more likely that the center tap has one rank between 1 and 25 than any other.

So

$$P[\text{hit}] = P_n = P[R_T > k] = \sum_{i=k+1}^{N+1} P[R_T=i] = \frac{N+1-k}{N+1}$$

Clearly P_n is independent of the distribution of the video.

In the general case, when there is some bias, the quantizer is no longer non-parametric. For example, when the input is log video, then the delay line samples are log-Rayleigh random variables. If the bias $\left(K_{log}\right)$ is an offset:

$$y = x - K_{log};\ K_{log} > 0$$

then P_n has been calculated in Reference 25:

$$P_n = \frac{N(N-1)(N-2)\ \ldots\ (N-k+1)}{(N+e^{2K_{log}})\ (N+e^{2K_{log}-1})\ldots\ (N+e^{2K_{log}-k+1})}$$

A similar calculation may be done for the case of linear video. The samples are, then, Rayleigh distributed and the bias $\left(K_{lin}\right)$ is of the form

$$y = K_{lin}x\ ;\ 0 < K_{lin} \leq 1$$

The corresponding probability of a hit in noise is:

$$P_n = \frac{N(N-1)(N-2)\ \ldots\ (N-k+1)}{(N+1/K_{lin}^2)(N+1/K_{lin}^2-1)\ \ldots\ (N+1/K_{lin}^2-k+1)}$$

Note that in both cases the processor is CFAR since although P_n now depends on the distribution of the video samples, if that distribution is Rayleigh or log-Rayleigh then P_n is independent of the Rayleigh parameter.

The biases K_{log} and K_{lin} are controlled by the 5 bit gain word, g, providing closed loop control of P_n. The specific bias implementations described in Reference 24 will produce biases that are linear functions of g:

$$K_{log} = ag + b \quad ; \quad g = 0, 1, \ldots, 31$$

$$K_{lin} = cg + d \quad ; \quad g = 0, 1, \ldots, 31$$

The constants (a, b, c, d) can be adjusted to set a desired range of P_n values by setting the ranges of K_{log} and K_{lin}. In the log case, b must be set to zero while a will vary depending on which base logarithms are used and on any scaling of the video between the log transformation and the variable bias.

The hits generated by the rank quantizer are required to pass an M/N azimuth correlation requirement before becoming target reports. This M/N requirement reduces the probability of a false hit, P_n, to the probability of a system false alarm P_{fa}. The ratio P_n/P_{fa} is a decreasing function of ρ_{IF} the azimuthal clutter correlation. For example, as $\rho_{IF} \to 1$, $P_{fa} \to P_n$ so to prevent P_{fa} from rising P_n must be lowered to 10^{-5}. But closed loop control cannot be maintained by SCF when $P_n < 10^{-3}$ since changes in P_n will have no affect on the most likely zone density count (zero). Although some form of open loop control might be used to stabilize P_n at values less than 10^{-3}, closed loop control is prohibited by the sample size and single scan memory implementation. Thus P_n is limited to values between $(N + 1 - k)/(N + 1)$ and 10^{-3}.

5.3.2.1.3 Accuracy of SCF Control Loop in Uncorrelated Clutter

The feedback gain, g, used to set the variable bias is a 5-bit word. Thus, with either linear or log video, only 32 equally spaced biases are available. This section estimates the fineness of control of P_n which can be achieved with SCF under this constraint. The primary tradeoff is fineness of control versus range of P_n desired since the control words can always be spaced more closely by giving up the capability for low P_n values. In view of the necessity for a very low P_n in highly correlated clutter, it will be assumed that control of P_n over the entire feasible range ($(N+1-k)/(N+1)$ to 10^{-3}) is desired.

The rank quantizer can be thought of as computing the center tap rank in order to estimate the Rayleigh parameter and then using this estimate to provide CFAR thresholding with the bias considered to be a threshold. Reference 25 derives the reference rank k which will provide the rank quantizer with the most efficient (minimum variance) estimate of the video Rayleigh parameter. Although these reference ranks are computed only for N between 1 and 20, the data may be extrapolated to the case N = 24 giving as the most desirable operating point k = 20. Suppose it is desired to have the P_n range $(N+1-k)/(N+1)$ to 10^{-3} for k values in some operating band about k = 20, say k = 17 to 24. Then, for fixed K_{lin} or K_{log}, P_n is a decreasing function of k so that for log video the desired operating range will be assured if the maximum bias

$$K_{log}(max) = ag(max)+b \qquad g=0,1,\ldots,31.$$

satisfies

$$\left.\frac{N(N-1)(N-2)\ldots(N-K+1)}{(N+e^{2K_{log}})(N+e^{2K_{log}-1})\ldots(N+e^{2K_{log}-K+1})}\right| \leq 10^{-3}$$

$$N=24,\quad k=17,\quad K_{log} = K_{log}(max)$$

The approximate solution of this equation is K_{log} (max) $\geq$ 1.0 (when a = 1). This implies a minimum quantization step for K_{log} of about 1/32 = .03125. Figure 5.19 shows the 32 P_n values obtainable for this choice of K_{log} (max). This curve will shift to the right or left depending on the operating value k which is selected. In the region P_n = .2, the quantization factor for P_n is:

$$K_S = P_n(g-1)/P_n(g) \simeq 1.1$$

This factor increases with decreasing P_n until $K_S \simeq 1.4$ at $P_n = 10^{-3}$.

Performing the identical procedure for linear video, gives K_{lin} quantized in steps of .0203 and varying between 1 and .35. The corresponding quantization factors vary between $K_S \simeq 1.07$ for P_n = .2 and $K_S \simeq 1.4$ for $P_n = 10^{-3}$. Since the quantization of P_n in linear video is so similar to that in log video, only the log video case need be analyzed for SCF accuracy.

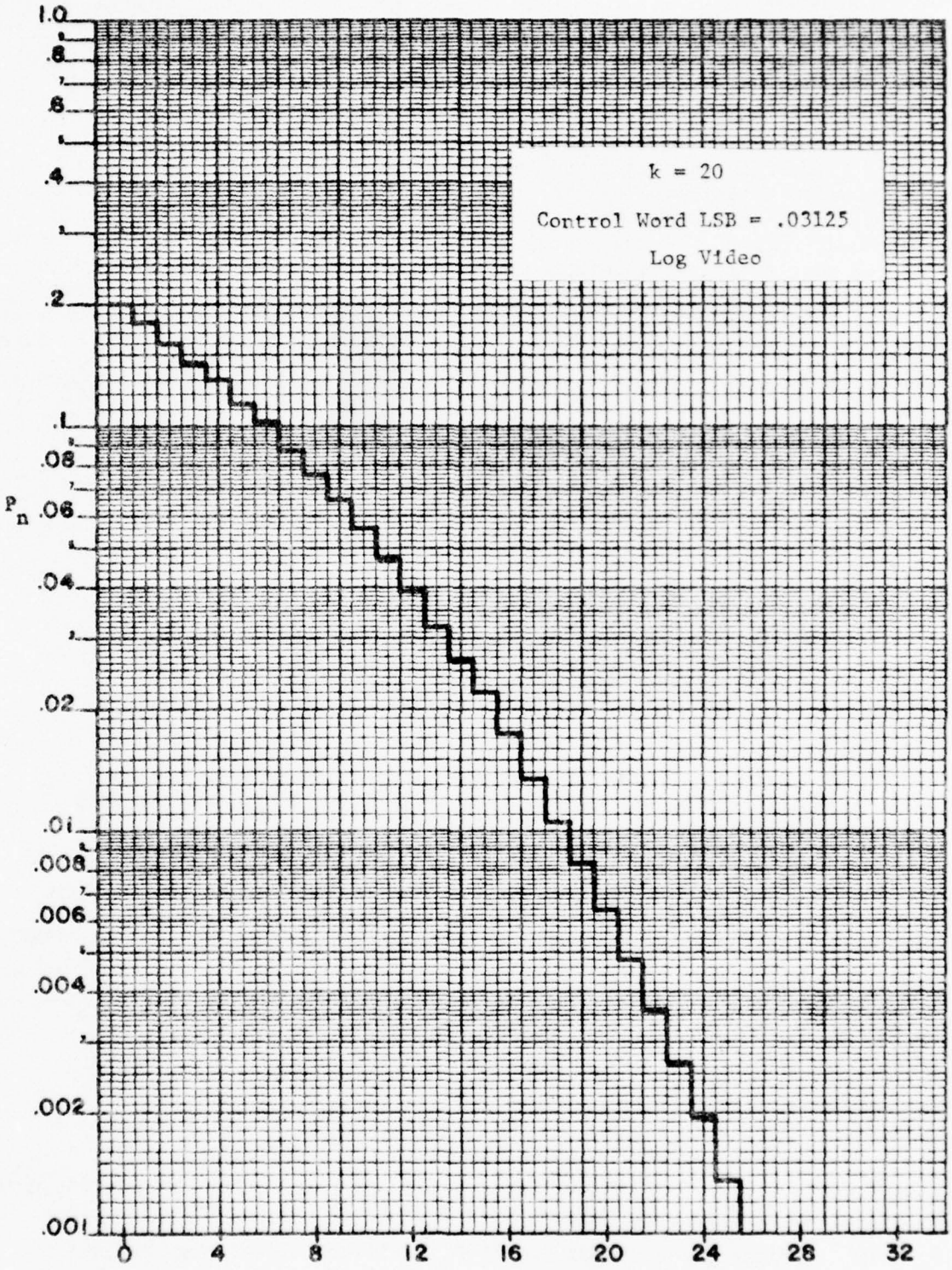

QUANTIZATION OF HIT PROBABILITY P_n

FIGURE 5.19

In Reference 27, a feedback loop used to control the threshold of a sample mean AVP is analyzed. Both dynamic and steady state characteristics of the closed loop system are investigated. The steady state characterization is accomplished by modeling the system as a Markov chain, deriving the state transition probabilities, and then iteratively computing the steady state Markov probabilities. Since each state corresponds to a specific false alarm probability, the profile of steady state probabilities specifies the steady state probabilities of the various possible false alarm rates. The extent to which this profile constrains the actual probability of false alarm to lie in a narrow band about the desired probability of false alarm is a measure of the fineness of the loop's control.

The same analysis may be applied to the SCF loop to specify its steady state performance in noise or uncorrelated clutter. Each of the 32 possible gain words g_i corresponds to a Markov state S_i. The software SCF decision logic presented in Reference 24 simply increments g if the zone density P_n exceeds that desired ($P_{n,ref}$), and decrements g if $P_n < P_{n,ref}$. The probabilities of these state transitions are calculated by assuming noise or uncorrelated clutter which makes each zone density count a binomial random variable with mean $1024\ P_n$ and variance $1024\ P_n(1-P_n)$.

Once the state transition probabilities are known, the chain can be iterated to compute the steady state probability of each state. Figure 5.20 shows the log video steady state probabilities of 9 gain words in the case where one of the gain words corresponds exactly to the desired zone density. That is, $P_n\ (g_o) = P_{n,ref}$. Figure 5.21 illustrates the case where the desired zone density falls in between two gain words: $P_n\ (g_o + 1/2) = P_{n,ref}$. In both cases, SCF holds P_n to within 20 - 30% of the desired value (about 2-3 LSB's). Finer control of P_n could be obtained by allowing a larger "dead zone" (values for hit density count for which g is not changed) at the expense of loop dynamic response characteristics (Reference 27).

It is now possible to estimate the fineness of control of P_{fa}, the probability of an M/N detection. P_{fa} is a monotonic increasing function of P_n and a decreasing function of the azimuthal clutter correlation ρ_{IF}. For the case $\rho_{IF} = 0$ (uncorrelated clutter or noise), the M/12 requirement gives

$$P_{fa} = \sum_{i=M}^{12} \binom{i}{12} P_n{}^i (1-P_n)^{12-i}$$

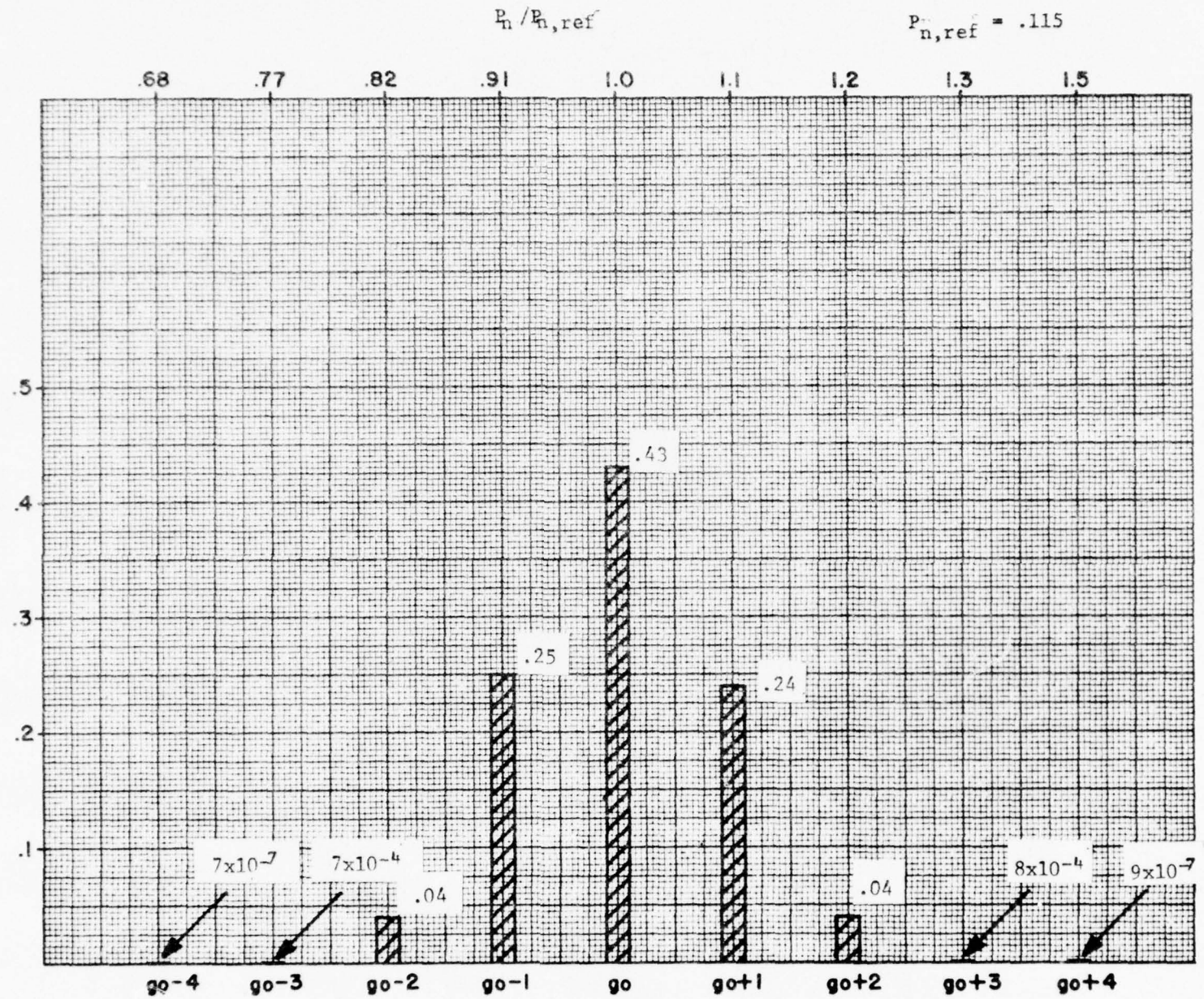

STEADY STATE MARKOV PROBABILITIES WITH $P_{\Pi}(\mathcal{E}_{\Phi}) = P_{n,ref}$

FIGURE 5.20

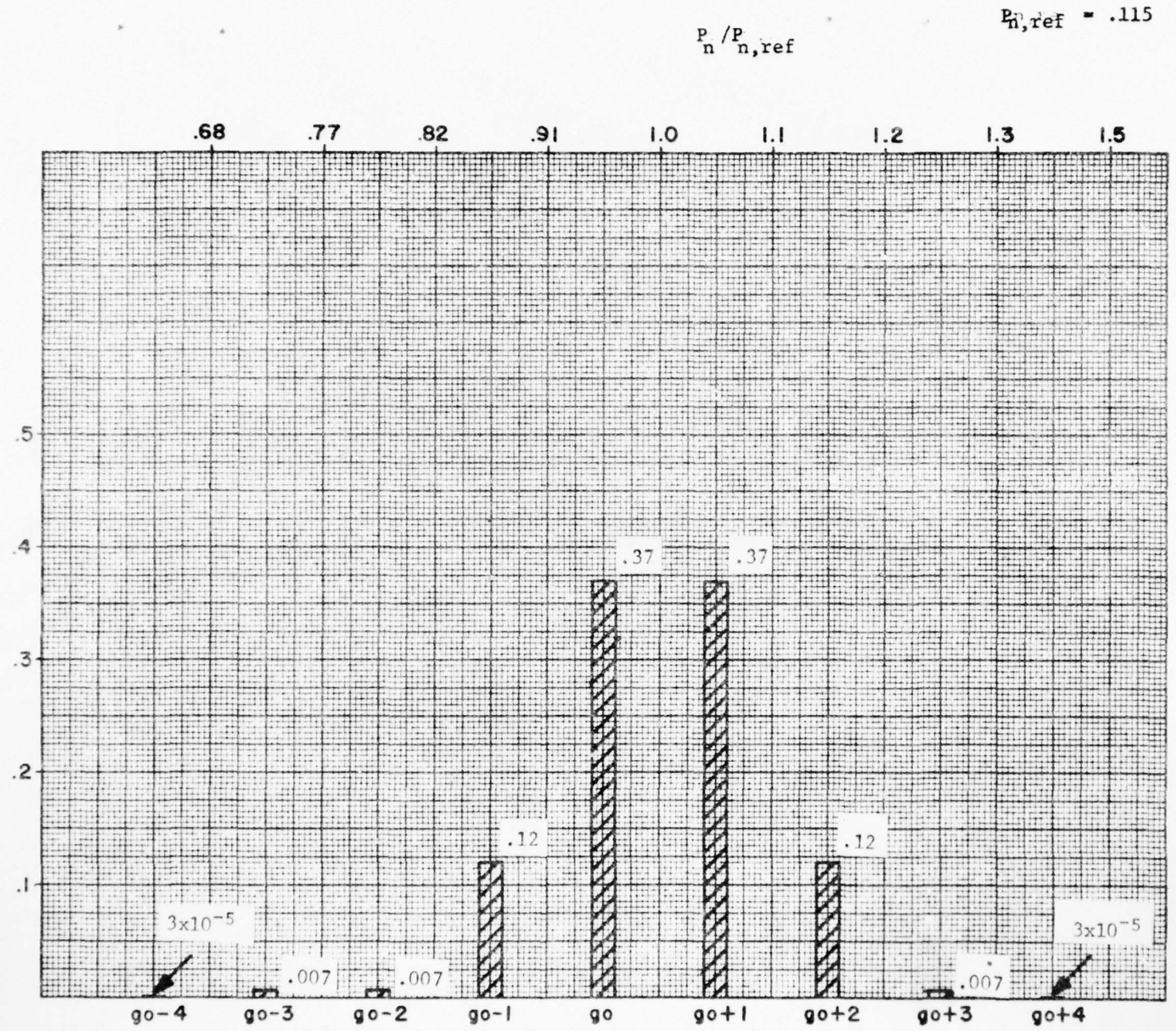

STEADY STATE MARKOV PROBABILITIES WIHT P_n $(g_0 + \frac{1}{2}) = P_{n,ref}$

FIGURE 5.21

The quantization levels of P_{fa} for log video are plotted in Figure 5.22 M/N=8/12. Control of g to 2 or 3 LSB's corresponds to control of P_{fa} to within about an order of magnitude in uncorrelated clutter.

5.3.2.1.4 Accuracy of SCF Loop in Correlated Clutter

Since P_{fa} is an increasing function of ρ_{IF}, as the clutter becomes correlated, the CD must respond in some way to keep P_{fa} from rising. Two responses are possible: 1) The ACE automatically increases the M in the M/N requirement; or, 2) P_n is lowered manually. Either of these responses will decrease P_{fa}. However, both have limitations. In particular, the M/N requirement cannot be made more stringent than 12/12 and P_n cannot be lowered below 10^{-3}. In addition, since P_n cannot be controlled individually for each zone, when P_n is lowered manually a detection loss is suffered for targets in clear regions of the radar's coverage.

Let ρ_{IF} be the azimuthal clutter correlation at IF and ρ_Q be the azimuthal correlation of the quantized video out of the rank quantizer. The relation between ρ_Q and ρ_{IF} is plotted in Reference 28 . Assuming the Markov model for correlated clutter (Reference 29) a lower bound on P_{fa} for a given ρ_Q is

$$P_{fa} \geq P_{fa_{12/12}} = P_n \left[(1-\rho_Q)\, P_n + \rho_Q\right]^{11}$$

As $\rho_Q \to 1$, then $P_{fa} \to P_n$. Thus, in heavily correlated clutter, P_{fa} must be controlled by adjusting P_n. If the detection loss associated with lowering P_n is deemed too high or if ρ_{IF} is so large that P_n must be lowered below 10^{-3}, then a high false alarm rate must be accepted.

Consider the following example of SCF performance in correlated clutter. Suppose a system false alarm probability of 10^{-5} is desired and that the desired P_n value has been set at .1. There are four cases to consider:

Case 1 ($\rho_{IF} = 0$) The SCF system performs as described in Section 5.3.2.1.2; P_n is held to within 20 - 30% of the desired value.

Case 2 ($0 < \rho_{IF} < .7$) P_n is still set at .1. $P_{fa} = 10^{-5}$ can be maintained by the ACE increasing M in the M/12 requirement. SCF suffers a small degradation of accuracy as ρ increases.

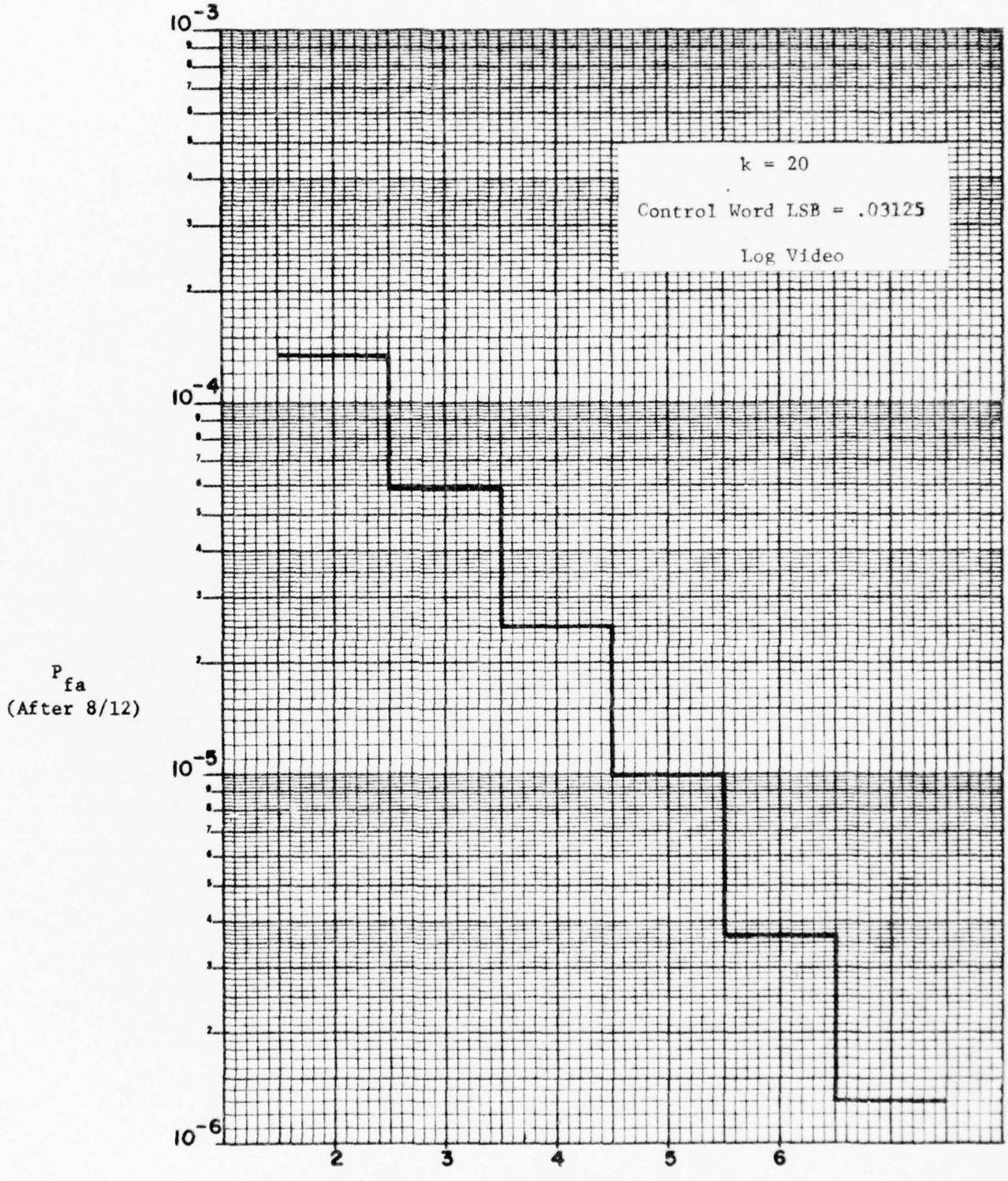

QUANTIZATION OF SYSTEM FALSE ALARM PROBABILITY P_{fa}

FIGURE 5.22

Case 3 ($.7 \leq \rho_{IF} < .9$) With $P_n = .1$, $P_{fa} = 10^{-5}$ cannot be maintained by the ACE even if a 12/12 requirement is imposed. In order to maintain $P_{fa} = 10^{-5}$, P_n must be lowered manually. As $P_{n,ref} \rightarrow 10^{-3}$, accuracy of SCF control of P_{fa} actually improves, but a detection loss occurs for targets in the clear.

Case 4 ($\rho_{IF} > .9$) $P_{fa} = 10^{-5}$ cannot be maintained using SCF.

As noted in Case 2, an increase in ρ_{IF} results in a decrease in SCF accuracy. The decrease is attributable to an increase in the variance of the zone density count by a factor of (Reference 29):

$$1 + \frac{2\rho_Q}{L}\left(\frac{L}{1-\rho_Q} - \frac{1-\rho_Q^L}{(1-\rho_Q)^2}\right)$$

where L = 64 is the number of sweeps (pulses) ACP's per zone.

Figure 5.23 illustrates the effect of clutter correlation on the fineness of SCF control. The steady state probabilities of various P_n's are plotted for the case $\rho_{IF} = .7$ ($\rho_Q = .36$). This is a point on the boundary of Cases 2 and 3 and so represents a worst case for Case 2 SCF accuracy. Notice that the clutter correlation results in only a slight broadening of the distribution of P_n values. Thus for $\rho_{IF} < .7$ SCF accuracy is only slightly affected by clutter correlation.

When ρ_{IF} is so large that P_n is decreased manually (Case 3), control of P_n becomes much coarser. However, this is more than offset by decline of the ratio P_{fa}/P_n for large ρ_Q. The net effect is that control of the system false alarm rate, P_{fa}, improves as P_n is decreased. Figure 5.24 illustrates the fineness of SCF control at a point within Case 3. The IF correlation is $\rho_{IF} = .8$. P_n has been lowered to .01 in order to maintain $P_{fa} = 10^{-5}$. Clearly, the fineness of control is degraded by lowering P_n. But for $\rho_{IF} = .8$ ($\rho_Q = .54$) and M/N = 12/12:

$$P_{fa} = P_n\left[(1-\rho_Q)\,P_n + \rho_Q\right]^{11} \simeq P_n\,\rho_Q^{11}$$

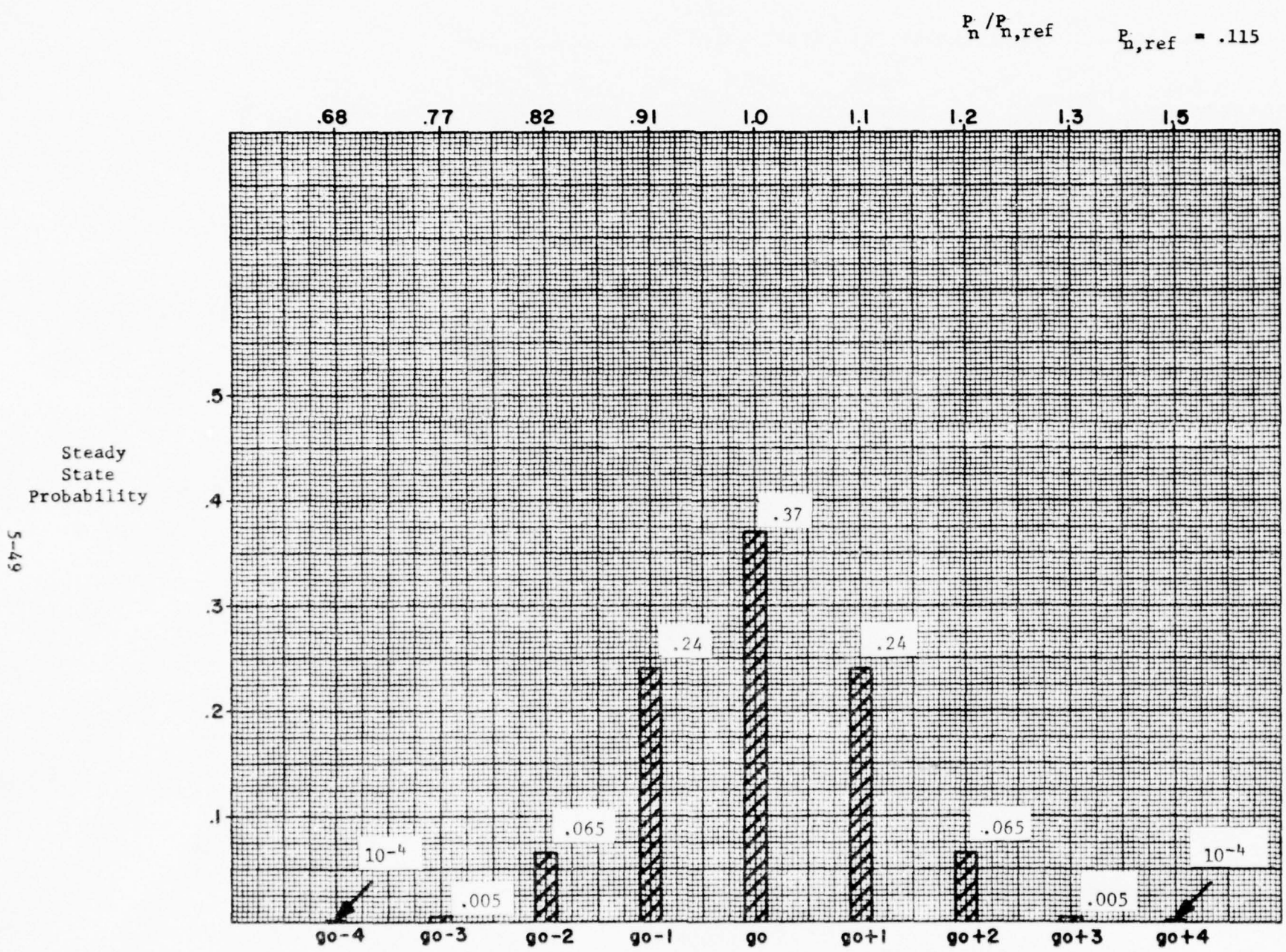

STEADY STATE MARKOV PROBABILITIES IN CORRELATED CLUTTER, $\rho_{IF} = .7$

FIGURE 5.23

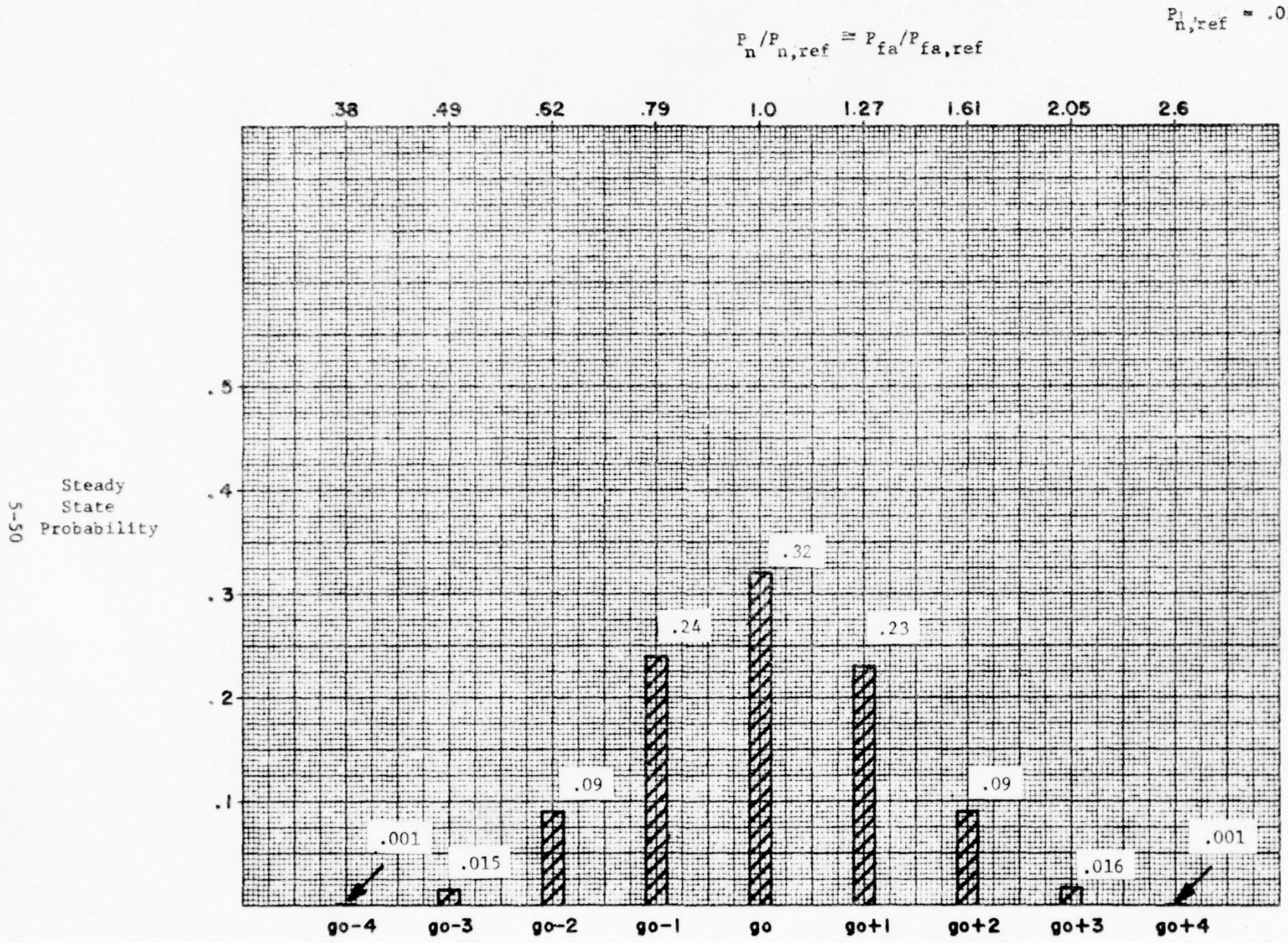

STEADY STATE MARKOV PROBABILITIES IN CORRELATED CLUTTER, $\rho_{IF} = .8$

FIGURE 5.24

So P_{fa}/P_n is a constant. Thus the fineness of control of P_n is also the fineness of control of P_{fa}. From Figure 5.24 then, P_{fa} can be controlled easily to within a factor of 2 or 3 (better performance than in uncorrelated clutter).

To put these results in perspective, typical correlation coefficients ρ_{IF} were computed for rain and land clutter. Assuming a Gaussian clutter spectrum (Reference 11).

$$\rho_{IF}(K) = \frac{c/N}{1+c/N} \exp(-8\pi^2(\frac{\sigma v}{\lambda fr})^2 K^2)$$

where the clutter-to-noise ratio C/N is assumed large; K, the separation in azimuth is taken to be 1; λ is .25 m (L-band), the pulse repetition frequency fr = 300 Hz, and σ_v the standard deviation of the clutter spectrum is taken as .2 m/s over land and 6.0 m/s in rain (Reference 11). The results are:

$$\rho_{IF}(\text{rain}) \simeq .6$$
$$\rho_{IF}(\text{land}) \simeq .99$$

so that for the particular parameters considered, SCF would be quite accurate in rain clutter but not usable at all in land clutter.

One alternative available in heavy clutter is the use of MTI video. Although empirical data on MTI performance was not available, some insight can be gained by modeling MTI by an ideal single delay canceller. In this case the improvement in the correlation coefficient can be derived as in Reference 11.

$$\rho_{MTI} = \frac{\rho_{IF} - 1 - \rho_{IF}^4}{2(1-\rho_{IF})}$$

With ideal MTI the rain and land correlation coefficients are:

$$\rho_{MTI}(\text{rain}) \simeq .1$$
$$\rho_{MTI}(\text{land}) \simeq .96$$

Rain clutter is still in Case 2 and land clutter is still in Case 4. Thus the rank quantizer with SCF would provide accurate control of P_n in rain but would not be usable in land clutter.

5.3.2.1.5 Summary and Conclusions

Effective control of P_n can be accomplished through the use of a rank quantizer with a center tap bias controlled by the scan correlated feedback technique. Scan correlated feedback can provide a hit probability easily regulated to within 20 - 30% in noise or lightly correlated clutter. This implies a system false alarm probability (P_{fa}) well regulated to within an order of magnitude.

The scan correlated feedback technique is, however, limited by the zone density sample size to hit probabilities (P_n) greater than 10^{-3}. Thus in heavily correlated clutter where the system false alarm and hit probabilities are nearly equal, system false alarm probabilities (P_{fa}) less than 10^{-5} cannot be maintained.

5.3.2.2 Scan Correlated Feedback Detection Loss

5.3.2.2.1 Discussion

Scan correlated feedback (SCF) provides zone by zone closed loop control of the rank quantizer hit probability, P_n, by varying the center tap bias. The bias is controlled by counting the number of hits in each zone on the previous scan and using this zone density count to adjust the variable bias either upward or downward decreasing or increasing the hit probability P_n. The analysis presented in the previous section (5.3.2.1) indicates that when the rank quantizer operates on thermal noise or slightly correlated clutter, SCF will provide a P_n controlled to within 20-30% of the desired value corresponding to regulation of the system false alarm rate to within an order of magnitude.

However, unlike the automatic clutter eliminator (ACE), SCF must include the target cells in its estimate of the hit probability P_n. As a result, the presence of a target in a given zone will bias upward the threshold used by the rank quantizer to detect that target. This results in a detection loss when SCF is used instead of a fixed threshold. For example, consider a strong target with 20 hits in azimuth. Suppose the desired P_n value is set at .05. Then in the absence of the target the expected number of hits due to noise is 50 (~1000 hit opportunities per zone) which is also the expected zone density count. Now let the 20 hit target appear in the zone. In order to maintain an average of 50 hits in the zone, the SCF loop will lower P_n to .03 giving 30 hits from noise, 20 hits from the target, and maintain an expected zone density count of 50. Of course, in reality, P_n will settle out at some value a little greater than .03 since the higher threshold will reject some of the original 20 target hits. Thus if, instead of having 20 hits, the target has only enough hits in azimuth to just pass the M/N second threshold requirement, then the increase in threshold due to SCF might be sufficient to suppress detection of the target at the second threshold.

The detection loss of interest is, then, the additional S/N ratio required to detect a target in a SCF system as opposed to an ideal system where the threshold always gives the desired probability of false alarm. To simplify the calculation, it will be assumed that about 1 dB of detection loss is suffered when the detection threshold is raised enough to reduce P_{fa} by a factor of ten. This is a good approximation for small detection losses and P_{fa} on the order of 10^{-5} or 10^{-6} (Reference 30). Since P_{fa} in an ideal system is exactly that desired ($P_{fa,ref}$) it is only necessary to calculate P_{fa} in a SCF system when there is a target with minimum detectable S/N ratio in the zone. It is shown in Appendix B that in uncorrelated clutter or noise:

$$P_{fa} \cong \sum_{i=M}^{12} \binom{i}{12} \left(P_{n,ref} - \frac{M}{N_{zone}}\right)^{i} \left(1-P_{n,ref} + \frac{M}{N_{zone}}\right)^{12-i}$$

when $P_{n,ref} > {}^{M}/_{N_{zone}} + P_n(min)$ and

$$P_{fa} \cong \sum_{i=M}^{12} \binom{i}{12} (P_n(min))^{i} \; (1 - P_n(min))^{12-i}$$

when $P_{n,ref} < {}^{M}/_{N_{zone}} + P_n(min)$,

where $N_{zone} = 1000$ is the number of hit opportunities per zone; M/12 is the second threshold detection requirement; and, $P_n(min)$ is the minimum obtainable P_n with SCF. $P_n(min)$ may be adjusted by setting the SCF gains, (a,b,c,d) in Section 5.3.2.1 and the reference rank k. The expressions for P_{fa} are a function of the M-value used in the M/N integrator. These expressions were evaluated by setting M=10 in the term $(P_{n,ref} - M/N_{zone})$. In uncorrelated clutter or thermal noise, use of an M greater than 10 is unlikely so that these calculations give worst case losses for zero correlation.

Figure 5.25 shows the results of these calculations. The loss resulting from use of SCF instead of a perfect threshold is plotted as a function of $P_{n,ref}$ for three $P_n(min)$ values. Notice that at $P_n = .05$ (typical operating point) a .6 dB detection loss is suffered for all 3 minimum P_n values. As P_n decreases, the three detection loss curves separate. The maximum detection loss decreases as $P_n(min)$ increases. Thus by raising the minimum P_n value the maximum detection loss can be limited. Figure 5.26 is an idential plot for the case where two targets (both of the same S/N ratio) are in the zone. Clearly the losses are larger (1.3 dB at $P_n = .05$) but as before, the maximum loss can be limited by limiting the range of SCF P_n values.

These results indicate the desirability of setting $P_n(min)$ greater than 10^{-3}. Such a limitation would decrease the maximum detection loss if it was desired to operate with P_n at low values (say .01). However, since the purpose of a SCF loop is to handle non-Rayleigh clutter, some capability for P_n's less than those actually desired must be retained. When the clutter is non-Rayleigh, more variable bias range than for Rayleigh clutter may be required.

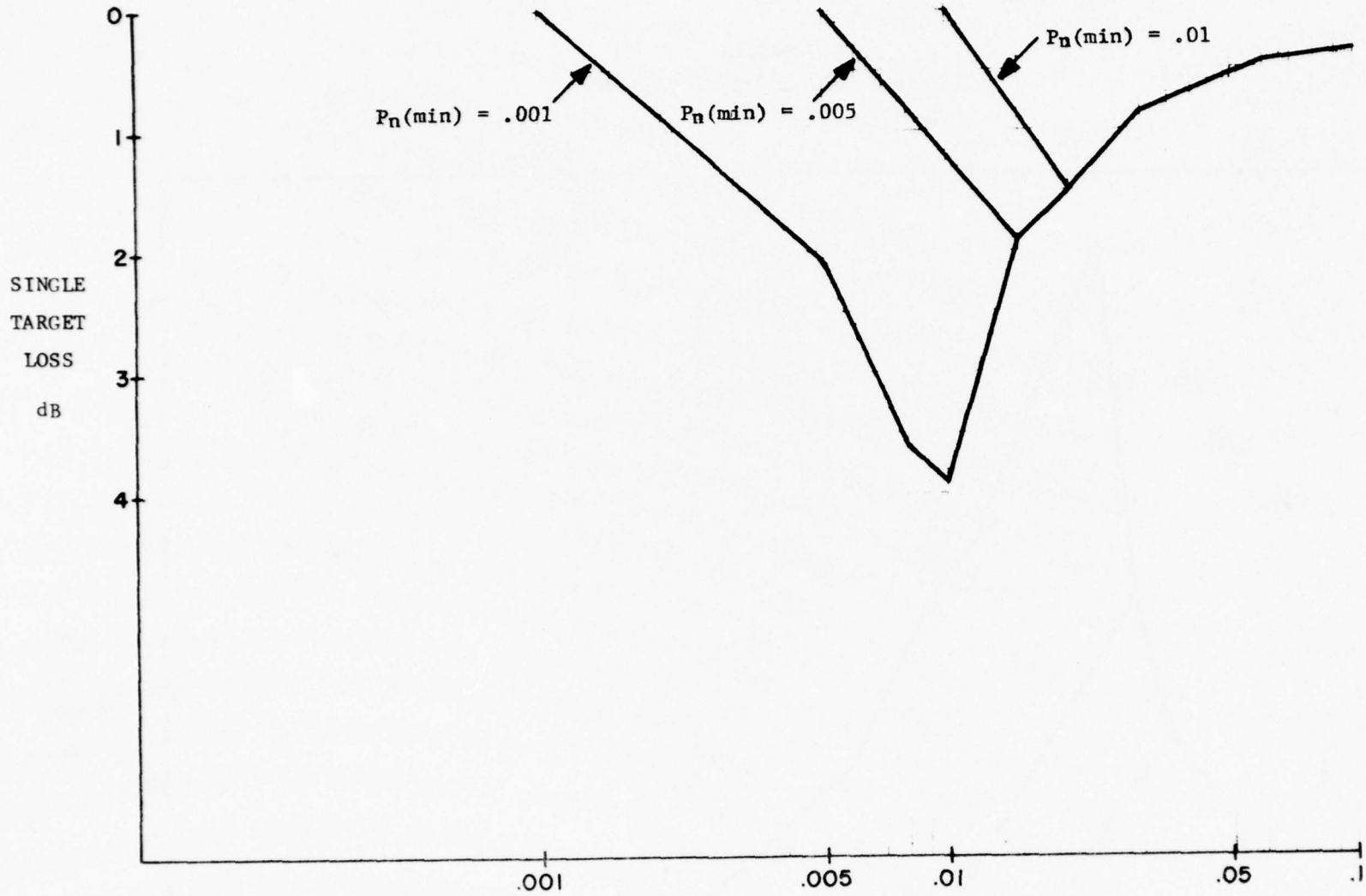

FIGURE 5.25

SINGLE TARGET SCF DETECTION LOSS AFTER MANY SCANS

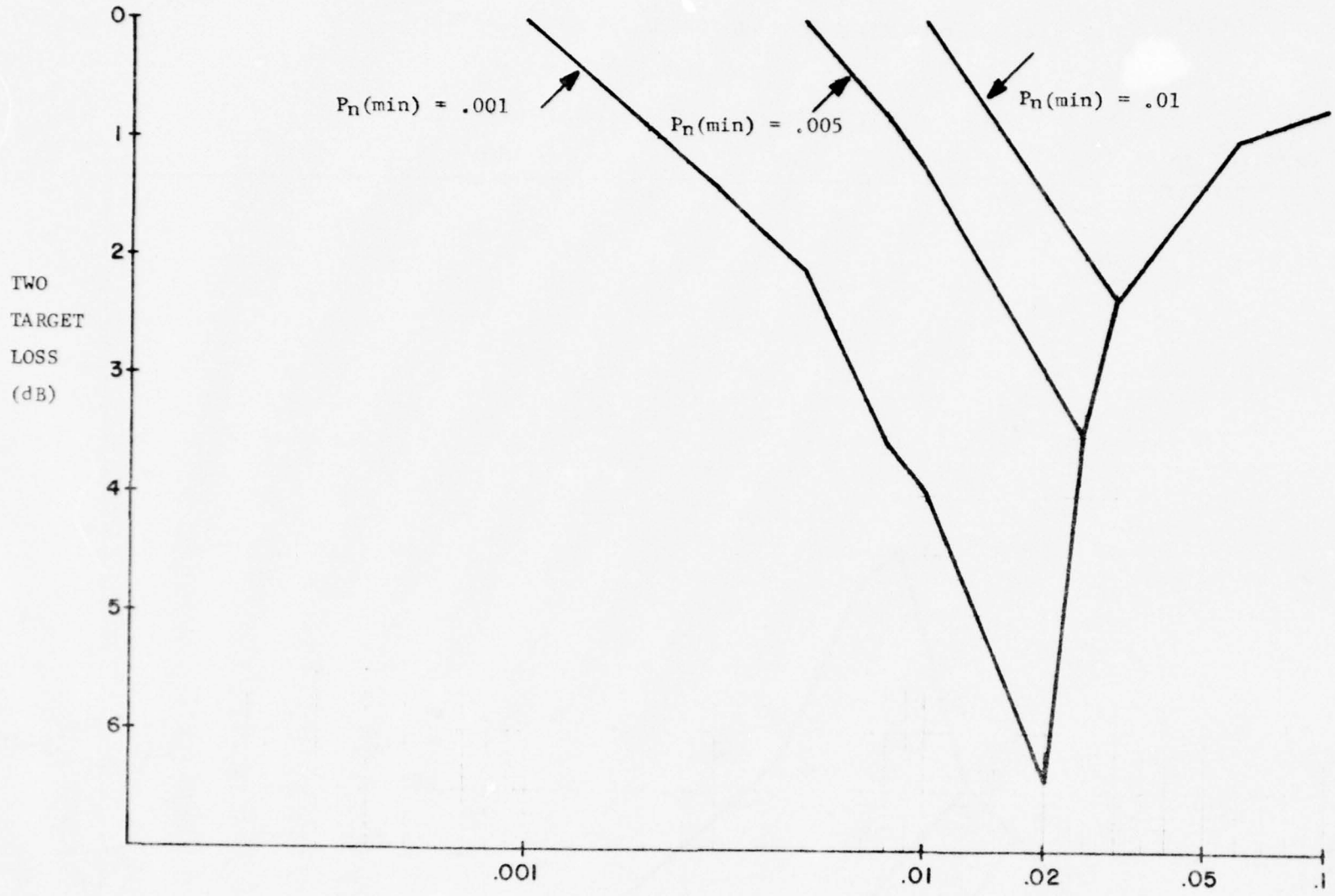

DESIRED P_n VALUE (SET MANUALLY)

FIGURE 5.26

TWO TARGET SCF DETECTION LOSS AFTER MANY SCANS

5.3.2.2.2 Summary and Conclusions

The rank quantizer with SCF operates with a detection loss when compared to an ideal thresholding system, because the presence of a target will trigger the SCF loop to bias the first detection threshold upward. The magnitude of this loss is computed and found to be less than .6 dB over a typical range of operating values (P_n = .05 to .1). If operation at lower P_n values is desired, the detection loss can be minimized by adjusting the SCF gains to limit the downward range of P_n.

5.3.2.3 Performance of Scan Correlated Feedback in Non-Rayleigh Clutter with the Use of Guard Bands

5.3.2.3.1 Introduction

In the previous sections the accuracy and range of P_n control for a rank quantizer with SCF control of the center tap bias was analyzed. This analysis indicates that effective P_n control can be obtained with SCF. Also, additional analysis is required to determine P_n control performance in non-Rayleigh clutter. This subsection presents an analysis of the non-Rayleigh clutter case and expands the analysis to include the effect of hit density guard bands. Guard bands are used to improve the steady state response of the SCF loop.

5.3.2.3.2 Range of SCF Control in Non-Rayleigh Clutter

Figure 5.18 of Section 5.3.2.1 presents a block diagram of the rank quantizer with SCF control of P_n. The probability of a false target report (P_{fa}) out of the M/N binary integrator must be held below a certain level (in the region of 10^{-6} or 10^{-5}) to prevent overloading. When there is no azimuthal correlation between video samples, the false alarm rate out of a 12 hit ($M/_{12}$) sliding window integrator, P_{fa}, is related to the false hit rate prior to azimuth integration, P_n by:

$$P_{fa} = \sum_{i=M}^{12} \binom{i}{12} P_n{}^{i} \, (1-P_n)^{12-i}$$

The degree of control of P_n required for a given degree of control of P_{fa} is plotted in Figure 5.27. It is assumed that the azimuth threshold M for the $M/_{12}$ azimuth sliding window is controlled perfectly. That is, it is assumed some mechanism (such as an ACE auto-select) always selects the M-value which will give P_{fa} closest to 10^{-5}. This uncorrelated case represents the worst correlation case since the fineness of control of P_{fa} increases with increasing azimuth correlation.

The rank quantizer operating with a constant center tap bias maintains a constant hit probability in thermal noise or Rayleigh clutter independent of the clutter power. The purpose of a closed loop system such as scan correlated feedback is to maintain the desired probability of false alarm not only when the clutter power changes but when the clutter distribution changes as well. In particular, if the clutter becomes more "spiky," it acquires a longer tail. (The probability density function falls off more slowly as its argument goes to infinity.) This longer tail causes a given center tap bias to result in a higher hit probability and can also make the hit probability a function

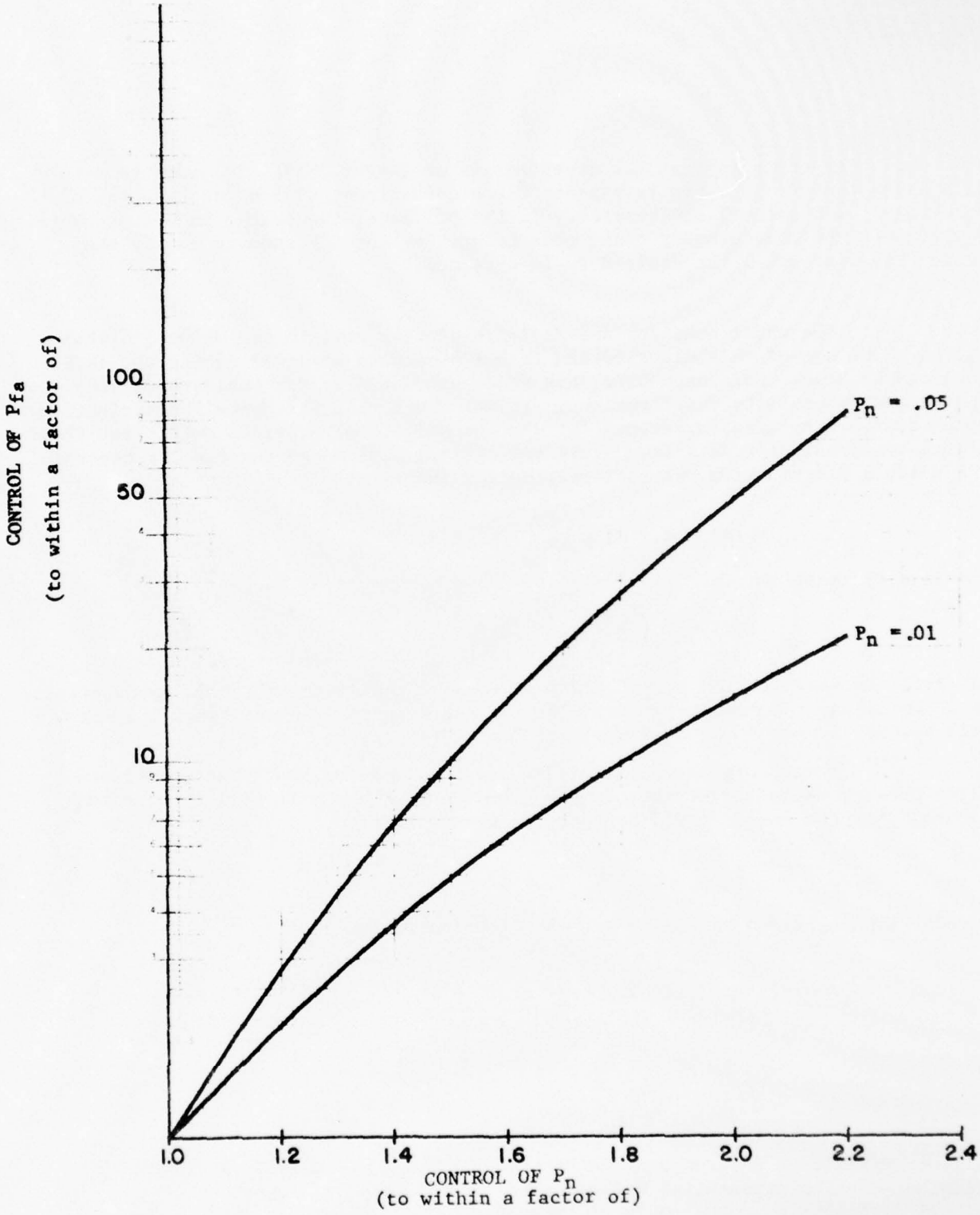

FIGURE 5.27

EFFECT OF $^{M}/_{12}$ BINARY AZIMUTH

INTEGRATION ON CONTROL OF FALSE ALARMS

of the clutter power so that the quantizer is no longer CFAR. In order to maintain a constant false alarm rate under these conditions, closed loop control of the threshold (such as SCF) can be used. In the SCF mode, the change in hit probability, P_n, changes the zone density count thus triggering the SCF loop to modify the center-tap bias until the desired P_n is obtained.

The model used for non-Rayleigh clutter will be the Weibull distribution. The use of this distribution is based on data analyzed during the ARTS Enhancement Study (Reference 33). This study attempted to fit observed radar video to various probability distributions. It was found that the Weibull distribution (with appropriate transformations for log and MTI video) provided sufficient flexibility to closely fit data from clear and clutter regions of the radar's coverage. The Weibull distribution has the distribution function:

$$F(x) = 1 - e^{-\frac{1}{\beta}\left(\frac{X}{\sigma}\right)^{\beta}}$$

and density function:

$$f(x) = \frac{1}{\sigma}\left(\frac{x}{\sigma}\right)^{\beta-1} e^{-\frac{1}{\beta}\left(\frac{x}{\sigma}\right)^{\beta}}$$

For $\beta=2$, the distribution is Rayleigh and for $\beta=1$ the distribution is exponential. As β decreases, the mean-to-median ratio of the distribution increases and the tail becomes longer (thus modeling more "spiky" clutter.)

For the purposes of this study it will be assumed that normal and MTI video are Weibull distributed with β between 1 and 2. It will further be assumed that the radar uses a perfect log transformation

$$Y = \alpha \ell n X$$

so that the log video has a log-Weibull distribution:

$$F(y) = 1 - e^{-\frac{1}{\beta\sigma^{\beta}} e^{\beta y/\alpha}}$$

$$f(y) = \frac{1}{\alpha\sigma^{\beta}} e^{\frac{\beta}{\alpha} y} e^{-\left[\frac{1}{\beta\sigma^{\beta}} e^{\beta y/\alpha}\right]}$$

In fact, results in Reference 33 indicate that MTI video may be more closely distributed as an exponential Weibull. However, since the exponential Weibull distribution corresponds to even less "spiky" clutter than Weibull, the Weibull distribution will be assumed as a worst case for MTI video. Also, it was suspected in the ARTS study that the ASR radar from which data was taken had a log transform with the imperfect characteristic:

$$Y = \alpha \ell n(X+\Delta)$$

This problem is ignored here because of its complexity and because for small Δ, the effect on the tail of the distribution of Y will be small.

The probability of a hit in Weibull clutter is computed in Reference 33,

$$P_n = \frac{N(N-1) \cdot \cdot \cdot (N-k+1)}{(N+K_{lin}^{-\beta}) \cdot \cdot \cdot (N+K_{lin}^{-\beta}-k+1)}$$

where K_{lin} is the center tap multiplicative bias, k is the reference rank and N is the number of taps.

Similarly in log video:

$$P_n = \frac{N(N-1) \cdot \cdot \cdot (N-k+1)}{(N+e^{-\beta K_{log}}) \cdot \cdot \cdot (N+e^{-\beta K_{log}}-k+1)}$$

where K_{log} is the additive center tap bias. Notice that with $\beta=2$ these two expressions are the same as those for Rayleigh clutter (Section 5.3.2.1.2). Notice also that the processor is CFAR in Weibull clutter for any fixed β value.

Suppose that in log Weibull clutter with a β-value equal to β_o an additive bias $K_{log,o}$ is required for some hit probability P_n. It is easily shown, then, that in arbitrary log Weibull clutter with parameter β the bias required for a hit probability P_n will be:

$$K_{log} = K_{log,o}\left(\frac{\beta_o}{\beta}\right)$$

Similarly, if the multiplicative bias $K_{lin,o}$ is required when $\beta=\beta_o$, then

$$K_{lin} = \left(K_{lin,o}\right)^{\beta_o/\beta}$$

is required for arbitrary β. In particular, if it is desired to have the capability for P_n values as low as P_n (min) in all expected clutter conditions, then the SCF gains are adjusted so that the maximum gain word g_{max} gives $P_n=P_n$(min) in the "spikiest" clutter expected.

During actual adjustment of the SCF gains, video with spiky clutter will probably not be available. It is, therefore, necessary to specify a method for adjusting the SCF gains when only Rayleigh video (thermal noise) is available. Assuming $\beta=1$ is the "spikiest" clutter expected, then $P_n=P_n$(min) is desired when $\beta=1$. Thus in thermal noise ($\beta=2$) the SCF gains should be adjusted so that the gain word g_R will give

$$K_{log}(g_R) = K_{log}(g_{max})^{\frac{1}{2}}$$

in log video and

$$K_{lin}(g_R) = (K_{lin}(g_{max}))^{\frac{1}{2}}$$

in linear video.

In Section 5.3.2.1 it is shown that a necessary condition for CFAR operation is that:

$$K_{log} = ag \quad \text{and} \quad K_{lin} = 1-cg$$

where a and c are positive constants. It follows then in log video that the gain should be set to

$$g_R = \tfrac{1}{2}\, g_{max} = \tfrac{1}{2}\, 31 = 15 \text{ or } 16$$

with $P_n = P_n(\min)$ and receiver noise into the rank quantizer. This will ensure that $P_n(\min)$ will be obtainable in the spikiest clutter expected (exponential).

In linear video the procedure is more complicated. In receiver noise with $P_n=P_n(\min)$ the parameter c must be adjusted so that with $g=g_R$

$$K_{lin}(g_R) = \left[K_{lin}(g_{max})\right]^{\frac{1}{2}}$$

Substituting for K_{lin} gives:

$$1 - cg_R = (1-cg_{max})^{\frac{1}{2}} = (1-31c)^{\frac{1}{2}}$$

This is a quadratic equation in g_R and can be solved:

$$g_R = \frac{1 \pm \sqrt{1-31c}}{c}$$

Discarding the root which gives $g_R > 31$ gives:

$$g_R = \frac{1 - \sqrt{1-31c}}{c}$$

Substituting for c:

$$g_R = 31\, \frac{1-\sqrt{K_{lin}(g_{max})}}{1 - K_{lin}(g_{max})}$$

The calibration procedure is carried out as follows:

1) Using the equation for P_n in linear video find the K_{lin} value which corresponds to $P_n = P_n(\min)$ for $\beta=1$. Call it $K_{lin}(gmax)$.

2) Either:

Set c so that g=31 gives a bias of $K_{lin}(gmax)$

or

In thermal noise set c s.t. $P_n=P_n(\min)$ when

$$g = 31 \frac{1-\sqrt{K_{lin}(gmax)}}{1 - K_{lin}(gmax)}$$

5.3.2.3.3 Effect of Guard Bands in SCF Decision Logic

The SCF decision logic operates as described in Reference 24 by incrementing or decrementing the 5 bit gain word g. The decision to increment, decrement or leave g unchanged is based upon the current zone density count X_c. The SCF loop increments the gain word if X_c exceeds the desired hit density count and decrements the gain word if X_c is less than the desired zone density count. (The desired zone density count is just the number of hit opportunities per zone multiplied by the desired false hit probability P_n, ref.) A more complicated decision logic allowing a guard band is discussed in this section.

When a guard band is provided in the decision logic, the gain word is incremented only if the hit density count exceeds some upper threshold, X_u, and is decremented only if the hit density count is less than some lower threshold X_ℓ. The thresholds X_u and X_ℓ are chosen so that the desired hit density count lies in between them. The purpose of the guard band is to improve the steady state characteristics of the loop by damping out oscillations.

As described in References 27, 37 and Section 5.3.2.1, a digital feedback loop such as SCF can be modeled by a Markov chain. With a 5 bit feedback gain word, the center tap bias can assume only 25-32 different values. The value of a gain word during any given scan depends only on the value of that gain word during the prevous scan and the current hit density count. Thus the system may be modeled by a Markov chain with 32 states. Each state corresponds to a particular gain word. The probability that the state changes is just the probability that the hit density count, X_c, exceeds the upper threshold or is less than the lower

threshold. Assuming all of the cells in the zone are uncorrelated, then the zone density count is binomially distributed. If the expected value of the zone density count is large compared to one, then this distribution is approximately normal. The state transition probabilities are then computed in Reference 27.

$$P[X_c > X_u] = \text{Erfc}\left[\sqrt{N\, P_{n,ref}\, K_s^{-i}}\,(K_u R - K_s^{i})\right]$$

$$P[X_c < X_\ell] = \text{Erfc}\left[\sqrt{N\, P_{n,ref}\, K_s^{-i}}\,(K_s^{i} - R K_\ell)\right]$$

where:

N = number of hit opportunities per zone

$P_{n,ref}$ = desired hit probability

P_o = P_n value of Markov state closest to $P_{n,ref}$

R = $P_{n,ref}/P_o$

X_u = $K_u N\, P_{n,ref}$

X_ℓ = $K_\ell\, N\, P_{n,ref}$

i = Difference between gain word corresponding to $P_n = P_o$ and gain word of present state (i is an integer)

K_s = proportional change in P_n when the gain word changes by one LSB:

$$K_s = \frac{P_n\,(g)}{P_n(g+1)}$$

$$\text{Erfc}(x) = \int_x^\infty e^{-u^2/2}\, du$$

A control loop modeled by a Markov chain may be evaluated with respect to its steady state and dynamic response just as a classical control system would be. In the Markov case, the steady state response corresponds to the steady state probabilities of being in a particular state. That is, the steady state probability distribution gives the probability of a particular gain word no matter what the initial gain word, providing a large number of scans

have elapsed and the hit density count statistics have remained constant. The extent to which these probabilities are substantially different from zero only in a narrow band around the desired gain word is a measure of the fineness of the loop's control. A measure of the loop's dynamic response characteristics is the number of scans required for the probability that the gain word is that desired to reach, say 50%, given some initial state. This corresponds to the settling time of the step response of a classical control system.

The steady state Markov probabilities are determined by first computing the state transition probabilities, then iteratively solving the state equations for the steady state (Reference 32). This process was performed for 4 different guard band widths: 1 hit, 5 hits, 10 hits, 15 hits. A guard band symmetric about the desired hit density count was assumed. Assuming 1000 hit opportunities per zone would mean a desired zone density count of 50 hits. The guard band would, then, have an upper threshold X_u = 60 hits and a lower threshold X_ℓ=40 hits. (Note this is referred to as a "10 hit guardband" rather than a "20 hit guard band.") The steady state performance of the loop with this guard band choice is shown in Figure 5.30. Figures 5.28, 5.29 and 5.31 present the 1, 5, and 15 hit guard band results.

5.3.2.3.4 Accuracy of SCF Control in Non-Rayleigh Clutter

The previous section derived the range of center tap bias values needed for a desired range of P_n in different clutter distributions. In general, as the clutter becomes more "spiky", additional bias range is required. The additional range is achieved by adjusting the SCF gains. However, the same SCF gains must be used for all zones. Therefore, in zones where thermal noise or Rayleigh clutter predominates, much of the available bias range will not be used. For example, if in log video SCF is configured so that g=31 gives $P_n=P_n(\text{min})$ in exponential clutter, then in Rayleigh clutter $P_n=P_n(\text{min})$ can be achieved with g=15. The gain words 16 through 31 will never be used in the zones of the radar's coverage where thermal noise or Rayleigh clutter predominates. This implies that control of P_n will be coarser in Rayleigh video than in exponential since the same range of P_n values (non-parametric to $P_n(\text{min})$) must be covered using only half as many gain words.

This section examines the accuracy of SCF control when the SCF gains have been set to allow operation in non-Rayleigh clutter distributions. The worst case for accuracy will be in the least "spiky" clutter, assumed here to be Rayleigh. It also appears that for reasonable values of $P_{n,\text{ref}}$ and $P_n(\text{min})$, control will be coarser in log video than in linear video. The case considered here, then, will be the accuracy of SCF control in log-Rayleigh video when the SCF gains have been set to provide P_n values down to $P_n(\text{min})$ in log exponential video.

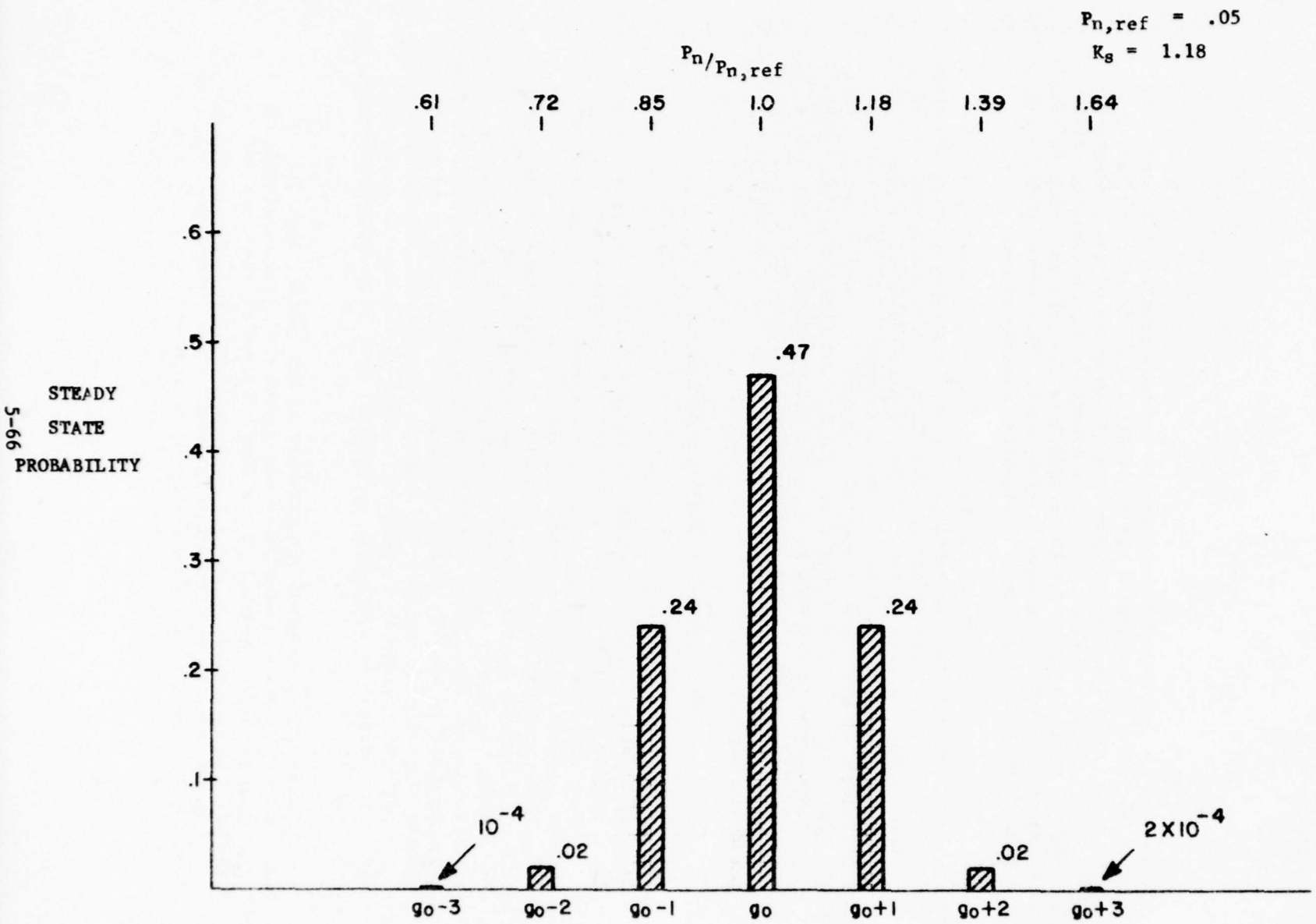

FIGURE 5.28

STEADY STATE MARKOV PROBABILITIES WITH 1 HIT GUARD BAND

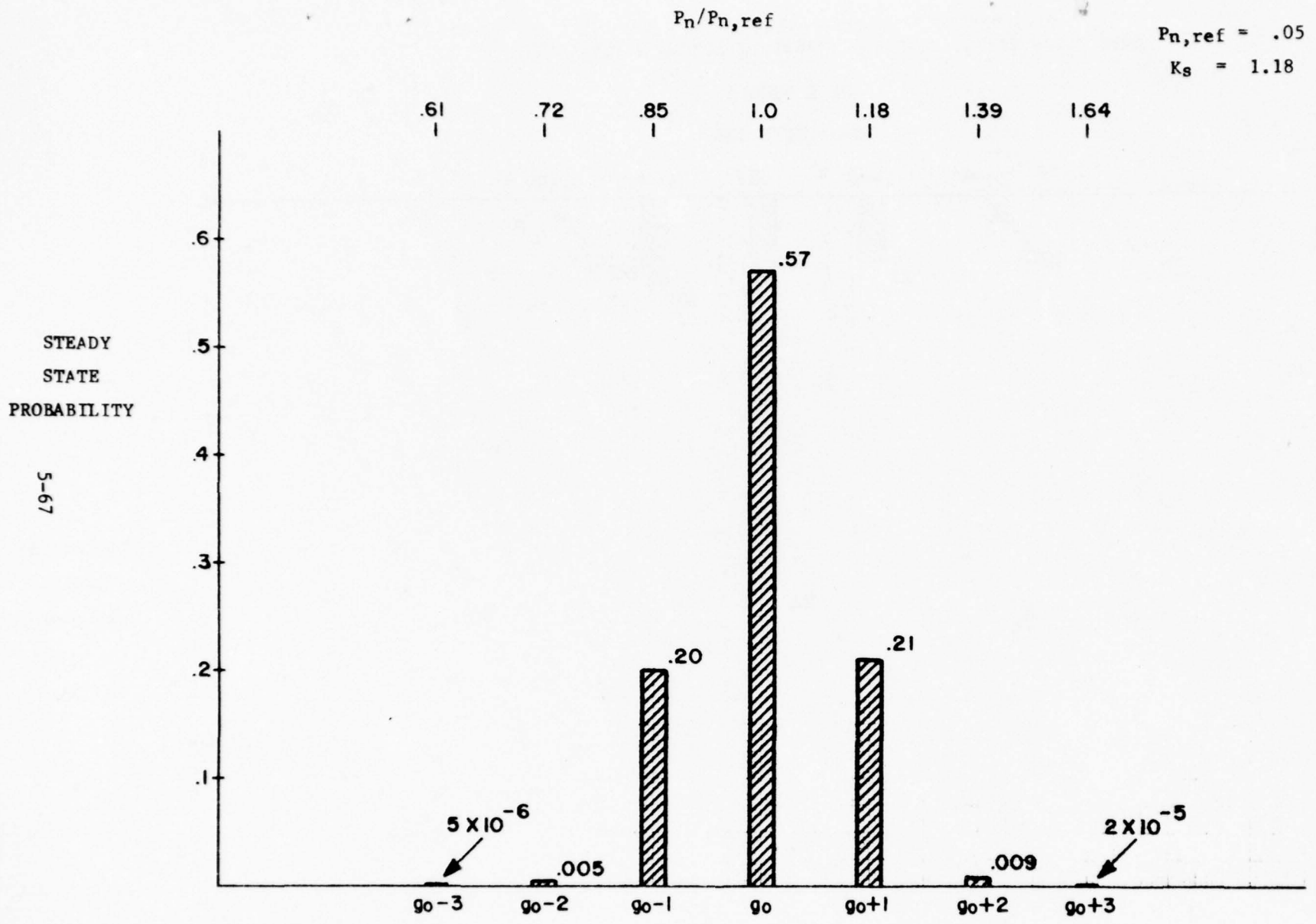

FIGURE 5.29

STEADY STATE MARKOV PROBABILITIES WITH 5 HIT GUARD BAND

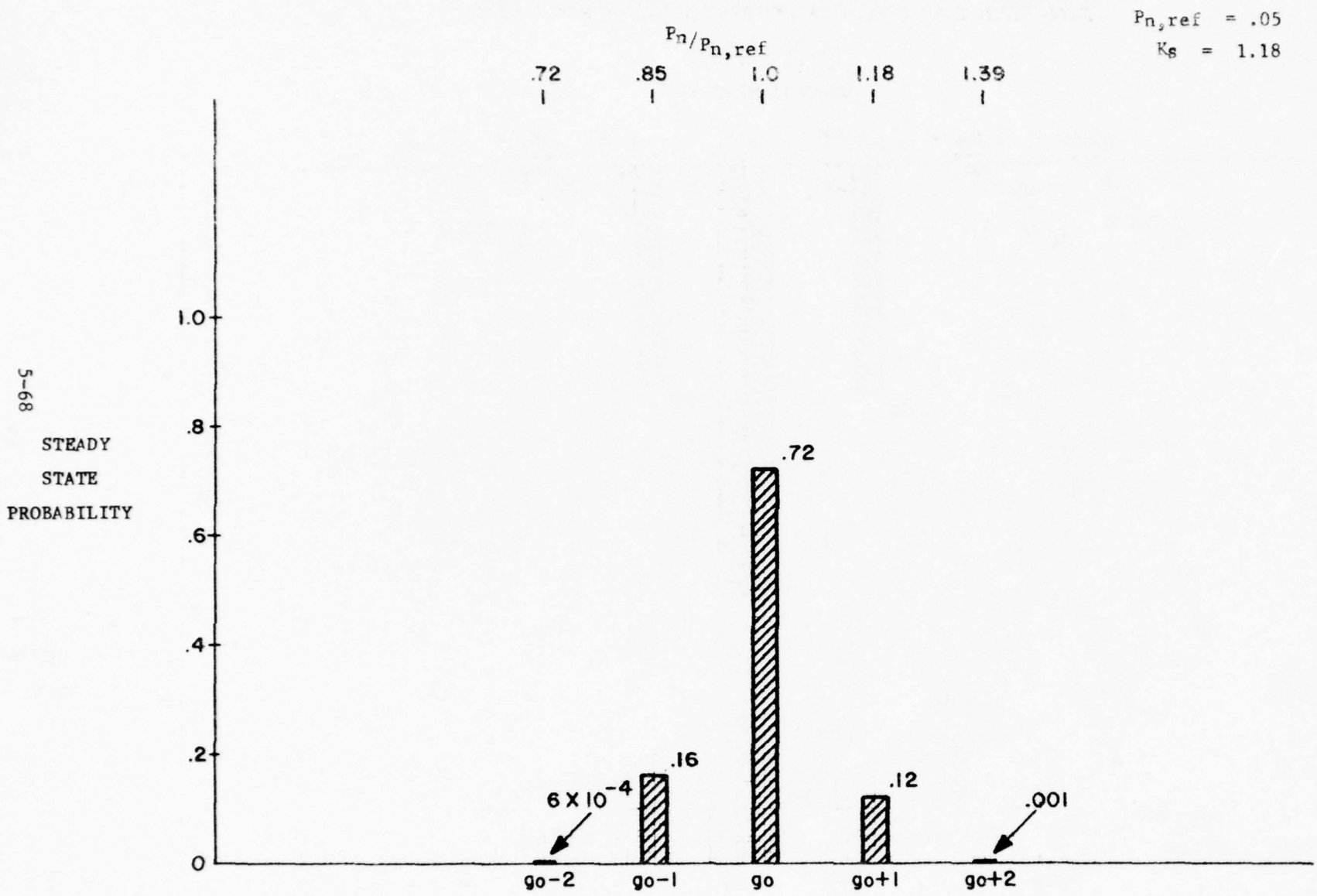

FIGURE 5.30

STEADY STATE MARKOV PROBABILITIES WITH 10 HIT GUARD BAND

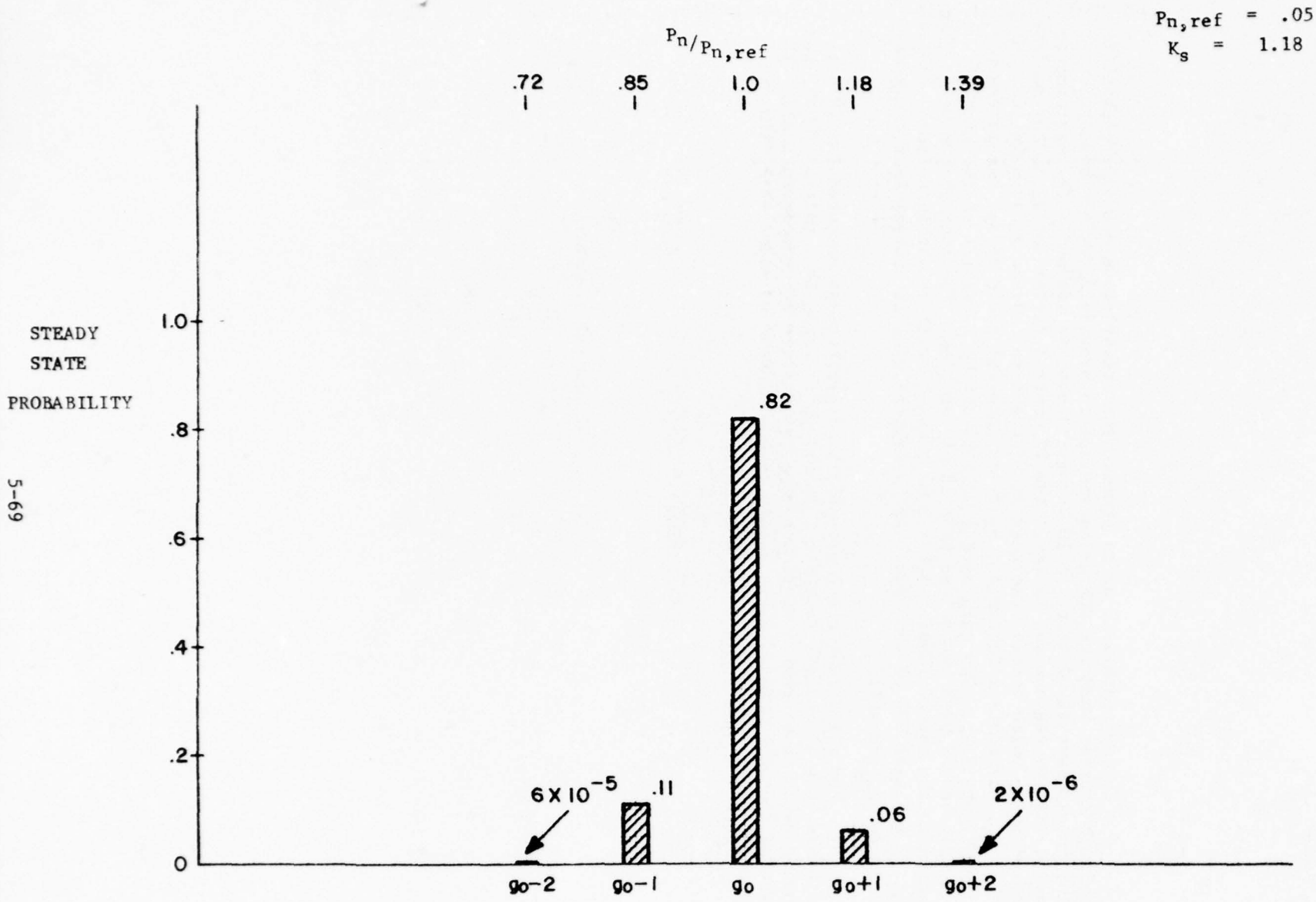

FIGURE 5.31

STEADY STATE MARKOV PROBABILITIES WITH 15 HIT GUARD BAND

The approach will be to compute the steady state Markov probabilities in Rayleigh clutter when the SCF gains are set to provide P_n values down to $P_n(\min)$ in exponential clutter. A 10 hit guard band is assumed. The performance criterion will be the control factor. The 1% control factor for P_n is the maximum variation in P_n which occurs less than 1% of the time. Since P_n is quantized in steps of K_s, the control factor for P_n is an integral power of K_s. As an example, consider Figure 5.31. The gain word g will be off by 1 LSB 17% of the time. But it will be off by 2 LSB's less than 1% of the time. The control factor is then K_s raised to the second power: $K_s^2 = 1.4$. Thus P_n will be within a factor of 1.4 of $P_{n,ref}$ at least 99% of the time. Using Figure5.27 a 1% control factor can be computed for P_{fa} as well.

For all steady state probability distributions computed for 10 hit guard bands, the 1% control factor for P_n was K_s^2. Using this rule-of-thumb, the following table shows the 1% control factor for various SCF configurations. (It is assumed that the SCF gains are set to give a minimum P_n value of $P_n(\min)$ in exponential clutter.)

SCF CONTROL FACTORS

		1% Control Factor	
$P_n(\min)$	$P_{n,ref}$	P_n	P_{fa}
.001	.05	1.7	20
.001	.01	2.2	20
.01	.05	1.4	7
.01	.01	1.7	8

5.3.2.3.5 Summary and Conclusions

Scan correlated feedback control of the rank quantizer center tap bias maintains the desired probability of false alarm when the clutter power changes as well as when the clutter distribution changes. When "spiky" clutter is encountered, the center tap bias range required to maingain P_n control must be larger than when controlling for thermal noise or Rayleigh clutter. The center tap bias range must therefore be adjusted for the "spiky" clutter situation in order to insure that P_n will be controlled for all clutter situations. Adjustment in this manner will result in a coarser control of P_n for the thermal noise and Rayleigh clutter situations.

The use of a SCF guard band in the control of the center tap bias improves the steady state characteristics of the control loop by damping out oscillations. The decision to increment, decrement or leave the bias unchanged is based upon the zone density count. A guard band with 10 hits in a zone with 1000 hit opportunities is recommended.

5.4 TESTING OF THE CD MODIFICATIONS

A test plan was developed to confirm analysis and to determine whether the various modifications resulted in enhanced CD operational performance. The test plan (Reference 34) was designed to evaluate each modification individually and as a component of a system test. A system test consists of playing an FR-950 analog tape through the CD and measuring specified performance criteria. The performance criteria would be used as a yardstick to measure performance improvement against a reference standard.

The reference would be the system performance obtained by playing the FR-950 tapes through the CD with the CD in the baseline configuration (see Section 5.1).

The pertinent performance criteria to be measured and the applicable FAA clear-air radar performance standards are as follows:

System Performance Parameter	FAA Clear-Air Standard
1. Blip scan ratio	$\geq$ 70%
2. Split rate	$\leq$ 2%
3. False target rate	$\leq 1 \times 10^{-6}$
4. Track life	----
5. Total blanked area	$\leq$ 0.1%

The Search Radar Target Detection and Statistical Definitions required to support the performance criteria are as follows:

Search Radar Target Detection and Tracking -

Statistical Definitions

1. Types of Tracks:

   (A) Fixed - A slow moving, velocity less than 70 knots, or stationary track that has established a definite scan-to-scan correlation (6 correlated scans with less than 8 successive misses).

(B) Firm - A moving track, velocity greater than 70 knots and less than 700 knots, which has established a definite scan-to-scan correlation (6 correlated scans with less than 7 successive misses).

(C) Tentative - A track which has not yet established a definite scan-to-scan correlation (1 correlated scan with less than 3 successive misses).

(D) New Tentative - A track which has just entered the system.

2. Track Life:

The number of correlated target reports in an aircraft track beginning and ending with a correlated target report.

3. Track Scans:

The number of antenna scans occurring during the track life.

4. Blip Scan Ratio:

Track Life/Track Scans.

5. Tracks per Scan:

The number of tracks (tentative, firm, fixed)/The number of scans.

6. False Targets:

A target report not associated with a firm, fixed or tentative aircraft track.

7. False Targets per Scan:

The total number of false targets/The number of antenna scans.

8. Total Blanked Area:

The ratio of the number of zones exhibiting blanking (ACE) to the number of zones in the radar coverage area.

9. Split Target:

Range - A pair of targets in adjacent range cells separated by less than or equal to a beamwidth in azimuth.

Azimuth - A pair of targets at the same range but differing by less than a beamwidth in azimuth.

The FR-950 tapes selected for the system tests exhibit rain clutter and clear conditions at Elwood, N.J. and terrain clutter at Paso Robles, California. Both tapes have MTI and log normal video data recorded.

Prior to the system tests individual tests were scheduled to be performed on the quantizer modifications. These tests were necessary to establish that the quantizers were operating properly, to measure their first threshold P_n control characteristic, to establish appropriate calibration procedures and to determine an optimal operating configuration.

Testing of the modifications was performed from July through November 1975. The test program did not progress satisfactorily because of numerous problems. Of fifteen tests proposed only two tests were completed before work was suspended.

5.4.1 Test Plan

Figure 5.32 presents a list of the proposed tests and a recommended sequence for enhancement testing and analyses. Reference 34 presents the detailed plan for testing the Common Digitizer enhancements. The objective of each test is presented in Table 5.6 in order to provide a brief summary of the intent of each test.

Test 1.1 provides test procedure guidelines to ensure that the test configuration was correct prior to testing and to assess, by using available on-line diagnostic indicators, whether the CD was operating properly during the test. Test 1.2 provides for the measurement of a set of reference statistics with which to determine whether the CD modifications resulted in improved system performance. Additionally the test also provides a means by which to perform an operational check of the Baseline configuration at several stages in the test program.

The 2. test series tests the Q3 quantizer. Tests 2.1, 2.2 and 2.4 provide data to examine the operation of the rank quantizer portion of Q3. The parametric and nonparametric control of P_n as well as the effect that the quantizer delay line tap spacing has on P_n control are tested. Tests 2.1 and 2.3 provide data to examine the signal processing effects of the input buffer circuit and the output hit width discrimination circuit. Tests 2.5 and 2.6 are system tests to determine the dynamic effects of operating the rank quantizer parametrically or nonparametrically and the Q3 quantizer with and without clutter switching between the thermal noise quantizer loop (clear air) and the rank quantizer (clutter situation).

The 3. test series tests the improved Q2 quantizer modification. Test 3.1 provides data to determine the input buffer signal conditioning effects on target detection sensitivity using a test target. A static test of P_n control using the scan correlated feedback bias control loop is performed with test 3.2. Tests 3.3 and 3.4 check the dynamic operation of the quantizer when operated with SCF and the quantizer with and without clutter switching between the thermal noise quantizer loop (clear air) and clutter quantizer loop (clutter situation).

Test 4. tests the preliminary SCF algorithm provided by Burroughs with the SCF modification. The quantizers were to be operated in their optimal configuration as determined by the previous tests. Tests 5, 6, and 7 test three modifications to the second threshold target detection and processing group. The modifications are Zone Control of T_L, Automatic ACE Selection (based on correlation measurement) and Delayed Decision Integration (manual smoothing of T_L). The Zone Control of T_L test was to have been accomplished not as a unique test, but by using data obtained from several of the other tests.

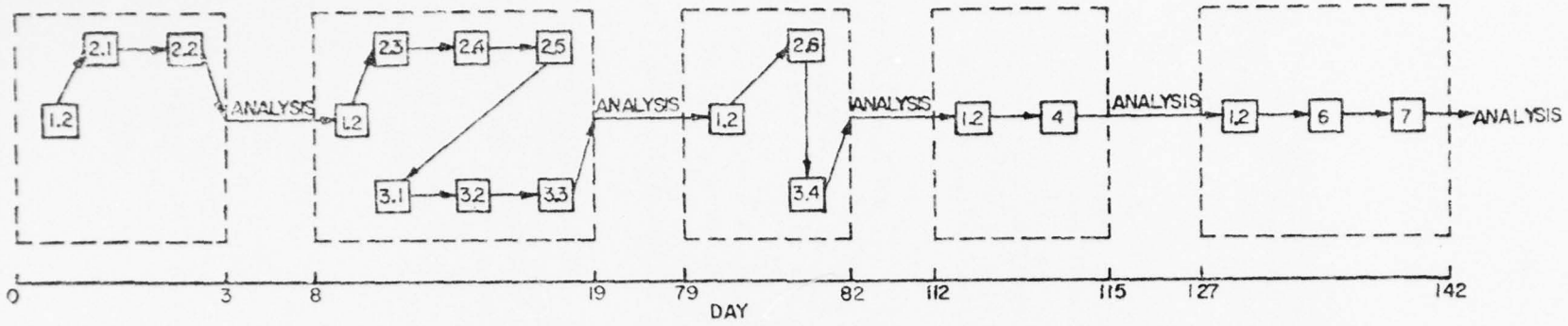

TEST INDEX

1.2 Baseline

2. Q3 Quantizer
   - 2.1 Nonparametric False Alarm Rate Control
   - 2.2 Delay Line Tap Spacing
   - 2.3 Sensitivity of Signal Conditioning to Noise Bandwidth
   - 2.4 Parametric False Alarm Rate Control
   - 2.5 Dynamic Operation of Parametric and Nonparametric Rank Quantizer
   - 2.6 Evaluation of Q3 Thermal Quantizer

3. Improved Q2 Quantizer
   - 3.1 Signal Conditioning Effects
   - 3.2 Scan Correlated Feedback P_N Control
   - 3.3 Scan-Correlated Feedback Operation
   - 3.4 Evaluation of Q2 Thermal Quantizer

4. Quantizer Select

5. Zone Control of T_L

6. ACE AUTO SELECT

7. Delayed Decision Integration

NOTE: 1. Test 1.2 rerun at selected intervals to verify CD operation.
2. The evaluation of Test 5 (Zone Control of T_L) will be accomplished from data obtained on the other tests.

FIGURE 5.32 RECOMMENDED SEQUENCE FOR ENHANCEMENT TESTING AND ANALYSES

TABLE 5.6

TEST OBJECTIVES

Test No.	Objective
1.	Preliminary Tests
1.1	Go/No Go
	In order to prevent the collection of invalid data, a Go/No Go test will be performed to check the test configuration prior to each test and to observe the test data during the test for correctness.
1.2	Baseline
	To measure the false hit rate and target detection statistics of the Common Digitizer prior to the installation of the improvement modifications, and thereby provide a reference with which to compare the performance of the modification. To provide a confidence check of system operation throughout the test period.
2.	Quantizer Q3 Tests
2.1	Nonparametric False Hit Rate Control
	To measure the false hit rate control in log normal and MTI receiver noise with the input buffer circuit enabled and disabled, and to determine the effect that noise amplitude and frequency bandwidth have on P_n.
2.2	Delay Line Tap Spacing Test
	To determine whether a difference in the false hit rate (P_n) occurs when the delay line tap spacing is changed from non-independent (1 μsec) to independent (2 μsec) clutter measurements.
2.3	Sensitivity of Signal Conditioning to Noise Bandwidth
	To measure the false hit rate control at the output of the hit width discriminator as a function of minimum pulse width criteria and CD input signal bandwidth.
2.4	Parametric False Hit Rate Control
	To measure the static scan correlation controls of the false hit rate when the rank quantizer is operated in the parametric mode.

TABLE 5.6 (cont'd)

Test No.	Objective
2.5	Dynamic Operation of the Parametric and Nonparametric Rank Quantizer
	To determine, for log normal and MTI video, if the false hit rate of the rank quantizer and the target detection statistics are affected by different types of clutter when the rank quantizer is operated with and without scan correlated feedback; i.e., parametrically and nonparametrically.
2.6	Evaluation of Q3 Thermal Quantizer
	To determine, for log normal and MTI video, whether the false hit rate (P_n) and target detection statistics of the Q3 quantizer are affected by different types of clutter when operated under its hardware clutter switching mechanism, compared to operating only as a rank quantizer under the same clutter conditions.
3.	Improved Quantizer Q2 Tests
3.1	Input Signal Conditioning Effects
	To measure the target detection sensitivity of the improved Q2 clutter quantizer for three input signal processing conditions. The three conditions are: o No input signal processing o FTC-rectifier o 60 Hz filter with a dead time clamp The sensitivity will be measured as a function of a DC offset voltage which will be added to log normal receiver video. The 60 hertz filter with a dead time clamp is the input buffer circuitry used to condition the input signal to the Q3 quantizer.
3.2	Scan Correlated Feedback P_n Control
	To determine that the scan correlated feedback control can maintain a constant P_n in receiver noise.
3.3	Scan Correlated Feedback Operation
	To measure the ability of the clutter quantizer to maintain a constant P_n from zone to zone when using a noise meter controlled threshold gain and a scan feedback controlled gain. Compare the target reports from both processes to determine if scan correlated feedback control adversely affects target detection.

TABLE 5.6 (cont'd)

Test No.	Objective
3.4	Evaluation of Q2 Thermal Quantizer To determine if target detection is enhanced in clear regions by using the thermal quantizer instead of the clutter quantizer, and whether any target detection variations occur in transition regions due to thermal/clutter quantizer switching.
4.0	Quantizer Select Test To determine if the quantizer select logic provides an improvement in the control of false hit rates and increased target detection capability compared to the optimal quantizer configuration of the CD without scan correlated feedback.
5.0	Zone Control of T_L To determine some typical probability density functions of aircraft count per zone and false alarm count per zone.
6.0	Automatic Clutter Elimination (ACE) Selection Test To measure the azimuth and range correlation recognition capability of the automatic ACE curve selection method for a 12 hit sliding window at selected first threshold false hit rates (P_n). To operate the CD with automatic ACE selection to determine its effect on second threshold detection. Previous runs without automatic ACE selection will be used for comparison purposes.
7.0	Delayed Decision Integration (DDI) To determine the effect of DDI on target detection and in reducing false targets and target splits from the CD. Target report data will be collected using the baseline CD and DDI, and ACE auto select and DDI.

5.4.2 Test Results

CD testing was performed during seven test intervals from July through November 1975. The seven test intervals were as follows:

- o 7,8,9,10 July
- o 30,31 July, 1 August
- o 13,14,15 August
- o 17,18,19 September
- o 24,25,26 September
- o 1,2,3 October
- o 14 November

An abridged summary of each test interval is presented in the following paragraphs. The testing concentrated on trying to accomplish four tests; 1.2 (Baseline), 2.1 (Rank Quantizer-Nonparameter False Alarm Rate Control), 2.2 (Rank Quantizer-Delay Line Tap Spacing) and 2.3 (Rank Quantizer-Sensitivity of Signal Conditioning to Noise Bandwidth). A detailed discussion of tests 2.1, 2.2 and 2.3 commences with Section 5.4.2.1. Test 1.2 is not discussed since quantizer and "D" machine recording problems prevented the attainment of meaningful data.

7,8,9 July

Tests Performed - 1.2, 2.1, and 2.2.

Test Results - None of the tests produced satisfactory results. Test 1.2 data was incorrect because the Improved Quantizers 1 and 2 were in swapped positions. Test 2.1 only worked for log video when the video was AC coupled to the rank quantizer. The rank quantizer was not calibrated prior to the test. Test 2.2 did not work, possibly due to incorrect modification of comparator circuit to disable selected delay line taps.

30,31 July, 1 August

Tests Performed - Investigated equipment to determine reasons for the unsatisfactory results obtained during the previous test interval. Three items were investigated:

1. Unsatisfactory rank quantizer operation with MTI video.
2. The required use of AC coupling of the input video to obtain correct rank quantizer operation.
3. The correct method to disable selected rank quantizer delay line taps.

Test Results - A solution to the MTI video problem could not be determined due to the presence of an additive noise signal. Investigation of the rank quantizer operation revealed the requirement to make center tap gain and bias calibration adjustments prior to testing. AC coupling was determined to be necessary because the rank quantizer delay line and associated circuitry is not presently built to compensate for the impedance variations at all frequencies. The designer compensated by using an average attenuation rather than the low frequency attenuation. The correct method of disabling selected rank quantizer delay line taps was determined. The comparators must be turned on rather than off to get the correct P_n effect.

13,14,15 August

Tests Performed - The elimination of the MTI noise signal and rank quantizer operations were investigated. Test 2.1 was performed and a Test 2.2 delay line configuration (10 taps) was checked under Test 2.1 conditions.

Test Results - The MTI noise signal was eliminated as an input to the delay line by installing an existing NAFEC circuit, used to AC couple the video to a test terminal radar rank quantizer, in place of the Burroughs input buffer circuit. The gain vs. frequency response of the NAFEC circuit was measured and found to be satisfactory. The attenuation compensation for each delay line tap used to adjust the center tap voltage prior to comparison was measured and found to be satisfactory. Using the latest estimate of how to calibrate the rank quantizer, Test 2.1 was performed and satisfactory P_n control obtained only with log video. Satisfactory performance was adjudged to be a measured P_n resulting in a P_n error of less than 10 percent from the selected value. A 10 percent error approximately doubles the number of false targets obtained at a selected P_n. Rank quantizer test results so far indicate that the quantizer, as implemented with this modification, is not a distribution free device.

17,18,19 September

Tests Performed - Testing commenced after a two week delay to correct several CD equipment failures. Test 1.2 and a functional nonparametric rank quantizer test were performed.

Test Results - The baseline test (1.2) was run without difficulty. The functional rank quantizer test produced unsatisfactory results. CD output target blanking occurred in rain clutter areas. A revised rank quantizer calibration adjustment procedure was tried and the blanking problem eliminated. However, ACE had to be enabled to eliminate continuous Output Buffer Overload Alarms. The overall test results indicated the need for a better rank quantizer calibration procedure.

24,25,26 September

Tests Performed - The rank quantizer calibration procedure was investigated further and tests 2.1 and 2.2 again performed.

Test Results - A correct calibration procedure was finalized that covered all rank quantizer circuit adjustments. Test 2.1 was completed with satisfactory results (both log and MTI video) using the 24 tap Burroughs designed delay line configuration. Three other delay line candidates for Test 2.2 were checked using the Test 2.1 procedure. Quantizer operation was affected considerably by the delay line configuration. Of the three configurations, only the 10 tap, 2 μsec tap spaced, 3 μsec buffer zone configuration produced acceptable performance. Test 2.2 produced inconclusive results. Manual data taken with digital counters resulted in large P_n errors and the tape recordings could not be processed due to numerous short records and parity errors. Photographs taken of the video during Test 2.2 showed MTI limiting in rain clutter. Target information is lost when the signal limits, therefore the recorded rain clutter MTI video was not used in future testing.

1,2,3 October

Tests Performed - Test 2.3 was completed, the rank quantizer comparator signal response was measured, Test 2.2 was again attempted and a P_n Mode 1 calibration recording was made with the hit width discrimination (HWD) circuit connected.

Test Results - Test 2.3 results were satisfactory. The HWD circuit has a pronounced effect on P_n. It is sensitive to the input video distribution and changes P_n according to the discrimination selected. Operation at 1/32 nmi minimum discrimination produces the least effect. The P_n error is still large at 1/32 nmi; 1.2 percent measured vs. 4 percent selected. No hits are output when 3/32 nmi minimum discrimination is selected. The HWD destroys the constant P_n characteristics of the theoretical rank quantizer.

The comparator signal response was measured for all comparators. The response was the same for all comparators; a slow rise time (1.25 μsec) and a rapid fall time was measured. Since the LM311N comparator response time specification is 0.2 μsec, input capacitive effects are most likely causing the slow rise time.

The P_n calibration recording was successful. The data shows that, even though the HWD reduces the P_n count, the P_n occurring in the M/N is more than double the P_n selected after the 1/4 nmi peak detection.

14 November

Test Performed - A major "D" machine recording problem had developed (parity errors and short records), so testing was delayed a month. A one day test interval was scheduled and the following was accomplished:

- Determined the latest status of the "D" machine recording problem.
- Completed a bandwidth vs. P_n rank quantizer test for the 18 tap, 1 μsec tap spaced, 3 μsec buffer zone delay line configuration.
- Obtained en route VQR tapes for analysis
- Attempted to perform Test 3.1 (Improved Q_2 Quantizer - Signal conditioning effects).

Test Results - The "D" machine recording problem still existed. Assistance was required from Burroughs since the FAA had no information to troubleshoot the problem.

The bandwidth vs P_n test showed that the 18 tap configuration was too bandwidth sensitive. This rank quantizer delay line configuration should not be considered as a candidate for Test 2.2. Test 3.1 would not work because the Improved Q_2 Quantizer would not regulate P_n correctly. Additionally, a 11/16 VDC power supply failed and the 5 VDC power supply output terminal board began to burn. Due to the numerous problems, testing was suspended.

5.4.2.1 Test 2.1 (Nonparametric False Hit Rate Control)

5.4.2.1.1 Discussion

The objective of Test 2.1 was to measure the false hit rate control in log normal and MTI video thermal noise with the input buffer circuit enabled and disabled, and to determine the effect that noise amplitude and frequency bandwidth have on P_n.

A constant false hit rate is obtained for the rank quantizer by comparing the output of each tap against the center tap. The comparator outputs are summed and the result compared to a fixed threshold.

The rank quantizer, when operating without center tap bias, has a first threshold false hit rate (P_n) of:

$$P_n = 1 - \frac{TR}{n+1}$$

where n is the number of taps, excluding the center tap, and TR is the rank threshold (the number of taps that the center tap must be greater than). The P_n for the 24 tap rank quantizer can be varied in four percent increments.

Figure 5.33 presents the equipment setup for the performance of Test 2.1. The test approach was implemented as follows:

For selected threshold P_n values, the radar was configured to provide random noise at signal levels from 0.1 to 2.0 volts mean peak while operating in the log normal and MTI receiver modes. The various noise voltage levels were obtained by attenuating the signal with an attenuator. An additional wide band amplifier was required to boost the signal to account for attenuation across the filter. The filter was used to change the noise bandwidth. The quantizer output hit count rate was sampled every 1/32 nmi and recorded with an electronic counter.

Considerable time was spent trying to obtain successful nonparametric rank quantizer P_n control. Satisfactory performance was not obtained until a calibration procedure was determined that accounted for all the circuit adjustments provided by the Burroughs design engineer.

Test 2.1 data for the first test interval (7,8,9,10 July) was taken without doing any calibration adjustments. The results of the first test interval are summarized in Table 5.7.

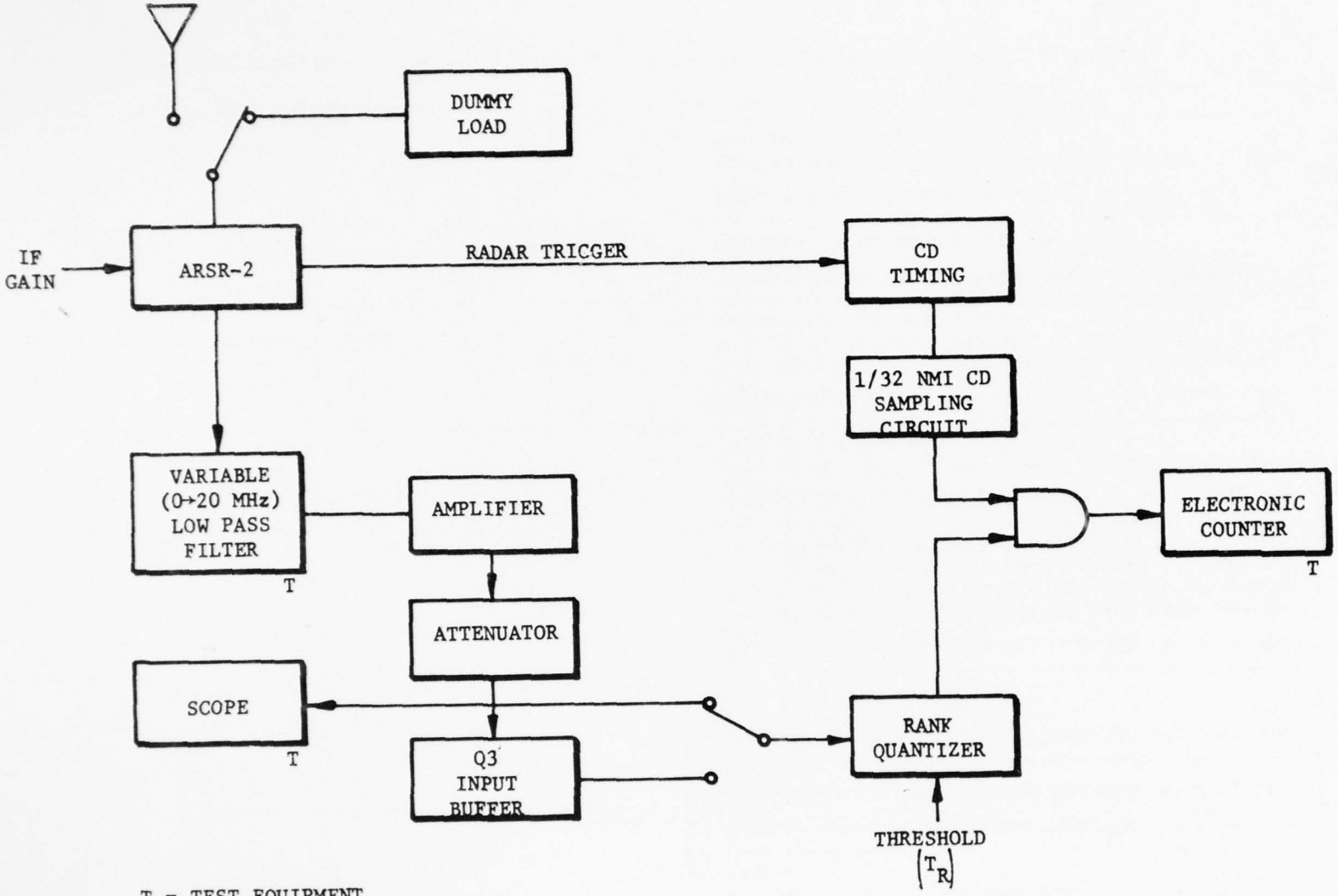

FIGURE 5.33 EQUIPMENT SETUP FOR P_N MEASUREMENT

Date	Video	Input Buffer	Filter (500 kHz)	Quantizer Input Volts p/p	Remarks
7 July	Log	Enabled	Disabled	2.0 to 0.25 *	Satisfactory - ΔP_N less than 10% for all ranks and voltages. Slight rank and voltage sensitivity indicated.
7 July	MTI	Enabled	Disabled	2.0 to 0.25 *	Unsatisfactory - ΔP_N greater than 10% for most ranks and voltages. Large voltage and rank sensitivity.
7 July	MTI	Disabled	Disabled	2.0 to 0.25 *	Unsatisfactory - ΔP_N greater than 10% for voltages less than 1.0 volt p/p.
8 July	MTI	Disabled	Disabled	1.0 to 0.125 **	Unsatisfactory - ΔP_N greater than 10% for most ranks and voltages. Large voltage and rank sensitivity. Determined that input buffer drops input voltage by 1/2. Adjusted test voltages to obtain a consistant voltage input to delay line.
8 July	MTI	Disabled	Enabled	1.0 to 0.125 **	Unsatisfactory - Large variations in ΔP_N. ΔP_N greater than 10% for most ranks and voltages. Large voltage and rank sensitivity.
8 July	Log	Disabled	Enabled	1.0 to 0.125 **	Unsatisfactory - Excessively large ΔP_N values. It was determined that the quantizer will not operate without input buffer circuit. The video must be AC coupled to the delay line.
8 July	Log	Disabled	Disabled		
8 July	Log	Enabled	Enabled	0.75 to 0.125 **	Satisfactory - ΔP_N less than 10% for all ranks and voltages. Rank sensitivity indicated.
8 July	MTI	Enabled	Enabled	0.75 to 0.125 **	Unsatisfactory - Large variations in ΔP_N. ΔP_N greater than 10% for most ranks and voltages. Large rank and voltage sensitivity.

* Measured at input to input buffer circuit

** Measured at input to the delay line.

SUMMARY OF RANK QUANTIZER NONPARAMETRIC P_n CONTROL TEST RESULTS WITH RECEIVER NOISE 7, 8 JULY 1975
TABLE 5.7

The following observations were made:

- Satisfactory results could only be obtained for log video with the input video AC coupled to the delay line (input buffer circuit enabled).
- Reducing the video bandwidth with the filter (set at 500 kHz) produced a small change in the measured P_n (4 percent change).
- The quantizer operated satisfactorily for low log normal input voltage but showed unsatisfactory performance for MTI at low voltages.
- Rank sensitivity was indicated for all tests.

Data supporting these observations are presented in Tables 5.8 through 5.10. At this point in the testing it was thought that a hardware failure was present in the rank quantizer circuitry. The quantizer had recently been adjusted and operated for sell-off tests that were accepted by the FAA. Methods of testing the rank quantizer to determine the problem and explain the results of the first test interval were investigated and implemented in the next test interval (30, 31 July, 1 August).

During the next test interval the video signals were traced through the rank quantizer, the gain and frequency response of the input buffer circuit and delay line were measured and initial calibration procedures to adjust the rank quantizer center tap gain and bias were checked.

The MTI video could not be checked because of an interference problem; a 60 Hz modulation with a lot of harmonics was added to the signal. This could be a grounding problem, power supply coupling, or oscillation in the high pass filter (input buffer); as is typical of these sorts of problems, a number of hours were spent without finding a solution. The interference was present on the MTI but was not found on the log video. Also, the high pass filter amplified the problem; the input to the filter had about 80 mv pp on a 5 v pp MTI signal, whereas the output of the filter had about 400 mv pp on a 2 1/2 v pp signal. (This was measured at the beginning of the delay line; i.e., the filter output after the 200 Ω driving resistor.)

The AC coupling was determined to be necessary because the low frequency attenuation of the delay line is not the same as that above 200 kHz and when the circuit designer compensated for attenuation in the comparator circuits, an "average" (across frequency) sort of attenuation was used rather than the low frequency attenuation. The reason for the AC coupling is that any DC voltage, which is often present on video amplifiers, is not correctly compensated and thus gives incorrect rank results.

AD-A038 491 JOHNS HOPKINS UNIV LAUREL MD APPLIED PHYSICS LAB F/G 17/7
SYSTEM DEFINITION AND INVESTIGATION OF THE ON-SITE PROCESSING O--ETC(U)
SEP 76 J W THOMAS, E C WETZLAR, L H ZITZMAN DOT-FA75WA-3553
UNCLASSIFIED APL/JHU-FP8-E-024-1 FAA-RD-77-12-1 NL

3 OF 3
AD A038491

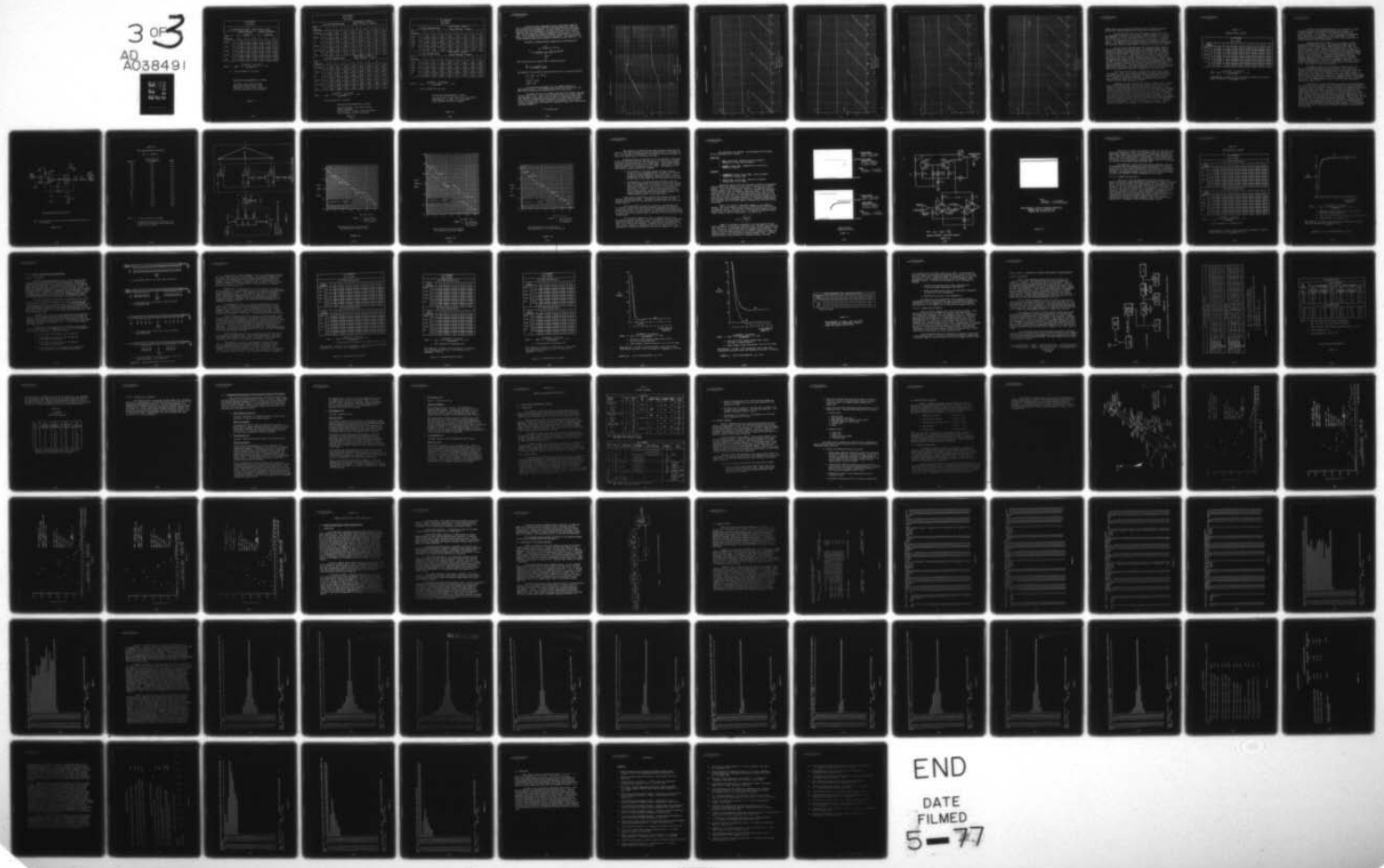

END
DATE FILMED
5-77

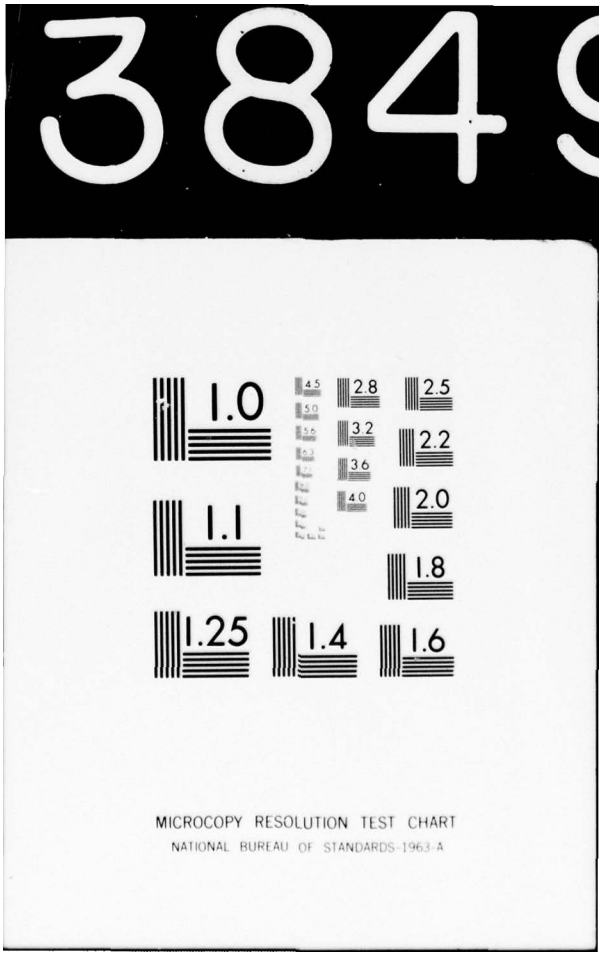
3849
1.0
1.1
1.25
1.4
1.6
1.8
2.0
2.2
2.5
2.8
3.2
3.6
4.0
4.5
5.0
5.6
MICROCOPY RESOLUTION TEST CHART
NATIONAL BUREAU OF STANDARDS-1963-A

P_N% MEASURED (ΔP_N% ERROR)							
LOG VIDEO RECEIVER NOISE: INPUT BUFFER DISABLED							
		Filter (500 kHz) enabled			Filter (500 kHz) disabled		
P_N% Selected		4	8	12	4	8	12
Delay	1.0	2.36 (-41)	5.37 (-33)	8.54 (-29)	2.67 (-33)	5.84 (-27)	9.24 (-23)
Line	0.75	2.47 (-38)	5.53 (-31)	8.78 (-27)	2.67 (-33)	5.88 (-27)	9.28 (-23)
Input	0.50	2.55 (-36)	5.64 (-30)	8.93 (-26)	2.71 (-32)	5.92 (-26)	9.32 (-22)
Volts	0.20	2.94 (-26)	6.38 (-20)	9.98 (-17)	2.90 (-28)	6.34 (-21)	9.86 (-18)
p/p	0.25	3.56 (-11)	7.58 (-5)	11.68 (-3)	3.25 (-19)	6.96 (-13)	10.75 (-10)

Notes: 1. $\Delta P_N\% = \dfrac{P_N \text{ measured} - P_N \text{ selected}}{P_N \text{ selected}} \times 100$

2. Test performed on 8 July 1975

RECEIVER NOISE NONPARAMETRIC P_n CONTROL

Log Video - Input Buffer disabled, filter enabled and disabled. Rank Quantizer - 24 taps, 1 μsec tap spacing. Center tap gain and bias not adjusted.

TABLE 5.8

P_N% MEASURED (ΔP_N% ERROR)									
LOG VIDEO RECEIVER NOISE: Input Buffer - Enabled, Filter (500 kHz) - Disabled									
P_N% Selected		4	8	12	16	20	24	28	32
Voltage	2.0	4.01 (0)	8.04 (1)	12.33 (3)	16.79 (5)	21.15 (6)	25.52 (6)	29.89 (7)	34.37 (7)
Input	1.5	3.97 (-1)	8.01 (0)	12.28 (2)	16.71 (4)	21.06 (5)	25.44 (6)	29.79 (6)	34.26 (7)
To	1.0	3.96 (-1)	7.93 (-1)	12.21 (2)	16.58 (4)	20.92 (5)	25.31 (5)	29.64 (6)	34.06 (6)
Buffer	0.5	3.83 (-3)	7.74 (-3)	11.98 (0)	16.19 (1)	20.57 (3)	24.89 (4)	29.11 (4)	33.64 (5)
Circuit	0.4	3.60 (-10)	7.52 (-5)	11.71 (-2)	15.72 (-2)	20.37 (2)	24.40 (2)	28.64 (2)	33.13 (4)
p/p	0.25	3.75 (-6)	7.48 (-7)	11.65 (-3)	15.62 (-2)	20.41 (2)	24.32 (1)	28.53 (2)	33.10 (3)
MTI VIDEO RECEIVER NOISE: Input Buffer - Enabled, Filter (500 kHz) - Disabled									
P_N% Selected		4	8	12	16	20	24	28	32
Voltage	2.0	4.23 (6)	8.75 (9)	13.38 (12)	18.40 (15)	23.62 (18)	28.80 (20)	34.18 (22)	39.63 (24)
Input	1.5	4.21 (5)	8.74 (9)	13.38 (12)	18.40 (15)	23.82 (19)	29.42 (23)	34.64 (24)	40.21 (26)
To	1.0	4.21 (5)	9.01 (13)	13.84 (15)	18.95 (18)	24.63 (23)	31.32 (31)	34.07 (22)	41.95 (31)
Buffer	0.5	5.01 (25)	11.17 (40)	16.39 (55)	22.04 (38)	30.58 (53)	36.34 (51)	40.40 (44)	45.62 (43)
Circuit	0.4	6.19 (55)	13.34 (67)	18.95 (58)	25.09 (57)	33.25 (66)	38.16 (59)	42.84 (53)	46.78 (46)
p/p	0.25	6.77 (69)	14.89 (186)	20.61 (72)	28.15 (76)	35.61 (78)	40.09 (67)	44.08 (57)	45.56 (42)

Notes: 1. $\Delta P_N\% = \dfrac{P_N \text{ measured} - P_N \text{ selected}}{P_N \text{ selected}} \times 100$

2. Test performed on 7 July 1975

RECEIVER NOISE NONPARAMETRIC P_n CONTROL

Log and MTI Video - Input Buffer enabled,
Filter - disabled.
Rank Quantizer - 24 taps, 1 μsec tap spacing.
Center tap gain and bias not adjusted.

TABLE 5.9

P_N% MEASURED (ΔP_N ERROR)									
LOG VIDEO RECEIVER NOISE:					Input Buffer - Enabled Filter (500 kHz) - Enabled				
P_N% Selected		4	8	12	16	20	24	28	32
Delay Line Input Volts p/p	0.75	3.67 (-8)	7.66 (-4)	11.87 (-1)	16.32 (2)	20.61 (3)	24.94 (4)	29.27 (5)	33.64 (5)
	0.50	3.71 (-7)	7.66 (-4)	11.87 (-1)	16.32 (2)	20.57 (3)	24.94 (4)	29.23 (4)	33.56 (2)
	0.20	3.71 (-7)	7.66 (-4)	11.87 (-1)	16.28 (2)	20.57 (3)	24.90 (4)	29.19 (4)	33.56 (2)
	0.125	3.87 (-3)	7.96 (0)	12.33 (3)	16.90 (6)	21.27 (6)	25.60 (7)	29.96 (7)	34.45 (8)
MTI VIDEO RECEIVER NOISE:					Input Buffer - Enabled Filter (500 kHz) - Enabled)				
P_N% Selected		4	8	12	16	20	24	28	32
Delay Line Input Volts p/p	0.75	4.14 (4)	8.55 (7)	13.11 (9)	18.09 (13)	23.47 (17)	28.77 (20)	34.57 (23)	40.21 (26)
	0.50	4.14 (4)	8.55 (7)	13.07 (9)	18.21 (14)	23.47 (17)	28.61 (19)	34.80 (24)	40.40 (26)
	0.20	5.18 (30)	9.67 (21)	14.77 (23)	20.88 (31)	29.77 (49)	32.86 (37)	39.44 (41)	44.08 (38)
	0.125	6.84 (71)	13.18 (65)	18.13 (51)	24.36 (52)	30.74 (54)	36.61 (53)	41.37 (48)	46.20 (44)

Notes: 1. $\Delta P_N = \dfrac{P_N \text{ measured} - P_N \text{ selected}}{P_N \text{ selected}} \times 100$

2. Test performed on 8 July 1975

RECEIVER NOISE NONPARAMETRIC P_n CONTROL

Log and MTI Video - Input Buffer and Filter Enabled.
Rank Quantizer - 24 taps, 1 μsec tap spacing.
Center tap gain and bias not adjusted.

TABLE 5.10

In order to better understand the gain compensation trade-offs and AC coupling, the transfer function of the high pass filter (HPF) and the delay line were both measured. The HPF transfer function was measured from its input to the beginning of the delay line (after a 200 Ω driving resistor); the delay line transfer was measured from its input to the 24th tap. This is probably not the most desirable configuration but it was not known at the time that the 200 Ω resistor was present. The resulting plots of the transfer functions are presented in Figures 5.34 and 5.35(a, b, c, d).

The HPF is a standard design configuration (see Reference 35):

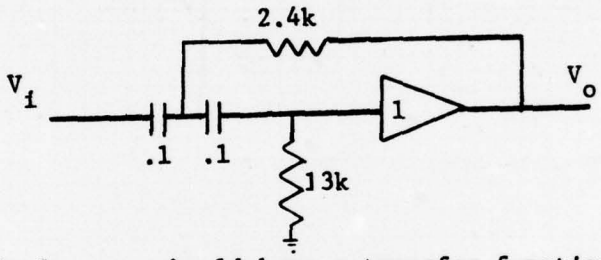

and this particular one should have a transfer function:

$$\frac{V_o}{V_1} = \frac{S^2}{S^2 + 1538S + 3.21E6}$$

The magnitude of the transfer function should have the following parameters:

$W_o = 1790, \quad f_o = 285$ Hz

$\delta = .43$

f peak ~ 310 Hz

peak ~ 3 dB

As can be seen from Figure 5.34, the transfer function is approximately correct. The attenuation and ripple are probably due to the 200 Ω drive resistor and the characteristics of the delay line.

The delay line acts as an almost ideal delay line between 4 kHz and 200 kHz (Figure 5.35). Below 4 kHz the gain is good but the phase peaks and then disappears; there appears to be no delay for frequencies below 1 kHz. Above 200 kHz, the phase is reasonably good but the gain starts decreasing. To get the best match of phase, the delay was estimated by least squares fitting a straight line to the phase for frequencies between 200 k and 400 kHz. The delay estimate is

$$\hat{T} = 24.3446 \text{ μsec};$$

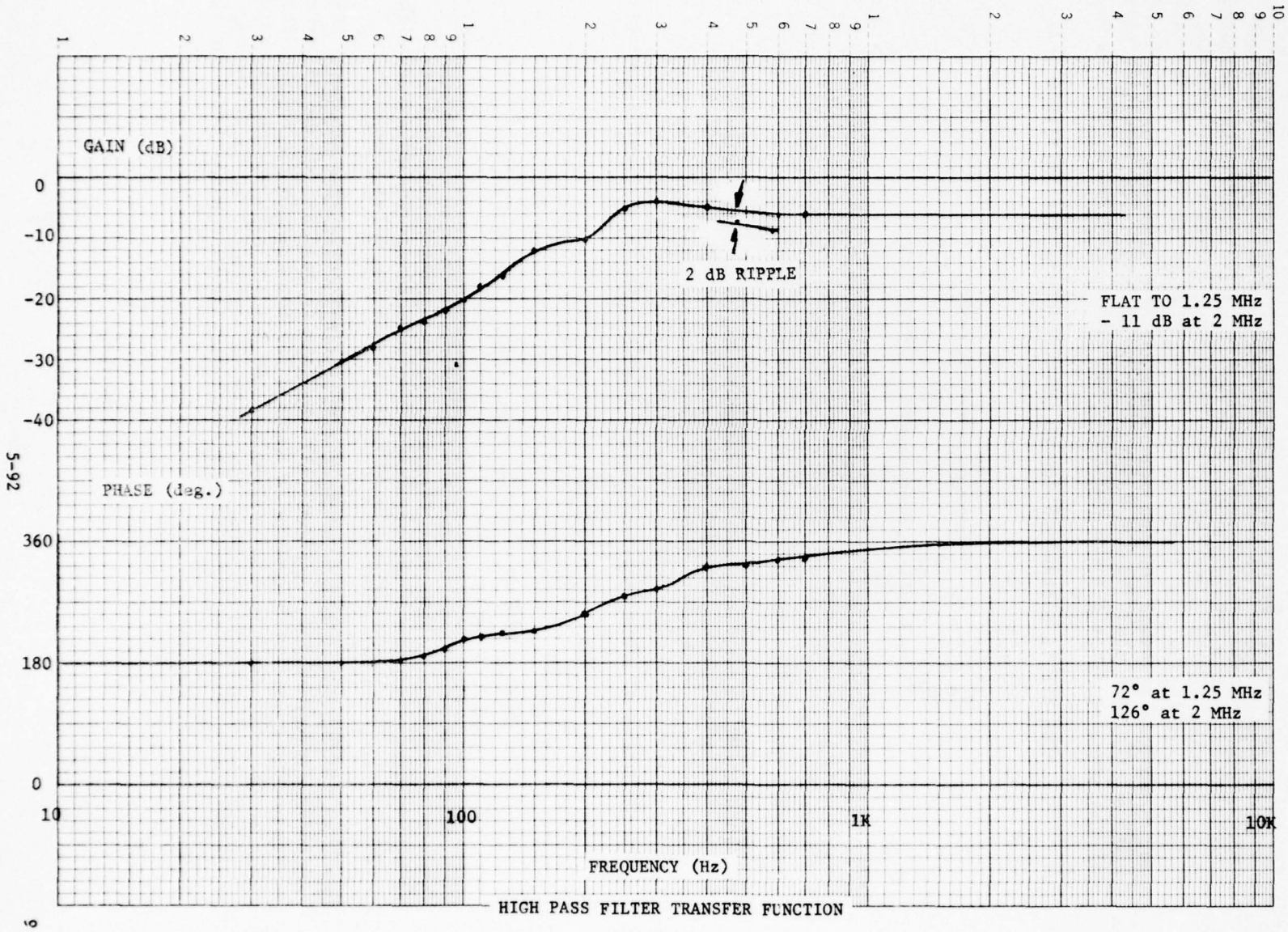

HIGH PASS FILTER TRANSFER FUNCTION

FIGURE 5.34

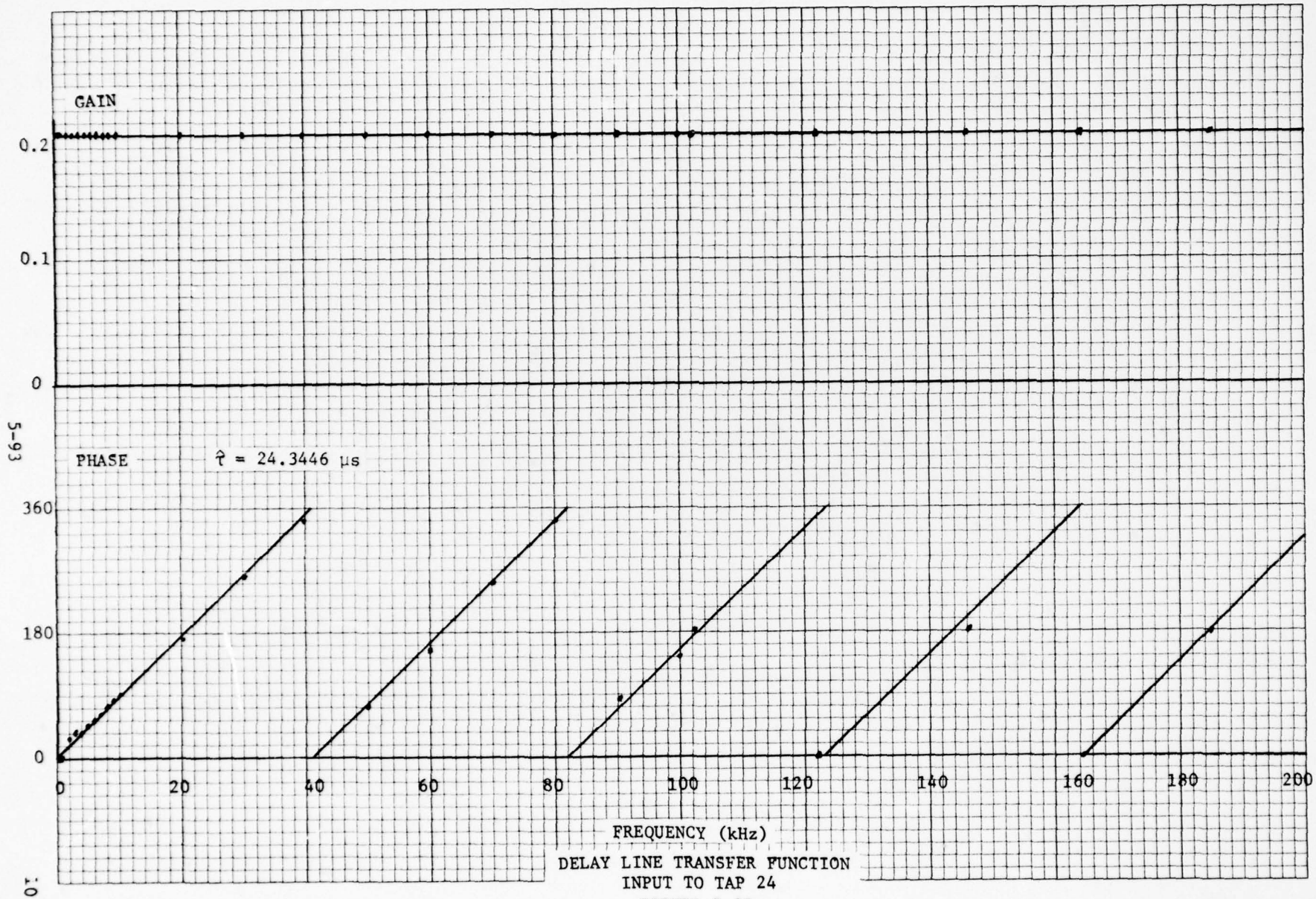

DELAY LINE TRANSFER FUNCTION
INPUT TO TAP 24
FIGURE 5.35a

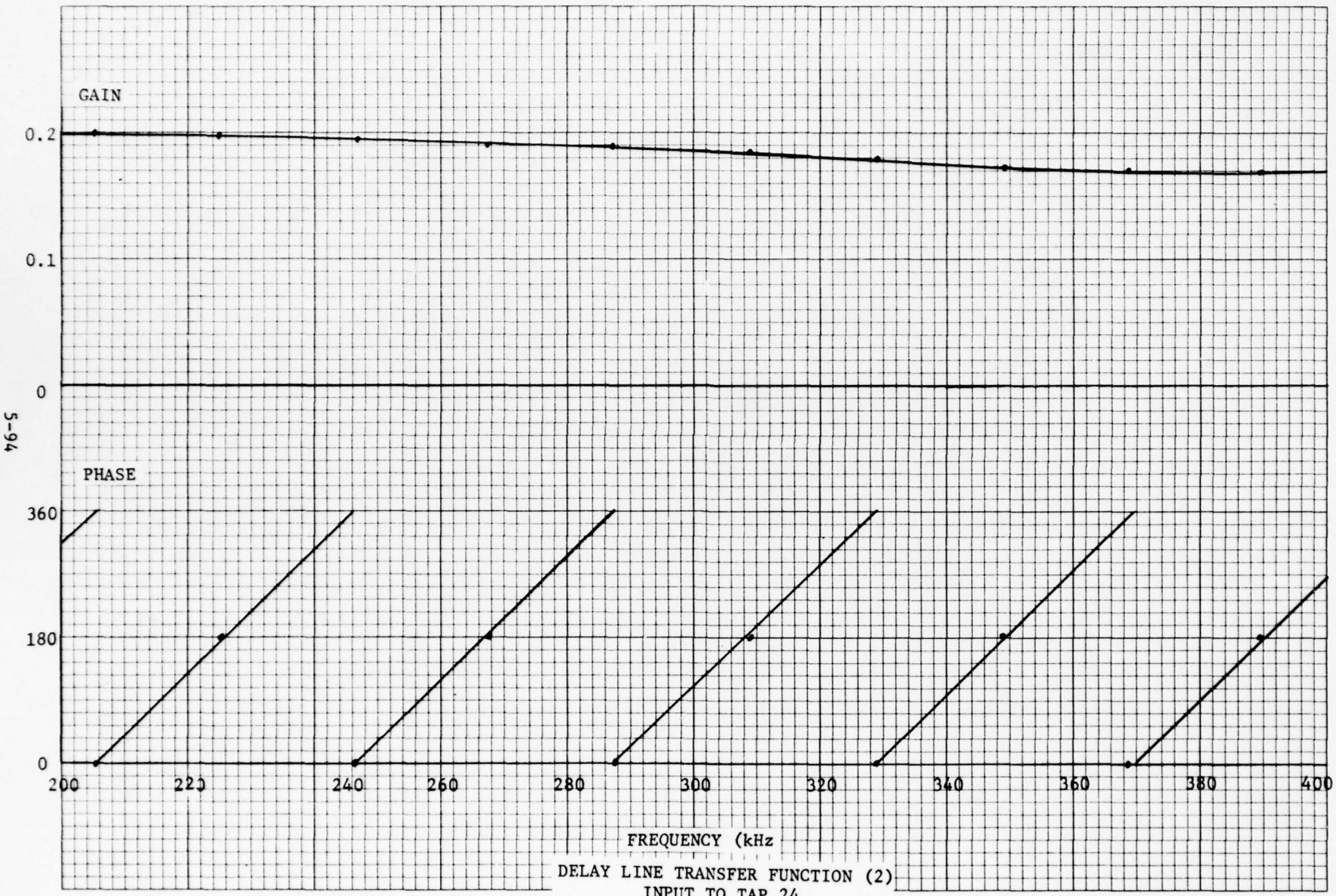

DELAY LINE TRANSFER FUNCTION (2)
INPUT TO TAP 24

FIGURE 5.35b

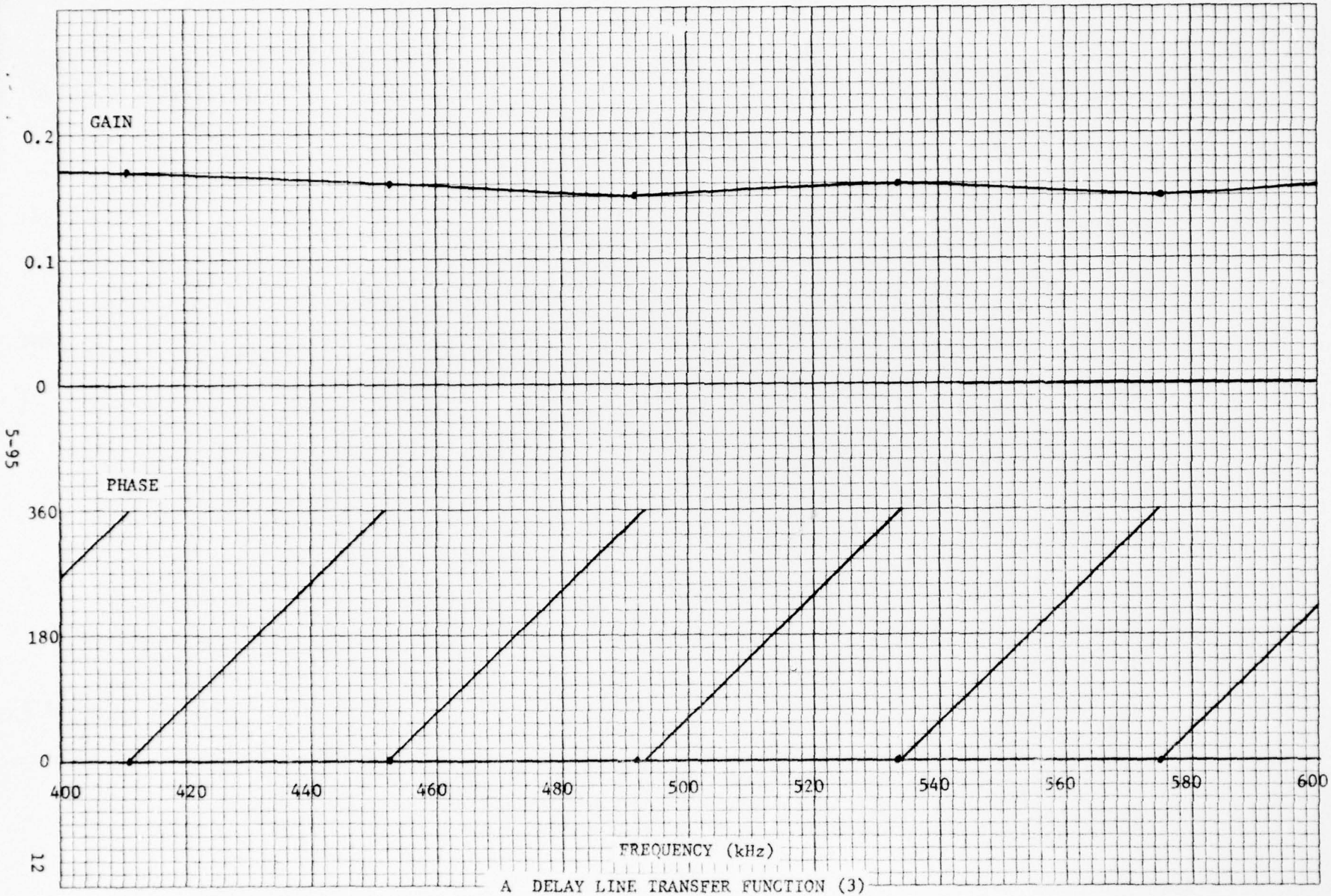

A DELAY LINE TRANSFER FUNCTION (3)
INPUT TO TAP 24
FIGURE 5.35c

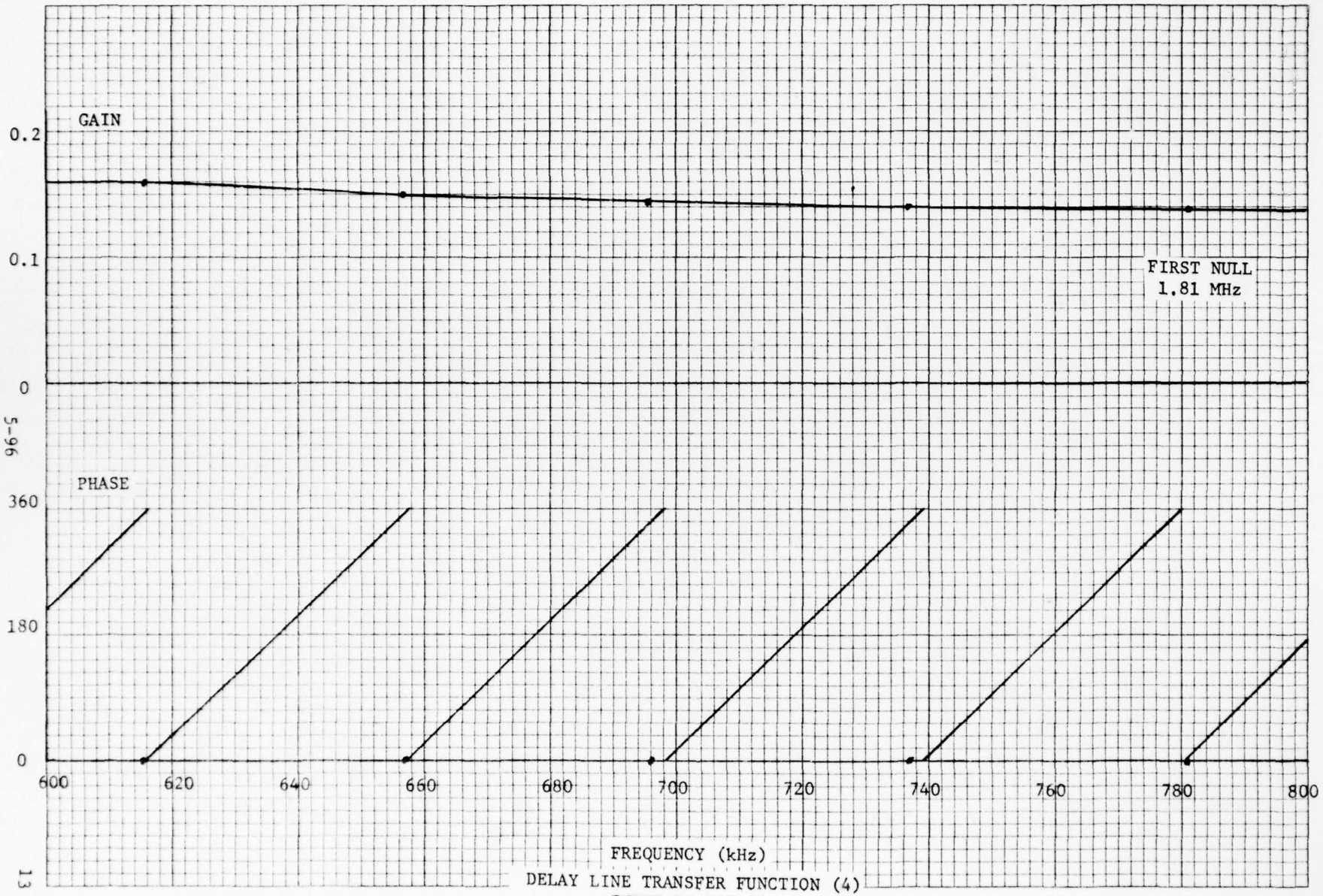

DELAY LINE TRANSFER FUNCTION (4)
INPUT TO TAP 24

FIGURE 5.35d

simply using 24 μsec results in large phase errors at higher frequencies and does not adequately characterize the quality of the delay line.

An investigation of the delay line bandwidth specifications and the measurement of the delay line frequency response revealed that the delay line bandwidth is 500 kHz. The small change in P_n, observed after setting the low pass filter to 500 kHz during the first test interval, thus appears correct. The additional serial filtering reduces the bandwidth a small amount. The simulation of correlation effects by varying the video bandwidth thus requires a lesser bandwidth before a significant P_n effect can be seen.

The two curves of HPF and delay line transfer functions should provide some idea of the trade-offs made in the Burroughs design. How the delay line attenuation was compensated and why the exotic HPF with peaking at 300 Hz is anyone's guess; the argument for the HPF is just as valid at 100 kHz as it is at 300 Hz. However, the one fact which is certain is that the device is not ideal. A better approach would be to get a delay line while has at least as good phase, a constant attenuation out to about 1 MHz, to compensate the comparators for the low frequency attenuation, and to remove the HPF. The cost of such a delay line has not been investigated, but a large cost would suggest consideration of alternate techniques such as analog or digital shift registers. The present delay line acts like a succession of low pass filters, with some sort of gain compensations, and the effect is likely to make the false alarm rate depend on the parameters of the input video.

Test results indicate that a revised input buffer circuit should be considered. There is no reason to incorporate an exotic filter with its associated peaking at 300 Hz, a frequency which probably causes rank errors due to incorrect attenuation compensation. A simple buffered RC would be just as effective, would have no low frequency peaking, and might even eliminate the MTI signal interference problem.

Examination of the rank quantizer circuitry revealed that a calibration procedure was necessary. Numerous adjustments were designed into the system but no adjustment procedure had been documented that could be found. A method to adjust the center tap gain and bias pots was suggested by Burroughs. The method adjusted the gain pot for the correct P_n with a large input voltage (2 volt p/p) and then adjusted the bias pot for the correct P_n with a small input voltage (.125 volt p/p). While performing this procedure it was found that better results could be obtained by iterating the procedure 2 or 3 times. Table 5.11 presents P_n control results for log video noise using this procedure. The results (rank sensitivity) seem to indicate that the gain and bias pots are correctly adjusted but the two rank threshold pots are not. The rank threshold adjustment was scheduled to be investigated at a later date.

TABLE 5.11

RECEIVER NOISE P_n CONTROL

		P_n % MEASURED (ΔP_n % ERROR							
P_n% SELECTED		4	8	12	16	20	24	28	32
DELAY LINE INPUT VOLTS P/P	2.0	3.94 (-1.5)	7.81 (-2.4)	12.02 (.1)	16.55 (3.4)	21.19 (5.95)	25.90 (7.9)	30.58 (9.2)	35.3 (10.3)
	1.5	3.98 (-.5)	7.88 (-1.5)	12.10 (.8)	16.66 (4.1)	21.34 (6.7)	26.02 (8.4)	30.78 (9.9)	35.53 (11.0)
	1.0	4.02 (.05)	7.96 (- .5)	12.26 (2.2)	16.85 (5.3)	21.57 (7.8)	26.29 (9.5)	31.05 (10.9)	35.84 (12.0)
	.75	4.09 (2.25)	8.16 (2)	12.49 (4.08)	17.17 (7.3)	21.96 (9.8)	27.76 (11.5)	31.55 (12.7)	36.34 (13.6)
	.50	3.98 (-.05)	8.27 (3.4)	12.84 (7.0)	17.59 (9.9)	22.46 (12.3)	27.45 (14.4)	32.32 (15.4)	37.27 (16.5)
	.25	4.56 (14)	9.94 (24.3)	15.89 (32.4)	22.31 (39.4)	29.19 (45.9)	36.30 (51.3)	43.30 (18.9)	50.49 (57.8

NOTE: $\Delta P_n\% = \dfrac{P_n \text{ measured} - P_n \text{ selected}}{P_n \text{ selected}} \times 100$

Rank Quantizer - 24 taps, 1 μsec tap spacing, nonparametric operation, center tap adjusted for Log Video at 4% P_n.

A change in test philosophy appeared to be in order as a result of investigating the rank quantizer during this test interval. As originally specified in the task, APL was supposed to perform only system type tests. An involvement in the actual design of the equipment was not determined to be necessary in order to understand the design trade-offs and the adjustments which must be made, and to ensure that the mathematical models include these effects.

During the third test interval (13, 14, 15 August) the rank quantizer investigation continued. The additive MTI noise signal was eliminated by the installation of a NAFEC designed circuit, used to AC couple the video to a test terminal radar rank quantizer, in place of the Burroughs designed circuit. Future testing did not result in improved P_n control with MTI receiver noise after the additive noise signal was removed. The circuit was used for all further testing because it presented a cleaner signal to the rank quantizer. The NAFEC circuit designated the rank quantizer delay line driver, is presented in Figure 5.36. The Gain vs. Frequency response of the NAFEC circuit was measured to determine its operating characteristics. This data is presented in Table 5.12. The gain is flat for frequencies from 60 Hz to 1 mHz and drops off rapidly below 60 Hz. Satisfactory AC coupling is indicated.

The transfer function of the delay line between the input and tap 24 was measured during the last test interval. This time it was decided to measure the relationship between the center tap (Pin 2) and each tap (Pin 3) at the input to each comparator for a 1 volt peak to peak signal input to the delay line. Variation of the input signal frequency will show the delay line attenuation changes with frequency, the tap to tap attenuation at a given frequency, and the center tap compensation prior to comparison to each tap. The rank quantizer circuitry involved in this measurement is presented in Figure 5.37.

Figures 5.38, 5.39 and 5.40 present the results of these measurements for a 50 kHz and 500 kHz sinewave, and a 2 microsecond 100 kHz pulse signal. The figures show the comparison of each tap voltage to the respective attenuation compensated center tap voltage. The measured center tap voltage has been adjusted mathematically for the best gain value since the gain was not fine tuned prior to the test. The comparison for the 50 kHz sinewave and the pulse signal indicates that the center tap voltage is properly compensated at all taps. The delay line attenuation is also satisfactory, being -0.16 and -0.18 dB/microsecond for the 50 kHz and pulse signal respectively. Typical delay line attenuation for a lumped constant delay line is 0.001 to 0.1 dB/microsecond. Center tap voltage compensation and tap attenuation (-0.29 dB/microsecond) at 500 kHz is not as good as for the 50 kHz and pulse signals. This is expected since 500 kHz is the -3 dB attenuation frequency that defines the bandwidth of the delay line.

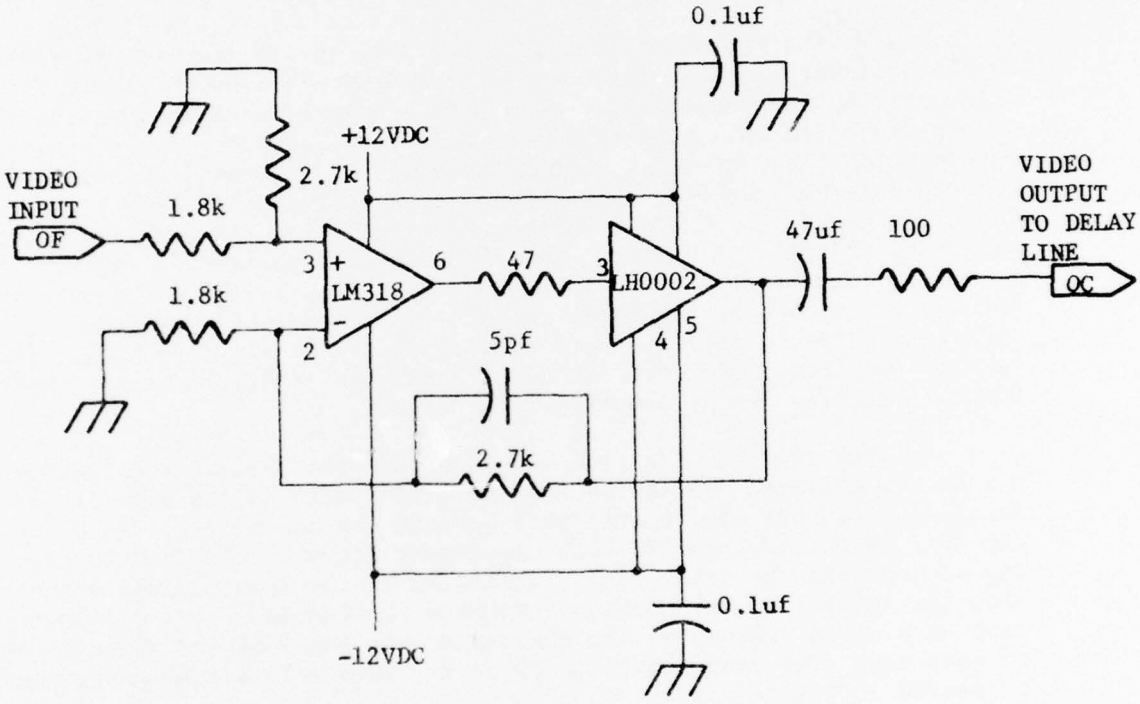

RANK QUANTIZER DELAY LINE DRIVER

NOTE: Delay line driver used to replace Burroughs input buffer on card DE DA67.

FIGURE 5.36

TABLE 5.12

RANK QUANTIZER DELAY LINE DRIVER

Gain vs. Frequency

Frequency	Output Volts[1] p/p (Pin DA6C)	Gain[2]
100k	1.50	0.75
94k	1.45	0.73
83k	1.45	0.73
74k	1.50	0.75
64k	1.46	0.73
55k	1.50	0.75
40k	1.47	0.74
32k	1.50	0.75
10k	1.50	0.75
1k	1.50	0.75
500	1.49	0.75
100	1.47	0.74
60	1.45	0.73
10	1.00	0.50
5	0.70	0.35
3	0.30	0.25
1	0.15	0.08

Notes: 1. 2 volts p/p input at pin DA6F.

2. No phase shift except at 5 and 10 hz. 36 degree shift occurred at these frequencies. Gain is flat to 1 mHz.

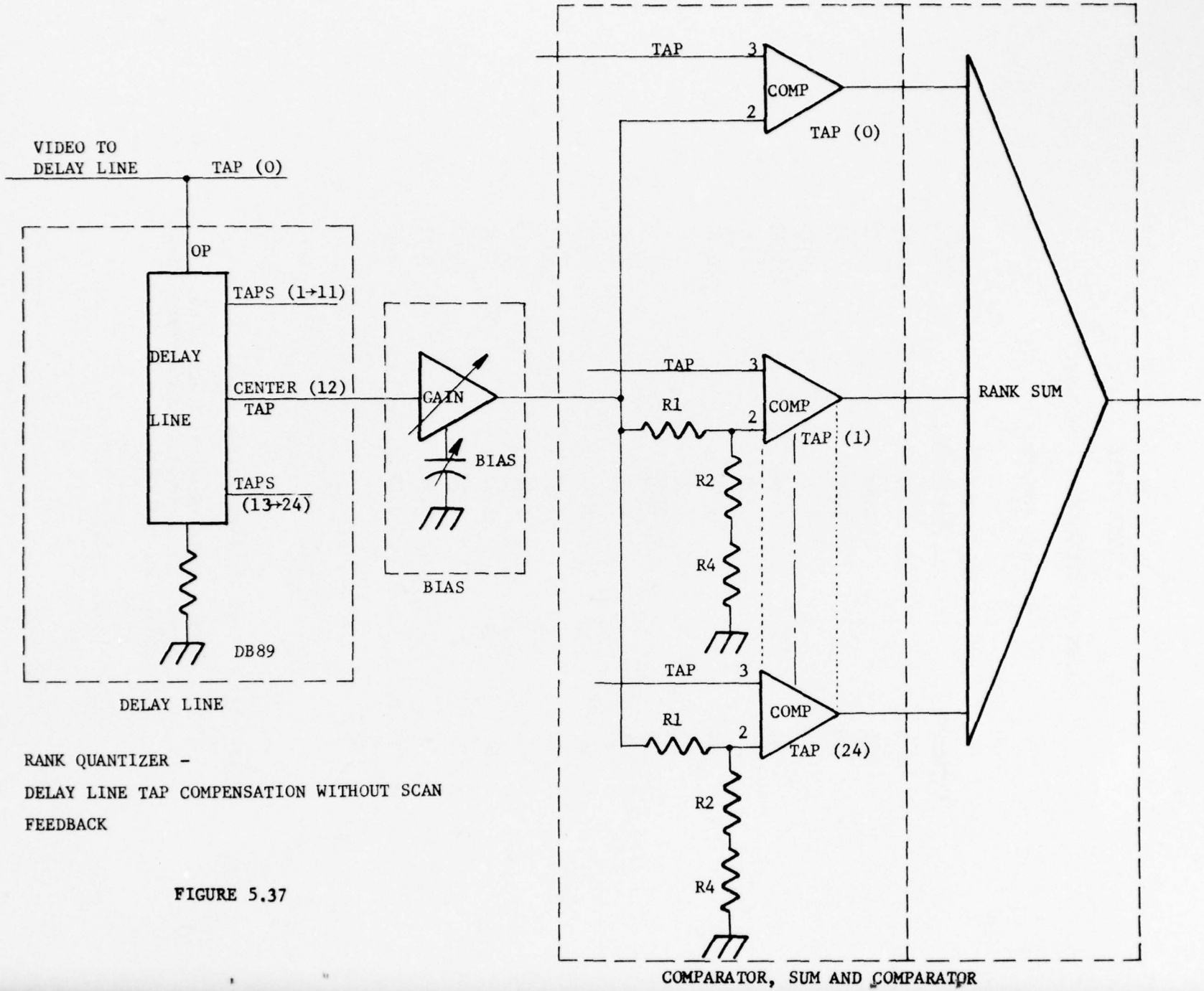

RANK QUANTIZER -
DELAY LINE TAP COMPENSATION WITHOUT SCAN
FEEDBACK

FIGURE 5.37

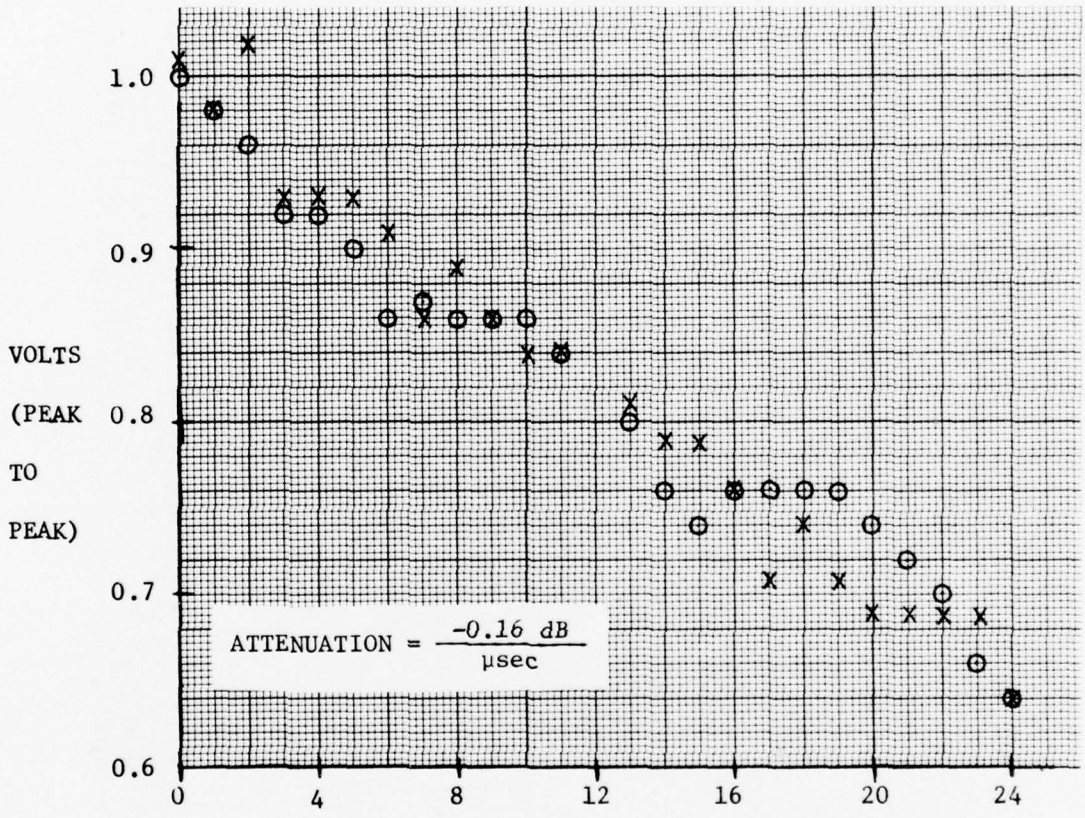

LEGEND: 1. Tap voltage, ⊙
2. Adjusted center tap voltage, X

Rank Quantizer Delay Line/Comparator
Gain Compensation-50 kHz Sinewave

FIGURE 5.38

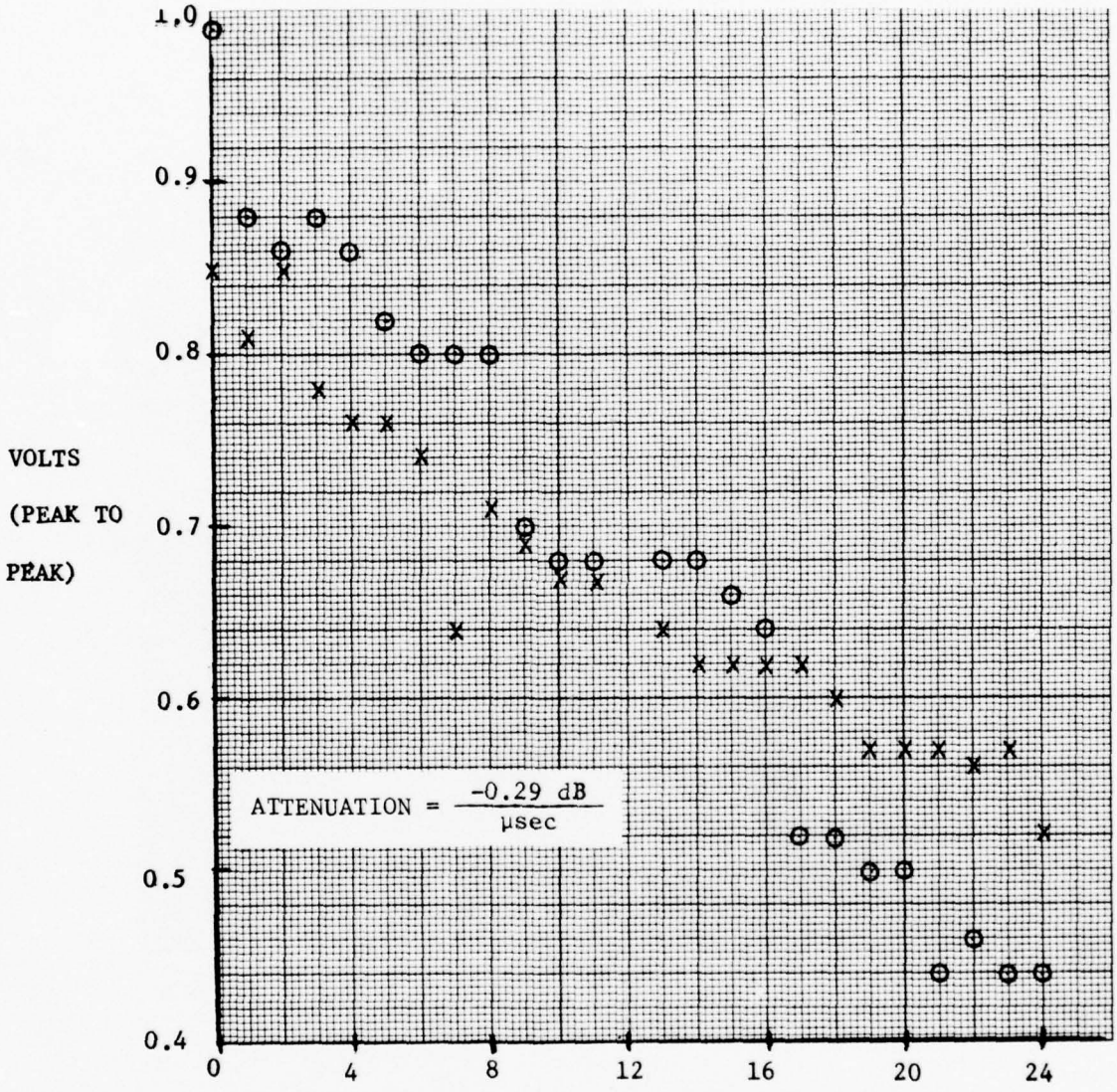

Rank Quantizer Delay Line/Comparator
Gain Compensation-500 kHz Sinewave

FIGURE 5.39

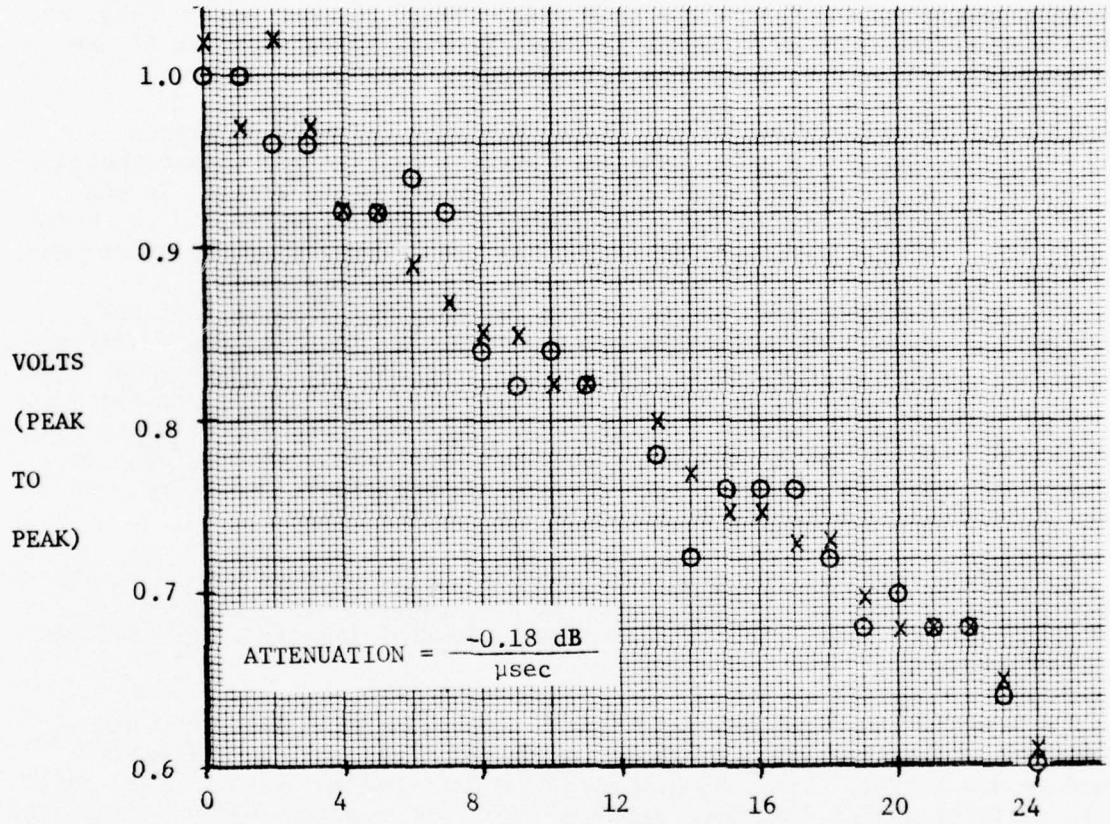

LEGEND: 1. Tap voltage, ⊙
2. Adjusted center tap voltage, X

Rank Quantizer Delay Line/Comparator
Gain Compensation-2 μsec pulse, 100 kHz PRF

FIGURE 5.40

Rank quantizer P_n control data was again obtained during this test interval. The center tap gain and bias were adjusted prior to performing the test. The log data was satisfactory but the MTI data showed unacceptable P_n control for selected P_n's of 16 percent and larger.

During the fourth test interval (17, 18, 19 September) a functional CD test was performed using the rank quantizer as the second range quantizer with theCD in the Baseline Test (1.2) configuration. Unsatisfactory target detection performance occurred for both video types. Output Buffer Overload alarms occurred as well as blanking in rain clutter. Investigation of the rank quantizer signals revealed the following:

1. The adjustment of the center tap gain and bias to obtain a known hit count nonparametrically in receiver noise resulted in quantizer output blanking in rain clutter areas. It was determined that this adjustment procedure resulted in the mean voltage level of the center tap to be lower than the other taps.

2. The adjustment of the center tap gain and bias so that the center tap voltage equals the true rms. receiver noise voltage level of tap "zero" for a 2 volt p/p and 0.25 volt p/p receiver noise input, resulted in a hit count P_n of 5.2 percent for a selected P_n of 4 percent. This is a 29.5 percent error in the P_n value selected. Operation with recorded rain clutter, however, appeared normal with this adjustment procedure. No target blanking occurred in the clutter areas.

These results indicated that problems still existed with the rank quantizer calibration procedure. Successful P_n control with log normal receiver noise obviously did not guarantee successful dynamic P_n control and target detection.

During the fifth and sixth test intervals, 24-26 September and 1-3 October, a satisfactory rank order quantizer nonparametric calibration procedure was tested. The rank quantizer, as implemented by Burroughs, could now be calibrated with log video receiver noise and operated with satisfactory P_n control with both log and MTI video at all selected P_n's and expected video voltage levels.

The successful completion of Test 2.1 required that the rank quantizer be properly calibrated. Since no established calibration procedure was provided with the rank modification, a procedure had to be derived and tested over numerous test intervals. Although a better understanding of the rank circuitry resulted, a considerable loss of test time occurred. The nonparametric calibration procedure and circuitry is presented in Appendix C.

Four adjustments are required. The adjustments and the reason for each adjustment are as follows:

Center Tap

1. GAIN, resistor R2. Amplifies center tap signal to compensate for delay line attenuation.

2. BALANCE, resistor R29. Compensates for low level DC offsets in circuits.

Threshold

1. INCREMENTAL Voltage, resistor R38. Adjusts threshold voltage level between ranks.

2. BIAS Voltage, resistor R40. Adjusts the threshold voltage level for all ranks.

During the tests in which the calibration procedure was determined, numerous signals were examined to verify that the quantizer was operating properly. All circuits showed proper operation. The comparator output response, however, could be improved. Figure 5.41 presents two photographs of the comparator output for different pulse width inputs. The two pulse widths are 2 μsec and 6 μsec. The photographs show a slow pulse rise time (1.25 μsec and a rapid fall time. The rise time should be the same as the pulse input in order to accurately represent, via an analog voltage sum, the time the center tap exceeded each rank (N taps). Capacitive effects should be investigated since the LM311N comparator response rise time specification is 0.2 μsec.

Figure 5.42 presents a simplified schematic of the summation network. The circuit operates by switching the HEX Inverter circuit with the Comparator output. This provides a conductive path through the 6.3K ohm resistor when the inverter circuit is on. The simplified summation network output voltage is then as follows when $I_1 = I_2$ and $R_2 = R_F$

$$V_{out} = I\left[\frac{R_2 \cdot R_F}{R_1}\right]$$

Figure 5.43 presents a photograph of the rank summation network output voltage for a log receiver noise input and a threshold level reference for a rank of 24. The photograph shows the voltage sum corresponding to each rank (1 through 24 taps) as the center tap randomly exceeds each rank. The output of the rank order quantizer is controlled by comparing the summation network voltage to the rank threshold voltage (brightest line). A voltage quantized pulse is output whenever the threshold voltage is exceeded.

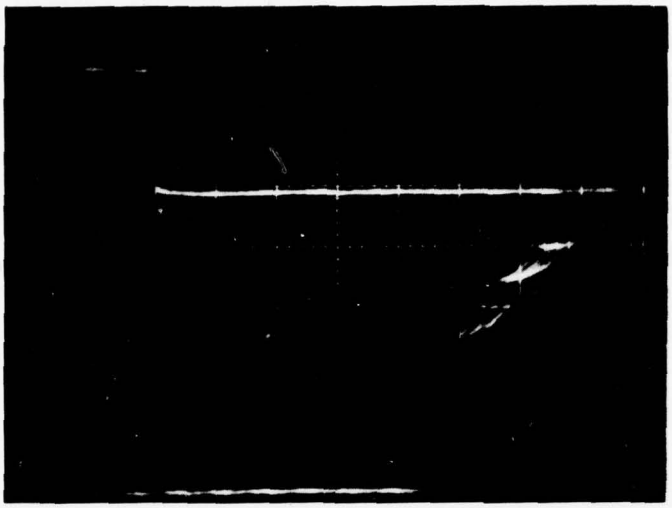

A. Upper Signal
1 μsec, 2 volt pulse input to delay line

0 Volts

Lower Signal
Comparator Output for tap 3. Measured at inverter output.

Scale
Vertical - 1 volt/CM
Horizontal - 0.5 μsec/CM

0 volts

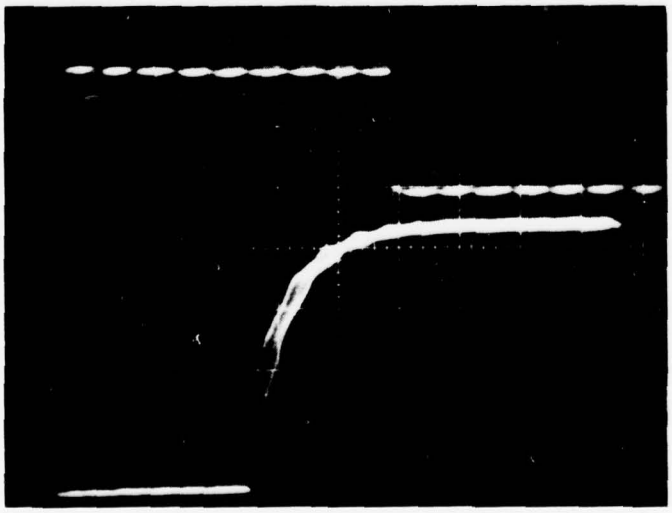

B. Upper Signal
6 μsec, 2 volt pulse input to delay line.

0 volts

Lower Signal
Comparator Output for tap 3. Measured at inverter output.

Scale
Vertical - 1 volt/CM
Horizontal - 1.0 μsec/CM

0 volts

RANK QUANTIZER
COMPARATOR RESPONSE

FIGURE 5.41

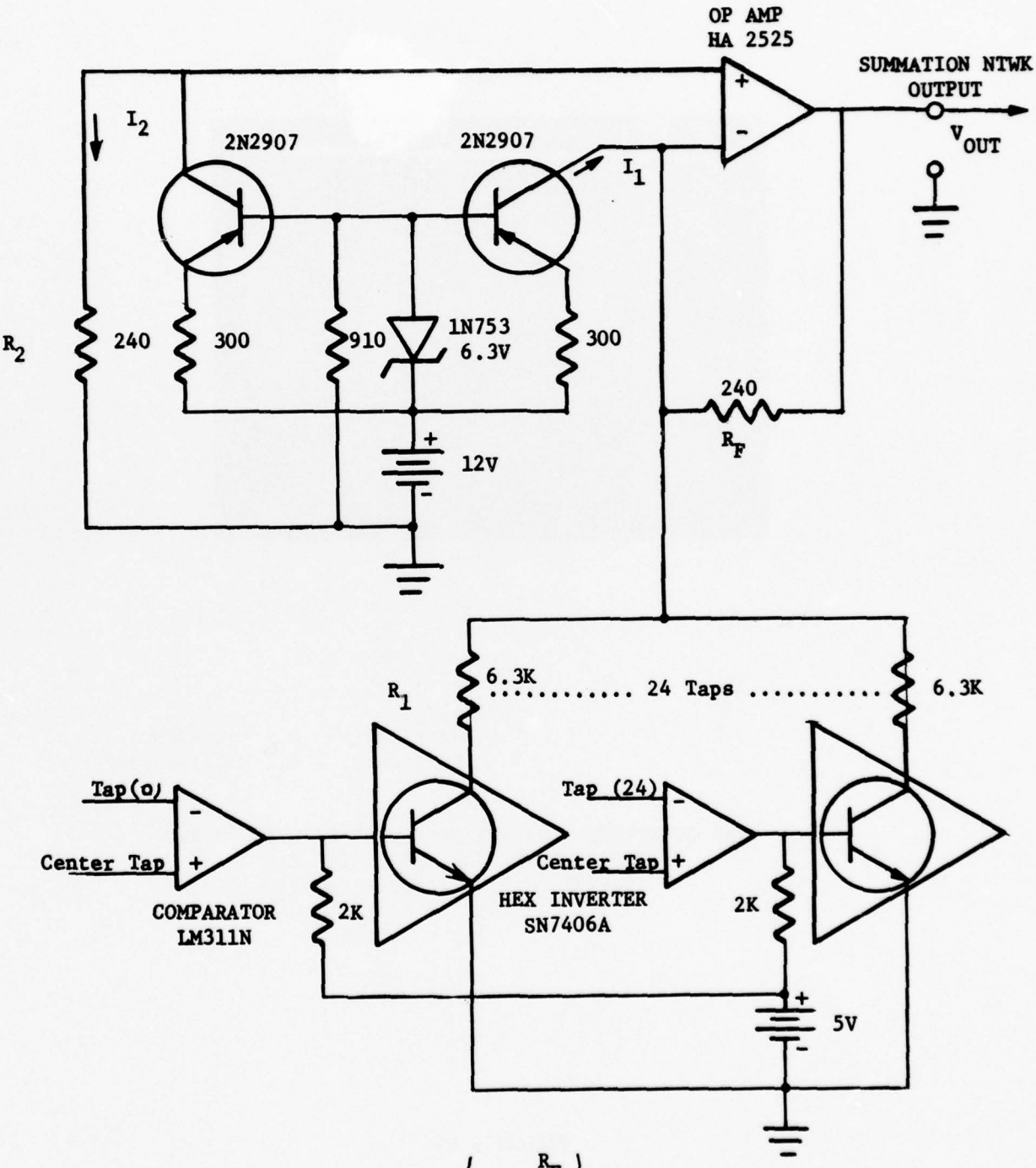

$$VOUT = -I_1R_F + I_2R_2\left(1 + \frac{R_F}{R_1}\right)$$

SUMMATION NETWORK - SIMPLIFIED SCHEMATIC

FIGURE 5.42

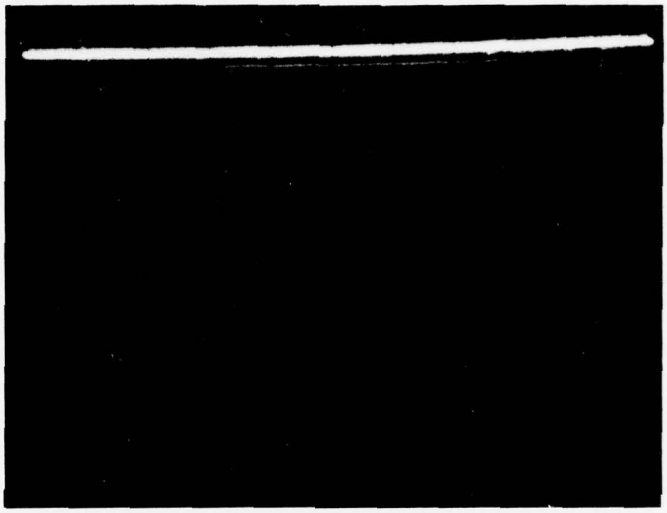

Scale:
Vertical - 0.5 volts/CM
Horizontal - 0.2 millisecond/CM

RANK QUANTIZER - OUTPUT OF SUMMATION NETWORK AND THRESHOLD SET FOR THE CENTER TAP GREATER THAN 24 TAPS (P_N = 4%)

FIGURE 5.43

Final Test 2.1 results are presented in Table 5.12 and Figure 5.46. The properly calibrated 24 tap, 1 μsec tap spaced delay line rank quantizer shows little sensitivity to the rank selected, voltage input level and the type of input video (distribution free indication). These observations are based on the use of receiver noise. Operation with live or recorded video with targets is still necessary to assess the dynamic operation and determine the effects of not having a target tap buffer zone.

The simulation of video correlation effects obtained by reducing the bandwidth shows that significant P_n errors (ΔP_n greater 10%) will not occur until the pulse return expands beyond 5 μsec (0.2 MHz). An additional satisfactory P_n control effect is that the P_n is reduced as the correlation increases. The negligible change in P_n from 2 MHz to 0.3 MHz occurs because the delay line bandwidth (0.5 MHz) predominates in this region.

5.4.2.1.2 Summary and Conclusions

The 24 tap, 1 μsec tap spaced delay line rank quantizer, when properly calibrated, produces satisfactory nonparametric P_n control in receiver noise. The quantizer shows little sensitivity to the rank selected, voltage input level and the type of input video (distribution free indication). An increase in the video correlation results in a reduction in the value of P_n. The 24 tap rank quantizer provides for a nonparametric P_n control as low as 4 percent. Because of the low P_n control capability, the reduction in P_n with increased video correlation, and the potential distribution free characteristic, the 24 tap rank quantizer should be tested further. Future testing should determine the dynamic target detection and P_n control characteristics in various clutter situations. Test 2.5 of the test plan (Reference 34) is designed to make these measurements at NAFEC.

TABLE 5.13

RECEIVER NOISE P_n CONTROL

P_N % MEASURED (ΔP_N % ERROR)									
LOG VIDEO RECEIVER NOISE									
P_N% SELECTED		4	8	12	16	20	24	28	32
DELAY LINE INPUT VOLTS P/P	2.0	3.98 (-0.5)	8.16 (2.0)	12.29 (2.4)	16.47 (2.9)	20.72 (3.6)	24.82 (3.4)	28.68 (2.4)	32.63 (1.9)
	1.5	3.98 (-0.5)	8.16 (2.0)	12.29 (2.4)	16.47 (2.9)	20.68 (3.4)	24.82 (3.4)	28.65 (2.3)	32.63 (1.9)
	1.0	3.98 (-0.5)	8.16 (2.0)	12.29 (2.4)	16.47 (2.9)	20.68 (3.4)	24.82 (3.4)	28.57 (2.0)	32.55 (1.7)
	0.75	3.98 (-0.5)	8.12 (1.5)	12.29 (2.4)	16.47 (2.9)	20.68 (3.4)	24.82 (3.4)	28.57 (2.0)	32.59 (1.8)
	0.50	3.98 (-0.5)	8.16 (2.0)	12.26 (2.2)	16.47 (2.9)	20.68 (3.4)	24.82 (3.4)	28.61 (2.2)	32.55 (1.7)
	0.25	3.94 (-1.5)	8.08 (1.0)	12.26 (2.2)	16.39 (2.4)	20.61 (3.0)	24.78 (3.3)	28.57 (2.0)	32.59 (1.8)
MTI VIDEO RECEIVER NOISE									
P_N% SELECTED		4	8	12	16	20	24	28	32
DELAY LINE INPUT VOLTS P/P	2.0	3.98 (-0.5)	8.12 (1.5)	12.26 (2.2)	16.35 (2.2)	20.49 (2.4)	24.51 (2.1)	28.07 (0.3)	32.13 (0.4)
	1.5	3.98 (-0.5)	8.12 (1.5)	12.21 (1.8)	16.35 (2.2)	20.49 (2.4)	24.51 (2.1)	28.07 (0.3)	32.09 (0.3)
	1.0	3.98 (-0.50)	8.12 (1.5)	12.21 (1.8)	16.35 (2.2)	20.45 (2.3)	24.51 (2.1)	28.03 (0.1)	32.09 (0.3)
	0.75	3.94 (-1.5)	8.08 (1.0)	12.21 (1.8)	16.35 (2.2)	20.45 (2.3)	24.51 (2.1)	28.03 (0.1)	32.13 (0.4)
	0.50	3.94 (-1.5)	8.08 (1.0)	12.21 (1.8)	16.35 (2.2)	20.49 (2.4)	24.51 (2.1)	28.03 (0.1)	32.09 (0.3)
	0.25	3.94 (-1.5)	8.08 (1.0)	12.26 (2.2)	16.47 (2.9)	20.60 (3.0)	24.71 (3.0)	28.22 (0.8)	32.24 (0.7)

NOTES: 1. $\Delta P_N\% = \dfrac{P_N \text{ measured} - P_N \text{ selected}}{P_N \text{ selected}} \times 100$

2. Test performed on 24 September 1975

Rank Quantizer - 24 taps, 1 μsec tap spacing, nonparametric operation, center tap adjusted for Log Video at 4% P_N.

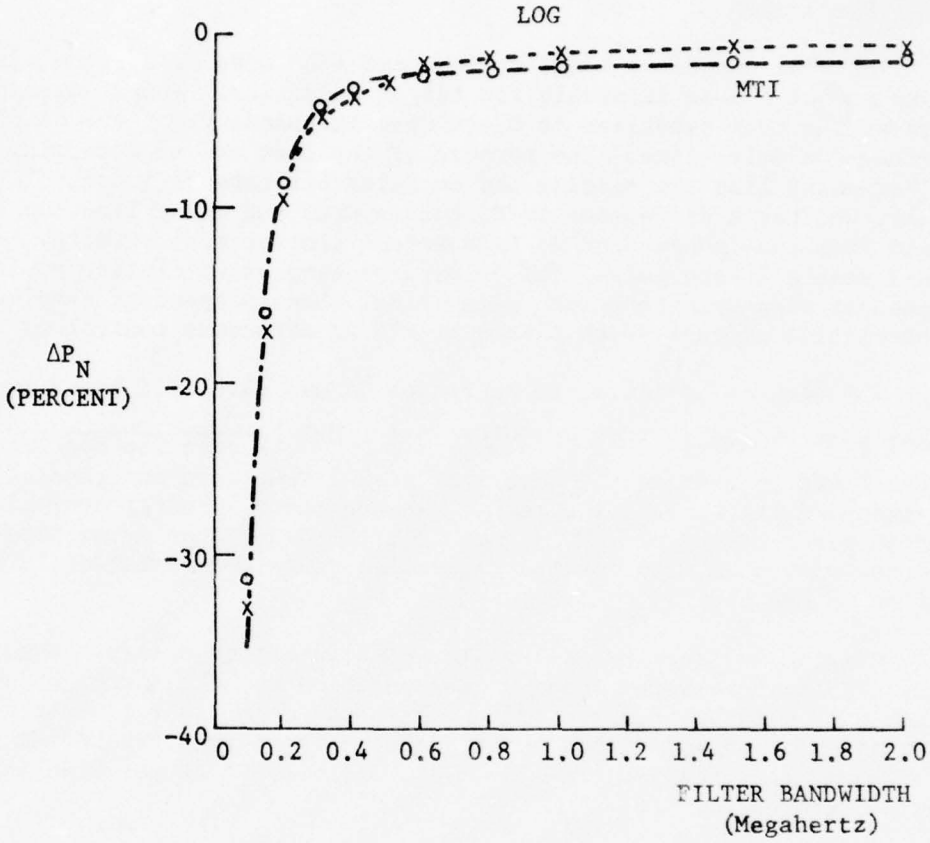

NOTES: 1. $\Delta P_N\% = \dfrac{P_{N\ \text{measured}} - P_{N\ \text{selected}}}{P_{N\ \text{selected}}} \times 100$

2. Krohn Hite filter inserted between radar receiver and input to common digitizer

3. Input voltage to delay line equals 1 volt P/P (0.21 Vrms)

4. Test performed on 24 September 1975

Rank Quantizer - 24 taps, 1 μsec tap spacing, nonparametric operation, Center Tap adjusted for Log Video at 4% P_N.

FIGURE 5.44 ΔP_N VS FILTER BANDWIDTH; P_N = 4%

5.4.2.2 Test 2.2 (Delay Line Tap Spacing Test)

5.4.2.2.1 Discussion

The rank quantizer modification uses a 24 μsec delay line with 24 taps spaced at 1 μsec intervals for target detection. Nonparametric operation of the rank quantizer is based upon independence of the samples (taps) along the delay line. The purpose of the test was to determine the effect that delay line tap spacing has on false hit rate (P_n) control. In particular, whether a difference in P_n occurs when the delay line tap spacing is changed from non-independent to independent clutter measurements. Since the ARSR-2 uses a 2 μsec pulse, the delay line samples of clutter would not be independent when using a 1 μsec delay line. Non-independent samples cause correlation effects which should result in erroneous control of P_n.

The test as specified in Reference 34 was developed based on the assumption that the delay line bandwidth was 1 MHz $\left(\frac{1}{1\ \mu\text{sec Tap Spacing}}\right)$. The approach was to operate the quantizer with 1 μsec (non-independent) and 2 μsec (independent) tap spacing and to measure the P_n control over clear and clutter zones for Elwood, N. J. rain clutter video tape input into the CD. Rain clutter was to be used for the test since range decorrelation is on the order of one pulse width.

Originally, only two delay line configurations were proposed for the test. The Burroughs recommended configuration and the Burroughs configuration with a target tap buffer zone were added in order to test the quantizer as designed and with a buffer zone. The target tap buffer zone is recommended by Reference 29 (page 330, Vol. 2) to avoid target blanking by wide target returns.

Each delay line configuration was calibrated and tested under Test 2.1 conditions prior to attempting Test 2.2. The four configurations are presented in Figure 5.45. They are as follows:

A. 24 μsec delay, 24 taps with 1 μsec tap spacing.

B. 24 μsec delay, 18 taps with 1 μsec tap spacing, 3 μsec target tap buffer zone.

C. 24 μsec delay, 10 taps with 2 μsec tap spacing, 3 μsec target tap buffer zone.

D. 16 μsec delay from a 24 μsec delay line, 10 taps with 1 μsec tap spacing, 3 μsec target tap buffer zone.

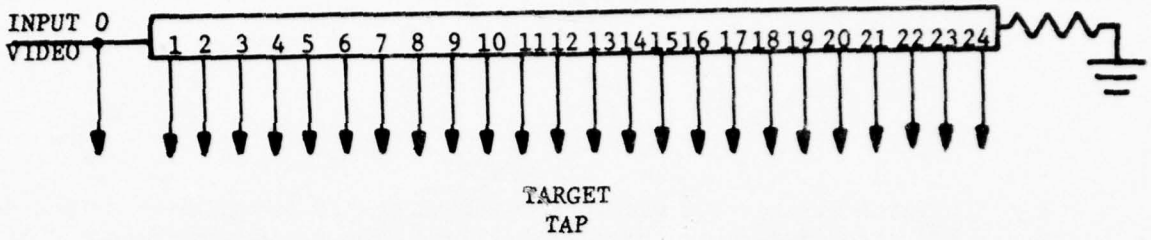

A. 24 μSEC DELAY LINE, 24 TAPS WITH 1 μSEC TAP SPACING.

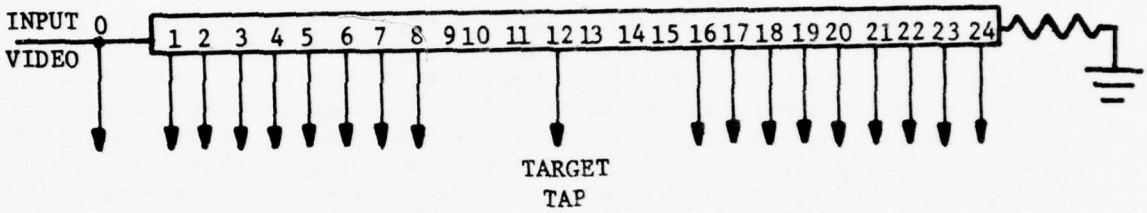

B. 24 μSEC DELAY LINE, 18 TAPS WITH 1 μSEC TAP SPACING, 3 μSEC BUFFER ZONE.

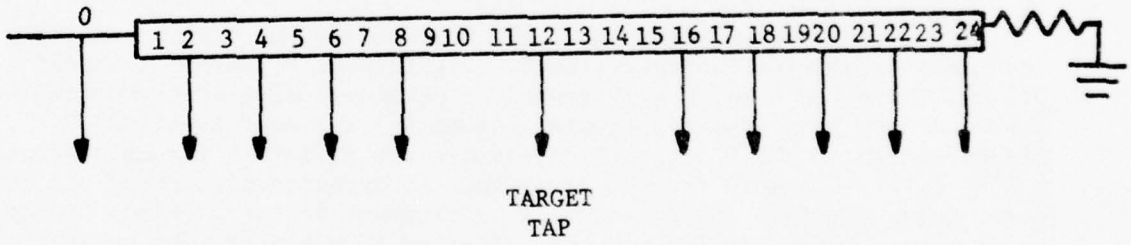

C. 24 μSEC DELAY LINE, 10 TAPS WITH 2 μSEC TAP SPACING, 3 μSEC BUFFER ZONE.

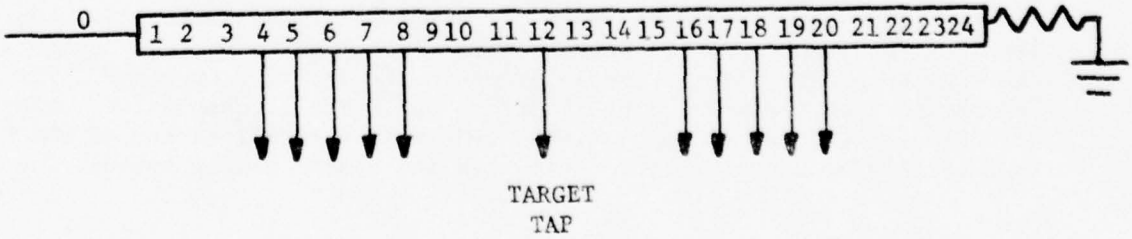

D. 16 μSEC DELAY FROM A 24 μSEC DELAY LINE, 10 TAPS WITH A 1 μSEC TAP SPACING, 3 μSEC BUFFER ZONE.

FIGURE 5.45 RANK QUANTIZER DELAY LINE CONFIGURATIONS

Tests 2.1 and 2.2 were performed on the 10 tap configurations during the second, third and fourth test intervals. The tests were repeated after the correct rank quantizer calibration procedure was completed (fifth test interval 24, 25, 26 September). Satisfactory Test 2.2 results were never obtained. Manual data taken with digital counters resulted in large P_n errors and the "D" machine tape recordings could not be processed due to numerous short records and parity errors.

Tables 5.14 - 5.16 and Figures 5.46, 5.47 and Table 5.17 present the static P_n receiver noise nonparametric tests and the bandwidth tests respectively. for configurations B, C and D. The bandwidth of the video was changed by placing a Krohn Hite filter in series with the video prior to the quantizer input. Decreasing the bandwidth simulates the response of the quantizer to wide pulse return. Configuration A is the rank quantizer delay line configuration provided by Burroughs. Test results for this configuration are discussed in Section 5.4.2.1.

The application of Test 2.1 to the other configurations (B, C, D) showed that the quantizer delay line configuration has a pronounced effect on P_n control. Configuration C (2 μsec tap spacing) was the only one that produced acceptable P_n control in both log and MTI receiver noise. Configurations B and D (1 μsec tap spacing) show considerable sensitivity to video type and rank sensitivity for MTI video. Log video operation was satisfactory.

Video correlation, simulated by reducing the video bandwidth, showed the least effect for Configuration C. Significant P_n errors occurred around 0.3 MHz while the B and D configurations developed similar errors around 0.5 MHz. The P_n errors increased positively (higher P_n) for configurations B, C, and D. The direction of the P_n control divergence was different for configurations A and B, C, D. A reason for the divergence in opposite directions was not determined. This is not a desirable operational feature. Since Configurations B and D show a considerable video distribution effect on P_n and greater correlation sensitivity, they should not be used.

While performing Test 2.2 it was observed that the MTI video signal was limiting in rain clutter areas. Since target information is lost when the signal limits, ARSR-2 MTI video should not be used in rain clutter situations unless the receiver can be adjusted to eliminate the limiting.

The testing of the Test 2.2 rank quantizer configurations under Test 2.1 conditions and the investigations required to properly calibrate the rank quantizer pointed out an error in the Test 2.2 approach. The assumption that the delay line bandwidth was 1 MHz (1 μsec pulse) when it actually was 0.5 MHz (2 μsec pulse) results in the calibration of the quantizer in a correlated condition for the 1 μsec tap spaced configuration. Operation

P_N % MEASURED (ΔP_N % ERROR)								
LOG VIDEO RECEIVER NOISE								
P_N % SELECTED		5.26	10.53	15.79	21.05	26.32	31.58	36.84
DELAY LINE INPUT VOLTS P/P	2.0	5.26 (0)	10.63 (0.9)	15.81 (0.1)	20.57 (-2.2)	25.94 (-1.4)	31.39 (-0.6)	36.73 (-0.3)
	1.5	5.26 (0)	10.63 (0.9)	15.81 (0.1)	20.53 (-2.5)	25.90 (-1.6)	31.36 (-0.7)	36.69 (-0.4)
	1.0	5.26 (0)	10.63 (0.9)	15.81 (0.1)	20.49 (-2.7)	25.87 (-1.7)	31.32 (-0.8)	36.65 (-0.5)
	0.75	5.26 (0)	10.63 (0.9)	15.77 (-0.1)	20.49 (-2.7)	25.83 (-1.9)	31.28 (-0.9)	36.65 (-0.5)
	0.50	5.26 (0)	10.59 (0.6)	15.74 (-0.3)	20.45 (-2.8)	25.79 (-2.0)	31.24 (-1.1)	36.58 (-0.7)
	0.25	5.26 (0)	10.52 (0)	15.66 (-0.8)	20.26 (-3.8)	25.60 (-2.7)	31.12 (-1.5)	36.42 (-1.1)
MTI VIDEO RECEIVER NOISE								
P_N % SELECTED		5.26	10.53	15.79	21.05	26.32	31.58	36.84
DELAY LINE INPUT VOLTS P/P	2.0	6.34 (20.5)	11.41 (8.36)	16.12 (2.1)	20.11 (-4.5)	25.36 (-3.7)	30.70 (-2.8)	35.88 (-2.6)
	1.5	6.34 (20.5)	11.41 (8.36)	16.12 (2.1)	20.11 (-4.5)	25.36 (-3.7)	30.66 (-2.9)	35.88 (-2.6)
	1.0	6.38 (21.3)	11.41 (8.36)	16.12 (2.1)	20.03 (-4.9)	25.32 (-3.8)	30.62 (-3.0)	35.88 (-2.6)
	0.75	6.42 (22.0)	11.33 (7.6)	16.08 (1.8)	19.99 (-5.0)	25.25 (-4.1)	30.62 (-3.0)	35.84 (-2.7)
	0.50	6.38 (21.3)	11.29 (7.2)	16.08 (1.8)	19.99 (-5.0)	25.21 (-4.1)	30.54 (-3.3)	35.84 (-2.7)
	0.25	6.38 (21.3)	11.25 (6.8)	16.01 (1.4)	19.87 (-5.6)	25.05 (-4.8)	30.39 (-3.8)	35.80 (-2.8)

NOTE: 1. $\Delta P_N\% = \dfrac{P_N \text{ measured} - P_N \text{ selected}}{P_N \text{ selected}} \times 100$

2. Test performed on 30 September 1975 (NAFEC personnel only)

Rank Quantizer - 18 taps, 1 μsec tap spacing, 3 μsec buffer zone, nonparametric operation, center tap adjusted for Log Video at 5.26% P_N.

TABLE 5.14 RECEIVER NOISE P_N CONTROL

P_N % MEASURED (ΔP_N % ERROR)						
LOG VIDEO RECEIVER NOISE						
P_N % SELECTED		9.09	18.18	27.27	36.36	45.45
DELAY LINE INPUT VOLTS P/P	2.0	9.08 (-0.1)	18.33 (0.8)	27.41 (0.5)	36.49 (0.4)	45.85 (0.9)
	1.5	9.12 (0.3)	18.28 (0.6)	27.37 (0.3)	36.42 (0.2)	45.66 (0.5)
	1.0	9.08 (-0.1)	18.25 (0.4)	27.37 (0.3)	36.46 (0.3)	45.62 (0.4)
	0.75	9.08 (-0.1)	18.28 (0.6)	27.30 (0.1)	36.38 (0.1)	45.62 (0.4)
	0.50	9.08 (-0.1)	18.28 (0.6)	27.34 (0.3)	36.38 (0.1)	45.58 (0.3)
	0.25	9.08 (-0.1)	18.25 (0.4)	27.34 (0.3)	36.42 (0.2)	45.51 (0.1)
MTI VIDEO RECEIVER NOISE						
P_N % SELECTED		9.09	18.18	27.27	36.36	45.45
DELAY LINE INPUT VOLTS P/P	2.0	9.43 (3.7)	18.55 (2.0)	27.30 (0.1)	36.31 (-0.1)	45.08 (-0.8)
	1.5	9.43 (3.7)	18.60 (2.3)	27.22 (-0.2)	36.23 (-0.4)	45.08 (-0.8)
	1.0	9.43 (3.7)	18.55 (2.0)	27.30 (0.1)	36.23 (-0.4)	45.04 (-0.9)
	0.75	9.43 (3.7)	18.55 (2.0)	27.34 (0.3)	36.11 (-0.7)	45.04 (-0.9)
	0.50	9.43 (3.7)	18.55 (2.0)	27.34 (0.3)	36.07 (-0.8)	45.00 (-1.0)
	0.25	9.39 (3.3)	18.55 (2.0)	27.26 (0)	36.00 (-1.0)	44.89 (-1.2)

NOTES: 1. $\Delta P_N \% = \dfrac{P_N \text{ measured} - P_N \text{ selected}}{P_N \text{ selected}} \times 100$

2. Test performed on 25 September 1975

Rank Quantizer - 10 taps, 2 μsec tap spacing, 3 μsec buffer zone, nonparametric operation, center tap adjusted for Log Video at 9.09% P_N.

TABLE 5.15 RECEIVER NOISE P_N CONTROL

P_N % MEASURED (ΔP_N % ERROR)						
LOG VIDEO RECEIVER NOISE						
P_N % SELECTED		9.09	18.18	27.27	36.36	45.45
DELAY LINE INPUT VOLTS P/P	2.0	9.09 (0)	18.09 (-0.4)	26.79 (-1.8)	33.91 (-6.7)	42.80 (-5.8)
	1.5	9.09 (0)	18.13 (-0.3)	26.75 (-1.9)	33.83 (-6.9)	42.76 (-5.9)
	1.0	9.12 (0.3)	18.09 (-0.4)	26.75 (-1.9)	33.87 (-6.8)	42.76 (-5.9)
	0.75	9.16 (0.8)	18.09 (-0.4)	26.75 (-1.9)	33.87 (-6.8)	42.72 (-6.0)
	0.50	9.09 (0)	18.06 (-0.7)	26.75 (-1.9)	33.87 (-6.8)	42.65 (-6.2)
		9.05 (-0.4)	17.94 (-1.3)	26.72 (-2.0)	33.75 (-7.2)	42.57 (-6.3)
MTI VIDEO RECEIVER NOISE						
P_N % SELECTED		9.09	18.18	27.27	36.36	45.45
DELAY LINE INPUT VOLTS P/P	2.0	10.67 (17.4)	18.98 (4.4)	27.06 (-0.8)	33.02 (-9.2)	41.72 (-8.2)
	1.5	10.67 (17.4)	18.94 (4.2)	27.03 (-0.9)	33.02 (-9.2)	41.72 (-8.2)
	1.0	10.67 (17.4)	18.94 (4.2)	27.03 (-0.9)	32.98 (-9.3)	41.68 (-8.3)
	0.75	10.67 (17.4)	18.87 (3.8)	26.99 (-1.0)	32.94 (-9.4)	41.64 (-8.4)
	0.50	10.67 (17.4)	18.83 (3.6)	26.91 (-1.3)	32.94 (-9.4)	41.60 (-8.5)
		10.67 (17.4)	18.83 (3.6)	26.83 (-1.6)	32.75 (-9.9)	41.37 (-8.9)

NOTES: 1. $\Delta P_N\% = \dfrac{P_N \text{ measured} - P_N \text{ selected}}{P_N \text{ selected}} \times 100$

2. Test performed on 26 September 1975.

Rank Quantizer - 10 taps, 1 μsec tap spacing, 3 μsec buffer zone, nonparametric operation, center tap adjusted for Log Video at 9.09% P_N.

TABLE 5.16 RECEIVER NOISE P_N CONTROL

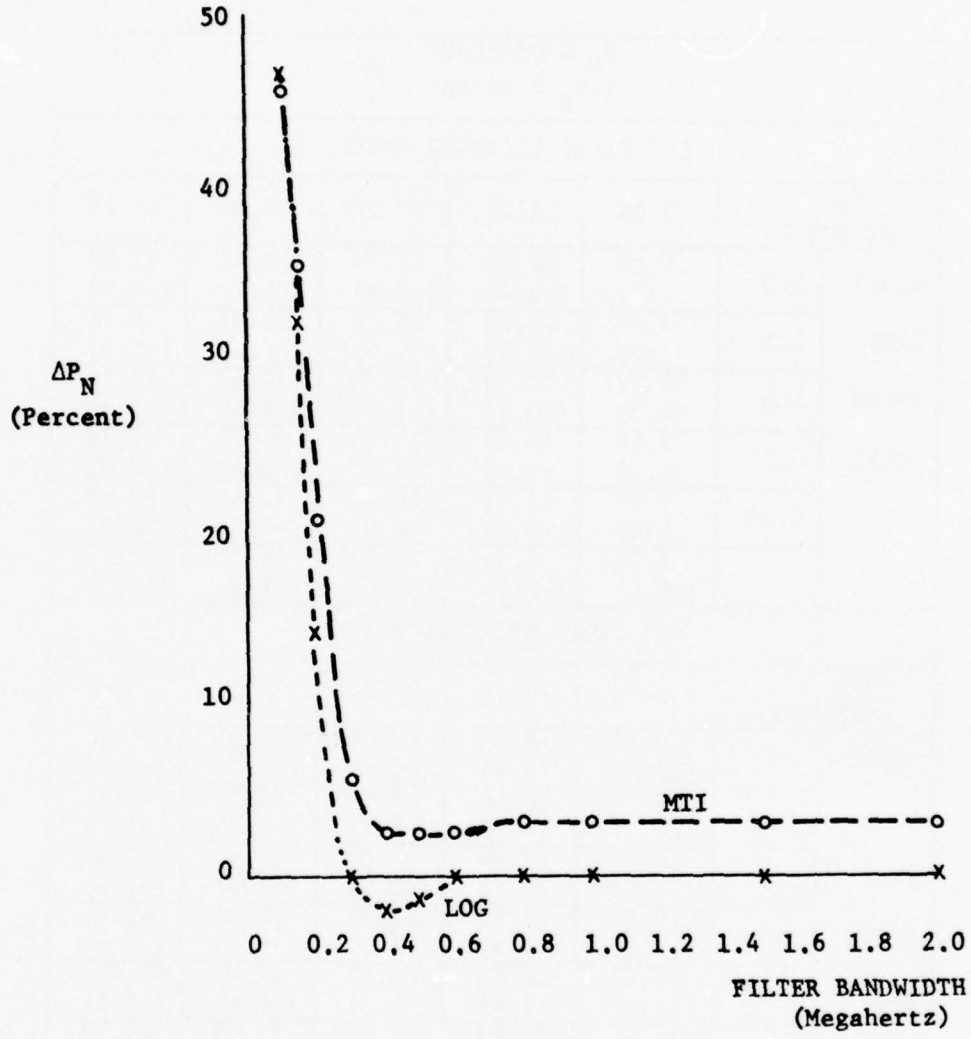

NOTES: 1. $\Delta P_N\% = \dfrac{P_N \text{ measured} - P_N \text{ selected}}{P_N \text{ selected}} \times 100$

2. Krohn Hite filter inserted between radar receiver and input to common digitizer.

3. Input voltage to delay line equals 1 volt P/P (0.21 Vrms)

Rank Quantizer - 10 taps, 2 μsec tap spacing, 3 μsec buffer zone, nonparametric operation, center tap adjusted for Log Video at 9.09% P_N.

FIGURE 5.46 ΔP_N VS FILTER BANDWIDTH; P_N = 9.09

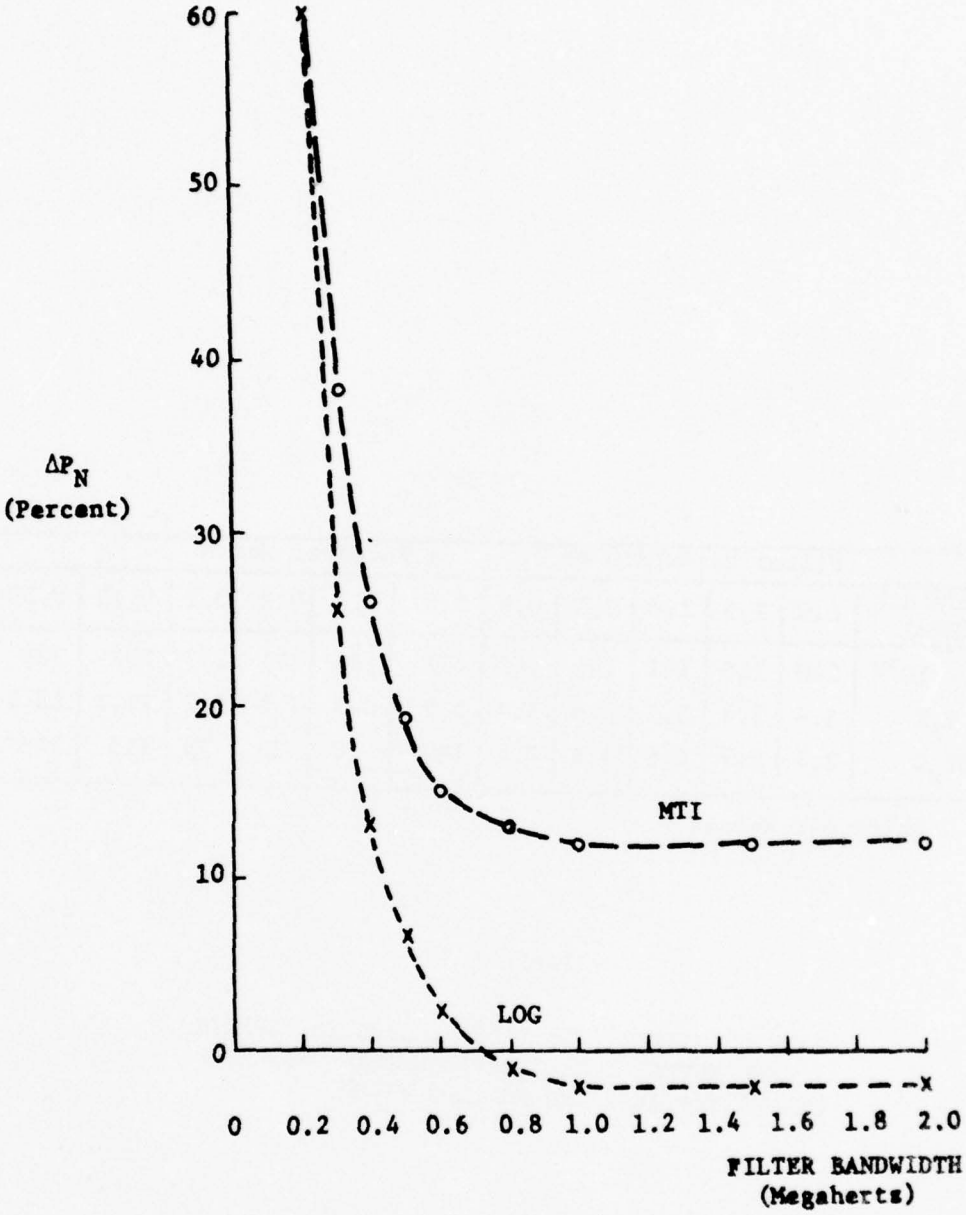

NOTES: 1. $\Delta P_N\% = \frac{P_N \text{ measured} - P_N \text{ selected}}{P_N \text{ selected}} \times 100$

2. Krohn Hite filter inserted between radar receiver and input to common digitizer.

3. Input voltage to delay line equals 1 volt P/P (0.21 Vrms)

Rank Quantizer - 10 taps, 1 μsec tap spacing, 3μsec buffer zone, nonparametric operation, center tap adjusted for Log Video at 9.09% P_N.

FIGURE 5.47 ΔP_N VS FILTER BANDWIDTH; P_N = 9.09%

Filter Bandwidth vs P_N - Log Receiver Noise											
Bandwidth (MHz)	2.0	1.5	1.0	0.8	0.6	0.5	0.4	0.3	0.2	0.15	0.10
$P_N \cdot 10^3$*	140	140	141	143	147	153	164	181	237	292	338
P_N%	5.4	5.4	5.5	5.5	5.7	5.9	6.3	7.0	9.2	11.3	13.1
ΔP_N%	2.7	2.7	4.6	4.6	8.4	12.2	20	33	75	115	149

*hits per second

TABLE 5.17

RANK QUANTIZER - 18 TAPS, 1 μSEC TAP SPACING,
3 μSEC BUFFER ZONE, NONPARAMETRIC OPERATION
CENTER TAP ADJUSTED FOR LOG VIDEO.

of the quantizer with correlated video (2 μsec video, 1 μsec tap spacing) would most likely not have shown any difference in P_n control for the clear and rain clutter areas. Because the delay line bandwidth does not match the tap spacing, it will be difficult to devise a test as intended to obtain meaningful results. A possible revised approach could be implemented as follows:

1. Calibrate the quantizer with receiver noise using the 2 μsec tap spacing (independent, uncorrelated).

2. Remove the signal used to turn on the appropriate comparators to obtain the 2 μsec configuration.

3. Measure the P_n for the 1 μsec configuration.

Any error in P_n can be attributed to the correlation effect if configuration sensitive circuit effects, such as having selected comparators continuously on, can be neglected or recorded video could be utilized in each case to see if the change in P_n is the same under dynamic conditions.

5.4.2.2.2 Summary and Conclusions

Test 2.2 was not completed due to tape recording problems. Short records and parity errors prevented the removal of test data from the "D" machine tape recordings. Four rank quantizer delay line configurations were considered as candidates for the performance of Test 2.2. Each configuration was tested under Test 2.1 conditions (receiver noise) prior to performing Test 2.2. The Test 2.1 results showed that the delay line configuration has a pronounced effect on P_n control. The static P_n testing indicated that only the Burroughs 24 tap, 1 μsec tap spaced delay line (minimum P_n = 4%) and the 10 tap, 2 μsec tap spaced, 3 μsec buffer zone delay line (minimum P_n = 9.09%) should be used for dynamic testing. These quantizer configurations should be tested further in order to determine their relative target detection and dynamic P_n control characteristics.

The rank quantizer offers the potential for improved CD performance. A rank quantizer should be tested that incorporates independent sample taps, a sufficient number of taps to produce a low P_n, and a target tap buffer zone.

5.4.2.3 Test 2.3 (Sensitivity of Signal Conditioning to Noise Bandwidth)

5.4.2.3.1 Discussion

Test 2.3 was completed satisfactorily during the sixth test interval (1-3 October). The purpose of the test was to determine the effect of post quantizer signal conditioning on P_n regulation. This was accomplished by measuring the false hit rate control at the output of the Hit Width Discriminator (HWD) as a function of minimum pulse width criteria and input video bandwidth. The test setup configuration for the measurement of P_n is presented in Figure 5.48. The purpose of the HWD is to prevent multiple range reporting of single targets that span more than a single radar range cell. Narrow width targets are also rejected. The video is passed through a one-clock period discriminator which eliminates any video spikes that are less than 386 nanoseconds wide (1/32 nmi).

The test results presented in Tables 5.18 and 5.19 show that the HWD circuit has a pronounced effect on P_n. For a log video 4% P_n out of the rank quantizer, the P_n out of the HWD for a 1/32 nmi discrimination is 1.2%. This is a -70% error in the P_n selected. As the minimum width discrimination is increased, the P_n count drops drastically, so that there are no noise hits out of the HWD for a discrimination equal to or greater than 3/32 nmi.

The response of the HWD to varying pulsewidth returns was checked by varying the bandwidth of the receiver noise video. The HWD shows the largest effect from variations in the bandwidth of the log video. Changing the filter bandwidth from 2 to 0.5 MHz results in +20% change in the P_n for a selected P_n of 4%. For the same interval the P_n changed +10% for MTI video. The percentages indicated are adjusted for the quantizer bandwidth effects on P_n1. The HWD is also sensitive to the input video distribution (log vs MTI). When the HWD is operated with a minimum discrimination of 1/32 nmi, there are 44% more hits/second output with MTI video as compared to log video (filter at 2 MHz).

At the conclusion of the sixth test sequence two Mode 1 recordings were made with log video receiver noise in order to calibrate the M/N integrator with 1/4 nmi peak detection, versus quantizer P_n and to provide data to check out the CD Data List and Analysis Program. The block diagram for this process is illustrated as follows.

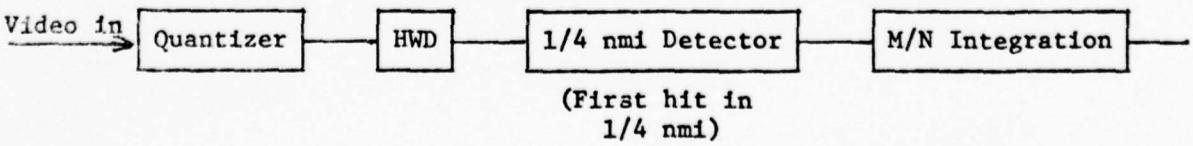

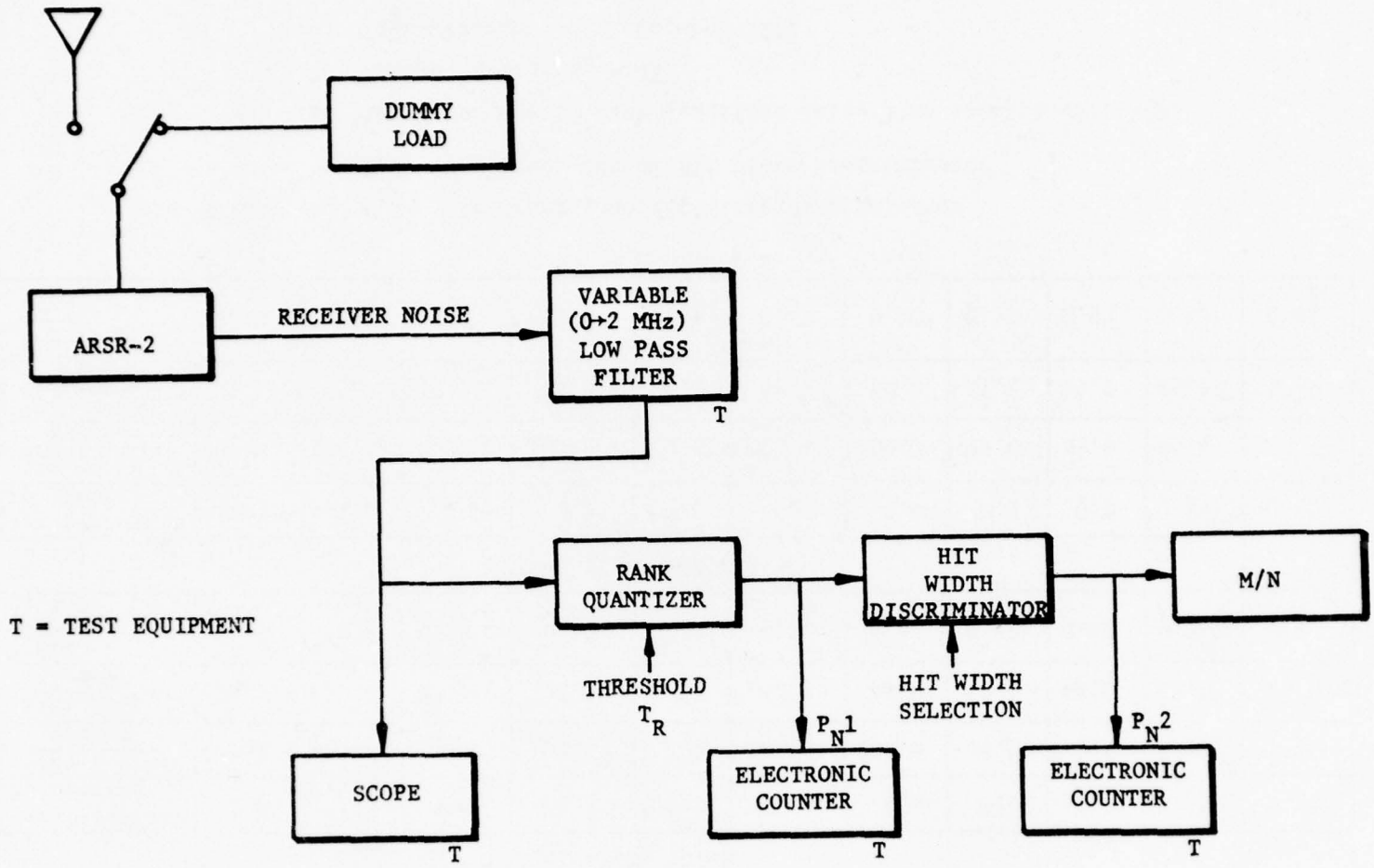

FIGURE 5.48

TEST SETUP FOR P_N MEASUREMENT; POST-QUANTIZER SIGNAL CONDITIONING EFFECTS

HIT WIDTH DISCRIMINATION = 1/32 NMI											
LOG RECEIVER NOISE											
Filter Bandwidth (10^6 Hertz)	2.0	1.5	1.0	0.8	0.6	0.5	0.4	0.3	0.2	0.15	0.10
P_N1 $\frac{\text{Hits X } 10^3}{\text{Second}}$	103.9	103.6	103.0	103.0	102.5	102.0	101.6	99.0	93.0	83.0	58.0
P_N2 $\frac{\text{Hits X } 10^3}{\text{Second}}$	30.7	30.9	32.6	35.5	39.5	42.7	46.0	49.0	48.0	42.0	23.0
$\frac{P_N2}{P_N1}$	0.29	0.30	0.32	0.34	0.38	0.42	0.45	0.49	0.52	0.51	0.40
MTI RECEIVER NOISE											
Filter Bandwidth (10^6 Hertz)	2.0	1.5	1.0	0.8	0.6	0.5	0.4	0.3	0.2	0.15	0.10
P_N1 $\frac{\text{Hits X } 10^3}{\text{Second}}$	103.2	103.2	102.8	102.8	102.0	101.4	100.7	99.0	93.9	85.0	63.5
P_N2 $\frac{\text{Hits X } 10^3}{\text{Second}}$	43.7	43.7	44.2	45.0	46.4	48.2	50.0	51.1	49.7	44.2	27.9
$\frac{P_N2}{P_N1}$	0.42	0.42	0.43	0.44	0.45	0.47	0.50	0.52	0.53	0.52	0.44

NOTES: 1. P_N1: Hit Count into Hit Width Discriminator
P_N2: Hit Count out of Hit Width Discriminator

2. Input voltage to rank quantizer delay line equal 1 volt P/P.
3. Rank quantizer P_N = 4%
4. Test performed on 1 October 1975

TABLE 5.18 HIT WIDTH DISCRIMINATOR P_N VS FILTER BANDWIDTH

LOG RECEIVER NOISE						
HIT WIDTH DISCRIM. (NMI)	FILTER BANDWIDTH					
	2×10^6 Hertz			0.5×10^6 Hertz		
	P_N1 Hits x 10^3 / Second	P_N1 Hits x 10^3 / Second	$\frac{P_N2}{P_N1}$	P_N1 Hits x 10^3 / Second	P_N2 Hits x 10^3 / Second	$\frac{P_N2}{P_N1}$
1/32	103.9	30.9	0.30	101.9	42.3	0.42
2/32	103.9	4.8	0.05	101.9	9.1	0.09
3/32	103.9	0.0	0.0	101.9	0.0	0.0
4/32	103.9	0.0	0.0	101.9	0.0	0.0
MTI RECEIVER NOISE						
1/32	103.5	43.5	0.42	101.4	47.7	0.47
2/32	103.5	10.5	0.10	101.4	12.4	0.12
3/32	103.5	0.0	0.0	101.4	0.0	0.0
4/32	103.5	0.0	0.0	101.4	0.0	0.0

NOTES: 1. P_N1: Hit Count into Hit Width Discriminator

P_N2: Hit Count out of Hit Width Discriminator

2. Input voltage to rank quantizer delay line equal 1 volt P/P

3. Rank Quantizer $P_N = 4\%$

4. Test performed on 1 October 1975

P_N VS HIT WIDTH DISCRIMINATION

TABLE 5.19

The rank quantizer configurations A and B were used for the test recordings. The configuration A recording was the only one useable since the other had too many parity errors. The P_n values obtained are presented as follows. The data shows that even though the HWD reduces the P_n count, the P_n occurring in the M/N is double the quantizer P_n after the 1/4 nmi peak detection.

TABLE 5.20

P_n CONTROL

M/N VS RANK QUANTIZER

Rank	P_N Selected (Percent)	P_N Measured (Percent)	M/N Zone Count (Hits)	P_N M/N* (Percent)
24	4	4	69	8
23	8	8.2	164	19
22	12	12.4	247	28.6
21	16	16.6	333	38.6
20	20	20.6	406	47.1
19	24	24.7	474	54.8
18	28	28.9	532	61.6
17	32	33.1	589	68.2

*Based on a maximum possible zone count of 864 hits.
M/N refers to M target hits out of N sweeps.

5.4.2.3.2 Summary and Conclusions

The results of Test 2.3 show that the HWD changes the P_n characteristics of the rank quantizer. The combined operation of the HWD and 1/4 nmi peak detector approximately doubles P_n. Since the nonparametric P_n is changed the rank quantizer will have to be operated parametrically to obtain the desired P_n. Further analysis and testing are required to determine the best method of P_n control that includes the HWD and detector effects. The minimum hit width target discrimination (1/32 nmi) presently used by the CD is the preferred value. Values greater than 1/32 nmi drastically reduce noise hits out of the discriminator.

5.4.3 Recommended Modifications to Future Testing of Proposed Enhancements

Due to the test problems that developed, the original scope of the test plan (Reference 34) was not completed. Prior to the end of NAFEC testing the proposed tests were examined to see if any short cuts could be taken and still obtain meaningful test results. It was determined that several tests could be deleted or delayed. Future testing should incorporate these modifications. The tests that can be deleted or delayed and the reason for each deletion/delay are presented as follows:

A. Tests Deleted (2.6 and 3.4)

Test 2.6 - Evaluation of Q3 Thermal Quantizer, and Test 3.4 - Evaluation of Improved Q2 Thermal Quantizer.

Reason for Deletion

The operation of the Q3 (rank) and Improved Q2 quantizers, in areas where the thermal quantizer loop would normally be utilized, should indicate whether the respective thermal quantizer loops are required. The tests were originally proposed in order to provide a direct comparison of the two operations.

B. Test Deleted (3.1)

Test 3.1 - Improved Q2 Quantizer Signal Conditioning Effects.

Reason for Deletion

In the process of evaluating the CD it was observed that a similar input signal conditioning circuit exists in the terminal system RVD-3 processor. An analysis presented in Reference 1 (ARTS Multisensor System Study) indicates that the Fast Time Constant (FTC)/rectifier circuit causes an approximate 1 dB target detection loss compared to an adaptive first threshold device, when both circuits measure the DC bias of the input video without error. This calculation was based on video that is Rayleigh distributed and stationary.

Test 3.1 proposed that the rank quantizer input signal conditioning circuit be tested in place of the FTC/rectifier circuit to see if an improvement in target detection might occur. The rank quantizer circuit consists of a 60 Hz filter and a dead time clamp. Dead time is the time between gating the receiver off and the time of the next pulse transmission. Rank quantizer testing indicated the presence of excessive noise amplification when using the Burroughs circuit so the circuit was replaced with an FAA/NAFEC designed AC coupled circuit.

The original intent of Test 3.1 is still applicable i.e., the AC coupled circuit could be installed in place of the FTC/ rectifier circuit and the test performed. Since the existence of the 1 dB loss is based on a simplified statistical model, and it is questionable whether a 1 dB improvement can be measured, the test should be deleted.

C. Test Delayed (4.0)

Test 4.0 - Quantizer Select

Reason for Delay

The purpose of Test 4.0 was to check out the Burroughs designed scan correlated feedback (SCF) quantizer and thermal/clutter loop selection algorithm. Documentation was never provided to explain why the particular algorithm was selected. The algorithm was reviewed, using educated guesses, to see if any errors existed. Aside from reasons for the quantizer gain tests and the clutter in adjacent zone decisions, the algorithm looks acceptable.

One area of the algorithm appears questionable. The type of video used for each quantizer should be specified for the algorithm. Tests show that MTI video limits in rain clutter while log normal does not. The present SCF algorithm switches from quantizer Q2 to quantizer Q1 when Q2 limits. If MTI is used for Q1 and log normal is used for Q2, a limiting situation existing with log normal video will not be corrected by switching to MTI video.

The results of the rank quantizer Q3 and improved Q2 quantizer tests will provide sufficient information as to whether SCF zone control of P_n works for a given quantizer and whether clutter/ thermal loop switching is not required. If such is the case, the proposed SCF algorithm can be significantly simplified.

Test 4.0 would provide information on whether or not SCF as implemented with one proposed algorithm enhances or does not enhance system performance. It would be advantageous to evaluate the quantizer tests and use the results of these tests to optimize the SCF algorithm.

D. Test Deleted (5.0)

Test 5.0 - Zone Control of T_L

Reason for Deletion

Test 5.0 was not a test that was to be performed as a specific field exercise. Instead, data obtained from other tests would be analyzed to see whether the target count in a zone could be used to control the magnitude of the target leading edge (T_L) parameter for the second threshold detector.

This test should be deleted because it is highly speculative. The distribution of aircraft within the radar coverage area will not be uniform. Air traffic density varies significantly over the radar coverage area due to traffic patterns, the time of day, and because the area covered by a zone (4 nmi x 5.6 degrees) increases with range. It is questionable whether it will be possible to select a value for the expected number of targets in a zone that will be constant with respect to time and be applicable for all zones in the radar coverage area.

E. Test Delayed (6.0)

Test 6.0 - Automatic Clutter Elimination (ACE) Selection

Reason for Delay

The CD does not presently have the capability for logically setting the leading edge target detection threshold (T_L) based upon the existing correlation between consecutive radar returns. Several methods have been proposed that will give the CD this capability. If they work, the target detection performance of the CD in clutter will be improved. The analyses presented in Section 5.3.1 indicates that the method will be only marginally successful. Since, a method developed by the MITRE Corporation has recently been tested; the results of that testing should be evaluated prior to commencing testing this ACE method.

6.0 INPUT SIGNAL CHARACTERISTICS (RADAR)

6.1 INTRODUCTION

The objective of the input signal characteristics task was to measure the statistical characteristics of the various types of clutter contained in the ARSR video. These statistical models can then be used to predict how the CD modifications can be expected to perform when tested.

The data used for this task was obtained from FR-950 Recorder/Reproducer analog tape recordings of log/normal and MTI video made at three ARSR sites. The three sites were Elwood, N.J.; Seattle, Washington; and Paso Robles, California. The analog recordings were converted to digital form to facilitate computer data processing. The Video Quantizer Recorder (VQR) was used to make the conversion. The recorded radar video illustrates weather, ocean and groud radar clutter returns.

The intent of the CD input signal characteristics analysis plan was never fulfilled. The VQR tapes arrived late in the CD analysis schedule and work was stopped prior to receiving a reference gain calibration recording. Weather information was also not provided so the tapes could not be labeled by weather characteristics.

In order to account for several gain settings, it was stipulated (Reference 36) that reference gain recordings should be made by first recording receiver noise with the gain set initially for normal operating conditions. On succeeding scans the IF gain should have been increased in steps of 10 dB until the full tape was recorded or full gain was achieved.

6.2 VQR TAPE EDITING

Nine tapes were edited with the VQR display program. The program allows the video amplitude to be displayed in color over a selected area. Five colors are available with four variable amplitude thresholds. The four thresholds divide the amplitudes into five color regions; black, blue, red, green and white. The nature of the recorded data does not allow rejection of bad data statistically during processing; therefore the data must be manually edited scan by scan prior to processing. Table 6.1 presents a summary of pertinent information on each tape. In general, the data recording quality was satisfactory. Tape Number 1, however, had a large number of bad data scans. Bad data can be characterized as follows:

TABLE 6.1

EN ROUTE VQR TAPES

TAPE DATA								
FR-950 Source	Tape No.	Video Type	VQR Date	Range (nmi) Start	Range (nmi) Stop	Azimuth (Deg) Start	Azimuth (Deg) Stop	Tape Edited
Elwood, N.J. No. 2 1/11/74 (7407)	1	Log	10/21/75	15	48	310	330	Yes
	2	MTI						Yes
	3	Log	10/27/75	40 ①	73	320	340	Yes
	4	MTI						Yes
Paso Robles, Cal. No. 2 4/14/74 (102)	5	Log	10/27/75	80 ②	111	50	76	Yes
	6	MTI						Yes
	7	Log		5	36	210	236	Yes
	8	MTI						Yes
Seattle, Wash. No. 5 (205)	9	Log	11/19/75	20	47	290	310	Yes
	10	MTI						No
	11	Log		28	55	75	95	No
	12	MTI						No

Notes: ① Range offset required (32 nmi).
② Range offset required (64 nmi).

EDIT COMMENTS						
Tape No.	No. of Scans	Scans with all bad data	Thresholds Utilized ①	Scans with at least 1 bad sweep	Targets Observed	Type Clutter
1	79	---	10,20,35,60	1,2,3,12,17,42,45 49,56,58,70,74,75	No	Rain
2	>55	---	10,30,40,90	4,13,18,25,28,42,43	No	
3	82	---	15,25,40,70		Yes	
4	82	---	15,25,45,100		Yes	
5	103	4,12,59	15,20,35,40		No	Mountain Ranges
6	103	---	4,8,12,16		No	
7	100	6,59	20,30,45,50		Yes	Mountain Ranges, Ocean
8	79	---	4,8,12,16		Yes	
9	>32	7,15,23,29	4,15,25,100		No	Mountain Ranges, Ocean
10		NOT EDITED				
11	100 ②					Mountain Ranges
12						

Notes: ① In order blue, red, green, white thresholds.
② 2 files, 50 scans each file.

1. Several bad sweeps in a scan. Data for the bad sweeps are either of zero amplitude or are of proper amplitude but are displaced in range.

2. The entire scan is incorrect. The data from a portion of the VQR gate area are displaced to fill the total gate area. The preamble information would be correct.

3. The entire scan is incorrect. The preamble is in error and would change from scan to scan.

6.3 ANALYSIS APPROACH

Prior to beginning this study several texts and papers were consulted to determine what is known about statistical modeling of the radar environment (References 1, 11, 38, 39, 40). The literature search indicates that no simple model has ever been determined. At best, a sufficient number of samples to determine a statistical model for each clutter type can be obtained. These statistics can then be used to predict the performance of a detection device for each clutter condition.

Clutter returns are very complex. Ground clutter depends on the type of terrain and season. Significant spatial variations occur because of contour variations of the terrain. The moisture content of the soil and snow conditions are seasonal variations. In mountainous areas a large amplitude return will occur from the near side of a mountain while a small return will occur from the far side (shadowing effect). Wind velocity effects on trees should also be accounted for. Weather clutter is even more complex because it is affected by turbulence and wind shear, and also whether or not the rainfall fills the entire radar beam.

Previous studies show (Reference 1) that radar weather clutter is non-stationary and that the statistics will vary depending on the size of the sample area. The statistics derived should thus be based on the specific area of interest.

The analysis approach selected for this study was as follows:

1. Analyze the Paso Robles ground clutter first, since it is spatially constant from scan to scan. Analyze the Elwood and Seattle weather tapes after gaining experience with ground clutter statistics.

2. Since the statistics will vary with the size of the area selected, the scan correlated feedback sample zone size of 4 nmi by 64 ACP's (5.6 degrees) would be used as the sample base.

3. Select areas that have distinguishing characteristics for the labeling of data. Tentative areas selected are as follows:

   a. Ground Clutter

      1. Rolling hills
      2. High mountains and valleys
      3. High mountains with canyons (rough terrain)
      4. Mountain slope and coastal plain
      5. Coastal plain
      6. Ocean

   b. Weather Clutter

      1. Heavy rain
      2. Light rain
      3. Rain transition regions
      4. Turbulent areas

The ground clutter regions can be selected with a topographical map, whereas the weather clutter selection would be very subjective and be based upon signal intensity.

4. Perform the following statistical analysis:

   a. Obtain sample amplitude probability density and cumulative distribution functions. Consider weighting of data, where feasible, to eliminate range effects. Range weighting of log normal data does not appear feasible because of the need to measure two gain constants; a and b for the equation Vout = a log (1 + b Vin).

   b. Compare sample amplitude probability density functions to each other and to previously established models to determine whether they are the same or significantly different (Chi Square and Kolmogorov Smirnov tests).

   c. Determine the effect of the sampling period on the statistical model.

   d. Determine correlation effects for range and azimuth lags.

6.4 GROUND CLUTTER STATISTICS

Figure 6.1 through 6.6 present data obtained from an initial analysis of the Paso Robles ground clutter return. Figure 6.1 is a map of pertinent topographical features covered by the VQR sample area. This map was traced from the Interior Department Geological Survey Map "San Luis Obispo, Number N1-10-3 revised 1969." The area was divided into five sections for preliminary data labeling. They are as follows:

1. Mountains and valleys - 5 nmi to 9 nmi
2. Mountains with canyons - 9 nmi to 13 nmi
3. Mountain slope and coastal plain - 13 nmi to 17 nmi
4. Coastal plain - 17 nmi to 21 nmi
5. Pacific Ocean - 21 nmi to 25 nmi

Due to the difficulty in obtaining a 3 dimensional picture by following elevation lines on a 2 dimensional map, the terrain labels should be verified with a 3 dimensional map and modified as required. A comparison of the five graphs (Figures 6.2 through 6.6) and the respective statistics stated on each graph indicates that each is different. Statistical tests should be applied to verify the degree of difference.

6.5 SUMMARY AND CONCLUSIONS

A literature search of several texts and papers on statistical modeling of the radar environment shows that it has been determined that radar clutter returns are very complex. Ground clutter returns are effected by the terrain and season. Contour variations of the terrain cause significant spatial variations. Seasonal variations result from the amount of foliage on trees and the moisture content of the soil. Weather clutter is even more complex because it is affected by turbulence and wind shear and whether the rainfall fills the radar beam.

The objective of this task was to measure the various statistical characteristics of the ARSR-2 video. A library of models would then be available that could be used to predict how the CD modifications would perform when tested. Some preliminary statistics on ground clutter were measured prior to suspension of the task. These measurements verify that different statistics are obtained from area to area. Approximately 10 percent of the task was completed.

The analysis of radar signals is enhanced by the availability of digitized radar signal recordings. Future work should include a method to calibrate the VQR amplitude to the input signal amplitude (Appendix A Reference 40). This would enhance the statistical modeling effort by providing a scaled amplitude for power spectrum analysis and the comparison of amplitude data between different recordings made at the same site or at different sites.

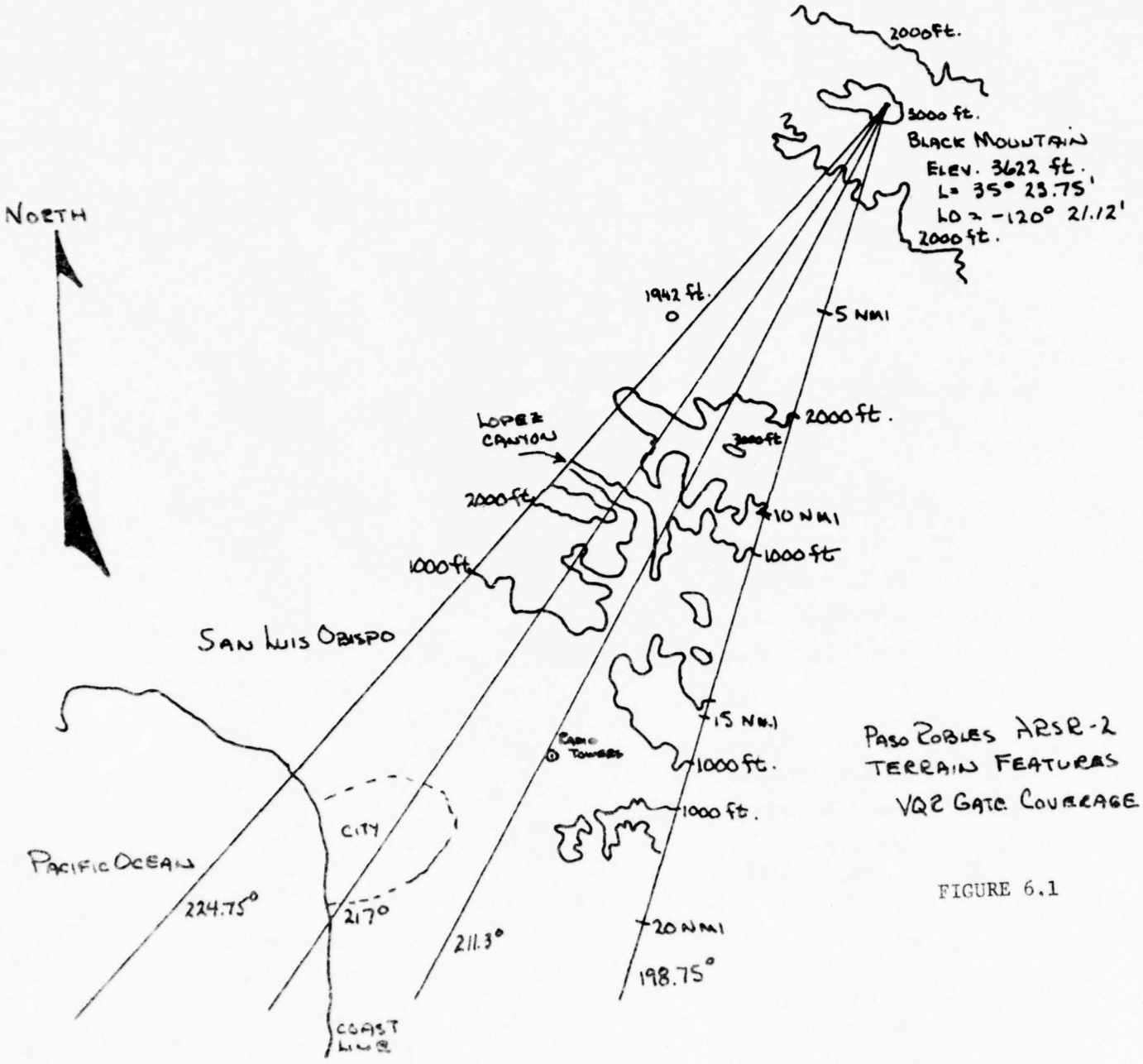

PASO ROBLES ARSR-2
TERRAIN FEATURES
VQ2 GATE COVERAGE

FIGURE 6.1

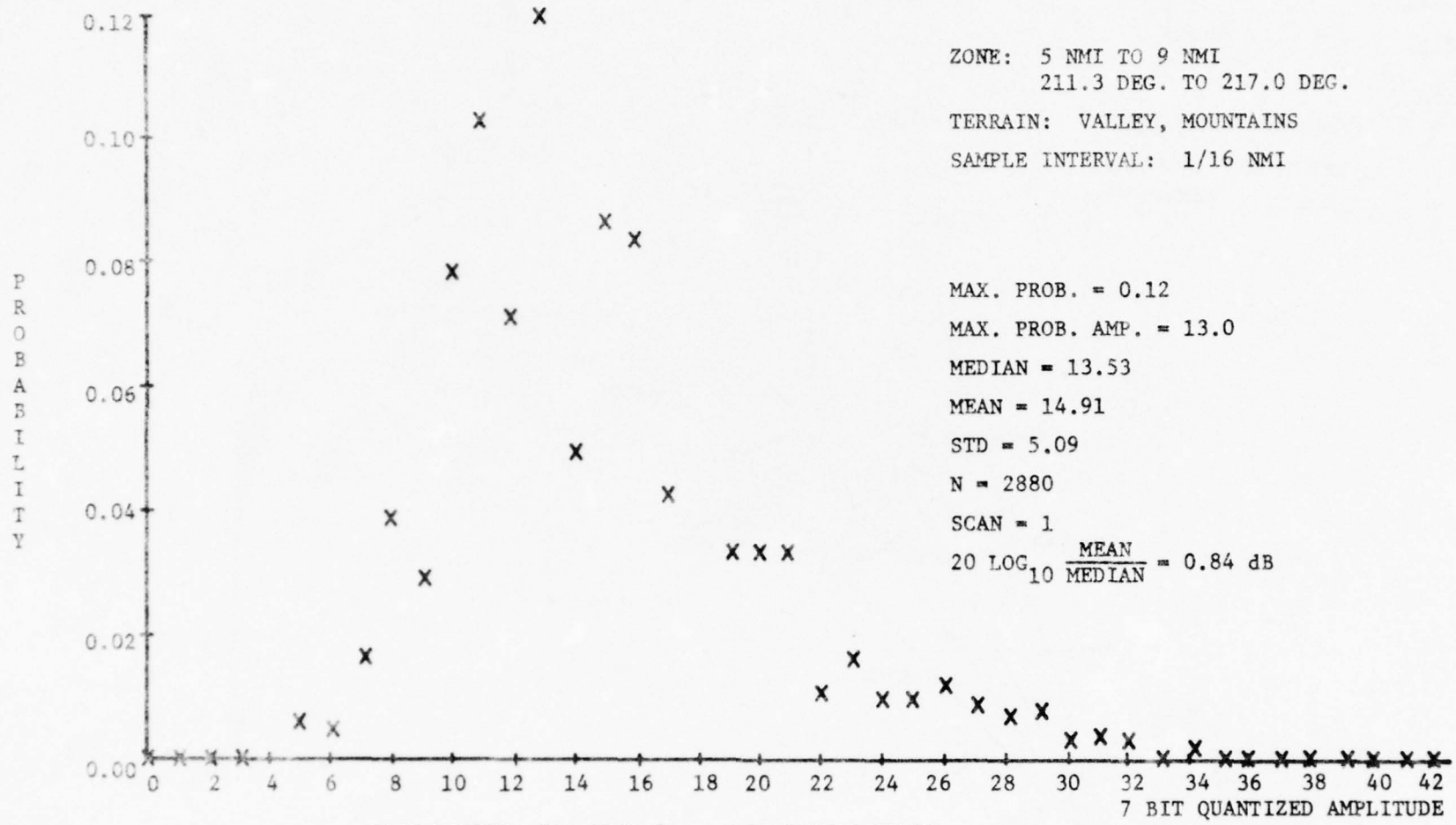

PASO ROBLES, CA. ARSR-2 LOG NORMAL VIDEO
SAMPLE UNWEIGHTED AMPLITUDE DENSITY 5 NMI TO 9 NMI

FIGURE 6.2

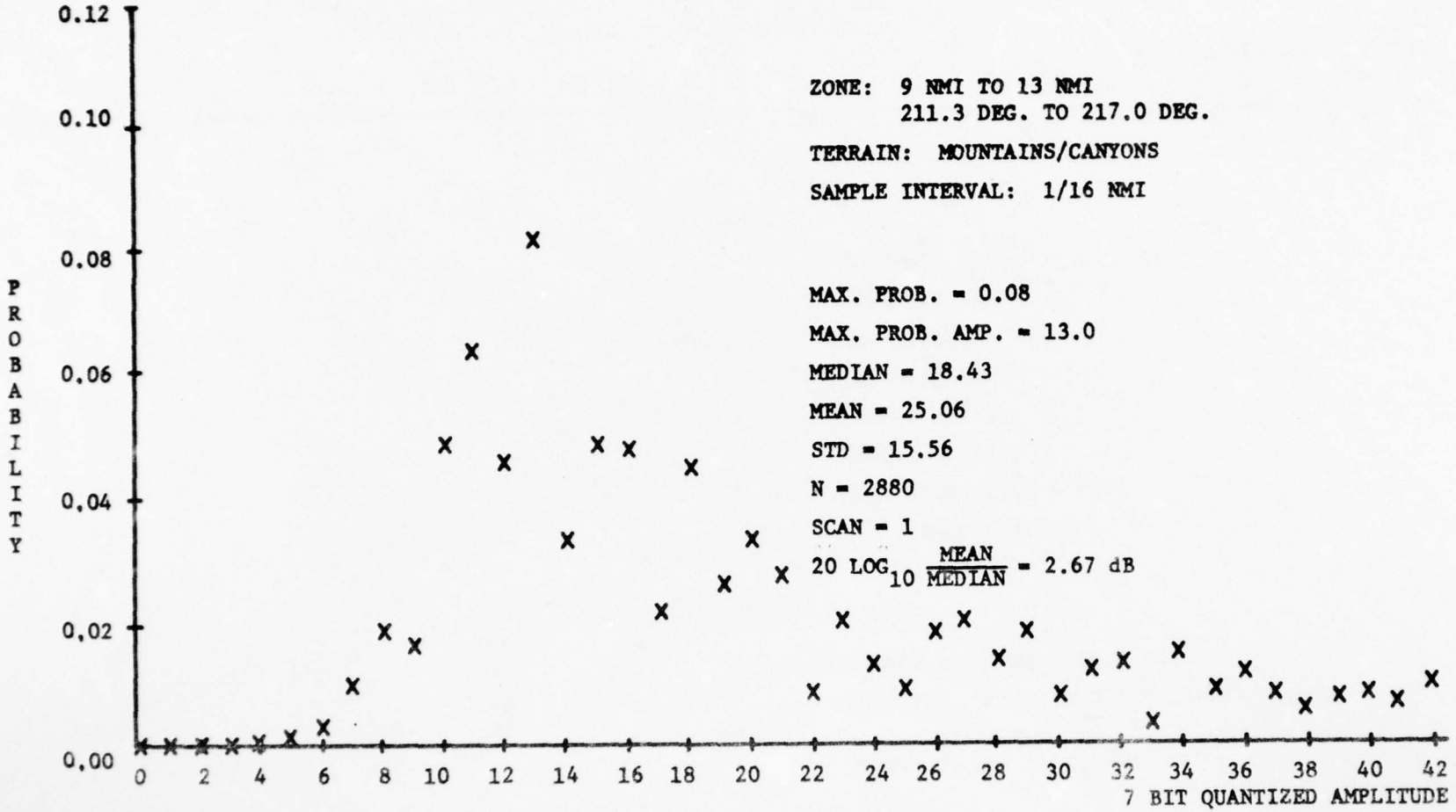

PASO ROBLES, CA. ARSR-2 LOG NORMAL VIDEO
SAMPLE UNWEIGHTED AMPLITUDE DENSITY 9 NMI TO 13 NMI

FIGURE 6.3

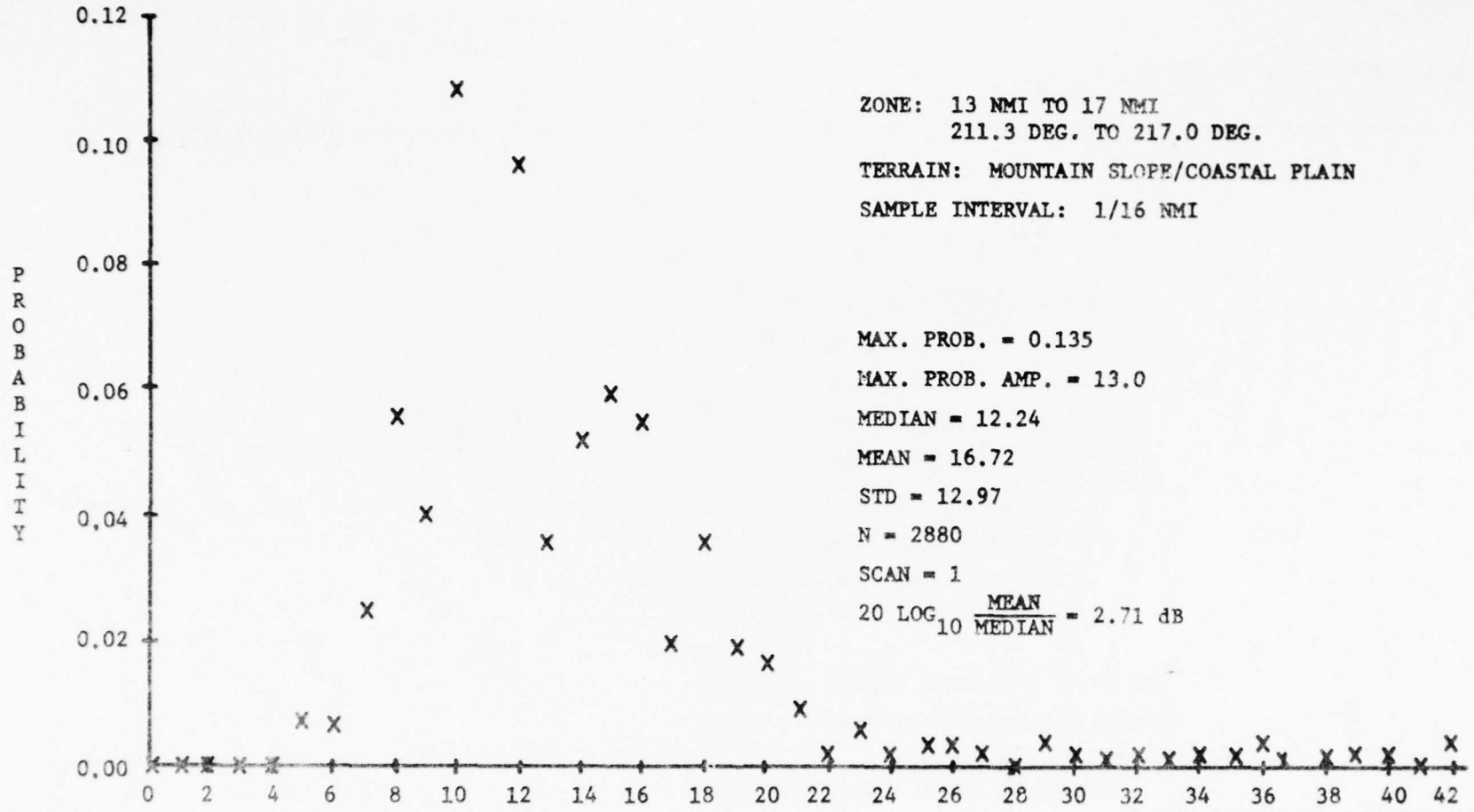

PASO ROBLES, CA. ARSR-2 LOG NORMAL VIDEO
SAMPLE UNWEIGHTED AMPLITUDE DENSITY 13 NMI TO 17 NMI

FIGURE 6.4

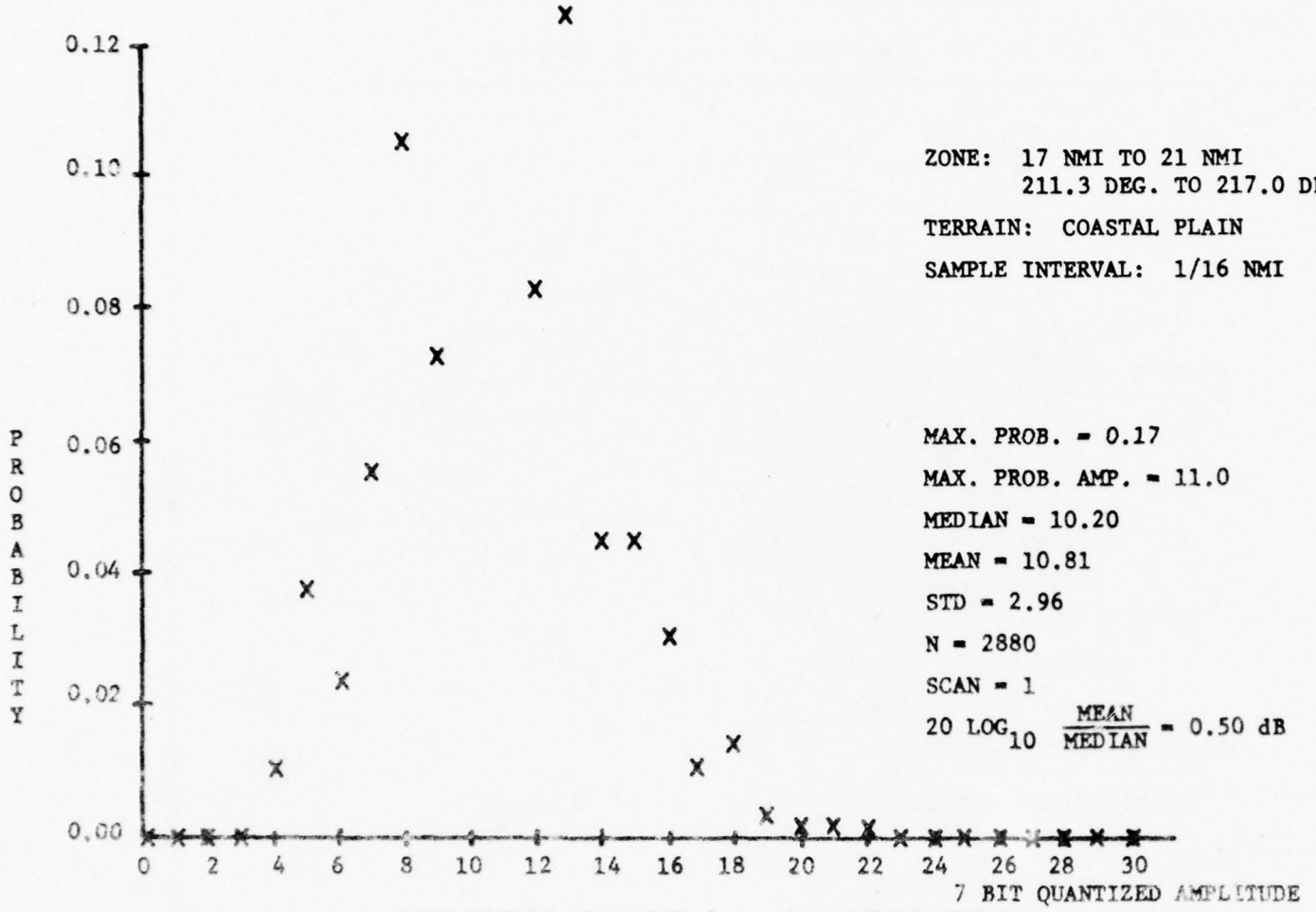

PASO ROBLES, CA. ARSR-2 LOG NORMAL VIDEO
SAMPLE UNWEIGHTED AMPLITUDE DENSITY 17 NMI TO 21 NMI

FIGURE 6.5

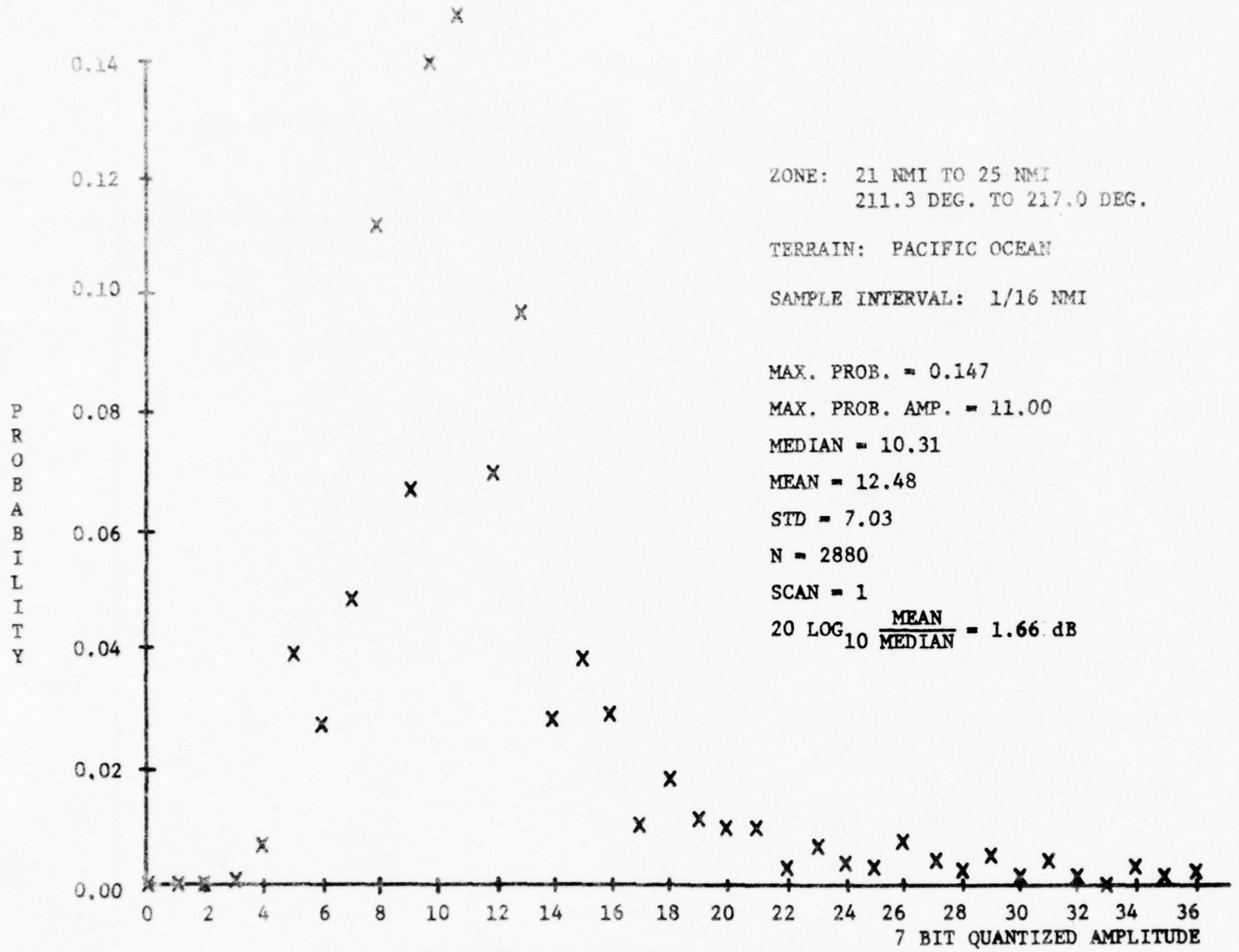

PASO ROBLES, CA. ARSR-2 LOG NORMAL VIDEO
SAMPLE UNWEIGHTED AMPLITUDE DENSITY 21 NMI TO 25 NMI

FIGURE 6.6

7.0 COMMON DIGITIZER OUTPUT SIGNAL CHARACTERISTICS

7.1 INTRODUCTION

In the NAS Stage A automation system the major function of the Common Digitizer (CD) is to form target reports using primary and secondary radar video as inputs. The objective of this section is to determine how well the CD performs this function by measuring the quality of the target reports as they exit the CD and before they enter the ARTCC. The ARTCC receives target reports from the CD, tracks them, correlates them with flight data, and displays aircraft tracks to the controller. The success with which it performs these tasks depends on the quality of the target reports from the CD. For example, if the CD fails to form target reports from aircraft returns on enough scans for a particular track, the ARTCC can not recognize that an aircraft is present. On the other hand if the CD creates too many false alarms, the ARTCC will produce false tracks or even become overloaded when the situation becomes bad enough. Therefore, it is advantageous to maintain a high quality on the target reports exiting the CD. Additionally, if the quality of reports is known, the tracking programs in the ARTCC can be tailored to most efficiently process those reports.

In order to measure target report quality, reports entering various ARTCC's around the country can be recorded in the form of CD Records. The CD Records are then processed at the Applied Physics Laboratory. Rather than make an exhaustive study of all the aspects of the target reports, a few key quality characteristics have been singled out and measured. These characteristics will now be described.

o Correlation Length - Target reports from aircraft returns will correlate from scan to scan and exhibit a definite velocity (speed and heading) which is within the capabilities of aircraft, while reports from noise, clutter, stationary targets, etc. tend to exhibit low velocities or fail to correlate for more than a few scans. Correlation length is defined as the number of target reports associated with a track when the target reports from the CD are processed by a tracker. Therefore, target reports which are associated with a track exhibiting a low correlation length as well as those reports associated with low velocity tracks will be classified as false and all remaining reports as true. Thus correlation length is a quantitative measurement of the quality of target reports exiting the CD.

o Blip/Scan Ratio - The blip/scan ratio is defined as the total number of target reports which correlate into a single track divided by the total number of scans that track exists. It is a measurement of the percentage of scans on which the CD detected a particular aircraft.

o Beacon Fade Statistics - A measurement is made of the number of times a beacon fade is backed up by a radar report.

o Radar Reinforcement Statistics - These statistics include the percentage of beacon reports that are radar reinforced. In addition radar reinforcement is cross correlated with correlation length. Beacon fade and radar reinforcement statistics indicate the amount to which primary radar information supplements and enhances secondary (beacon) radar track data in the Common Digitizer.

o Stationary Track Deviations - Histograms of deviations from scan to scan in both range and azimuth are made for target reports associated with stationary (low velocity) tracks. A knowledge of the magnitude of such deviations is important when designing a filter for stationary clutter. Histograms of deviations from the mean are also calculated.

o Moving Track Deviations - In calculating deviations involved with moving tracks one would like to subtract the true aircraft position (range and azimuth) from its measured position. However, since the true position is not known, it is estimated using a least squares fit to a second order polynomial through the preceding and following five measured positions of target reports along the track. Histograms are plotted of deviations from this smoothed position in both range and azimuth. The analysis yields a quantitative measurement of the positional errors associated with CD target reports.

o Run Length Statistics - Run length is defined as the azimuth extent of the radar hits or beacon replies which constitute a target report. In this part of the analysis cross correlation is made between run length and correlation length.

The parameters described above comprise a list of specific quantitative measurements which have been used to specify the quality of target reports from the CD. Although not applied here in this manner these parameters could also be used to evaluate the effectiveness of CD modifications or the field calibration of a particular CD. In fact the FAA already has a series of computer reduction programs which perform similar measurements that have been used for these purposes. In view of this, the question can be raised pertaining to the usefulness of this entire analysis. Although it does parallel work done previously in some respects there are differences in the ways the data is collected and presented.

In addition the major distinction here is the use of a different means for correlating reports from scan to scan (a different tracker). The crux of this entire line of analysis rests directly upon the accuracy of the tracker. Previous work in this area relied on the tracker in the ARTCC while this work uses a tracker developed at APL and provides a second source of analysis. For this reason alone it is justified and beneficial.

The following sections discuss the details of the analysis program and the results obtained along with conclusions.

7.2 DESCRIPTION OF THE ANALYSIS PROGRAMS

Figure 7.1 shows the entire data reduction process for the Output Signal Characteristics analysis. Circles represent data usually in the form of digital magnetic tape recordings, and rectangles represent computer programs. First of all the CD Records are converted from a 9 to 7 track tape format. For historical reasons the ARSR tracker needs its input in a special format and the Intermediate Format Tape (IFT) program provides that function. Next the ARSR tracker performs scan correlation of the target reports. This program is a non real time simulated range/bearing tracker using an α/β filter with gains modeled after a Kalman filter. Details of the tracker are listed in Appendix D.

The tracking program has two separate outputs. One is a Standard Sweep Tape (SST) upon which is listed a dump of the track stores from the tracker once a scan. This data is arranged in scan order (i.e., all reports occurring on scan N followed by all reports from scan N + 1, etc.). The SST tape contains all target reports except those which correlated with an established track but were not selected for update of that track. This is a characteristic of the original tracker which had to be modified in a manner such that the reports which correlated but were not selected for track update were written on a separate output tape, the Unselected Centroid tape (UC).

In order to efficiently analyze characteristics of a single aircraft track the data is reformatted from a scan order to a target order (i.e., all reports associated with track N followed by all reports associated with track N + 1, etc.). The Target Ordered Tape program performs this reformatting. Both the UC and the TOT tape recordings become the data inputs to the Target Report Quality Analysis (TRQA) program which calculates the various target report quality parameters described in section 7.1.

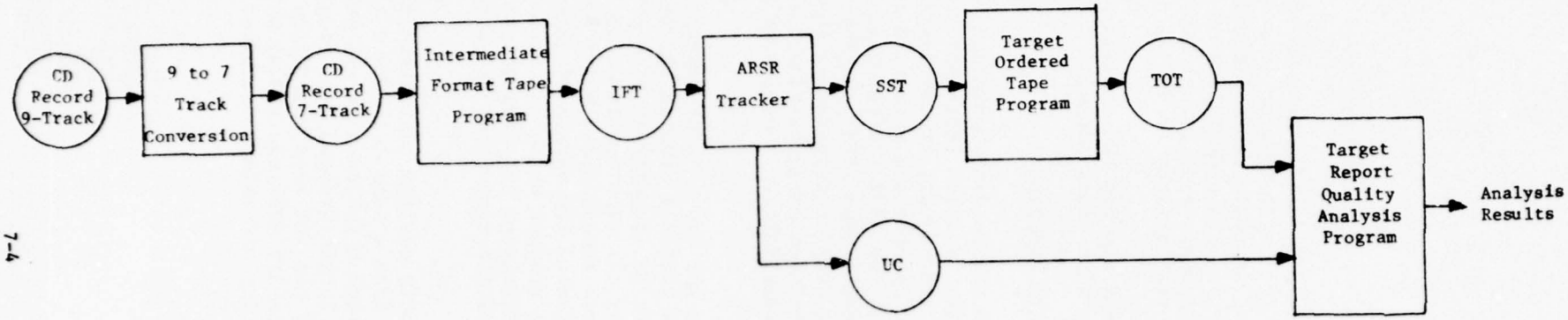

FIGURE 7.1 DATA REDUCTION FOR OUTPUT SIGNAL CHARACTERISTICS ANALYSIS

7.3 ANALYSIS RESULTS

Results in this section must be labeled as preliminary. Work on the task was suspended before a large scale data reduction could be accomplished. The only results available are those obtained while testing various subroutines of the TRQA program, and for some subroutines there existed bugs in the program which introduced errors into the results. Therefore, the exact values of the results in this section must not be taken too seriously, only general trends can be alluded. It should also be noted that this data primarily represents one data collection from one site and is not necessarily representative of all Common Digitizers. The primary reason for this section is to give examples of the form of the output from the TRQA program. The following figures are actual printouts from TRQA.

Figure 7.2 is the title and summary page for the TRQA output. Alphanumeric information is supplied via input control cards to designate the Run, Date, and Type of Data. For example the data used in this example was collected in Los Angeles on 8/6/75 and is Run 2-5-1 of the Laboratory's multisensor data collection on another FAA contract. The analysis can be restricted by track number, time, and range. The values for these restrictions are listed. Minimum and Maximum times refer to the times read directly from the data. Finally Figure 7.2 lists totals for various categories of target reports being analyzed.

Figures 7.3 to 7.6 deal directly with correlation lengths. They tabulate the total number of radar and beacon target reports found in tracks of varying correlation lengths. The column labeled "PER CNT" merely gives the percentage of the total reports that occurred on tracks of the given correlation length. The "CUM PER CNT" column shows the cumulative percentage of reports found in tracks of the given correlation length and all tracks of a lower correlation length. The column labeled "CUM PER CNT FIX" is a cumulative percentage as before only including all reports from fixed (stationary) tracks which in this case have, by definition, a correlation length of one. To interpret these tables one must remember that tracks with short correlation lengths are false and those with longer lengths are true. As an example arbitrarily pick the cutoff between 6 and 7. This would say that 84% of all the radar reports (88% if fixed reports are included) are false while only 18% of the beacon reports are false.

COMMON DIGITIZER OUTPUT SIGNAL CHARACTERISTICS
STATISTICAL ANALYSIS OF TARGET REPORTS

RUN:251 DATE:08/06/75 TYPE OF DATA:SPD ARSR
MINIMUM TIME:23:10: 9.5 MAXIMUM TIME:23:31:59.5

TOTAL NUMBER OF REPORTS(RADAR AND BEACON):	56422
TOTAL NUMBER OF BEACON REPORTS:	26101
TOTAL NUMBER OF RADAR REPORTS:	30321
TOTAL NUMBER OF RADAR REPORTS FROM FIXED TRACKS:	7785
TOTAL NUMBER OF RADAR REPORTS WHICH CORRELATED BUT WERE NOT SELECTED FOR UPDATE:	5855
TOTAL NUMBER OF BEACON REPORTS WHICH CORRELATED BUT WERE NOT SELECTED FOR UPDATE:	1663
TOTAL NUMBER OF REPORTS(BEACON AND RADAR)WHICH CORRELATED BUT WERE NOT SELECTED FOR UPDATE:	7518
TOTAL NUMBER OF BEACON REPORTS WHICH WERE RADAR REINFORCED:	9960

START TRACK NUMBER: 0 STOP TRACK NUMBER: 1000

START TIME: 0: 0: 0.0 STOP TIME:25: 0: 0.0
MINIMUM RANGE: 2.00 MAXIMUM RANGE: 256.00

FIGURE 7.2

TABLE INCLUDES: 1. RADAR REPORTS AS A FUNCTION OF CORRELATION LENGTH
2. CUMULATIVE PERCENTAGE(WITH AND WITHOUT REPORTS FROM FIXED TRACKS) OF THE REPORTS IN THE SPECIFIED AND LOWER CORRELATION LENGTHS. FIXED TRACK CORR LNG IS ONE

CORR LNG	NUM OF REPORTS	CUM PER CNT	CUM PER CNT FIX	CORR LNG	NUM OF REPORTS	CUM PER CNT	CUM PER CNT FIX	CORR LNG	NUM OF REPORTS	CUM PER CNT	CUM PER CNT FIX
1	9575	42.49	57.25	36	45	94.63	96.01	71	39	98.38	98.79
2	4716	63.41	72.81	37	0	94.63	96.01	72	15	98.44	98.84
3	2034	72.44	79.52	38	67	94.92	96.23	73	17	98.52	98.90
4	1277	78.11	83.73	39	16	94.99	96.28	74	0	98.52	98.90
5	1016	82.61	87.08	40	58	95.25	96.47	75	11	98.57	98.93
6	294	83.92	88.05	41	32	95.39	96.58	76	18	98.65	98.99
7	171	84.68	88.61	42	17	95.47	96.63	77	15	98.71	99.04
8	180	85.48	89.21	43	1	95.47	96.64	78	3	98.73	99.05
9	140	86.10	89.67	44	31	95.61	96.74	79	9	98.77	99.08
10	136	86.70	90.12	45	22	95.71	96.81	80	0	98.77	99.08
11	83	87.07	90.39	46	9	95.75	96.84	81	18	98.85	99.14
12	110	87.56	90.75	47	19	95.83	96.90	82	12	98.90	99.18
13	141	88.18	91.22	48	57	96.09	97.09	83	31	99.04	99.28
14	116	88.70	91.60	49	26	96.20	97.18	84	0	99.04	99.28
15	92	89.11	91.90	50	34	96.35	97.29	85	8	99.07	99.31
16	138	89.72	92.36	51	35	96.51	97.40	86	3	99.09	99.32
17	59	89.98	92.55	52	12	96.56	97.44	87	3	99.10	99.33
18	134	90.58	92.99	53	54	96.80	97.62	88	1	99.10	99.33
19	121	91.11	93.39	54	18	96.88	97.68	89	9	99.14	99.36
20	58	91.37	93.59	55	2	96.89	97.69	90	14	99.21	99.41
21	42	91.56	93.72	56	26	97.00	97.77	91	9	99.25	99.44
22	111	92.05	94.09	57	13	97.06	97.82	92	13	99.30	99.48
23	37	92.21	94.21	58	3	97.08	97.83	93	12	99.36	99.52
24	23	92.31	94.29	59	14	97.14	97.87	94	6	99.38	99.54
25	68	92.62	94.51	60	0	97.14	97.87	95	7	99.41	99.56
26	88	93.01	94.80	61	32	97.28	97.98	96	13	99.47	99.61
27	33	93.15	94.91	62	22	97.38	98.05	97	9	99.51	99.64
28	72	93.47	95.15	63	23	97.48	98.13	98	0	99.51	99.64
29	3	93.49	95.16	64	16	97.55	98.18	99	26	99.63	99.72
30	39	93.66	95.29	65	26	97.67	98.27	100	12	99.68	99.76
31	44	93.85	95.43	66	2	97.67	98.27	101	22	99.78	99.84
32	23	93.96	95.51	67	0	97.67	98.27	102	4	99.80	99.85
33	48	94.17	95.67	68	11	97.72	98.31	103	9	99.84	99.88
34	43	94.36	95.81	69	33	97.87	98.42	104	9	99.88	99.91
35	15	94.43	95.86	70	75	98.20	98.66	105	13	99.93	99.95

FIGURE 7.3

TABLE INCLUDES: 1. RADAR REPORTS AS A FUNCTION OF CORRELATION LENGTH
2. CUMULATIVE PERCENTAGE (WITH AND WITHOUT REPORTS FROM FIXED TRACKS) OF THE REPORTS IN THE SPECIFIED AND LOWER CORRELATION LENGTHS. FIXED TRACK CORR LNG IS ONE

CORR LNG	NUM OF REPORTS	CUM PER CNT	CUM PER CNT FIX	CORR LNG	NUM OF REPORTS	CUM PER CNT	CUM PER CNT FIX	CORR LNG	NUM OF REPORTS	CUM PER CNT	CUM PER CNT FIX
106	5	99.96	99.97	138	0	100.00	100.00	170	0	100.00	100.00
107	3	99.97	99.98	139	0	100.00	100.00	171	0	100.00	100.00
108	2	99.98	99.98	140	0	100.00	100.00	172	0	100.00	100.00
109	5	100.00	100.00	141	0	100.00	100.00	173	0	100.00	100.00
110	0	100.00	100.00	142	0	100.00	100.00	174	0	100.00	100.00
111	0	100.00	100.00	143	0	100.00	100.00	175	0	100.00	100.00
112	0	100.00	100.00	144	0	100.00	100.00	176	0	100.00	100.00
113	0	100.00	100.00	145	0	100.00	100.00	177	0	100.00	100.00
114	0	100.00	100.00	146	0	100.00	100.00	178	0	100.00	100.00
115	0	100.00	100.00	147	0	100.00	100.00	179	0	100.00	100.00
116	0	100.00	100.00	148	0	100.00	100.00	180	0	100.00	100.00
117	0	100.00	100.00	149	0	100.00	100.00	181	0	100.00	100.00
118	0	100.00	100.00	150	0	100.00	100.00	182	0	100.00	100.00
119	0	100.00	100.00	151	0	100.00	100.00	183	0	100.00	100.00
120	0	100.00	100.00	152	0	100.00	100.00	184	0	100.00	100.00
121	0	100.00	100.00	153	0	100.00	100.00	185	0	100.00	100.00
122	0	100.00	100.00	154	0	100.00	100.00	186	0	100.00	100.00
123	0	100.00	100.00	155	0	100.00	100.00	187	0	100.00	100.00
124	0	100.00	100.00	156	0	100.00	100.00	188	0	100.00	100.00
125	0	100.00	100.00	157	0	100.00	100.00	189	0	100.00	100.00
126	0	100.00	100.00	158	0	100.00	100.00	190	0	100.00	100.00
127	0	100.00	100.00	159	0	100.00	100.00	191	0	100.00	100.00
128	0	100.00	100.00	160	0	100.00	100.00	192	0	100.00	100.00
129	0	100.00	100.00	161	0	100.00	100.00	193	0	100.00	100.00
130	0	100.00	100.00	162	0	100.00	100.00	194	0	100.00	100.00
131	0	100.00	100.00	163	0	100.00	100.00	195	0	100.00	100.00
132	0	100.00	100.00	164	0	100.00	100.00	196	0	100.00	100.00
133	0	100.00	100.00	165	0	100.00	100.00	197	0	100.00	100.00
134	0	100.00	100.00	166	0	100.00	100.00	198	0	100.00	100.00
135	0	100.00	100.00	167	0	100.00	100.00	199	0	100.00	100.00
136	0	100.00	100.00	168	0	100.00	100.00	200	0	0.00	0.00
137	0	100.00	100.00	169	0	100.00	100.00				

FIGURE 7.4

TABLE INCLUDES: 1.NUMBER OF BEACON REPORTS AS A FUNCTION OF CORRELATION LENGTH.
2.PERCENTAGE OF BEACON REPORTS AT EACH CORRELATION LENGTH.
3.CUMULATIVE PERCENTAGE OF BEACON REPORTS AT THE SPECIFIED AND LOWER CORR.LENGTHS.

CORR LNG	NUM OF REPORTS	PER CNT	CUM PER CNT	CORR LNG	NUM OF REPORTS	PER CNT	CUM PER CNT	CORR LNG	NUM OF REPORTS	PER CNT	CUM PER CNT
1	2918	11.18	11.18	36	27	0.10	41.48	71	316	1.21	69.53
2	685	2.62	13.80	37	0	0.00	41.48	72	273	1.05	70.58
3	415	1.59	15.39	38	275	1.05	42.54	73	421	1.61	72.19
4	362	1.39	16.78	39	296	1.13	43.67	74	0	0.00	72.19
5	269	1.03	17.81	40	182	0.70	44.37	75	214	0.82	73.01
6	147	0.56	18.37	41	173	0.66	45.03	76	210	0.80	73.81
7	186	0.71	19.09	42	277	1.06	46.09	77	293	1.12	74.94
8	132	0.51	19.59	43	42	0.16	46.25	78	153	0.59	75.52
9	175	0.67	20.26	44	233	0.89	47.15	79	228	0.87	76.40
10	194	0.74	21.01	45	158	0.61	47.75	80	0	0.00	76.40
11	280	1.07	22.08	46	83	0.32	48.07	81	225	0.86	77.26
12	154	0.59	22.67	47	122	0.47	48.54	82	316	1.21	78.47
13	171	0.66	23.32	48	183	0.70	49.24	83	218	0.84	79.30
14	262	1.00	24.33	49	366	1.40	50.64	84	0	0.00	79.30
15	118	0.45	24.78	50	266	1.02	51.66	85	417	1.60	80.90
16	246	0.94	25.72	51	220	0.84	52.50	86	169	0.65	81.55
17	213	0.82	26.54	52	300	1.15	53.65	87	84	0.32	81.87
18	298	1.14	27.68	53	264	1.01	54.66	88	87	0.33	82.20
19	278	1.07	28.75	54	252	0.97	55.63	89	169	0.65	82.85
20	202	0.77	29.52	55	108	0.41	56.04	90	166	0.64	83.49
21	252	0.97	30.49	56	422	1.62	57.66	91	264	1.01	84.50
22	263	1.01	31.49	57	215	0.82	58.48	92	263	1.01	85.51
23	147	0.56	32.06	58	171	0.66	59.14	93	174	0.67	86.17
24	145	0.56	32.61	59	222	0.85	59.99	94	182	0.70	86.87
25	232	0.89	33.50	60	0	0.00	59.99	95	278	1.07	87.94
26	328	1.26	34.76	61	212	0.81	60.80	96	179	0.69	88.62
27	264	1.01	35.77	62	226	0.87	61.67	97	185	0.71	89.33
28	124	0.48	36.24	63	229	0.88	62.55	98	0	0.00	89.33
29	55	0.21	36.45	64	240	0.92	63.46	99	271	1.04	90.37
30	201	0.77	37.22	65	429	1.64	65.11	100	188	0.72	91.09
31	142	0.54	37.77	66	196	0.75	65.86	101	281	1.08	92.17
32	297	1.14	38.91	67	0	0.00	65.86	102	200	0.77	92.93
33	117	0.45	39.35	68	125	0.48	66.34	103	506	1.94	94.87
34	229	0.88	40.23	69	312	1.20	67.53	104	199	0.76	95.63
35	300	1.15	41.38	70	205	0.79	68.32	105	512	1.96	97.59

FIGURE 7.5

TABLE INCLUDES: 1. NUMBER OF BEACON REPORTS AS A FUNCTION OF CORRELATION LENGTH.
2. PERCENTAGE OF BEACON REPORTS AT EACH CORRELATION LENGTH.
3. CUMULATIVE PERCENTAGE OF BEACON REPORTS AT THE SPECIFIED AND LOWER CORR. LENGTHS.

CORR LNG	NUM OF REPORTS	PER CNT	CUM PER CNT	CORR LNG	NUM OF REPORTS	PER CNT	CUM PER CNT	CORR LNG	NUM OF REPORTS	PER CNT	CUM PER CNT
106	207	0.79	98.39	138	0	0.00	100.00	170	0	0.00	100.00
107	211	0.81	99.20	139	0	0.00	100.00	171	0	0.00	100.00
108	106	0.41	99.60	140	0	0.00	100.00	172	0	0.00	100.00
109	104	0.40	100.00	141	0	0.00	100.00	173	0	0.00	100.00
110	0	0.00	100.00	142	0	0.00	100.00	174	0	0.00	100.00
111	0	0.00	100.00	143	0	0.00	100.00	175	0	0.00	100.00
112	0	0.00	100.00	144	0	0.00	100.00	176	0	0.00	100.00
113	0	0.00	100.00	145	0	0.00	100.00	177	0	0.00	100.00
114	0	0.00	100.00	146	0	0.00	100.00	178	0	0.00	100.00
115	0	0.00	100.00	147	0	0.00	100.00	179	0	0.00	100.00
116	0	0.00	100.00	148	0	0.00	100.00	180	0	0.00	100.00
117	0	0.00	100.00	149	0	0.00	100.00	181	0	0.00	100.00
118	0	0.00	100.00	150	0	0.00	100.00	182	0	0.00	100.00
119	0	0.00	100.00	151	0	0.00	100.00	183	0	0.00	100.00
120	0	0.00	100.00	152	0	0.00	100.00	184	0	0.00	100.00
121	0	0.00	100.00	153	0	0.00	100.00	185	0	0.00	100.00
122	0	0.00	100.00	154	0	0.00	100.00	186	0	0.00	100.00
123	0	0.00	100.00	155	0	0.00	100.00	187	0	0.00	100.00
124	0	0.00	100.00	156	0	0.00	100.00	188	0	0.00	100.00
125	0	0.00	100.00	157	0	0.00	100.00	189	0	0.00	100.00
126	0	0.00	100.00	158	0	0.00	100.00	190	0	0.00	100.00
127	0	0.00	100.00	159	0	0.00	100.00	191	0	0.00	100.00
128	0	0.00	100.00	160	0	0.00	100.00	192	0	0.00	100.00
129	0	0.00	100.00	161	0	0.00	100.00	193	0	0.00	100.00
130	0	0.00	100.00	162	0	0.00	100.00	194	0	0.00	100.00
131	0	0.00	100.00	163	0	0.00	100.00	195	0	0.00	100.00
132	0	0.00	100.00	164	0	0.00	100.00	196	0	0.00	100.00
133	0	0.00	100.00	165	0	0.00	100.00	197	0	0.00	100.00
134	0	0.00	100.00	166	0	0.00	100.00	198	0	0.00	100.00
135	0	0.00	100.00	167	0	0.00	100.00	199	0	0.00	100.00
136	0	0.00	100.00	168	0	0.00	100.00	200	0	0.00	0.00
137	0	0.00	100.00	169	0	0.00	100.00				

FIGURE 7.6

HISTOGRAM OF THE NUMBER OF BEACON REPORTS AS A FUNCTION OF CORRELATION LENGTH

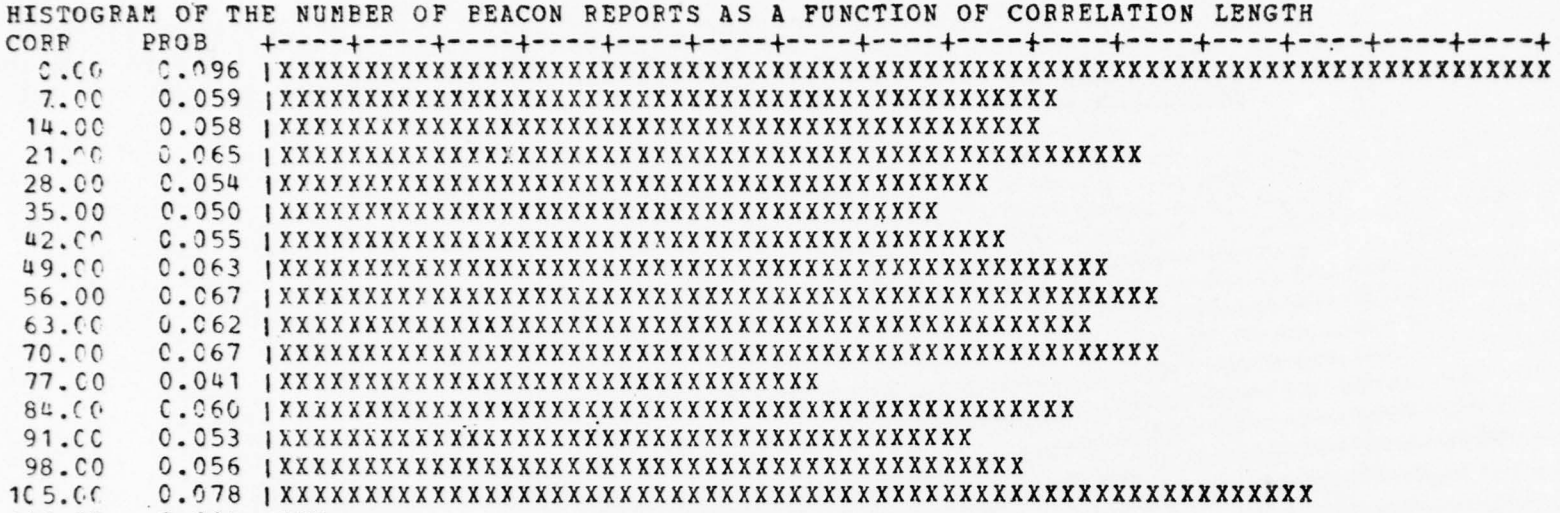

TOTAL NUMBER OF POINTS 24438 NUMBER OF POINTS OUTSIDE HISTOGRAM 0
MEAN 51.5660 RMS 61.5771
VARIANCE 1132.6876 STD DEV 33.6554

FIGURE 7.7

HISTOGRAM OF THE NUMBER OF RADAR REINFORCED BEACON REPORTS AS A FUNCTION OF CORRELATION LENGTH

```
CORR     PROB   +----+----+----+----+----+----+----+----+----+----+----+----+----+----+----+
  0.00    0.028 |XXXXXXXXXXXXXXXXXXXXX
  7.00    0.048 |XXXXXXXXXXXXXXXXXXXXXXXXXXXXXXXXXXXXX
 14.00    0.045 |XXXXXXXXXXXXXXXXXXXXXXXXXXXXXXXXXXXXX
 21.00    0.048 |XXXXXXXXXXXXXXXXXXXXXXXXXXXXXXXXXXXXX
 28.00    0.060 |XXXXXXXXXXXXXXXXXXXXXXXXXXXXXXXXXXXXXXXXXXXXXXXXX
 35.00    0.048 |XXXXXXXXXXXXXXXXXXXXXXXXXXXXXXXXXXXXX
 42.00    0.059 |XXXXXXXXXXXXXXXXXXXXXXXXXXXXXXXXXXXXXXXXXXXXXXXXX
 49.00    0.071 |XXXXXXXXXXXXXXXXXXXXXXXXXXXXXXXXXXXXXXXXXXXXXXXXXXXXXXXXX
 56.00    0.068 |XXXXXXXXXXXXXXXXXXXXXXXXXXXXXXXXXXXXXXXXXXXXXXXXX
 63.00    0.070 |XXXXXXXXXXXXXXXXXXXXXXXXXXXXXXXXXXXXXXXXXXXXXXXXX
 70.00    0.084 |XXXXXXXXXXXXXXXXXXXXXXXXXXXXXXXXXXXXXXXXXXXXXXXXXXXXXXXXXXXXXXXX
 77.00    0.053 |XXXXXXXXXXXXXXXXXXXXXXXXXXXXXXXXXXXXXXXXX
 84.00    0.078 |XXXXXXXXXXXXXXXXXXXXXXXXXXXXXXXXXXXXXXXXXXXXXXXXXXXXXXXXX
 91.00    0.066 |XXXXXXXXXXXXXXXXXXXXXXXXXXXXXXXXXXXXXXXXXXXXXXXXX
 98.00    0.068 |XXXXXXXXXXXXXXXXXXXXXXXXXXXXXXXXXXXXXXXXXXXXXXXXX
105.00    0.094 |XXXXXXXXXXXXXXXXXXXXXXXXXXXXXXXXXXXXXXXXXXXXXXXXXXXXXXXXXXXXXXXXXXXXXXXXXXXX
112.00    0.005 |XXXX
119.00    0.000 |
126.00    0.000 |
133.00    0.000 |
140.00    0.000 |
147.00    0.000 |
154.00    0.000 |
161.00    0.000 |
168.00    0.000 |
175.00    0.000 |
182.00    0.000 |
189.00    0.000 |
196.00    0.000 |
203.00    0.000 |
210.00    0.000 |
```

TOTAL NUMBER OF POINTS 9960 NUMBER OF POINTS OUTSIDE HISTOGRAM 0
MEAN 59.6757 RMS 67.2758
VARIANCE 964.8422 STD DEV 31.0619

FIGURE 7.8

Figure 7.7 is merely the data in Figure 7.5 and 7.6 presented in histogram form. In this as well as all following histograms it is important to remember that the histograms are normalized (that is the bin with the largest number of counts will always extend all the way to the top of the histogram). Figure 7.8 is the same as Figure 7.7 except that only beacon reports which are radar reinforced are plotted. It is interesting to note that on a percentage basis less reports exists at low correlation lengths and more at higher lengths for reinforced beacon reports than for nonreinforced. This indicates that radar reinforcement might be a discriminate for false versus true beacon reports.

Figures 7.9 through 7.18 show histogram plots ot track deviations. All tracks with correlation lengths less than eight have been excluded in order to eliminate false target reports. All histograms of moving track deviations were taken from a CD Record produced at NAFEC and have no connections with the rest of the data presented in this section which was recorded at Los Angeles. These histograms all possess a pronounced skewed symmetry about zero deviation with the radar reports deviations skewed in one direction and the beacon report deviations in the other. The skewing in range deviations is an indication that the beacon and radar processing are not properly aligned in time. The smoothed position will be a weighted value of beacon and radar reports lying closer to where the beacon reports are since there are more beacon reports than radar reports on tracks of long correlation length. The skewing in azimuth results from an improper adjustment of the const azimuth offset applied to beacon reports in order to align them with radar reports. Thus the skewed symmetry in these deviation histograms is readily explained by misalignments and should cause no further concern.

Figures 7.19 and 7.20 relate to blip/scan statistics. For these statistics only moving tracks are considered and there exists a minimum cutoff correlation length of six; below which the reports are neglected. In calculating blip/scan ratios there exist two types of tracks, radar and beacon. A radar track is composed of mainly radar reports and a beacon track, beacon reports. The ARSR tracker contains an algorithm for determining the type of track as well as allowing for transitions from one type to another. Figure 7.20 presents blip/scan ratios in matrix form for beacon tracks, radar tracks, and both beacon and radar tracks using only beacon reports, only radar reports and the combination of beacon and radar reports. A radar reinforced beacon report is considered a radar report in those sums which include only radar reports. This is done to give an indication of the CD performance without beacon input. However, because of the poor quality of the radar/beacon alignments (discussed in Section 8.4.4) many beacon reports are not classified as reinforced although a radar report was present and would have been correlated into the track if the beacon report were not present. Therefore, the 0.429 ratio for radar reports

HISTOGRAM OF THE SCAN-TO-SCAN FLUCTUATIONS IN RANGE(NMI)FOR STATIONARY TARGETS LASTING MORE THAN 7 SCANS

```
FLUCT   PROB   +----+----+----+----+----+----+----+----+----+----+----+----+----+----+----+----+
 -1.87   0.000 |
 -1.75   0.000 |
 -1.62   0.000 |
 -1.50   0.000 |
 -1.37   0.000 |
 -1.25   0.000 |
 -1.12   0.000 |
 -1.00   0.000 |
 -0.87   0.000 |
 -0.75   0.000 |
 -0.62   0.000 |
 -0.50   0.035 |XXXXXXXX
 -0.37   0.049 |XXXXXXXXXXX
 -0.25   0.075 |XXXXXXXXXXXXXXXXX
 -0.12   0.164 |XXXXXXXXXXXXXXXXXXXXXXXXXXXXXXXXXXX
  0.00   0.332 |XXXXXXXXXXXXXXXXXXXXXXXXXXXXXXXXXXXXXXXXXXXXXXXXXXXXXXXXXXXXXXXXXXXXXXXXXXXXXXX
  0.13   0.190 |XXXXXXXXXXXXXXXXXXXXXXXXXXXXXXXXXXXXXXXXXX
  0.25   0.071 |XXXXXXXXXXXXXXXX
  0.38   0.040 |XXXXXXXXX
  0.50   0.031 |XXXXXXX
  0.63   0.000 |
  0.75   0.000 |
  0.88   0.000 |
  1.00   0.000 |
  1.13   0.000 |
  1.25   0.000 |
  1.38   0.000 |
  1.50   0.000 |
  1.63   0.000 |
  1.75   0.000 |
  1.88   0.000 |
```

TOTAL NUMBER OF POINTS 6223 NUMBER OF POINTS OUTSIDE HISTOGRAM 0

MEAN -0.0040 RMS 0.2128

VARIANCE 0.0453 STD DEV 0.2127

FIGURE 7.9

```
HISTOGRAM OF THE SCAN-TO-SCAN FLUCTUATIONS IN AZIMUTH(DEG)FOR STATIONARY TARGETS LASTING MORE THAN
    7  SCANS
FLUCT    PROB   +----+----+----+----+----+----+----+----+----+----+----+----+----+----+----+
 -3.00    0.000 |
 -2.80    0.000 |
 -2.60    0.000 |
 -2.40    0.000 |
 -2.20    0.000 |
 -2.00    0.000 |
 -1.80    0.004 |X
 -1.60    0.004 |X
 -1.40    0.016 |XXXX
 -1.20    0.016 |XXXX
 -1.00    0.020 |XXXXX
 -0.80    0.036 |XXXXXXXXX
 -0.60    0.044 |XXXXXXXXXXX
 -0.40    0.068 |XXXXXXXXXXXXXXXXX
 -0.20    0.132 |XXXXXXXXXXXXXXXXXXXXXXXXXXXXXXXXX
 -0.00    0.300 |XXXXXXXXXXXXXXXXXXXXXXXXXXXXXXXXXXXXXXXXXXXXXXXXXXXXXXXXXXXXXXXXXXXXXXXXXXXXXXXXXXXXXXX
  0.20    0.128 |XXXXXXXXXXXXXXXXXXXXXXXXXXXXXXXX
  0.40    0.072 |XXXXXXXXXXXXXXXXXX
  0.60    0.036 |XXXXXXXXX
  0.80    0.036 |XXXXXXXXX
  1.00    0.016 |XXXX
  1.20    0.012 |XXX
  1.40    0.012 |XXX
  1.60    0.004 |X
  1.80    0.000 |
  2.00    0.000 |
  2.20    0.000 |
  2.40    0.000 |
  2.60    0.000 |
  2.80    0.000 |
  3.00    0.000 |

TOTAL NUMBER OF POINTS   6223          NUMBER OF POINTS OUTSIDE HISTOGRAM      0
MEAN    -0.0302              RMS     0.5919
VARIANCE    0.3494           STD DEV     0.5911
```

FIGURE 7.10

HISTOGRAM OF THE RANGE DEVIATIONS(NMI)FROM THE MEAN FOR STATIONARY TARGETS LASTING MORE THAN 7 SCANS

```
DEVIA    PROB   +----+----+----+----+----+----+----+----+----+----+----+----+----+----+----+----+
 -4.50   0.000 |
 -4.20   0.000 |
 -3.90   0.000 |
 -3.60   0.000 |
 -3.30   0.000 |
 -3.00   0.000 |
 -2.70   0.004 |X
 -2.40   0.008 |XX
 -2.10   0.015 |XXXX
 -1.80   0.015 |XXXX
 -1.50   0.023 |XXXXXX
 -1.20   0.031 |XXXXXXXX
 -0.90   0.042 |XXXXXXXXXX
 -0.60   0.069 |XXXXXXXXXXXXXXXXX
 -0.30   0.119 |XXXXXXXXXXXXXXXXXXXXXXXXXXXXX
 -0.00   0.288 |XXXXXXXXXXXXXXXXXXXXXXXXXXXXXXXXXXXXXXXXXXXXXXXXXXXXXXXXXXXXXXXXXXXXXXXXXXXXXXX
  0.30   0.135 |XXXXXXXXXXXXXXXXXXXXXXXXXXXXXXXX
  0.60   0.062 |XXXXXXXXXXXXXXXX
  0.90   0.042 |XXXXXXXXXXX
  1.20   0.031 |XXXXXXXX
  1.50   0.023 |XXXXXX
  1.80   0.015 |XXXX
  2.10   0.012 |XXX
  2.40   0.008 |XX
  2.70   0.008 |XX
  3.00   0.004 |X
  3.30   0.000 |
  3.60   0.000 |
  3.90   0.000 |
  4.20   0.000 |
  4.50   0.000 |
```

TOTAL NUMBER OF POINTS 6425 NUMBER OF POINTS OUTSIDE HISTOGRAM 20
MEAN 0.0000 RMS 1.0645
VARIANCE 1.1331 STD DEV 1.0645

FIGURE 7.11

```
HISTOGRAM OF THE AZIMUTH DEVIATIONS(DEG)FROM THE MEAN FOR STATIONARY TARGETS LASTING MORE THAN
    7   SCANS
DEVIA    PROB    +----+----+----+----+----+----+----+----+----+----+----+----+----+----+----+
-11.25   0.000   |
-10.50   0.000   |
 -9.75   0.000   |
 -9.00   0.000   |
 -8.25   0.000   |
 -7.50   0.000   |
 -6.75   0.000   |
 -6.00   0.000   |
 -5.25   0.000   |
 -4.50   0.006   |X
 -3.75   0.006   |X
 -3.00   0.018   |XXX
 -2.25   0.024   |XXXX
 -1.50   0.047   |XXXXXXXX
 -0.75   0.135   |XXXXXXXXXXXXXXXXXXXXXXX
 -0.00   0.442   |XXXXXXXXXXXXXXXXXXXXXXXXXXXXXXXXXXXXXXXXXXXXXXXXXXXXXXXXXXXXXXXXXXXXXXXXXXXX
  0.75   0.141   |XXXXXXXXXXXXXXXXXXXXXXXX
  1.50   0.047   |XXXXXXXX
  2.25   0.029   |XXXXX
  3.00   0.018   |XXX
  3.75   0.006   |X
  4.50   0.006   |X
  5.25   0.000   |
  6.00   0.000   |
  6.75   0.000   |
  7.50   0.000   |
  8.25   0.000   |
  9.00   0.000   |
  9.75   0.000   |
 10.50   0.000   |
 11.25   0.000   |

TOTAL NUMBER OF POINTS   6425          NUMBER OF POINTS OUTSIDE HISTOGRAM     27
MEAN    0.0055                RMS     2.1924
VARIANCE     4.8067           STD DEV     2.1924
```

FIGURE 7.12

```
HISTOGRAM OF THE RANGE DEVIATIONS(NMI)FROM THE SMOOTHED RANGE FOR RADAR REPORTS ON MOVING TRACKS
LASTING MORE THAN     7 SCANS
DEVIA    PROB   +----+----+----+----+----+----+----+----+----+----+----+----+----+----+----+
 -1.87    0.000 I
 -1.75    0.000 I
 -1.62    0.000 I
 -1.50    0.000 I
 -1.37    0.000 I
 -1.25    0.000 I
 -1.12    0.000 I
 -1.00    0.000 I
 -0.87    0.000 I
 -0.75    0.000 I
 -0.62    0.000 I
 -0.50    0.000 I
 -0.37    0.000 I
 -0.25    0.078 IXXXXXXXXXX
 -0.12    0.241 IXXXXXXXXXXXXXXXXXXXXXXXXXXXXXXX
  0.00    0.584 IXXXXXXXXXXXXXXXXXXXXXXXXXXXXXXXXXXXXXXXXXXXXXXXXXXXXXXXXXXXXXXXXXXXXXXXXXX
  0.13    0.054 IXXXXXXX
  0.25    0.008 IX
  0.38    0.000 I
  0.50    0.000 I
  0.63    0.000 I
  0.75    0.000 I
  0.88    0.000 I
  1.00    0.000 I
  1.13    0.000 I
  1.25    0.000 I
  1.38    0.000 I
  1.50    0.000 I
  1.63    0.000 I
  1.75    0.000 I
  1.88    0.000 I

TOTAL NUMBER OF POINTS     559          NUMBER OF POINTS OUTSIDE HISTOGRAM      0
MEAN    -0.0443              RMS    0.1328
VARIANCE    0.0157           STD DEV    0.1251
```

FIGURE 7.13

```
HISTOGRAM OF THE RANGE DEVIATIONS(NMI)FROM THE SMOOTHED RANGE FOR BEACON REPORTS ON MOVING TRACKS
LASTING MORE THAN     7 SCANS
DEVIA    PROB    +----+----+----+----+----+----+----+----+----+----+----+----+----+----+----+----+
 -1.87   0.000  I
 -1.75   0.000  I
 -1.62   0.000  I
 -1.50   0.000  I
 -1.37   0.000  I
 -1.25   0.000  I
 -1.12   0.000  I
 -1.00   0.000  I
 -0.87   0.000  I
 -0.75   0.000  I
 -0.62   0.000  I
 -0.50   0.000  I
 -0.37   0.000  I
 -0.25   0.000  I
 -0.12   0.052  IXXXXX
  0.00   0.780  IXXXXXXXXXXXXXXXXXXXXXXXXXXXXXXXXXXXXXXXXXXXXXXXXXXXXXXXXXXXXXXXXXXXXXXXXXXXXXX
  0.13   0.146  IXXXXXXXXXXXXXX
  0.25   0.000  I
  0.38   0.000  I
  0.50   0.000  I
  0.63   0.000  I
  0.75   0.000  I
  0.88   0.000  I
  1.00   0.000  I
  1.13   0.000  I
  1.25   0.000  I
  1.38   0.000  I
  1.50   0.000  I
  1.63   0.000  I
  1.75   0.000  I
  1.88   0.000  I

TOTAL NUMBER OF POINTS    2029          NUMBER OF POINTS OUTSIDE HISTOGRAM      0
MEAN     0.0130                RMS     0.0645
VARIANCE     0.0040            STD DEV     0.0631
```

FIGURE 7.14

```
HISTOGRAM OF THE RANGE DEVIATIONS(NMI)FROM THE SMOOTHED RANGE FOR BEACON AND RADAR REPORTS ON
MOVING TRACKS LASTING MORE THAN     7 SCANS
DEVIA    PROB    +----+----+----+----+----+----+----+----+----+----+----+----+----+----+----+
 -1.87    0.000 |
 -1.75    0.000 |
 -1.62    0.000 |
 -1.50    0.000 |
 -1.37    0.000 |
 -1.25    0.000 |
 -1.12    0.000 |
 -1.00    0.000 |
 -0.87    0.000 |
 -0.75    0.000 |
 -0.62    0.000 |
 -0.50    0.000 |
 -0.37    0.000 |
 -0.25    0.010 |X
 -0.12    0.088 |XXXXXXXXX
  0.00    0.737 |XXXXXXXXXXXXXXXXXXXXXXXXXXXXXXXXXXXXXXXXXXXXXXXXXXXXXXXXXXXXXXXXXXXXXXXXXXXXXX
  0.13    0.128 |XXXXXXXXXXXXX
  0.25    0.010 |X
  0.38    0.000 |
  0.50    0.000 |
  0.63    0.000 |
  0.75    0.000 |
  0.88    0.000 |
  1.00    0.000 |
  1.13    0.000 |
  1.25    0.000 |
  1.38    0.000 |
  1.50    0.000 |
  1.63    0.000 |
  1.75    0.000 |
  1.88    0.000 |

TOTAL NUMBER OF POINTS   2588          NUMBER OF POINTS OUTSIDE HISTOGRAM      0
MEAN    0.0006              RMS    0.0840
VARIANCE    0.0070          STD DEV    0.0840
```

FIGURE 7.15

```
HISTOGRAM OF THE AZIMUTH DEVIATIONS(DEG)FROM THE SMOOTHED AZIMUTH FOR RADAR REPORTS ON MOVING TRACKS
LASTING MORE THAN     7 SCANS
DEVIA    PROB    +----+----+----+----+----+----+----+----+----+----+----+----+----+----+----+----+
 -3.00    0.000 |
 -2.80    0.000 |
 -2.60    0.000 |
 -2.40    0.000 |
 -2.20    0.000 |
 -2.00    0.000 |
 -1.80    0.000 |
 -1.60    0.000 |
 -1.40    0.000 |
 -1.20    0.000 |
 -1.00    0.020 |XXXX
 -0.80    0.046 |XXXXXXXXX
 -0.60    0.096 |XXXXXXXXXXXXXXXXXX
 -0.40    0.117 |XXXXXXXXXXXXXXXXXXXXX
 -0.20    0.182 |XXXXXXXXXXXXXXXXXXXXXXXXXXXXXXXXX
 -0.00    0.380 |XXXXXXXXXXXXXXXXXXXXXXXXXXXXXXXXXXXXXXXXXXXXXXXXXXXXXXXXXXXXXXXXXXXXXXXXXXXXXX
  0.20    0.111 |XXXXXXXXXXXXXXXXXXXX
  0.40    0.020 |XXXX
  0.60    0.000 |
  0.80    0.005 |X
  1.00    0.000 |
  1.20    0.000 |
  1.40    0.000 |
  1.60    0.000 |
  1.80    0.000 |
  2.00    0.000 |
  2.20    0.000 |
  2.40    0.000 |
  2.60    0.000 |
  2.80    0.000 |
  3.00    0.000 |

TOTAL NUMBER OF POINTS     559          NUMBER OF POINTS OUTSIDE HISTOGRAM      0
MEAN    -0.1669              RMS     0.3593
VARIANCE     0.1012          STD DEV     0.3181
```

FIGURE 7.16

```
HISTOGRAM OF THE AZIMUTH DEVIATIONS(DEG)FROM THE SMOOTHED AZIMUTH FOR BEACON REPORTS ON MOVING TRACKS
LASTING MORE THAN     7 SCANS
DEVIA    PROB    +----+----+----+----+----+----+----+----+----+----+----+----+----+----+----+
 -3.00    0.000  |
 -2.80    0.000  |
 -2.60    0.000  |
 -2.40    0.000  |
 -2.20    0.000  |
 -2.00    0.000  |
 -1.80    0.000  |
 -1.60    0.000  |
 -1.40    0.000  |
 -1.20    0.000  |
 -1.00    0.000  |
 -0.80    0.000  |
 -0.60    0.006  |X
 -0.40    0.026  |XXXX
 -0.20    0.136  |XXXXXXXXXXXXXXXXXXXXX
 -0.00    0.485  |XXXXXXXXXXXXXXXXXXXXXXXXXXXXXXXXXXXXXXXXXXXXXXXXXXXXXXXXXXXXXXXXXXXXXXXXXXX
  0.20    0.188  |XXXXXXXXXXXXXXXXXXXXXXXXXXXXX
  0.40    0.078  |XXXXXXXXXXXX
  0.60    0.032  |XXXXX
  0.80    0.006  |X
  1.00    0.000  |
  1.20    0.000  |
  1.40    0.000  |
  1.60    0.000  |
  1.80    0.000  |
  2.00    0.000  |
  2.20    0.000  |
  2.40    0.000  |
  2.60    0.000  |
  2.80    0.000  |
  3.00    0.000  |

TOTAL NUMBER OF POINTS    2029          NUMBER OF POINTS OUTSIDE HISTOGRAM      0
MEAN     0.0595                RMS     0.2787
VARIANCE     0.0741            STD DEV     0.2722
```

FIGURE 7.17

```
HISTOGRAM OF THE AZIMUTH DEVIATIONS(NMI)FROM THE SMOOTHED AZIMUTH FOR BEACON AND RADAR REPORTS ON
MOVING TRACKS LASTING MORE THAN    7 SCANS
DEVIA   PROB   +----+----+----+----+----+----+----+----+----+----+----+----+----+----+----+
 -3.00  0.000 |
 -2.80  0.000 |
 -2.60  0.000 |
 -2.40  0.000 |
 -2.20  0.000 |
 -2.00  0.000 |
 -1.80  0.000 |
 -1.60  0.000 |
 -1.40  0.000 |
 -1.20  0.000 |
 -1.00  0.006 |X
 -0.80  0.012 |XX
 -0.60  0.025 |XXXX
 -0.40  0.043 |XXXXXXX
 -0.20  0.142 |XXXXXXXXXXXXXXXXXXXXXXX
 -0.00  0.462 |XXXXXXXXXXXXXXXXXXXXXXXXXXXXXXXXXXXXXXXXXXXXXXXXXXXXXXXXXXXXXXXXXXXXXXXXXXXXX
  0.20  0.173 |XXXXXXXXXXXXXXXXXXXXXXXXXXXX
  0.40  0.068 |XXXXXXXXXXX
  0.60  0.025 |XXXX
  0.80  0.006 |X
  1.00  0.000 |
  1.20  0.000 |
  1.40  0.000 |
  1.60  0.000 |
  1.80  0.000 |
  2.00  0.000 |
  2.20  0.000 |
  2.40  0.000 |
  2.60  0.000 |
  2.80  0.000 |
  3.00  0.000 |

TOTAL NUMBER OF POINTS    2588          NUMBER OF POINTS OUTSIDE HISTOGRAM      0
MEAN    0.0106                RMS    0.2979
VARIANCE    0.0887            STD DEV    0.2977
```

FIGURE 7.18

BLIP/SCAN STATISTICS

(STATISTICS CALCULATED ON MOVING TRACKS WITH A CORRELATION LENGTH OF 6 OR GREATER)

TOTALS:

TOTAL NUMBER OF BEACON REPORTS ON BEACON TRACKS	20957
TOTAL NUMBER OF BEACON REPORTS ON RADAR TRACKS	486
TOTAL NUMBER OF BEACON REPORTS ON ALL TRACKS	21443
TOTAL NUMBER OF RADAR REPORTS ON RADAR TRACKS	3011
TOTAL NUMBER OF RADAR REPORTS ON BEACON TRACKS	1123
TOTAL NUMBER OF RADAR REPORTS ON ALL TRACKS	4134
TOTAL NUMBER OF SCANS ON BEACON TRACKS	24191
TOTAL NUMBER OF SCANS ON RADAR TRACKS	4130
TOTAL NUMBER OF SCANS ON ALL TRACKS	28321
TOTAL NUMBER OF TRACKS	838
TOTAL NUMBER OF BEACON AND RADAR REPORTS ON ALL TRACKS	25577
TOTAL NUMBER OF RADAR REINFORCED REPORTS ON BEACON TRACKS	9266
TOTAL NUMBER OF RADAR REINFORCED REPORTS ON RADAR TRACKS	215

FIGURE 7.19

BLIP/SCAN RATIOES

	BLIP/SCAN RATIOES UTILIZING		
	BEACON REPORTS ONLY	RADAR REPORTS ONLY	RADAR AND BEACON REPORTS
BLIP/SCAN RATIOES FOR BEACON TRACKS	0.866	0.429	0.913
BLIP/SCAN RATIOES FOR RADAR TRACKS	0.118	0.729	0.794
BLIP/SCAN RATIOES FOR ALL TRACKS	0.757	0.473	0.895
AVERAGE OF INDIVIDUAL TRACKS BLIP SCAN RATIOES	0.638		0.878

FIGURE 7.20

on beacon tracks is probably a little low. Some general trends can be determined from Figure 7.20; for instance, the ratios are lower for radar reports than for beacon reports (0.729 versus 0.866). Radar information is definitely supplementing and enhancing the beacon information. On beacon tracks the blip/scan ratio jumps from 0.866 to 0.913 when radar reports are included. Also for all tracks if only beacon reports are considered the ratio is 0.757. Finally on Figure 7.20 the average of the blip/scan ratios for individual tracks is calculated. The value 0.638 is low because the radar tracks have very low or zero ratios when considering only beacon reports.

Figure 7.21 shows the results of the beacon fade and code change analysis. The beacon fade statistics merely measure the number of scans in which a beacon fade is backed up with a radar report. Once a beacon track has been established, associated with that track is a particular beacon code referred to as the track code. (The establishment of this code is determined by an algorithm in the ARSR tracker.) Also associated with each beacon report is a code referred to as the measured code. There exist two situations where the measured code differs from the track code (1) when the code selected on the transponder has been changed, in which case the track code will also change shortly, and (2) when the CD fails to interpret the code correctly, in which case the measured code will return to the track code on subsequent scans. If for some reason the Common Digitizer is unable to decode the replies in a report, it reports a code of zero. The data in Figure 7.21 shows that with approximately 2% of the beacon reports an incorrect code was reported and with another 2% the CD was unable to decode the replies. Hamming distance is a measurement of the number of differences existing in reply code pulses between the track and measured codes in non code transition situations.

Figures 7.22 through 7.24 are histograms of radar target reports as a function of run length. In Figure 7.22 only reports with correlation lengths of seven or greater are plotted and in Figure 7.23 those reports with lengths less than seven are plotted. The distribution of these two histograms indicate a correlation between run length and the validity of the report. Many false reports have a short run length. The TRQA program will also perform the same calculations for beacon reports; however, no data was processed which contained beacon run length information.

BEACON FADE STATISTICS

NUMBER OF SCANS WHERE BEACON FADES OCCURRED IN A BEACON TRACK	3225
PER CENT OF SCANS WHERE BEACON FADES OCCURRED IN A BEACON TRACK	13.330
NUMBER OF SCANS WHERE BEACON FADES WERE BACKED UP WITH RADAR REPORTS	1123
PER CENT OF FADES WITHIN BEACON TRACKS BACKED UP WITH RADAR REPORTS	34.821

CHANGE STATISTICS FOR BEACON CODES

TOTAL NUMBER OF TIMES TRACK BEACON CODE CHANGED	222	
TRACK CODE CHANGES/NUMBER OF BEACON REPORTS ON BEACON TRACKS		0.011
TOTAL NUMBER OF TIMES BEACON CODE DIFFERED FROM THE TRACK CODE IN A NON CODE TRANSITION SITUATION		990
CODE DIFFERENCES/NUMBER OF BEACON REPORTS ON BEACON TRACKS		0.047
CODE DIFFERENCES WHERE THE MEASURED BEACON CODE IS ZERO		511
PER CENT OF CODE DIFFERENCES WHICH ARE ZERO		51.614

HAMMING DISTANCES FOR CODE DIFFERENCES

HAMMING DISTANCE	1	2	3	4	5	6	7	8	9	10	11	12
NUMBER OF DIFFERENCES	124	58	44	49	58	54	48	26	16	2	0	0

FIGURE 7.21

```
HISTOGRAM OF RUN LENGTH(IN ACP)OF RADAR REPORTS FROM MOVING TRACKS WITH CORRELATION LENGTHS   7
OR GREATER
ACP      PROB   +----+----+----+----+----+----+----+----+----+----+----+----+----+----+----+
  0.00    0.058 |XXXXXXXXXXXXXXXXXXX
  4.00    0.035 |XXXXXXXXXXXX
  8.00    0.107 |XXXXXXXXXXXXXXXXXXXXXXXXXXXXXXXXXXX
 12.00    0.217 |XXXXXXXXXXXXXXXXXXXXXXXXXXXXXXXXXXXXXXXXXXXXXXXXXXXXXXXXXXXXXXXXXXXXXXXXXXXXXXX
 16.00    0.186 |XXXXXXXXXXXXXXXXXXXXXXXXXXXXXXXXXXXXXXXXXXXXXXXXXXXXXXXXXXXXXXXXXXXXXX
 20.00    0.159 |XXXXXXXXXXXXXXXXXXXXXXXXXXXXXXXXXXXXXXXXXXXXXXXXXXXXXXXXXXXXX
 24.00    0.122 |XXXXXXXXXXXXXXXXXXXXXXXXXXXXXXXXXXXXXXXXXXX
 28.00    0.104 |XXXXXXXXXXXXXXXXXXXXXXXXXXXXXXXXXXXXX
 32.00    0.000 |
 36.00    0.000 |
 40.00    0.000 |
 44.00    0.000 |
 48.00    0.000 |
 52.00    0.000 |
 56.00    0.000 |
 60.00    0.000 |
 64.00    0.000 |
 68.00    0.000 |
 72.00    0.000 |
 76.00    0.000 |
 80.00    0.000 |
 84.00    0.000 |
 88.00    0.000 |
 92.00    0.000 |
 96.00    0.000 |
100.00    0.000 |
104.00    0.000 |
108.00    0.000 |
112.00    0.000 |
116.00    0.000 |
120.00    0.000 |

TOTAL NUMBER OF POINTS   3739          NUMBER OF POINTS OUTSIDE HISTOGRAM      0
MEAN   15.7539              RMS   17.4517
VARIANCE   56.3738          STD DEV    7.5082
```

FIGURE 7.22

```
HISTOGRAM OF RUN LENGTH(IN ACP)OF RADAR REPORTS FROM MOVING TRACKS WITH CORRELATION LENGTHS LESS
THAN    7
ACP       PROB    +----+----+----+----+----+----+----+----+----+----+----+----+----+----+----+
  0.00    0.373   |XXXXXXXXXXXXXXXXXXXXXXXXXXXXXXXXXXXXXXXXXXXXXXXXXXXXXXXXXXXXXXXXXXXXXXXXXXX
  4.00    0.020   |XXXX
  8.00    0.109   |XXXXXXXXXXXXXXXXXXXXXX
 12.00    0.189   |XXXXXXXXXXXXXXXXXXXXXXXXXXXXXXXXXXXXXX
 16.00    0.119   |XXXXXXXXXXXXXXXXXXXXXXXX
 20.00    0.080   |XXXXXXXXXXXXXXXX
 24.00    0.050   |XXXXXXXXXX
 28.00    0.040   |XXXXXXXX
 32.00    0.000   |
 36.00    0.000   |
 40.00    0.000   |
 44.00    0.000   |
 48.00    0.000   |
 52.00    0.000   |
 56.00    0.000   |
 60.00    0.000   |
 64.00    0.000   |
 68.00    0.000   |
 72.00    0.000   |
 76.00    0.000   |
 80.00    0.000   |
 84.00    0.000   |
 88.00    0.000   |
 92.00    0.000   |
 96.00    0.000   |
100.00    0.000   |
104.00    0.000   |
108.00    0.000   |
112.00    0.000   |
116.00    0.000   |
120.00    0.000   |

TOTAL NUMBER OF POINTS   19960            NUMBER OF POINTS OUTSIDE HISTOGRAM       0
MEAN     9.3279               RMS    12.7538
VARIANCE    75.6508           STD DEV     8.6977
```

FIGURE 7.23

HISTOGRAM OF RUN LENGTH(IN ACP)OF RADAR REPORTS FROM MOVING TRACKS

TOTAL NUMBER OF POINTS 17844 NUMBER OF POINTS OUTSIDE HISTOGRAM 0
MEAN 8.6117 RMS 12.3533
VARIANCE 78.4431 STD DEV 8.8568

FIGURE 7.24

7.4 CONCLUSIONS

Care should be taken in attaching too great a significance to the values of the results in this section. Several inconsistencies in the data itself indicate that errors still exist in the program. It must be reemphasized that the results presented were not obtained from a representative data based of CD Records from several sites processed under correct version of the TRQA program, rather they were gathered while testing the TRQA program with limit data and a program with errors in it.

In spite of this some general conclusions can be drawn. First the vast majority of radar reports exiting the CD are false. However, radar information does enhance the beacon information both in the form of radar back up increasing the blip/scan ratio and radar reinforcement increasing confidence in the validity of a beacon report. The approximate 90% false radar report rate indicates that there is room for some very effective improvements in this area and some efforts should be applied. (Section 5 describes some past effort to improve radar processing.) Run length and radar reinforcement are two measured parameters which might be useful in determining the validity of a target report. These parameters have been used in the past to discriminate against false reports; however, a careful examination of their characteristics might uncover more effective uses.

REFERENCES

1. "ARTS Enhancement Support Program, Multisensor Systems Study", Volumes I, II and III, APL/JHU Report MSO-F-183, February 1974.

2. "Radar Processing Subsystem Evaluation", APL/JHU Report FP8-T-013, March 1975.

3. "CPU Recovery via the IOCE", P. J. McKay, SAAR 14.2, IBM Federal Systems Division; Atlantic City, N.J., July 22, 1974.

4. "NAS Stage A Systems Engineering and Analysis, Capacity Testing", H. T. Morgan, Federal Aviation Administration SRDS, Washington, D. C. April, 1974.

5. "NAS Configuration Management Document" Introduction to Specification Series", NAS-MD-310 revision C; Federal Aviation Administration, October 1973.

6. "NAS Configuration Management Document: Performance Criteria", NAS-MD-318 Revision B, Federal Aviation Administration, August 1973.

7. "NAS Configuration Management Document: Multiple Radar Data Processing", NAS-MD-320 Revision C; Federal Aviation Administration, October 1973.

8. "NAS Configuration Management Document: Automatic Tracking", NAS-MD-321 Revision C, Federal Aviation Administration, October 1973.

9. "NAS Configuration Management Document: Software Design Requirements", NAS-MD-325, Federal Aviation Administration, May 1973.

10. "Final Report on ASR-( ) Portion of the FAA Radar Study", APL/JHU Internal Technical Memorandum F3E-401, R. L. Harris, 10 January 1975.

11. "Radar Design Principles", F. E. Nathanson, McGraw-Hill, New York, 1969.

12. "Air Traffic Control Radar Systems Definition Report", H. C. Moses, FAA Report FAA-EM-72-1, March 1972.

13. "Radar Technology Applied to Air Traffic Control", W. W. Schrader, IEEE Transactions on Communications, Vol. COM-21, No. 5, May 1973.

14. "ARSR-2 Operating Manual, Section 3 Theory of Operation, Revised" May 1973.

15. "Radar Precipitation Echoes", F. E. Nathanson and J. P. Reilly, APL/JHU Report No. TG-899, April 1967.

16. "Distribution of Radar Angels", G. E. Pollin, IEEE-AES, Vol. AES-8, No. 6, November 1972.

17. "Radar Equations for Jamming and Clutter", D. K. Barton, Supplement to IEEE Transactions on Aerospace and Electronic Systems, Vol. AES-3, No. 6, November 1967.

18. "Studies of Target Detection by Pulsed Radar", J. I. Marcum and P. Swerling, IRE Transactions, Vol. IT-6, No. 2, April 1960.

19. "Preliminary Instruction Book, Air Traffic Control Beacon Interrogator Model ATCBI-4", Tasker Industries, July 1969.

20. "Technical Manual, Service Instruction, Transmitting Set, Coordinate Data, Models AN/FYQ-47, AN/FYQ-49", Burroughs Corporation Contract No. FA67NS-33, FAA No. T.O. 31S5-2FYQ47-2, June 1974.

21. "U. S. National Standard for the IFF Mark X (SIF)/Air Traffic Control Radar Beacon System Characteristics", DOT/FAA Order 1010.51A, March 8, 1971.

22. "Single Clock Modification to the CD", J. W. Thomas, APL/JHU Report F3E-512, June 19, 1975.

23. "Evaluation of Improved Quantizer Detector Modification to the Production Common Digitizer", Howard L. McFann and William C. Swansen, FAA-RD-73-54, AD-761116, May 1973.

24. "Design Data PCD Enhancements" Burroughs Corporation Report No. 33300-74-2413-C, Specification FAA-E-2235, Supplement 13, 31 March 1975.

25. "A Comparison of the Efficiency of Estimators for Log Rayleigh Noise", R. J. Prengaman, APL/JHU Report MRD-3-443, June 5, 1972.

26. "Binary Integration in Correlated Clutter", R. M. Barnes, APL Memorandum MRD-3-455, July 18, 1972.

27. "Analysis of Slow CFAR Loop Proposed for Use in SPS-88 AVP", W. G. Bath, APL/JHU Report F3C-1-062, February 6, 1975.

28. "ARTS Enhancement Support Program Multisensor System Study", Vol. II, APL/JHU Report MSO-F-183, January 31, 1973.

29. "Maximum Likelihood Correlation Estimation", R. M. Barnes, APL/JHU Report F3E-130, February 21, 1974.

30. "Marcum's and Swerling's Data on Target Detection by a Pulsed Radar", L. F. Fehlner, APL/JHU Report TG-451, July 2, 1962.

31. "Recommended Radar Video Quantizing/Detection Modifications", APL/JHU MSO-F-120, March 22, 1972.

32. "Probability and Stochastic Processes With a View Towards Applications", Leo Breiman, Houghton Mifflin Co., 1969.

33. "ARTS Enhancement Support Program Multisensor System Study", Vol. II, III, APL/JHU MSO-F-183, January 31, 1973.

34. "Plan for Testing Common Digitizer Enhancements", E. L. Brickner, E. C. Wetzlar, APL/JHU FP8-E-008, April 1975.

35. "Operational Amplifiers", Burr-Brown, McGraw-Hill 1971, p.298.

36. "Study Plan for System Definition for On-Site Processing of Sensor Signals", APL/JHU Report FP8-E-002, December 1974.

37. "Introduction to Radar Systems", M. I. Skolnik, McGraw-Hill, 1962.

38. "Clutter Statistics Which Affect Radar Performance Analysis", F. E. Nathanson and J. P. Reilly, IEEE 1967.

39. "The Design of a Modern Surveillance Radar", A. K. Edgar, E. J. Dodsworth and M. P. Warden, IEEE.

40. "Test Plan for Recording and Documenting ASR-7 Weather Data", APL/JHU Report FP8-T-036, May 1976.

#U.S. GOVERNMENT PRINTING OFFICE: 1977 724-443/612 1-5